

## ABSTRACT

Title of Document: Degenerative Transfer Living Ziegler-Natta  
Polymerization of  $\alpha$ -Olefins

Yonghui Zhang, Doctor of Philosophy, 2005

Directed By: Professor Lawrence R. Sita  
Department of Chemistry and Biochemistry

A degenerative transfer (DT) living Ziegler-Natta polymerization system based on the cyclopentadienyl amidinate zirconium complex,  $(\eta^5\text{-C}_5\text{Me}_5)\text{ZrMe}_2[\text{N}(t\text{-Bu})\text{C}(\text{Me})\text{N}(\text{Et})]$  (**19**), has been studied in detail. Compound **19** is an active pre-catalyst for the living and stereospecific polymerization of  $\alpha$ -olefins, upon activation by a stoichiometric amount of  $[\text{PhNHMe}_2][\text{B}(\text{C}_6\text{F}_5)_4]$  (**18**). With a *substoichiometric* amount of **18**, degenerative transfer living Ziegler-Natta polymerization occurs. The extremely fast interconversion between an active cationic species and a dormant neutral species via a methyl (MeDeT) or chloride (ChloDeT) group is essential for degenerative transfer to occur ( $R_{ex} \gg R_p$ ). Under MeDeT conditions, atactic polyolefins are produced due to the configurational instability of the amidinate ligand in its dormant state, with the rate of epimerization being much faster than the rate of propagation ( $R_{epi} \gg R_p$ ). The configurational stability of all the zirconium species involved in ChloDeT ensures that this degenerative transfer living polymerization is stereospecific.

Methylating reagents ( $\eta^5\text{-C}_5\text{Me}_5\text{)ZrMe}_2[\text{N}(t\text{-Bu)C}(t\text{-Bu)N}(\text{Et})]$  (**34**) and ( $\eta^5\text{-C}_5\text{Me}_5\text{)ZrMe}_2[\text{NCH}_2(t\text{-Bu)C}(\text{Me)N}(\text{Et})]$  (**39**) were synthesized to provide a means by which a fully activated polymerization system could be brought under degenerative transfer conditions. Adding **18** and **34** or **39** alternatively to a living polymerization system produces well-defined atactic-isotactic stereoblock polyolefins. This allows, for the first time, the production of stereoblock polyolefins with controlled block length, block tacticity and block placement within a polymer backbone.

Living stereoselective propylene polymerizations were carried out by  $\{(\eta^5\text{-C}_5\text{Me}_5\text{)ZrMe}[\text{N}(t\text{-Bu)C}(\text{Me)N}(\text{Et})]\}\{\text{B}(\text{C}_6\text{F}_5)_4\}$  (**32**). A mmmm of 73% and a  $\sigma$  value of 94% were determined, which is the highest among living propylene polymerizations reported to date. Under degenerative transfer conditions, atactic PP was produced. Using the developed methodology, a family of different atactic-isotactic stereoblock polypropylene (*sb*-PP) was synthesized with controlled block length, block tacticity for the first time. Preliminary data shows excellent elastomeric properties for the *sb*-PPs that are synthesized.

The amidinate zirconium initiator was chemically immobilized to polystyrene-based solid support via deprotonation and nucleophilic addition reactions at the distal position of ( $\eta^5\text{-C}_5\text{Me}_5\text{)ZrCl}_2[\text{N}(t\text{-Bu)C}(\text{Me)N}(\text{Et})]$  (**40**). Heterogeneous initiator (**58**) polymerizes  $\alpha$ -olefins in a living and isospecific fashion. Also, a long shelf time was observed for **58** at room temperature. This is the first heterogeneous living Ziegler-Natta stereospecific catalyst reported to date.

DEGENERATIVE TRANSFER LIVING ZIEGLER-NATTA POLYMERIZATION  
OF  $\alpha$ -OLEFINS

By

Yonghui Zhang

Dissertation submitted to the Faculty of the Graduate School of the  
University of Maryland, College Park, in partial fulfillment  
of the requirements for the degree of  
Doctor of Philosophy  
2005

Advisory Committee:

Professor Lawrence R. Sita	Chair
Professor Bryan W. Eichhorn	
Professor Jeffery T. Davis	
Associate Professor Lyle Isaacs	
Professor Kyu-Yong Choi	

© Copyright by  
Yonghui Zhang  
2005



## **Dedication**

To my wife Jiemin and daughter Joyce.

## Acknowledgements

I'd like to thank my advisor, Professor Lawrence R. Sita, for his supervision during my four years research at the University of Maryland. Professor Sita's tremendous enthusiasm for chemistry, unique angles of observation, knowledge of organometallic chemistry and brilliant ideas have benefit my research significantly. I am also very grateful for his encouragement. I not only learned chemistry from him, but also how to be a scientist.

It has been an incredible four years. My committee has given me great support not only for course work, but also for advice and suggestions. Among which, especially, Dr. Davis, Dr. DeShong, Dr. Eichhorn, Dr. Isaacs, Dr. Falvey, Dr. Morehead, Dr. Vedernikov and Dr. Rokita have been especially helpful. Without their help, this work would not be possible.

Special thanks goes to the Sita group, both former and current members: Dr. Richard Keaton, Matthew B. Harney, Andrea E. Young, Lixin Wang, Dr. Denis A. Kissounko, Albert Epshteyn, Erin K. Reeder, Wei Zhang, Hao He and Samuel Hundert. I'd like to thank Dr. Keaton, Matthew and Lixin for their support, discussion and their partial contribution to this dissertation.

NMR and X-Ray diffraction are the two major analytical techniques used in this dissertation. Without the help from Dr. Yiu-Fai Lam, Dr. Yinde Wang and Dr. James Fettinger, this work would be impossible.

Finally, I would like to thank my family for their support, especially my parents Yizhong Zhang, Liujiao Chen and my wife Jiemin Lu.

## Table of Contents

Dedication.....	ii
Acknowledgements.....	iii
Table of Contents.....	iv
List of Abbreviations.....	vi
List of Figures.....	vii
List of Schemes.....	xii
List of Tables.....	xv
List of Numbered Compounds.....	xvi
Chapter 1 Introduction.....	1
1.1 Early Development of Ziegler-Natta Polymerization.....	1
1.1.1 Discovery.....	1
1.1.2 Metallocene Initiators.....	3
1.2 Dynamic Polymerization Systems.....	12
1.2.1 Chain End Epimerization.....	12
1.2.2 Site-Isomerization.....	16
1.2.3 Oscillating Metallocene.....	21
1.2.4 Binary System.....	25
1.3 Living Ziegler-Natta Polymerization and Post-Metallocene Polymerization..	27
1.3.1 Living Polymerization.....	27
1.3.2 Group 4 Post-Metallocene Initiators for Living Ziegler-Natta Polymerizations.....	28
1.4 Sita System: More Detailed Picture.....	38
Chapter 2 Methyl Group Degenerative Transfer Ziegler-Natta Polymerization MeDeT <sup>164</sup> .....	42
2.1 Background.....	42
2.2 Degenerative Transfer Ziegler-Natta Polymerization.....	43
2.3 Mechanistic Studies.....	49
2.4 Kinetic Analysis.....	51
2.5 Origin of the Loss of Stereospecificity.....	57
2.6 Synthesis of Multi-Stereoblocks.....	66
2.7 Hafnium MeDeT <sup>192</sup> .....	75
2.8 Conclusions.....	79
2.9 Experimental.....	79
Chapter 3 Chloride Group Degenerative Transfer Ziegler-Natta Polymerization ChloDeT.....	91
3.1 Background.....	91
3.2 Stereospecific Degenerative Transfer Living Polymerization.....	92
3.3 Halide Abstraction Reagents.....	96
3.4 Kinetic of ChloDeT.....	99
3.5 Applications of ChloDeT.....	101
3.6 Conclusion.....	106
Chapter 4 Heterogeneous Living Ziegler-Natta Polymerization of $\alpha$ -olefins.....	117

4.1 Background.....	117
4.2 Deprotonation of Zirconium Amidinate <sup>217</sup> .....	119
4.3 Reaction with Electrophiles .....	121
4.4 Preparation of the Solid-Supported Initiator <sup>224</sup> .....	126
4.5 Living Polymerization of 1-Hexene.....	127
4.6 Conclusions.....	130
4.7 Experimental.....	130
Chapter 5 Living 1-Butene and Propylene Polymerization .....	135
5.1 Background.....	135
5.2 Polymerization of 1-Butene Stereoblock.....	136
5.3 Polypropylene Polymerization.....	140
5.4 Kinetic Analysis.....	145
5.5 Methylating Reagents .....	151
5.6 Synthesis of PP Stereoblocks.....	152
5.7 Polypropylene Produced by Formamidinate Zirconium Complex .....	160
5.8 Conclusions.....	163
5.9 Experimental.....	164
Chapter 6 Conclusions .....	171
References.....	173

## List of Abbreviations

$\sigma$	stereoselectivity of pro-chiral monomer insertion into the cationic propagating centers
acac	acetylaceton
AFM	atomic force microscopy
<i>i</i> -Bu	<i>iso</i> -butyl
<i>t</i> -Bu	<i>tert</i> -butyl
CGC	constrained geometry catalyst
ChloDeT	chloro group degenerative transfer
Cp	cyclopentadienyl ( $\eta^5$ -C <sub>5</sub> H <sub>5</sub> )
Cp*	pentamethylcyclopentadienyl ( $\eta^5$ -C <sub>5</sub> Me <sub>5</sub> )
Cy	cyclohexyl
DMA	dynamic mechanic analysis
DSC	differential scanning calorimetry
DP	degree of polymerization
DT	degenerative transfer
EXSY	exchange NMR spectroscopy
GC	gas chromatography
GPC	gel permeation chromatography
Ind	indenyl
MAO	methylaluminoxane
mMAO	modified MAO
MeDeT	methy group degenerative transfer
mmmm	isotactic content for PP microstructure pentad analysis
$M_n$	number average molecular weight
$M_w$	weight average molecular weight
PDI	polydispersity index ( $M_w/M_n$ )
PE	polyethylene
PH	poly(1-hexene)
PMCP	poly(methylenecyclopentane)
PO	poly(1-octene)
PP	polypropylene
<i>a</i> -PP	atactic polypropylene
<i>el</i> -PP	elastomeric polypropylene
<i>iso</i> -PP	isotactic polypropylene
<i>sb</i> -PP	stereoblock polypropylene
<i>syndio</i> -PP	syndiotactic polypropylene
PVCH	poly(vinylcyclohexane)
R	any alkyl group
$R_p$	rate of propagation
$R_{epi}$	rate of epimerization
$R_{ex}$	rate of exchange
$T_m$	melting point

## List of Figures

Figure 1. Typical microstructures of polypropylenes .....	2
Figure 2. Typical metallocenes with different symmetries.....	4
Figure 3. Typical regioerror arising from a 2,1 misinsertion in a dominate 1,2 insertion propagation. ....	7
Figure 4. <sup>13</sup> C NMR (100 MHz, C <sub>6</sub> D <sub>5</sub> Cl, 0 °C) of the shown cation after 15 h at 0 °C. The two 1:1:1 triplets (□) centered at 27.2 and 25.8 ppm correspond to diastereotopic doubly labeled methyl groups ( <sup>13</sup> CH <sub>2</sub> D) of the isobutyl moiety. The singlet at 25.2 ppm and the triplets at 25.0 and 24.3 ppm are due to singly and doubly labeled decomposition products. ....	16
Figure 5. Several C <sub>1</sub> -symmetric metallocenes .....	17
Figure 6. Bulky ligands <i>ansa</i> -bridge C <sub>1</sub> -symmetric catalysts designed by Chien.....	20
Figure 7. Oscillating metallocenes and its <i>ansa</i> -bridged counterparts .....	22
Figure 8. diamido coordinated catalysts. ....	30
Figure 9. Titanium CGC catalyst designed by Ikeda ( <b>17</b> ). ....	31
Figure 10. General formula of FI catalyst.....	33
Figure 11. Modified FI pre-catalyst for living <i>iso</i> -PP polymerization developed by Coates.....	35
Figure 12. Amine bis(phenolate) catalysts for living polymerizations.....	36
Figure 13. The amine bis(phenolate) THF ligand.....	37
Figure 14. <sup>13</sup> C { <sup>1</sup> H} NMR (100 MHz, CDCl <sub>3</sub> , 25 °C) of PH obtained from pre- catalyst <b>19</b> , a), stoichiometric activation(up), <i>iso</i> -PH and b), half activation (bottom) with <b>19</b> : <b>18</b> = 2:1, <i>a</i> -PP. ....	44
Figure 15. Dependence of PH <i>M<sub>w</sub></i> (■) and PDI values (▲) on [1-hexene] <sub>0</sub> /[Zr] <sub>0</sub> at constant. [1-hexene] <sub>0</sub> = 0.50 M and [ <b>18</b> ] <sub>0</sub> = 2.5 mM. ....	45
Figure 16. <sup>1</sup> H NMR spectra (400 MHz, C <sub>6</sub> D <sub>5</sub> Cl, -10 °C) of <b>19</b> and <b>32</b> mixtures with various ratios. At the top: pure cationic <b>32</b> and at the bottom: pure neutral <b>19</b> .....	50

Figure 17. Typical simulation plot based on equilibrium. Equilibrium constants are shown in the insets of the figure. ....	54
Figure 18. Kinetic plot for different percentage activation. Linear curve fit only for guide of eye. ....	56
Figure 19. Bond lengths for three different zirconium species. ....	58
Figure 20. 2D $^{13}\text{C}\{^1\text{H}\}$ EXSY NMR (125 MHz, chlorobenzene- $d_5$ , -10 °C) spectrum of the diastereotopic methyl resonances for <b>42</b> * Me <sub>a</sub> / Me <sub>b</sub> mixture obtained with a mixing time of 400 ms <sup>185</sup> , a variety of mixing time from 200 ms to 800 ms were carried out for the calculation of rate constants. .	60
Figure 21. Partial $^{13}\text{C}\{^1\text{H}\}$ NMR (125 MHz, chlorobenzene- $d_5$ , -10 °C) spectra of methyl, polymeryl dormant species a-d prepared according to (a) upper reaction sequence of Scheme 32 (atactic) and (b) lower reaction sequence of Scheme 32 (isotactic). ....	63
Figure 22. 2D $^{13}\text{C}\{^1\text{H}\}$ EXSY NMR (125 MHz, chlorobenzene- $d_5$ , -10 °C) spectrum of methyl, polymeryl dormant species a-d of Scheme 30 and Figure 21a recorded with a mixing time of 100 ms. ....	65
Figure 23. $^{13}\text{C}\{^1\text{H}\}$ NMR (100 MHz, chlorobenzene- $d_5$ , -10 °C) spectrum of (a), upper, I and (b) lower, after addition of 1 equivalents of <b>42</b> followed by addition of 1 equivalent of <b>18</b> . ....	67
Figure 24. Inverse-gated $^{13}\text{C}\{^1\text{H}\}$ NMR (100 MHz, chloroform- $d_1$ , 298K) spectrum of <i>a</i> -poly(1-hexene)- <i>block-iso</i> -poly(1-octene). $^{13}\text{C}$ NMR resonances for the isotactic poly(1-octene) block are marked with an asterisk (*) .....	68
Figure 25. GPC trace for aliquots of the pentablock. From left to right are the 1 <sup>st</sup> block to the bulk pentablock. ....	72
Figure 26. Inverse gated $^{13}\text{C}\{^1\text{H}\}$ NMR (100 MHz, $\text{CDCl}_3$ , 25 °C) spectra for aliquots of the pentablock and the integration of PH and PO peaks. ....	73
Figure 27. Kinetic analysis of fully activated Hafnium 1-hexene polymerization system. ....	76
Figure 28. MeDeT mechanism for hafnium polymerization .....	77
Figure 29. Different percentage activation for hafnium polymerizations. ....	78
Figure 30. Polymers with Different microstructures. ....	92

Figure 31. Dependence of poly(1-hexene) $M_n$ (■) and PDI (▲) values on $[M]_0/[Zr]_{total}$ at constant $[M]_0 = 0.50$ M and $[18] = 2.5$ mM.....	95
Figure 32. $^1H$ NMR (400 MHz, chlorobenzene- $d_5$ , $-10$ °C) spectra of <b>41</b> (top), 1:1 of <b>42:18</b> (middle) and a 1:1:1 mixture of <b>41</b> , <b>42</b> and <b>18</b> (bottom). The peaks with asterisks are PhNMe <sub>2</sub> .....	98
Figure 33. Potential de-chloro reagent.....	99
Figure 34. $k_{obs}$ vs. percentage activation, dotted line is the simulation with $K = 0.13$ . .....	101
Figure 35. X-ray structure of the dinuclear initiator.....	104
Figure 36. Potential core for a tri-arm star polymer.....	106
Figure 37. $^{13}C\{^1H\}$ NMR (100 MHz, chloroform- $d$ , $25$ °C) spectrum of PH prepared using $[1\text{-hexene}]_0/[41+42] = 100 : 1$ .....	108
Figure 38. Full activation ChloDeT kinetic.....	110
Figure 39. 50% activation ChloDeT kinetic.....	111
Figure 40. 36.5% activation ChloDeT kinetic.....	112
Figure 41. 25% activation ChloDeT kinetic.....	113
Figure 42. 18% activation ChloDeT kinetic.....	114
Figure 43. 10% activation ChloDeT kinetic.....	115
Figure 44. IOLA solid supported activator.....	118
Figure 45. $^1H$ NMR spectrum (400 MHz, $C_6D_6$ , $25$ °C) of <b>46</b> .....	120
Figure 46. Molecular structure (30% thermal ellipsoids) of <b>46</b> . Hydrogen atoms have been removed for clarity.....	121
Figure 47. Molecular structure (30% thermal ellipsoids) of the nucleophilic addition reaction product of the hafnium derivative towards Me <sub>2</sub> SiCl <sub>2</sub> (left) and Me <sub>3</sub> SiCl (right). Hydrogen items have been removed for the sake of clarity.....	122
Figure 48. Molecular structure of <b>54</b> (left) and <b>55</b> (right). Hydrogen atoms removed for clarity.....	125
Figure 49. Dependence of $M_w$ for <i>iso</i> -PH on yield of isolated polymers.....	127

Figure 50. Inverse-gated $^{13}\text{C}\{^1\text{H}\}$ NMR (100 MHz, $\text{CDCl}_3$ , 25 °C) spectrum of <i>iso</i> -PH- <i>b</i> -PO block copolymer. Resonances for the PO block are marked with an asterisk (*).	129
Figure 51. GPC trace of <i>iso</i> -poly(1-hexene)- <i>b</i> - <i>iso</i> -poly(1-octene) block copolymer ( $M_n$ 23 700, PDI 1.07) (Solid line), and an aliquot of the <i>iso</i> -poly(1-hexene) block formed before addition of 1-octene monomer ( $M_n$ 8 500, PDI 1.05) (dashed line)	134
Figure 52. $^{13}\text{C}\{^1\text{H}\}$ NMR (100 MHz, $\text{CDCl}_3$ , 25 °C) spectra for <i>iso</i> -PB (top), and <i>a</i> -PB (bottom)	137
Figure 53. AFM height and phase maps for <i>iso</i> -PB before annealing	138
Figure 54. AFM height and phase maps for <i>iso</i> -PB after 120 °C annealing and cooling down slowly	139
Figure 55. AFM height and phase maps for <i>iso</i> - <i>a</i> -PB before annealing	139
Figure 56. AFM height and phase maps for <i>iso</i> - <i>a</i> -PB after 120 °C annealing and slowly cooling down to room temperature	140
Figure 57. Polypropylene polymerization setup	141
Figure 58. $^{13}\text{C}\{^1\text{H}\}$ (100 MHz, $\text{C}_2\text{D}_2\text{Cl}_4$ , 70 °C) NMR spectrum of <i>iso</i> -PP	142
Figure 59. 125 MHz $^{13}\text{C}\{^1\text{H}\}$ NMR ( $\text{C}_2\text{D}_2\text{Cl}_4$ , 70 °C) spectra of <i>a</i> -PP and <i>iso</i> -PP methyl region	144
Figure 60. 125 MHz $^{13}\text{C}\{^1\text{H}\}$ NMR spectrum (1,2- $\text{C}_2\text{D}_2\text{Cl}_4$ at 70 °C) of <i>iso</i> -PP sample	145
Figure 61. Kinetic plot of <i>a</i> -PP polymerization. ▼ represents number average molecular weight, and the hollow triangle represents polydispersity index	149
Figure 62. Kinetic data for <i>iso</i> -PP polymerization. ▼ represents number average molecular weight, and the hollow triangle represents polydispersity index	151
Figure 63. Tensile test results for three <i>sb</i> -PPs <sup>237</sup>	157
Figure 64. Ten cycle 300% elongation test for <i>a</i> - <i>iso</i> - <i>a</i> - <i>iso</i> -PP sample	158
Figure 65. DSC curves for three <i>sb</i> -PPs, <i>a</i> - <i>iso</i> - <i>a</i> (solid line), <i>a</i> - <i>iso</i> (dotted line) and <i>a</i> - <i>iso</i> - <i>a</i> - <i>iso</i> (dashed line)	159

Figure 66. ps-tm AFM phase maps for thin films on amorphous carbon. a). <i>iso</i> -PP (left); b) <i>iso-a-iso</i> -PP (middle) and c) a thin film of b (right). .....	160
Figure 67. $^1\text{H}$ NMR (400 MHz, $\text{C}_6\text{D}_5\text{Cl}$ , $-10\text{ }^\circ\text{C}$ ) spectrum of <b>60</b> .....	161
Figure 68. Methyl region $^{13}\text{C}$ $\{^1\text{H}\}$ NMR (125 MHz, $\text{C}_2\text{D}_2\text{Cl}_4$ , $70\text{ }^\circ\text{C}$ ) spectrum of polypropylene sample obtained from <b>60</b> .....	163

## List of Schemes

Scheme 1. Cossee-Arlman Mechanism .....	3
Scheme 2. Putative MAO activation mechanism for metallocenes.....	5
Scheme 3. Different microstructures generated by different enantioselectivities. ....	8
Scheme 4. $C_2$ -symmetric metallocene in a two site model.....	9
Scheme 5. $C_s$ -symmetric metallocene in a two site model .....	10
Scheme 6. $C_1$ -symmetric metallocene in a two site model.....	10
Scheme 7. Busico chain-end epimerization mechanism, Pn = polymer chain. ....	13
Scheme 8. Poly(1-D-propylene) microstructure at low propylene concentration. ....	14
Scheme 9. An enantioface dissociate-recoordination process proposed by Busico. ..	14
Scheme 10. Chain-end epimerization mechanism proposed by Resconi. ....	15
Scheme 11. Polymerization mechanisms for $C_1$ -symmetric metallocenes. ....	19
Scheme 12. Simplified model for oscillating metallocene catalyst.....	21
Scheme 13. Locked <i>rac</i> mechanism for unbridged metallocenes.....	24
Scheme 14. Polymer chain transfer between Zr and Al species.....	26
Scheme 15. Influence of solvent to the tacticity of polymer by Ikeda's catalyst .....	32
Scheme 16. General synthetic routes for amidinate based catalysts.....	39
Scheme 17. Configurational instability of the neutral pre-catalyst.....	40
Scheme 18. The origin of stereospecificity of amidinate based zirconium initiator. .	41
Scheme 19. Methyl, polymeryl groups exchange between cationic species .....	43
Scheme 20. Proposed Mechanism for Methyl group Degenerative Transfer Polymerization.....	46
Scheme 21. Slow dissociation of the monocationic Zr-Me-Zr dimer reported by Marks.....	47
Scheme 22. Basic mechanism of degenerative transfer polymerization.....	47
Scheme 23. Brief mechanisms for different systems controlled radical polymerizations.....	48
Scheme 24. Two enantiotopic propagating species and their isotactic polymer chains .....	57
Scheme 25. Preparation of alkyl methyl amidinate zirconium alkyl complex. ....	59

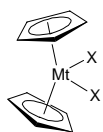
Scheme 26. Metal centered epimerization of alkyl methyl compound <b>42</b> . Me <sub>a</sub> is favored due to less interactions between the <i>i</i> -Bu group and the <i>t</i> -Bu group. ....	61
Scheme 27. Possible mechanism for the loss of stereo-control during MeDeT. ....	61
Scheme 28. Degenerative transfer based on polymeryl chain transfer.....	62
Scheme 29. <sup>13</sup> C labeled polymerization experiment to rule out the polymeryl chain transfer postulation.....	63
Scheme 30. Proposed mechanism for loss of stereo-control during MeDeT. For a and b, P = <i>a</i> -poly(1-hexene) chain, and for c and d, P = <i>iso</i> -poly(1-hexene) chain. ....	64
Scheme 31. General reaction scheme to make <i>t</i> -Bu amidinate derivatives .....	74
Scheme 32. Potential methylating reagent to turn on MeDeT.....	74
Scheme 33. ChloDeT polymerization using <i>i</i> -Bu derivatives <b>42</b> .....	93
Scheme 34. Chloride group degenerative transfer polymerization mechanism. ....	96
Scheme 35. Potential reactions for halide abstraction, counteranion borate omitted for clarity. ....	96
Scheme 36. Deprotonation vs. substitution.....	102
Scheme 37. Hydrogenolysis of Zr-Si bond.....	102
Scheme 38. Examples of the hydrozirconation of pro-chiral substrates.....	103
Scheme 39. Synthesis of the dinuclear initiators .....	103
Scheme 40. Potential mechanism for the dimer initiator polymerization.....	106
Scheme 41. Deprotonation of the distal methyl group by a sterically hindered base. ....	119
Scheme 42. Nucleophilic substitution reaction of <b>46</b> . ....	122
Scheme 43. Zwitterionic initiator remotely activated by B(C <sub>6</sub> F <sub>5</sub> ) <sub>3</sub> .....	123
Scheme 44. Electrophilic addition via THF ring-opening to produce <b>54</b> . ....	124
Scheme 45. Formation of the zwitterionic zirconium species <b>55</b> . ....	124
Scheme 46. The synthesis of solid-supported initiator <b>62</b> . Reagents and conditions: a) Ph <sub>3</sub> SiLi·(THF) <sub>3</sub> , THF, 25 °C, 2 h; b) Bio-beads <sup>TM</sup> S-X1, toluene, 2 h; c) MeLi, Et <sub>2</sub> O, -78 °C to 25 °C, 3 h; d) <b>18</b> , chlorobenzene, -10 °C, 5 min. ....	127

Scheme 47. Synthesis of <i>iso-a-iso</i> -PB .....	137
Scheme 48. Synthetic route for <b>58</b> .....	161
Scheme 49. an isotactic polypropylene stereoblock. ....	162
Scheme 50. Mechanism of Degenerative Transfer Polymerization.....	171

## List of Tables

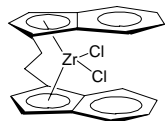
Table 1. Typical electron count for metallocene and post-metallocene catalysts.....	38
Table 2. Kinetic summary of MeDeT .....	55
Table 3. GPC data for each block aliquot and the final pentablock. ....	71
Table 4. Polymerization results for different potential methylating reagents.....	74
Table 5. Rate constants for different percentage activation of <b>43</b> . ....	78
Table 6. $M_n$ and PDI results for different zirconium concentration.....	93
Table 7. Different rate constants of polymerization under different activations%...	100
Table 8. Full activation kinetic data.....	109
Table 9. 50% activation kinetic data.....	110
Table 10. 36.5% activation kinetic data.....	111
Table 11. 25% activation kinetic data.....	112
Table 12. 18% activation kinetic data.....	113
Table 13. 10% activation kinetic data.....	114
Table 14. Kinetic data for <i>a</i> -PP polymerization .....	146
Table 15. Kinetic data of <i>iso</i> -PP polymerization. ....	150
Table 16. Detailed data for <i>a-iso</i> -PP diblock.....	154
Table 17. Detailed data for <i>a-iso-a</i> -PP triblock polymerization.....	154
Table 18. Detailed data for <i>a-iso-a-iso</i> -PP polymerizataion. ....	154
Table 19. 3 high molecular weight <i>sb</i> -PPs.....	156
Table 20. Analysis data for tensile test of <i>sb</i> -PPs.....	157

## List of Numbered Compounds

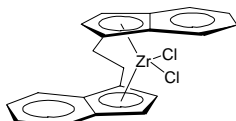


Mt: Ti, Zr, Hf  
X: Cl or Me

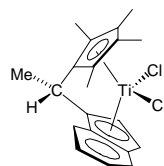
1



C<sub>5</sub>-2



C<sub>2</sub>-2

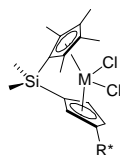


3



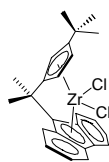
M = Ti, Zr, Hf  
X = C, Si

4

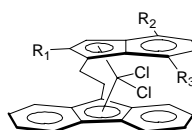


M = Zr, Hf  
R\* = (-)-menthyl, (+)-neomenthyl

5

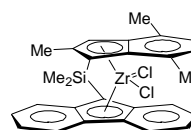


6

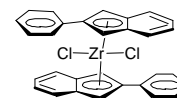


R<sub>1</sub>, R<sub>2</sub>, R<sub>3</sub> = H, Me

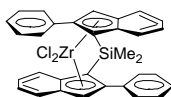
7



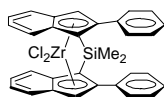
8



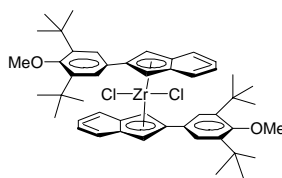
9



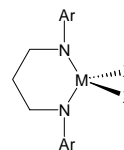
10



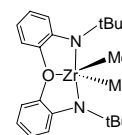
11



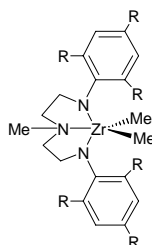
12



13a M = Ti, X = Me  
13b M = Ti, X = Cl  
13c M = Zr, X = CH<sub>2</sub>Ph

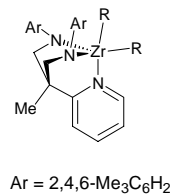


14



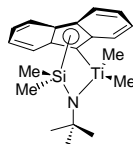
15a R = H  
15b R = Me

15a R = H  
15b R = Me



Ar = 2,4,6-Me<sub>3</sub>C<sub>6</sub>H<sub>2</sub>

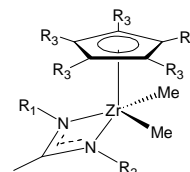
16



17

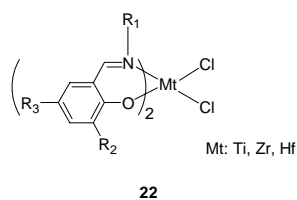
[PhNHMe<sub>2</sub>][B(C<sub>6</sub>F<sub>5</sub>)<sub>4</sub>]

18



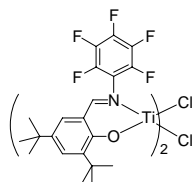
19 R<sub>1</sub> = Et, R<sub>2</sub> = *t*-Bu, R<sub>3</sub> = Me  
20 R<sub>1</sub> = R<sub>2</sub> = *i*-Pr, R<sub>3</sub> = Me  
21 R<sub>1</sub> = R<sub>2</sub> = *i*-Pr, R<sub>3</sub> = H

19

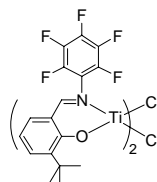


22

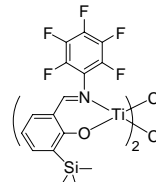
Mt: Ti, Zr, Hf



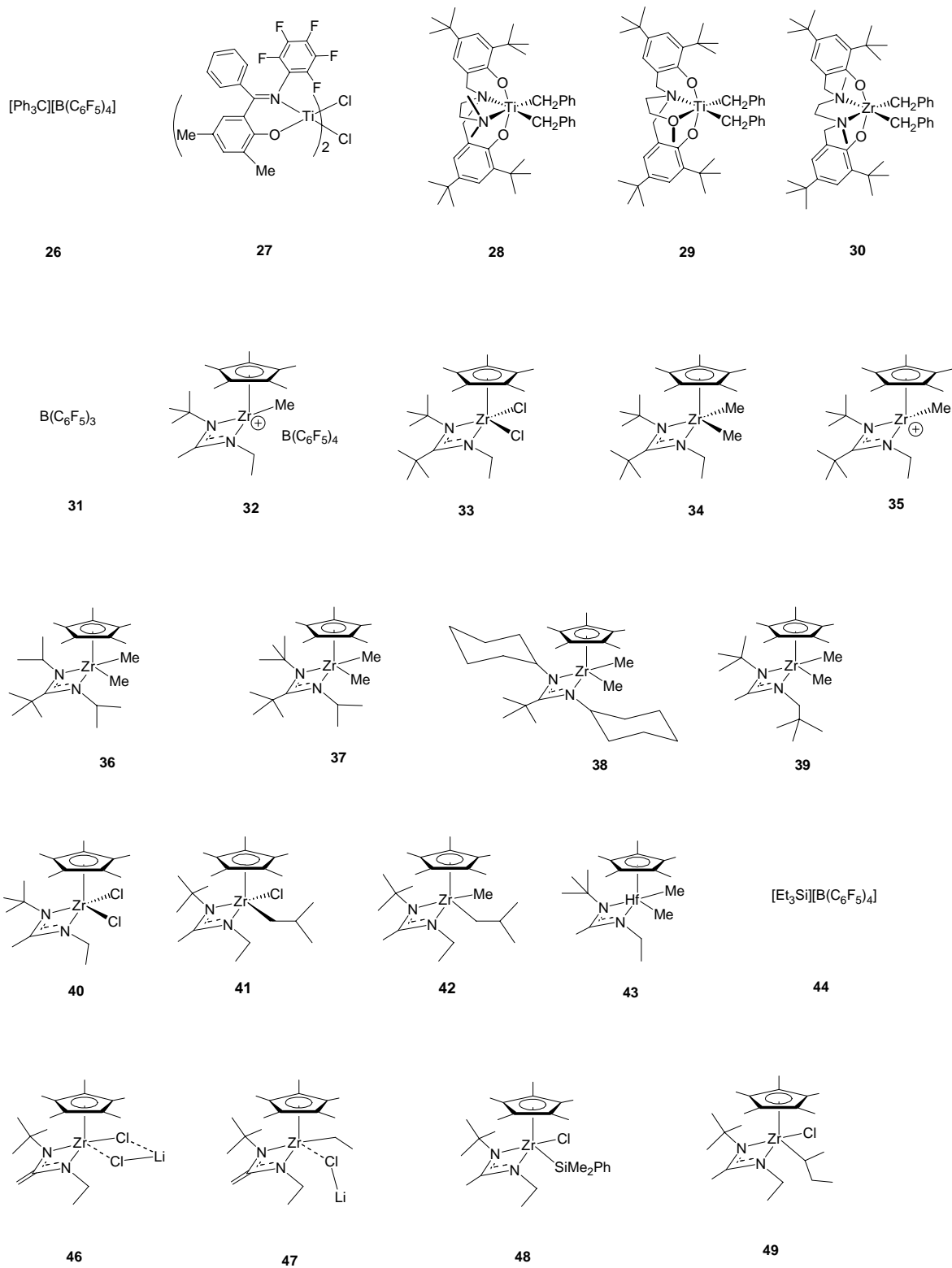
23

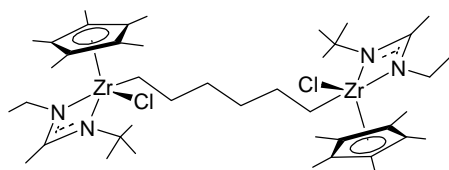


24

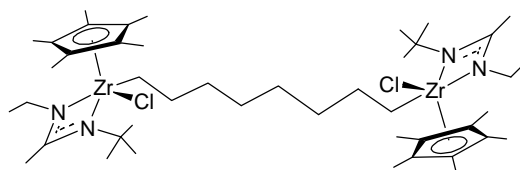


25

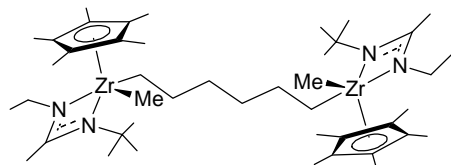




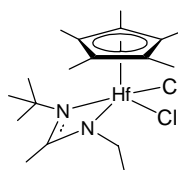
50



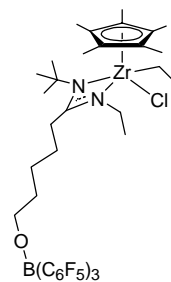
51



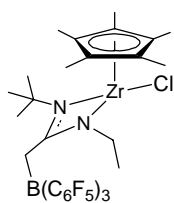
52



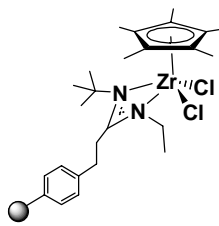
53



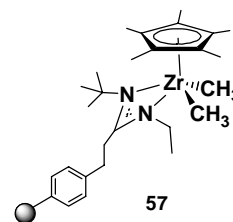
54



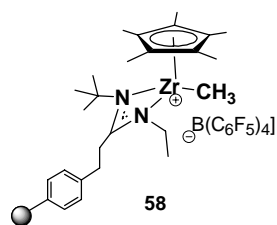
55



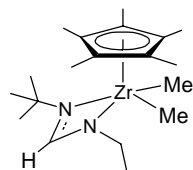
56



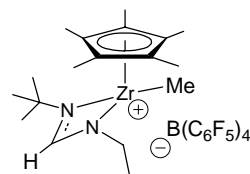
57



58



59



60

## Chapter 1 Introduction

### 1.1 Early Development of Ziegler-Natta Polymerization

#### 1.1.1 Discovery

It has been more than 50 years since Ziegler<sup>1</sup> and Natta<sup>2</sup> first discovered the transition metal-mediated polymerization of ethylene and propylene. Total polypropylene (PP) sales in the US in 2004 was 18.6 billion pounds and it is increasing 5 – 7% annually.<sup>3</sup> Production of polyethylene (PE) and polypropylene is now one of the largest chemical industries in the world accounting for more than 50% of the volume of manufactured plastic. Ziegler-Natta polymerization of  $\alpha$ -olefins is one of the most successful applications of organometallic chemistry in industry. Detailed molecular level mechanistic studies combined with elegant catalyst design have been the keys to success.

Shortly after Ziegler<sup>1</sup> discovered that a heterogeneous catalyst derived from  $\text{TiCl}_4/\text{AlEt}_3$  polymerizes ethylene at low pressure to form linear high density polyethylene (HDPE) in 1953, Natta<sup>2,4-7</sup> developed a heterogeneous catalyst, prepared from  $\text{TiCl}_3$  and  $\text{AlEt}_3$ , that initiates the polymerization of propylene to provide the first crystalline PP. The high activity of the  $\text{TiCl}_3/\text{AlEt}_3$  catalyst for both ethylene and propylene soon led to the commercialization of PE and PP. For polyolefins like PP, tacticity plays a very important role in the physical property of the material. Since propylene is a pro-chiral monomer, stereocenters are generated along the resulting

polymer backbone. If the stereocenters have the same relative stereochemistry, the polymer microstructure is referred to as isotactic, as shown in Figure 1. If all the stereocenters have random relative configurations, the polymer microstructure is referred to as being atactic. Finally, a syndiotactic microstructure is one in which the polymer backbone has stereocenters with alternating relative configurations. Most of commercialized PP is isotactic since it is a thermoplastic material with a relatively high melting point ( $T_m$  up to 165 °C). By adding a small percentage of nucleating agents, the highly crystalline PP can even be exceedingly transparent,<sup>8</sup> and can also be relatively flexible when combined with plasticizers. *iso*-PP is widely used in garbage bags, indoor-outdoor carpeting fibers, automotive parts and miniature golf courses. On the other hand, *a*-PP is tacky and amorphous. *a*-PP has limited commercial applications, such as adhesive and bitumen applications.<sup>9-13</sup>

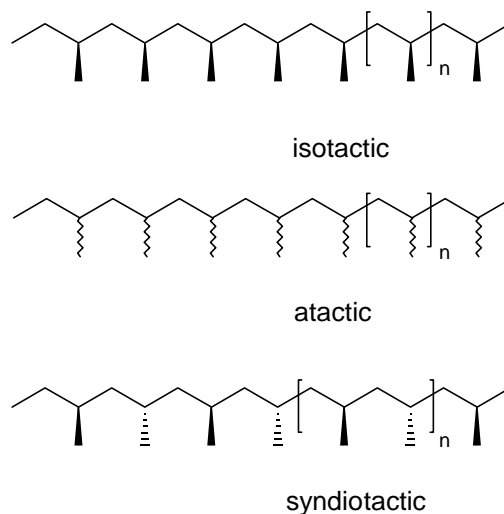
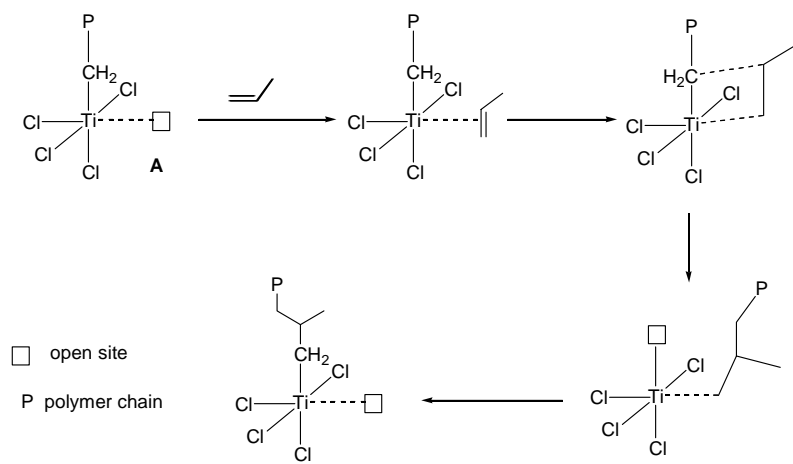


**Figure 1. Typical microstructures of polypropylenes.**

The PP industry is still using heterogeneous  $TiCl_3$  as a main catalyst for *iso*-PP because of its high activity. Due to the heterogeneous nature of the catalyst, the active sites and propagation mechanisms were not well understood for a long time. It

is believed that the isoselectivity of the  $\text{TiCl}_3$  system stems from the unique geometry of the initiator surface.



**Scheme 1. Cossee-Arlman mechanism**

The most widely accepted polymerization mechanism was proposed by Cossee and Arlman.<sup>14-17</sup> As shown in Scheme 1, polymerization occurs as follows: 1) olefin coordination to an open site in **A**; 2) migratory insertion of the  $\sigma$ -coordinated polymer chain to the  $\pi$ -coordinated olefin via a four-membered ring transition state. After migratory insertion, the metal site previously occupied by the  $\sigma$ -bonded polymer chain becomes vacant.

### 1.1.2 Metallocene Initiators

A metallocene is defined as a metal bis(cyclopentadienyl) complex.<sup>18</sup> For Ziegler-Natta polymerization, group 4 metals, such as Ti, Zr and Hf, a general structure of  $\text{Cp}_2\text{MtX}_2$  (**1**) (Cp = cyclopentadienyl, Mt = metal, X = methyl or halide), as shown in Figure 2, is commonly used. The neutral compound is commonly referred to as the pre-catalyst. A main group metal (B, Al, etc.) alkyl compound is often employed as

the co-catalyst, to activate the pre-catalyst to form the active cationic initiator involved in polymerization.

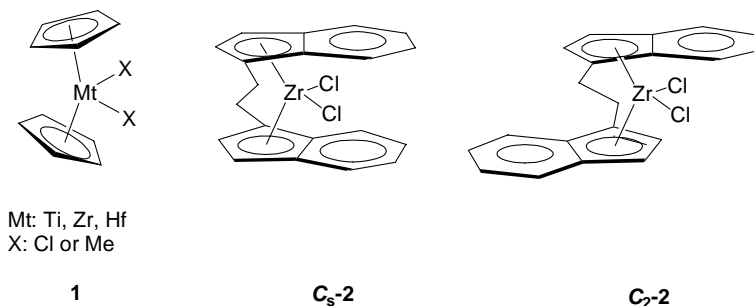
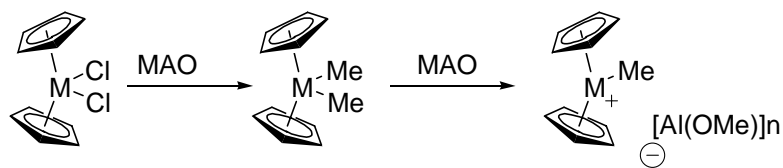


**Figure 2. Typical metallocenes with different symmetries.**

A typical combination of metallocene/ $\text{AlRCl}_2$  or  $\text{AlR}_3$  (R = alkyl group) was soon introduced after the discovery of  $\text{TiCl}_3/\text{AlEt}_3$ .<sup>19-21</sup> The homogeneous nature of metallocene provided insights into the mechanistic studies such as active sites, propagating centers and termination side reactions etc. In the early stages, metallocene catalyst systems, such as  $\text{Cp}_2\text{TiCl}_2/\text{AlMe}_3$ ,<sup>22</sup> had low polymerization activity for ethylene polymerization and almost no activity towards propylene polymerization.

It was not until 1980's that methylaluminoxane (MAO), a potent co-catalyst, was introduced by Kaminsky and Sinn.<sup>23-27</sup> A trace amount of water in the catalytic system of  $\text{Cp}_2\text{MtX}_2/\text{AlMe}_3$  (X = Me, or Cl) reacts with  $\text{AlMe}_3$  to form MAO, of which the actual structure is still unclear. MAO is generally considered as a mixture of  $\text{Al}(\text{O})\text{-Me}$  oligomers, with certain degree of free or possibly associated  $\text{AlMe}_3$ . With MAO, a dramatic increase in polymerization activity was observed.<sup>28</sup>



**Scheme 2. Putative MAO activation mechanism for metallocenes.**

MAO reacts with  $\text{Cp}_2\text{MtCl}_2$  to form a  $\text{Cp}_2\text{Mt}(\text{Me})$  cation, which is believed to be the active species involved in polymerization. Typically, a  $[\text{Al}] : [\text{Mt}]$  ratio of 1000 or higher is used for propylene polymerization due to the inefficiency by which MAO forms the active cationic species. The discovery of MAO is considered as one of the biggest breakthroughs since Ziegler and Natta's original finding and is still the dominant co-catalyst used in industry today.

Metallocene / MAO systems have high activity for ethylene polymerization, and it is also capable of copolymerization of ethylene with  $\alpha$ -olefins.<sup>29</sup> However, the polymerization activity of propylene is still much lower than the original  $\text{TiCl}_3/\text{AlEt}_3$  system. More importantly, only oily *a*-PP was originally produced with very low molecular weight.<sup>30,31</sup>

It is worth mentioning that for the Cp ligand, even with bulky substituents, the rotation of Cp ligand via Cp-Mt axils is very facile. A great discovery was the introduction of the *ansa*-bridged bis-Cp type of ligand to restrict the free rotation.<sup>23,32</sup> Typically, a silyl linkage such as  $\text{SiMe}_2$ , or ethylene (Et) linkage<sup>33</sup> is used as the bridge. For *ansa*-bridged metallocenes with two identically substituted Cp ligands, a mixture of racemic (*rac*) and *meso* diastereomers is typically generated during synthesis, such as with *ansa*-bridged  $\text{Et}(\text{Ind})_2\text{ZrCl}_2$  (Ind: indenyl), one *meso* ( $C_s$ -2) and one  $C_2$ -symmetric ( $C_2$ -2) diastereomer. Fractional recrystallization is commonly used to separate the *meso* compound out. Only the racemic ( $C_2$  symmetry) produces

isotactic polyolefin and the *meso* compound will only generate atactic polyolefin (*vide infra*). While it is often complicated to separate a pure diastereomer from the mixture, new synthetic methodology has been developed to increase the *rac:meso* ratio, such as the use of  $Zr(NMe_2)_4$  instead of  $ZrCl_4$  as the precursor.<sup>34-38</sup>

A significant advantage of metallocenes is their synthetic versatility. Since the early 1980's, hundreds of group 4 metallocene compounds have been synthesized, with different substituents on the Cp rings and with a variety of *ansa*-bridges.<sup>39</sup> Among these derivatives, many can produce highly isotactic PP, and many have similar or higher polymerization activity as compared to the  $TiCl_3/AlEt_3$  system.<sup>39</sup> These metallocenes are commonly referred to as single-site catalyst (SSC), since typically only one type of active species is involved in the polymerization.

For polymerizations of pro-chiral monomers, such as propylene, there are two types of enantiofacial selectivity: enantiomorphic site control, and chain end control. Enantiomorphic site control is the more effective way to control polymer tacticity where the symmetry of the metal's ligand environment, coupled with the steps involved in propagation determine the enantiofacial selectivity. On the other hand, if the relative stereochemistry of the last inserted monomer determines the enantiofacial selectivity of the incoming monomer, the mechanism is referred to as chain-end control.

In addition to stereoselectivity, there are two types of regioselectivity for olefin enchainment into the growing polymer chain: 1, 2 (primary) insertion and 2, 1 (secondary) insertion for  $\alpha$ -olefins. Due to the steric interactions, consecutive

primary or secondary insertions are common which will generate a head-to-tail microstructure as shown in Figure 3. In most cases, primary insertion is favored over secondary insertion due to the electrostatic interaction and less exchange repulsion.<sup>40</sup> For the insertion of propylene to the system  $\text{H}_2\text{Si}(\text{Cp})_2\text{ZrCH}_3(\text{propylene})^+$ , ab initio MO-MM study predicted a 3.5 kcal/mol energy difference between primary and secondary insertion, and the propagation is favored in primary insertion.<sup>41</sup> For different ligand set and metal, the preference of primary insertion and secondary insertion varies. Fujita and Coates's non-metallocene catalyst<sup>42</sup> favors secondary insertion, while with subtle change of the ligand set, primary insertion dominates.<sup>43</sup> Also, the regioselectivity is influenced by the co-catalyst and other factors.

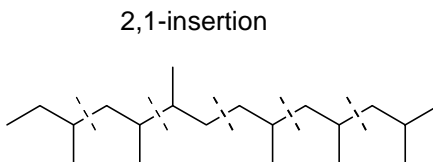


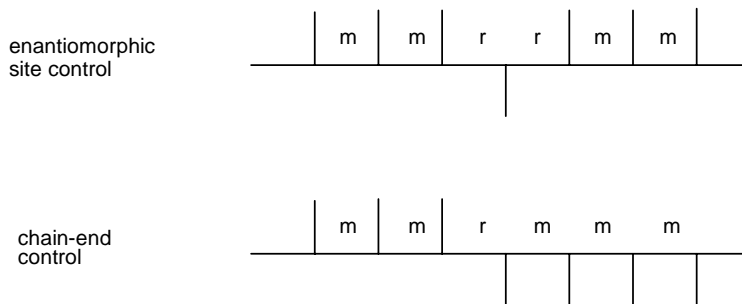
**Figure 3. Typical regioerror arising from a 2,1 misinsertion in a dominate 1,2 insertion propagation.**

A shorthand notation to describe different polyolefin microstructures based on the relative configurations of two consecutive chiral centers within the polymer backbone has been developed, as shown in scheme 3. If the two consecutive stereocenters along the backbone have the same relative configurations, “m” is used to represent a *meso* configuration; if the consecutive centers have opposite relative configurations, then “r” is used to denote the *rac* configuration.

For a propylene polymerization occurring under enantiomorphic site control, in which *iso*-PP is generated, if a misinsertion occurs, then an r dyad is generated. Since the configuration of the next insertion is governed only by the active metal center, the

next insertion should revert to the correct relative stereochemistry. This is referred to as self-correction. An mrrm sequence at the pentad of analysis is generated. Complete detailed statistical analysis at the pentad level shows the polymer should have a mmmr:mmrr:mrrm ratio of 2:2:1.<sup>39</sup> For chain end control, after a misinsertion, propagation will continue with the new relative configuration until another misinsertion occurs. As shown in Scheme 3, an isolated stereoerror generates a mrrm stereoerror at the pentad level.

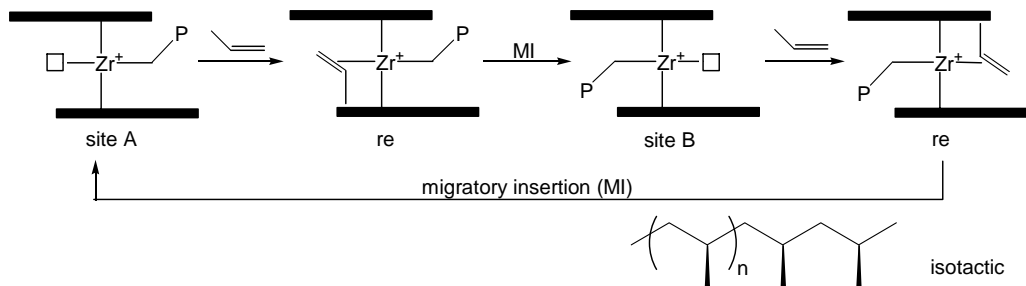
A parameter  $\sigma$  is commonly used to represent the stereoselectivity of the monomer insertion for a certain catalyst under enantiomorphic site control.  $\sigma$  is defined as the probability of a monomer adding to the R site on its *re* face, same as a *si* face to the S site.



**Scheme 3. Different microstructures generated by different enantioselectivities.**

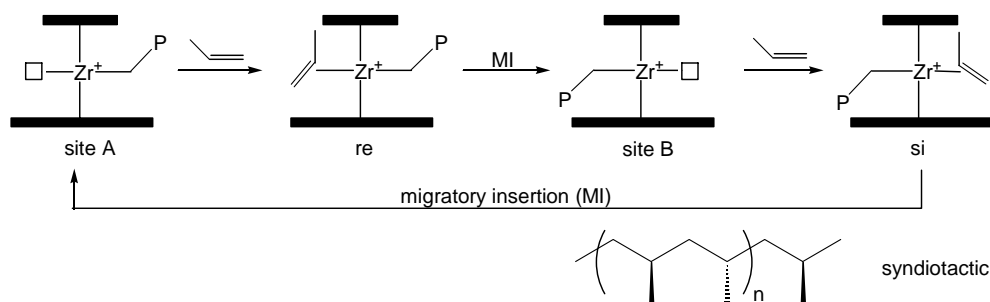
Structure/property relationship studies have been done extensively for catalysts under enantiomorphic site control. Changing the symmetry of a metallocene affects the microstructure of the polypropylene. This was mapped out by Ewen<sup>44</sup> and Kaminsky,<sup>45</sup> and is commonly referred to as Ewen's symmetry rules. In the case of weak site control with low or no stereoselectivity, nearly atactic or atactic polyolefins are produced. However, if the propylene insertion is under strong enantiomorphic

site control with high stereoselectivity, the microstructure of the polyolefin can be well anticipated. For metallocenes, propagation is viewed as occurring by alternating between two sites for olefin binding and propagation. If the two sites are homotopic, and stereoselectivity is high, isotactic polyolefin is produced. Scheme 4 shows a  $C_2$ -symmetric metallocene in which a solid bar is used to represent the cyclopentadienyl ligands, with the length of the bar depicting the steric configuration of the ligands. As the scheme shows in this representation of  $C_2$ -symmetric catalyst, sites A and B are homotopic. Monomer coordination to site A or site B should have the same enantiofacial stereoselectivity and as a result, isotactic polyolefin is produced.



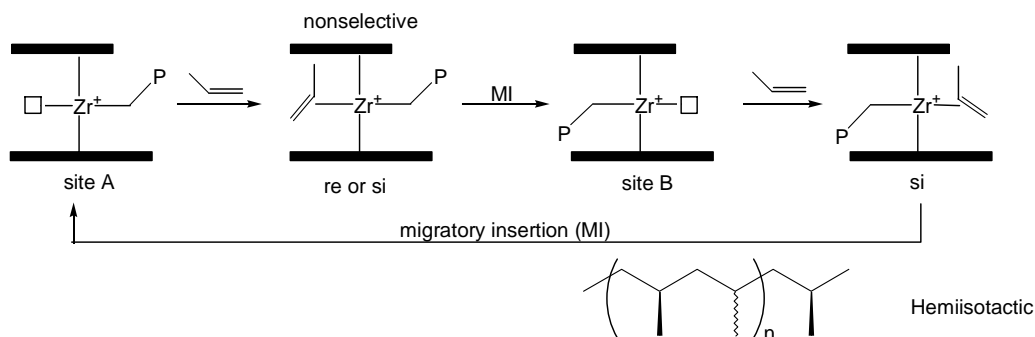
**Scheme 4.**  $C_2$ -symmetric metallocene in a two site model.

For a  $C_s$ -symmetric catalyst, such as  $Cp(Flu)ZrCl_2$ , as shown in Scheme 5, since the two sites are enantiotopic, site A and site B have a mirror image relationship, each insertion will alternate from *re* face to *si* face, therefore producing a syndiotactic polyolefin.



**Scheme 5.  $C_s$ -symmetric metallocene in a two site model.**

$C_1$ -symmetric metallocenes are much more complicated and two cases are of great interest. If site A is nonselective and site B is highly enantioselective, then every other insertion has the same relative configuration with those in between being random. This polymer microstructure is called hemiisotactic. Hemiisotactic PP can be amorphous or thermoplastic-elastomeric in nature.



**Scheme 6.  $C_1$ -symmetric metallocene in a two site model.**

In the extreme case where a bulky *tert*-butyl group is incorporated on the Cp ring, the steric interaction of this substituents can shut down the activity of site A, while site B is still enantioselective. In this example, after each migratory insertion, the

propagating chain can swing back to the previously occupied site A through a process referred to as back-skipping. If back-skipping happens after every migratory insertion, then an *iso*-PP is produced through a “one-site” model of propagation (*vide infra*).

The most powerful characterization of PP microstructure is high field  $^{13}\text{C}$  NMR analysis. The methyl region is the most informative region. For polypropylene, NMR can give very detailed information up to the nonad level or higher, or in other words, the microstructure for 10 consecutive units. Chemical shift is very sensitive to the configuration of the adjacent methines. It is important to remember that the NMR analysis only gives the statistical average of the polymer microstructure.

The degree of isotacticity can be described as dyad, triad, pentad, nonad content (m, mm, mmmm and mmmmmmmmm respectively), etc. In general, the degree of analysis depends on how precise the study needs to be. For example, a triad level of analysis is good for basic mechanistic analysis. In this case, an ideal atactic PP has a statistical mm:mr:rr ratio of 1: 2: 1, and a value of  $4[\text{mm}][\text{rr}]/[\text{mr}]^2$  equals 1 indicates a chain-end control mechanism. For enantiomorphic site control:  $[\text{mr}] = 2 [\text{rr}]$ ; and at the pentad level,  $[\text{mmmr}] = [\text{mmrr}] = 2[\text{mrrm}]$ . Also, at the pentad level, the degree of stereoselectivity ( $\sigma$  value) under enantiomorphic site control could be extracted from the equation:  $\text{mmmm}\% = 5\sigma^4 - 10\sigma^3 + 10\sigma^2 - 5\sigma + 1$ . Most NMR studies<sup>46</sup> are carried out in 1,1,2,2-tetrachloroethane- $d_2$  at 70 °C to 135 °C at a magnetic field higher than 400 MHz. Matrix multiplication methods can be used for statistical modeling, along with molecular modeling for detailed mechanistic studies.<sup>47,48</sup> Peak fitting programs can also be used to facilitate the analysis of the NMR spectra.<sup>46</sup>

Metallocenes can produce a variety of different types of polypropylene. However, not all polypropylenes can be made by metallocenes. For example,  $\beta$ -hydride elimination and  $\beta$ -hydride transfer to monomer are major termination processes for most of the metallocene catalysts; a well-defined polypropylene with narrow polydispersity cannot be obtained. Most commercial polypropylenes from heterogeneous catalysts have very broad polydispersity, while polypropylene produced by single-site metallocenes are still relatively narrow ( $\sim 2.0$ ). In addition, PP with unique microstructures such as a well-defined stereoblock PP is still of great technical challenge.

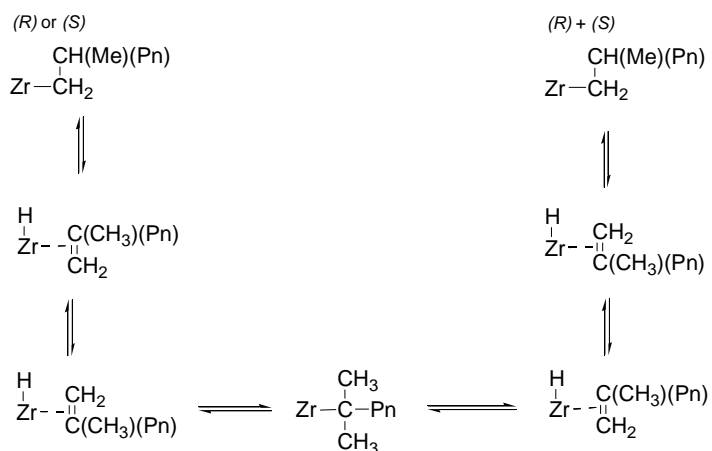
## 1.2 Dynamic Polymerization Systems

Besides the different microstructures generated by the unique symmetry of the metallocenes as described previously, other processes can also influence the microstructure. If a system is undergoing one or more of these processes competitive with propagation, we define this as a *dynamic polymerization system*. Based on the competitive processes involved, four main types of dynamic systems will be discussed here: chain end epimerization, site isomerization, oscillating metallocene and binary system.

### 1.2.1 Chain End Epimerization

For  $C_2$ -symmetric metallocenes, it is common that at low propylene concentration, the isotacticity drops.<sup>49,50</sup> This phenomenon has also been observed in non-metallocene systems.<sup>51</sup> In 1994, Busico<sup>52</sup> proposed a unimolecular chain end epimerization mechanism as the competitive process along with the bimolecular

propagating process, which scrambles the chirality of the last inserted unit. The detailed proposed mechanism is shown in Scheme 7.

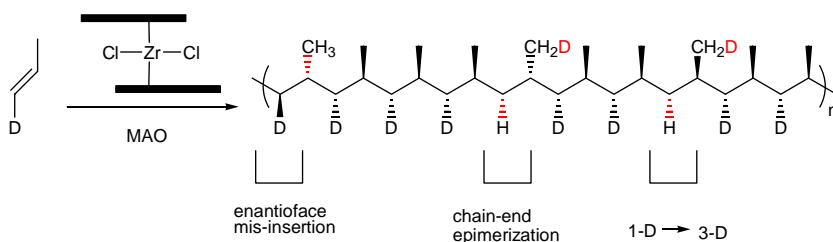


**Scheme 7. Busico chain-end epimerization mechanism, Pn = polymer chain.**

Based on Busico's mechanism, first, a zirconium hydride is generated after a typical  $\beta$ -hydride elimination of the propagated polymer chain, and the olefin chain end is still coordinated to the zirconium. The coordinated polymer chain is then in-plane rotated and 2,1 inserted again, upon which a *tertiary* center is generated. One more  $\beta$ -hydride elimination, rotation, and 1,2 primary insertion will give the opposite chirality inserted unit. This chain-end epimerization mechanism consists of two  $\beta$ -hydride eliminations, two rotations, one primary insertion and one secondary insertion.

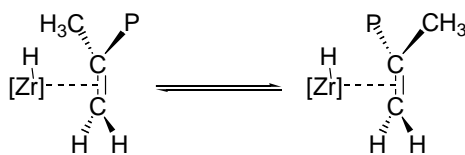
At the meantime, Brintzinger and Busico independently carried out a deuterium labeled propylene polymerization by these  $C_2$  isotactic metallocene catalysts, and interesting results were reported.<sup>53-56</sup> Without the 1-D labeled propylene, a stereo-error generated from chain-end epimerization or enantioface misinsertion is indistinguishable. A 1:1:1 ratio triplet (from the C-D coupling) in the  $^{13}\text{C}$  spectra is

observed for the deuterium labeled methyl group slightly upfield of the [mrrm] region when 1-D propylene is used. Further studies showed that the non-labeled [mrrm] pentad is independent of the monomer concentration, while deuterium labeled [mrrm] triplet changes when propylene concentration changes. This is consistent with what Busico<sup>52</sup> originally proposed.



**Scheme 8. Poly(1-D-propylene) microstructure at low propylene concentration.**

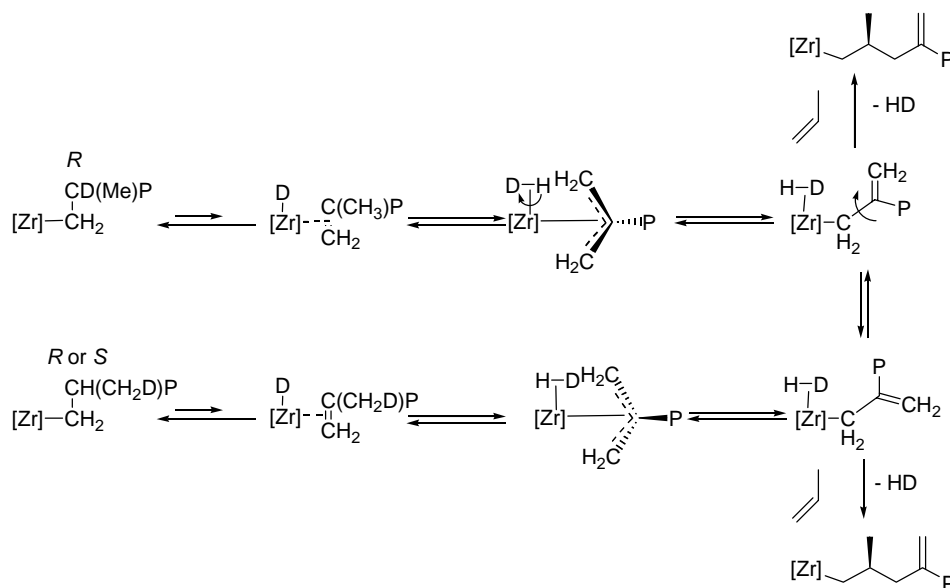
To explain the deuterium labeled (1-D to 3-D in Scheme 8.) in the methyl group with the right chiral center, a complete dissociation and re-coordination to the opposite olefin face of the disubstituted olefin is proposed by Busico. This is highly suspicious due to the large excess of monomer in the polymerization.



**Scheme 9. An enantioface dissociate-recoordination process proposed by Busico.**

In 1999, Resconi<sup>57</sup> proposed another mechanism, which includes a dihydrogen/ $\eta^3$ -allyl complex intermediate. Detailed mechanism is shown in scheme 10. This mechanism well explained the deuterium scramble in which a deuterium labeled propylene is used. A dihydrogen species generated along with an  $\eta^3$ -allyl

complex is proposed. The free rotation of allyl group is the key for the conversion of the last propagating chiral center. The free rotation of dihydrogen explains the scrambles the deuterium label. Based on the mechanism, the displacement of dihydrogen by propylene generated an internal vinylidene unsaturation and free H<sub>2</sub>, which is commonly observed at low concentration propylene condition.<sup>58,59</sup> Also, no *t*-Bu zirconium cation is involved in Resconi's mechanism.



**Scheme 10. Chain-end epimerization mechanism proposed by Resconi.**

To differentiate between these two mechanisms, a double labeled 2-D-3-<sup>13</sup>C propylene study was carried out by Bercaw and co-workers.<sup>60</sup> NMR assignments are consistent with Busico's mechanism and also provide that an allyl/dihydrogen complex does not mediate the chain end epimerization. Due to the facile  $\beta$ -hydride elimination, no model complexes have been reported for metallocenes.

In 2004, Sita and co-workers<sup>61</sup> reported a double labeled amidinate based cyclopentadienyl zirconium alkyl complex, which undergoes extremely slow  $\beta$ -

hydride elimination at  $-10\text{ }^{\circ}\text{C}$ . A double labeled isobutyl zirconium cation was incubated at  $0\text{ }^{\circ}\text{C}$  overnight, and upon isomerization, the deuterium label is always located on a  $^{13}\text{C}$ -labeled methyl position. This result is also consistent with what Busico proposed and contradicts Resconi's mechanism. Unfortunately, no tertiary alkyl zirconium species was detected.

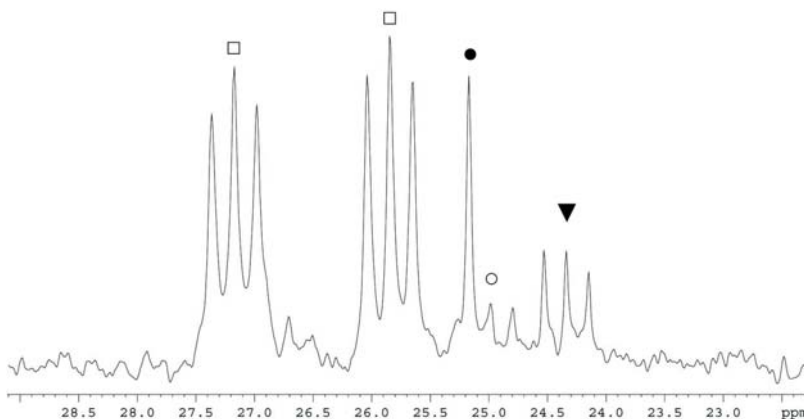


**Figure 4.**  $^{13}\text{C}$  NMR (100 MHz,  $\text{C}_6\text{D}_5\text{Cl}$ ,  $0\text{ }^{\circ}\text{C}$ ) of the shown cation after 15 h at  $0\text{ }^{\circ}\text{C}$ . The two 1:1:1 triplets (□) centered at 27.2 and 25.8 ppm correspond to diastereotopic doubly labeled methyl groups ( $^{13}\text{CH}_2\text{D}$ ) of the isobutyl moiety. The singlet at 25.2 ppm and the triplets at 25.0 and 24.3 ppm are due to singly and doubly labeled decomposition products.

Both Busico's and Resconi's mechanisms are reasonable at certain level, but neither of them is totally satisfied, while Busico's mechanism seems more reasonable. The lack of tertiary cation intermediate in literature, and the dubious dissociation/re-coordination are still an enigma.

### 1.2.2 Site-Isomerization

A metallocene with  $C_1$  symmetry can generate polypropylene with a variety of microstructures from hemiisotactic to isotactic, based on the activation energy for the

propylene coordination and the polymer chain occupation for two distinguishable sites.

For metallocenes with  $C_2$  symmetry, back-skipping is *invisible* since both sites are homotopic; while in the case of  $C_s$  symmetry, from where *syndio*-PP is produced, one back-skipping generates a unique *rmrr* sequence (c.f., misinsertion or chain-end-epimerization gives *rmmr* sequence only). This isolated *m* was observed by Ewen<sup>50</sup> and Chien<sup>62</sup> with a  $C_s$ -symmetric isopropylidene (1- $\eta^5$ -Cp)(9- $\eta^5$ -Flu)ZrCl<sub>2</sub> activated by MAO; a [rrrr] of 95%, and a [rmrr] ranged from 1 to 4% were observed, while at higher temperatures, more [rmrr] was detected.

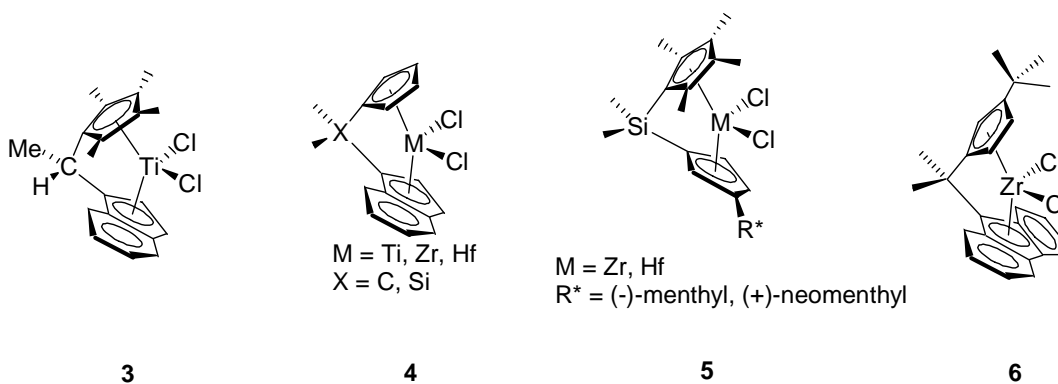


**Figure 5. Several  $C_1$ -symmetric metallocenes.**

In 1990, Chien and coworkers<sup>63</sup> reported the first intriguing  $C_1$ -symmetric titanocene **3**, by which a thermoplastic elastic polypropylene (*el*-PP) was produced upon activation by MAO. Only one diastereomer was obtained with the bridgehead methyl group anti to the indenyl ring. Polymerizations were carried out at different temperatures, upon activation by MAO. For all the samples obtained, relatively narrow (<2.0) polydispersities were observed. Dynamic mechanic analysis (DMA), thermal analysis and tensile test confirmed that the material is truly a thermoplastic

elastomer, with a recovery greater than 90% for 100% to 300% elongation. It is believed that the *el*-PP material consists of crystalline isotactic blocks and amorphous atactic blocks, randomly distributed along the linear polymer backbone. This is consistent with what Natta originally proposed for the elastic PP fraction isolated from the solid-supported polymerizations.<sup>64</sup>

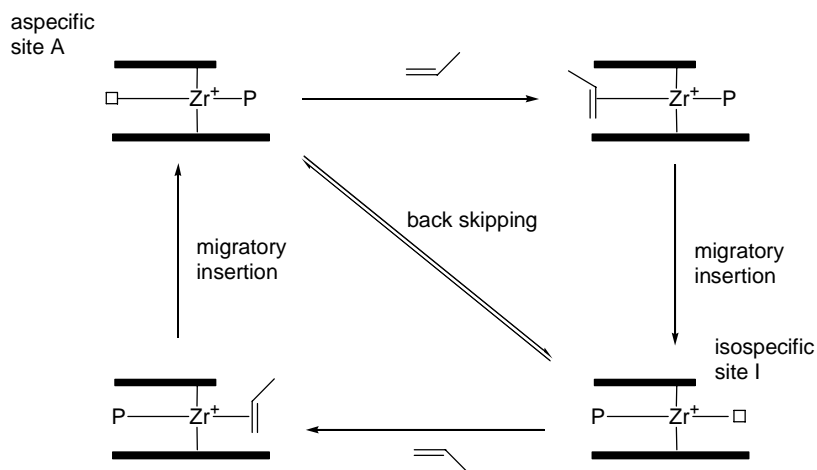
Crystal structure of a dimethyl derivative of **3** confirms the different Ti-C bond lengths of two methyl groups, where two propagating sites occupy.<sup>65</sup> A two-state switching propagation mechanism was first proposed by Chien and coworkers, with one aspecific site A and an isospecific site I.<sup>66,67</sup> An inter-conversion between the two sites occurs during the independent propagation in each site, and the site conversion happens after several propagations.

It is counterintuitive that the propagating center will remain in the same site after each propagation, since the propagation consists of olefin coordination and migratory insertion. Each insertion actually converts the active site, and for the polymer chain to stay at the same site, a back-skipping must occur after *each* insertion. The detailed mechanism is still unclear why the active center back skips every time to make isotactic block, and all of a sudden, the polymer chain stays in the isospecific site to generate an atactic blocks.

Compound **4**, which was developed by Collins,<sup>68,69</sup> has very similar structure and produces *el*-PP upon activation by MAO as well.

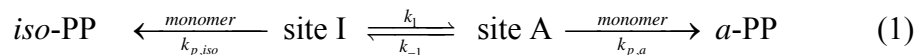
One thing worth mentioning is, for both **3** and **4**, a 2[rr]/[mr] value of 1 is obtained, which indicates that the propagation follows enantiomorphic site control during the polymerization. Collins<sup>68</sup> reported detailed statistical analysis based on

three possible models, which are 1). consecutive insertions at the isospecific site and another aspecific site; 2). random model, insertions can occur at either aspecific and isospecific sites and 3). strict alternating insertions at the two sites with the stereoselectivity of insertion at each site. Each model can fit the pentad analysis well. However, it is assumed that the microstructure of *el*-PP is rather random than proposed, and the block length of the atactic sequences is, on average, quite short.



**Scheme 11. Polymerization mechanisms for  $C_1$ -symmetric metallocenes.**

Temperature plays an important role in the microstructure of the *el*-PPs obtained. At lower temperature, **4** produces PP with higher stereoregularity ([*mmmm*] increases from 25.9% to 71.5% with the temperature change from 25 °C to -25 °C).<sup>69</sup> In contrast, the opposite behavior is observed for Chien's titanium catalyst **3**,<sup>66,70</sup> although the temperature influence is rather insignificant. The propylene produced at 0 °C or lower exhibits no crystallinity. A theoretical calculation suggests an approximate molecular structure of [(*a*-PP)<sub>16</sub>(*iso*-PP)<sub>7</sub>]<sub>100</sub>, and 7 consecutive isotactic unit is too short to be crystallized (c.f., a block length longer than 11<sup>71</sup>, 14<sup>71,72</sup> units is essential for the crystallization, as proposed by different research groups).



A simple kinetic model can be used to explain the temperature effect for these polymerizations. As shown in equation 1, for two sites, I (isospecific) and A (aspecific), a dynamic equilibrium exists competitively with monomer propagation. Since site isomerization is a unimolecular process, while propagation is bimolecular with initiator and monomer involved, adjusting the polymerization temperature or monomer concentration can be used to manipulate the microstructures of the PP, such as the isotactic block length.

Most  $C_1$ -symmetric catalyst produce isotactic<sup>73-76</sup> and hemiisotactic<sup>70,77,78</sup> polypropylenes. Chien<sup>79-82</sup> and Rieger<sup>83</sup> synthesized a series of unsymmetrical zirconocenes by changing the size of the rings, the substituents and the ansa bridges. Most of these catalysts have medium to high activity and high isotacticity, with limited *el*-PPs reported.<sup>84,85</sup> A benefit of these catalysts over  $C_2$ -symmetric metallocene is the readily accessibility, since no diastereomers need to be separated.

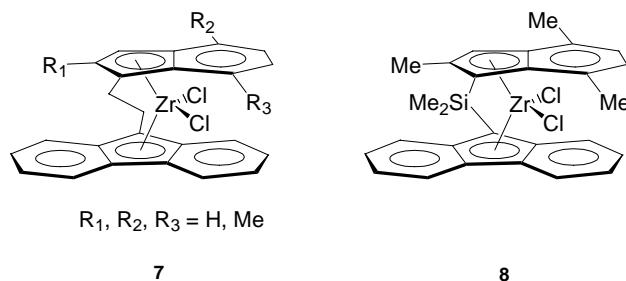


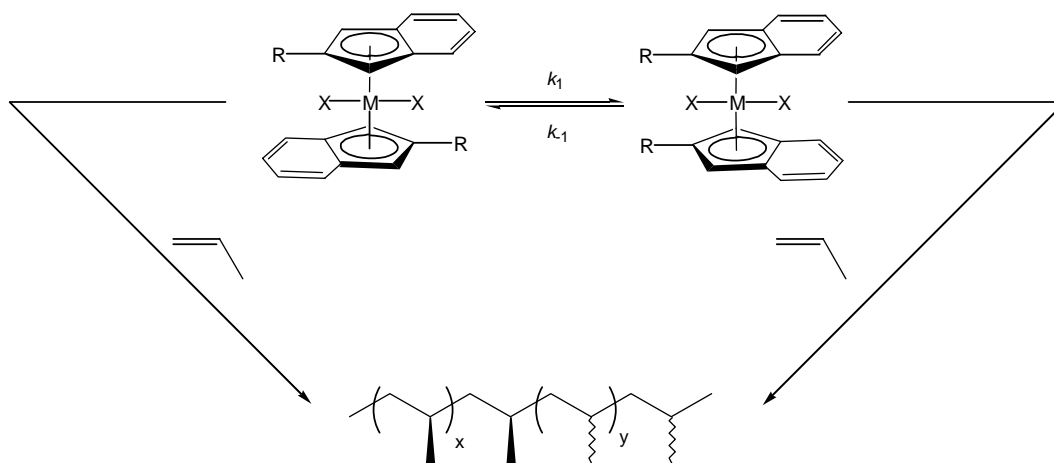
**Figure 6. Bulky ligands *ansa*-bridge  $C_1$ -symmetric catalysts designed by Chien.**

Since the development of  $TiCl_3/AlEt_3$  for propylene polymerization,  $C_s$  and  $C_1$  metallocenes produced polypropylenes with unique microstructures that the heterogeneous catalyst cannot produce. The dynamic competitive processes of back-

skipping, propagation and site-isomerization give metallocenes the potential capability to tailor design novel materials.

### 1.2.3 Oscillating Metallocene

Both Chien's and Collins' catalysts make *el*-PP. However, these catalysts do not have a wide range of variation, i.e., one catalyst typically generates a particular material. Temperature, pressure, monomer concentration and counterion effect are the only factors that can be tuned, and the influence is typically not significant enough to generate a polymer with dramatically different physical properties. In 1995, Coates and Waymouth<sup>86</sup> elegantly designed a non-bridged metallocene catalyst **9**, which has a dynamic structure that switches from *rac*-like to *meso*-like configurations.



**Scheme 12. Simplified model for oscillating metallocene catalyst.**

No *ansa*-bridge is used. A bulky substituent was placed in 2 position of the indenyl ring to restrict or slow down the rotation. And the rotation of the indenyl ring gives two minima energy states, a *rac*-like and a *meso*-like configurations, as shown in Scheme 12. Based on Ewen's rule,  $C_2$ -symmetric *rac* initiator gives *iso*-PP, and

the  $C_3$ -symmetric generates *a*-PP. A rubbery material was obtained which was believed to be a stereoblock *a*-*iso*-*el*-PP. *rac*-like and *meso*-like configurations of the pre-catalyst were both confirmed by X-ray structures.<sup>86</sup>

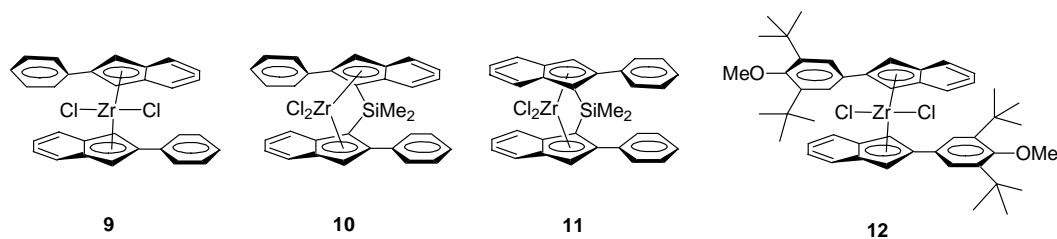


Figure 7. Oscillating metallocenes and its *ansa*-bridged counterparts.

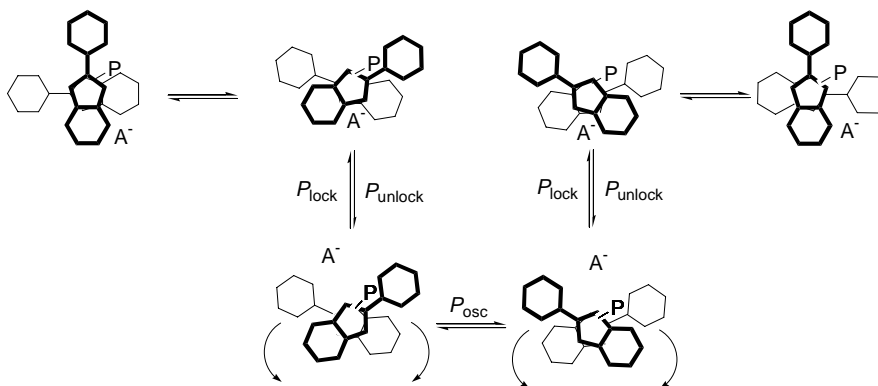
*ansa*-bridged counterparts of **9** were synthesized and polymerization carried out. For **10**, a [mmmm] of 87% was obtained and for **11**, [mmmm] of 6% was observed. All these evidences suggest that the mechanism of the polymerization follows a two site model, one stereospecific (*rac*-like) and one aspecific (*meso*-like). The rotation of the indenyl rings switches from the two configurations. Depending on the relative rates of the rotation and the propagation, different microstructures polymer could be obtained by changing the monomer concentration, pressure and polymerization temperature, thus influencing the average block length of the isotactic and atactic stereoblocks. Within the last 10 years, a variety of similar catalysts<sup>87-96</sup> have been reported with similar behavior, with different aryl substituents by many research groups.

Surprisingly, the polypropylene obtained has different fractions that can be separated by solvent extractions. The fractions include different microstructures from amorphous to highly crystalline polypropylenes with broad polydispersities. The

material certainly cannot be obtained from a single active site metallocene and it is believed that there are several active species involved in the polymerization. A surprisingly low energy barrier of the rotation was found; at 20 °C, catalyst generated from **9** has 7000 ligand rotations per second. Even a catalyst with bulkier aryl substituents, such as 3,5-di-*tert*-butylphenyl has 70 rotations at elevated temperatures, which is much faster than the monomer propagation.<sup>96</sup> This is not consistent with the oscillating mechanism proposed for the *el*-PP.

Detailed <sup>13</sup>C NMR pentad analysis of the *el*-PP generated by two oscillating metallocenes (**9** and **12**) has been carried out by Busico and co-workers.<sup>97,98</sup> For both catalysts, the polymerization is under enantiomorphic site control, and a major mmmmmmm nonad was observed. For steric hindered **12**, ligand rotation is relatively slower. A statistical model based on enantiomorphic site control fits the NMR data quite well, with a  $\sigma$  value of 0.985 and  $P_{osc} = 0.086$  ( $P_{osc}$ : probability of site inversion). An average isotactic block length of  $\langle L_{iso} \rangle = (1 - P_{osc}) / P_{osc} \approx 12$  is determined.

For the less hindered catalyst **9**, the rotation was reported 100 times faster than **12**.<sup>99</sup> At 20 °C, a non-crystalline PP was obtained with **9**/MAO at a [M] of 6.7 M. This could be well explained by the extremely fast oscillation between two propagating sites. However, a significantly mmmmm heptad (7.81% vs. 4.40% from enantiomorphic site model) indicates a more complicated mechanism. NMR analysis of this isotactic fraction suggests a PP with isotactic blocks of the same relative configuration for each block separated by very short atactic blocks.



**Scheme 13. Locked *rac* mechanism for unbridged metallocenes.**

To explain this phenomenon, a locked *rac* hypothesis was proposed, as shown in Scheme 13. A counteranion can freeze the ligand rotation, thus the catalyst will act like an *ansa*-bridged catalyst in the locked regime, where  $C_2$ -symmetric configuration (*rac*-like) is favored due to the less steric interaction. The active species keep their configuration long enough for the generation of the isotactic blocks.

Depending on the size of the two substituents, monomer concentration and the type of the counteranion, the percentage of the locked *rac*-like regime varies. For most cases, the locked regime is typically insignificant. A bulkier substituent probably prevents the formation of the locked *rac*-like configuration.

After 10 years extensive research, the full mechanism of the oscillating metallocene is still unclear, no one has demonstrated full control over the polypropylene microstructure, physical properties. One catalyst generates one polymer with limited control over the tacticity, molecular weight and block lengths.

#### 1.2.4 Binary System

Dynamic exchange also exists in binary systems. Theoretically, all metallocene activated by MAO have dynamic chain transfer between zirconium and aluminum. Typically, these chain transfers are not reversible, thus low molecular weight polymer chain is generated. A few examples have been reported recently for binary metallocene systems for the preparation of unique microstructure such as isotactic-atactic stereoblocks.

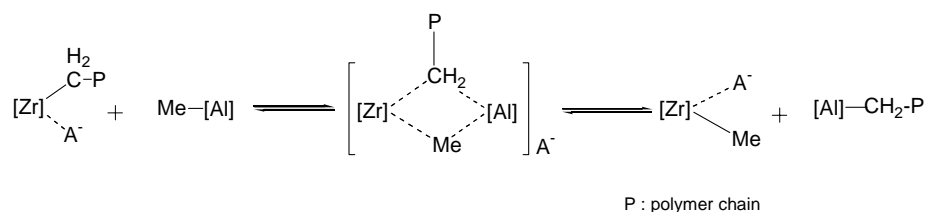
In 1997,<sup>100,101</sup> Chien and co-workers reported the first binary metallocene example with an isospecific  $C_2$ -symmetric catalyst combined with a nonspecific catalyst, *rac*-ethylene bis(1- $\eta^5$ -indenyl)zirconium dichloride or *rac*-dimethylsilylene bis(1- $\eta^5$ -indenyl)zirconium dichloride as isospecific catalyst precursors and ethylene bis(9- $\eta^5$ -fluorenyl)zirconium dichloride as an aspecific precursor. The combination produced a mixture of polymers, from which an isotactic-atactic stereoblock fraction was isolated. Besides the stereoblock, isotactic and atactic homo-polymer were also isolated. The stereoblock polypropylene was confirmed by solvent extraction and NMR analysis. Later, an isotactic and syndiotactic stereoblock was polymerized in the same manner with a syndioselective and an isoselective catalyst, while activated by  $[\text{Ph}_3\text{C}][\text{B}(\text{C}_6\text{F}_5)_4]$  and triisobutylaluminum.

Mechanistic hypotheses were proposed with three possibilities: 1). a polymer chain undergoes  $\beta$ -hydride elimination and reinsertion into another propagating species; 2) a direct chain transfer between two different propagating species; 3).  $\text{AlR}_3$  acts as a chain transfer reagent, which transfers a polymer chain from one propagating species to another. For the first one, with a large excess of monomer, the chances of

the eliminated chain to coordinate to another propagating center is extremely low, while a direct chain transfer, which involves a di-cationic species, is energetically not favored in the second case.

The stereoblock generated also shows good elastomeric properties. For the *a-iso-sb*-PP, a recovery better than 98% was observed after 500% elongation. The property of the *sb*-PP can be tuned by the mole ratio of the catalyst precursors.

Rieger<sup>84</sup> recently reported a reversible chain transfer to MAO from a Zr(IV) metallocene species.



**Scheme 14. Polymer chain transfer between Zr and Al species.**

Detailed study of the chain transfer via aluminum co-catalyst was reported by Brintzinger.<sup>102</sup> For different zirconocene catalysts, dramatically different behaviors were observed. For highly substituted metallocenes, an alkyl-polymeryl exchange is thermodynamically favored, since steric hindrance is released from a sterically encumbered zirconium to a “naked” aluminum center. For less hindered metallocenes, though kinetically the formation of the 4-centered heterocyclobutane is faster, the dissociation could be thermodynamically unfavorable. Thus, the combination of different zirconocenes will not necessarily give stereoblock polymers.

Also, Sita and coworkers<sup>103</sup> reported a methyl-polymeryl exchange between two different amidinate based zirconium catalysts. No polymeryl-polymeryl exchange

was detected. An *isotactic-atactic* polyolefin was synthesized via polymeryl methyl exchange.

All these dynamic systems generate unique PP microstructures. For each system, due to the competitive processes involved, by controlling the relative rate for these processes, a wide variety of polymers can be obtained. In addition, there are other dynamic polymerization systems that unique microstructure can be obtained, which will not be discussed in this dissertation.

### **1.3 Living Ziegler-Natta Polymerization and Post-Metallocene Polymerization**

#### **1.3.1 Living Polymerization**

While different microstructures could be easily achieved by large collection of metallocene catalysts, a well-defined block polyolefin was still out of reach.  $\beta$ -hydride elimination and  $\beta$ -hydride transfer to monomer are the major terminations for metallocene polymerizations. When  $\beta$ -hydride elimination is involved, a vinyl end group can be detected by NMR analysis for the terminated polymer chains.

Generally speaking, a living polymerization is a system that has no or negligible termination and chain transfer relative to propagation.<sup>104</sup> Every active center retains its activity, and as long as monomer is present, the active center continues to propagate. As a result, the number of active centers remains constant throughout the polymerization. Living polymerization was first reported in anionic polymerization.<sup>105-107</sup> Now it is well documented in radical polymerization<sup>108</sup> and other types of polymerizations systems.<sup>109-111</sup> Typically, a living system has the following characteristics:

- 1) Narrow polydispersity of the polymer obtained, i.e.  $PDI (M_w/M_n) (<1.1)$ .
- 2) Very fast initiation,  $R_i \gg R_p$ .
- 3) Polymerization is able to go to full conversion (100%).
- 4) Molecular weight increases linearly with conversion.
- 5) Active centers are stable in the absence of monomer.
- 6) Multiblock copolymers can be made by sequential addition of monomer.

Using living polymerization techniques, a telechelic<sup>112</sup> polymer can be synthesized by quenching the living polymer chain with desired functional groups, and the functional groups can be used for further polymer modification. Different microstructure polymers such as block copolymers, comb polymers and star polymers can be obtained.

It was not until the late 1990s that different research groups independently discovered post-metallocene catalysts,<sup>113</sup> and the Ziegler-Natta living polymerization of olefins by group 4 metals was made possible.

### **1.3.2 Group 4 Post-Metallocene Initiators for Living Ziegler-Natta**

#### **Polymerizations**

The first living Ziegler-Natta polyolefin polymerization was reported by Doi in 1979. The catalyst,  $V(acac)_3$ , upon activation by  $Et_2AlCl$ , is an efficient initiator for *syndio*-PP at  $-78\text{ }^\circ\text{C}$ .<sup>114</sup> It was not until late 1990's that few systems have been reported to be active towards Ziegler-Natta  $\alpha$ -olefin polymerization in living fashion based on group 4 metals. Among these are the systems independently developed by

McConville,<sup>115</sup> Schrock,<sup>116-121</sup> Fujita<sup>122</sup> / Coates,<sup>123</sup>, Sita.<sup>124-129</sup> Ikeda,<sup>130-132</sup> and Kol.<sup>133</sup> Several late transition metal complexes for living Ziegler-Natta polymerization of  $\alpha$ -olefins have been developed recently, and will not be discussed here.<sup>134</sup>

In 1996, McConville and co-workers<sup>135,136</sup> reported a diamido titanium complex **13**, which is an efficient initiator for the polymerization of higher  $\alpha$ -olefins with high activity after activation by  $B(C_6F_5)_3$ . More importantly, **13a** polymerizes 1-hexene in a living fashion at room temperature. Polar solvent, such as methylene chloride dramatically increases the polymerization activity, presumably due to the formation of loose ion-pair. Subsequent interesting results were reported by Uozumi and co-workers,<sup>137,138</sup> who demonstrated that **13b** produces highly *iso*-PP (mmmm% up to 83%) with PDI around 3.0 in the presence of cyclohexene, upon activation by  $Al(i-Bu)_3/Ph_3C[B(C_6F_5)_4]$ . In this system, polymerization undergoes primary insertion with enantiomorphic site control, but the catalyst is not  $C_2$ -symmetric, apparently in violation of the Ewen's symmetry rules. The coordination of cyclohexene, or a second propylene, to the active cationic site seems to be the reason for the high stereoselectivity. Furthermore, compound **13b**, when activated by dried mMAO, is active toward propylene polymerization in a living/controlled manner with narrow polydispersities (PDI = 1.1 – 1.4).<sup>139</sup>

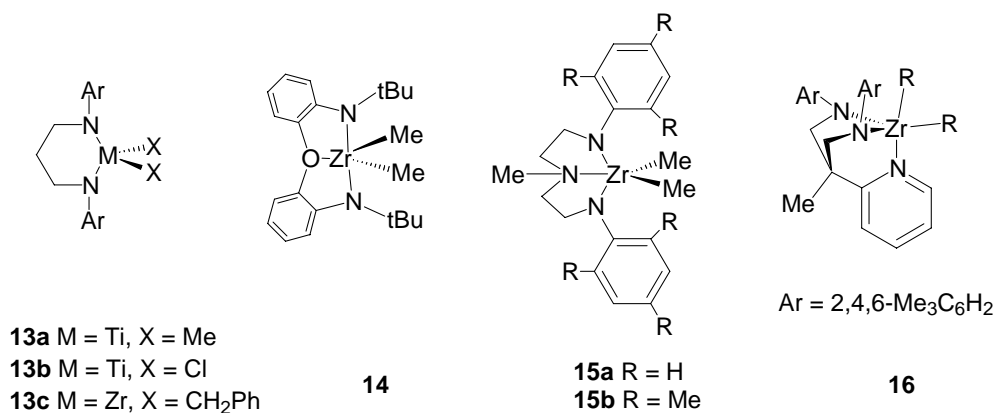


**Figure 8. diamido coordinated catalysts.**

In 1997, Schrock and co-workers reported another series of tridentate diamido group 4 complexes with ancillary ligand.<sup>116,140</sup> Three representatives, **14** - **16**, are shown in Figure 8, commonly referred to as NON and NNN catalysts. Besides two amido ligands, all of them have an extra coordination. Upon activation by borates, all these pre-catalysts are capable of 1-hexene polymerization, producing atactic polymers with narrow polydispersity.<sup>116</sup> Compound **15a** shows  $\beta$ -hydride elimination as the major termination reaction during 1-hexene polymerization, while polymerization by **15b** shows negligible  $\beta$ -hydride elimination at sub-ambient temperature (0 – 10 °C). Living poly(1-hexene) was reported when diamidopyridine complex **16** is used as the pre-catalyst, activated by Ph<sub>3</sub>C[B(C<sub>6</sub>F<sub>5</sub>)<sub>4</sub>]. An initiation effect was observed for complex **16**. When L<sub>n</sub>ZrMe<sub>2</sub> is used as the pre-catalyst, no living property is obtained; problem was solved by using L<sub>n</sub>Zr(*i*-Bu)<sub>2</sub> as the pre-catalyst. Also, the hafnium derivative of **16** is also proven to be an active pre-catalyst towards living polymerization of 1-hexene.<sup>141</sup> No ethylene or propylene activity has been reported for these catalysts.

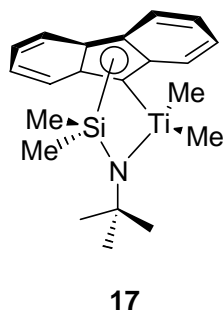
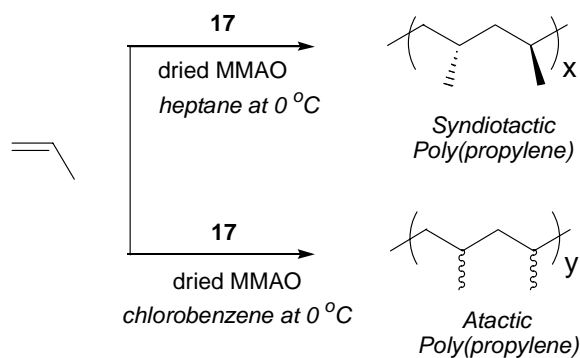


**Figure 9. Titanium CGC catalyst designed by Ikeda (17).**

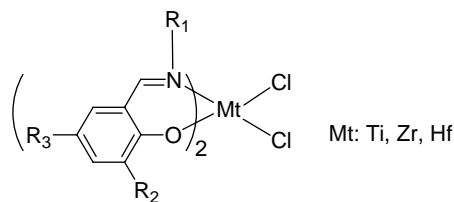
In 1998, Ikeda and co-workers reported a living polymerization of propylene and 1-hexene with **17** serving as the pre-catalyst at the presence of  $\text{Al}(\text{Oct})_3$ , which is activated by  $\text{B}(\text{C}_6\text{F}_5)_3$  at  $-50\text{ }^\circ\text{C}$ .<sup>130</sup>  $\text{Al}(\text{Oct})_3$  greatly decreased any chain transfer side reactions. The propagation undergoes primary insertion exclusively, and *syndio*-rich PP or poly(1-hexene) (PH) was obtained. Surprisingly, only half of the titanium centers are active. In 2004, it was reported<sup>132</sup> that by changing the polymerization solvent from heptane to chlorobenzene at  $0\text{ }^\circ\text{C}$ , *a*-PP is obtained using **17** as the pre-catalyst, upon activation with dried modified MAO (mMAO), in which free  $\text{AlMe}_3$  was greatly reduced. Since polymerizations in both solvents are living, by changing the polymerization solvents, a well-defined *syndio*-*a*-PP stereoblock with relatively narrow polydispersity (PDI = 1.27) was first synthesized. No physical properties of this material have been reported yet.



**Scheme 15. Influence of solvent to the tacticity of polymer by Ikeda's catalyst.**

In 2000, Sita and co-workers<sup>125,142</sup> discovered an amidinate based group 4 initiator for living  $\alpha$ -olefin polymerization. At  $-10$  °C, activated by co-catalyst  $[\text{PhNHMe}_2][\text{B}(\text{C}_6\text{F}_5)_4]$  (**18**), a  $C_1$ -symmetric pre-catalyst  $(\eta^5\text{-C}_5\text{Me}_5)\text{ZrMe}_2[\text{N}(t\text{-Bu})\text{C}(\text{Me})\text{N}(\text{Et})]$  (**19**) is efficient for the polymerization of 1-hexene in a living and isospecific fashion. This is the very first living and stereospecific  $\alpha$ -olefin Ziegler-Natta polymerization system. A  $C_s$ -symmetric pre-catalyst  $(\eta^5\text{-C}_5\text{Me}_5)\text{ZrMe}_2[\text{N}(i\text{-Pr})\text{C}(\text{Me})\text{N}(i\text{-Pr})]$  (**20**) produces atactic polyolefins, upon activation of **18**. Also, a dramatic increase of the activity was observed using  $(\eta^5\text{-C}_5\text{H}_5)\text{ZrMe}_2[\text{N}(i\text{-Pr})\text{C}(\text{Me})\text{N}(i\text{-Pr})]$  (**21**) as the pre-catalyst, a derivative of **19** with Cp ligand (*vide infra*).

A series of bis(phenoxyimine) group 4 metal complexes (**22**), referred to FI<sup>143</sup> catalyst, were designed for Ziegler-Natta polymerization by Fujita and co-workers in Mitsui Chemical Inc.<sup>42</sup> It's general formula is shown in Figure 10.

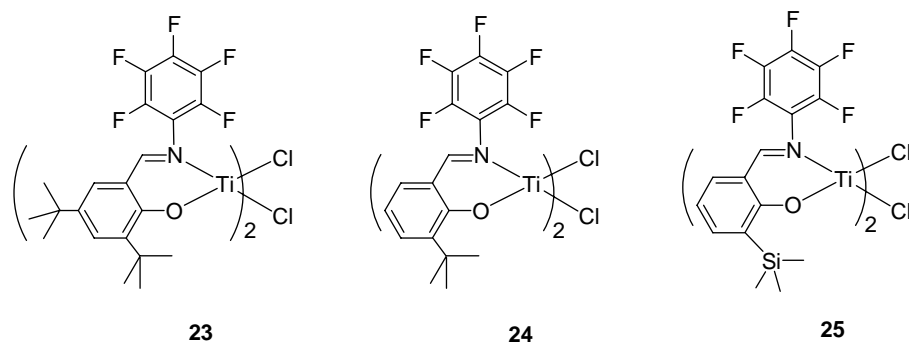


22

**Figure 10. General formula of FI catalyst.**

A wide collection of bis(phenoxyimine) complexes are efficient pre-catalysts for the polymerizations of ethylene,<sup>144,145</sup> propylene<sup>146,147</sup> and copolymerization of norbornene,<sup>148</sup> or higher  $\alpha$ -olefins<sup>149</sup> with ethylene, upon activation by MAO or borate co-catalysts.

The polymerization of propylene of these bis(phenoxyimine) catalysts is rather intriguing. Titanium derivatives typically produce *syndio*-rich PP via secondary insertion,<sup>147</sup> while zirconium and hafnium derivatives produce atactic to slightly syndiotactic PP.<sup>150,151</sup> Several titanium derivatives with sterically encumbered R<sub>1</sub> group were able to conduct quasi-living to living polymerizations via secondary insertion.<sup>146</sup> Propylene polymerizations by group 4 transition metal initiators via secondary insertion is highly unusual, while a hypothesis has been proposed by Cavallo and co-workers that a fluxional octahedral chiral site is the origin of the syndioselectivity.<sup>152</sup> The stereochemistry of the last inserted propylene unit influences the relative configuration of the fluxional octahedral site, which in turn dictates the enantiofacial selectivity of the incoming propylene. Research by Zambelli<sup>153</sup> and Fujita<sup>147</sup> uncovered that primary insertion is favored in the initiation steps for propylene polymerization, and then secondary insertion dominates in the propagation.



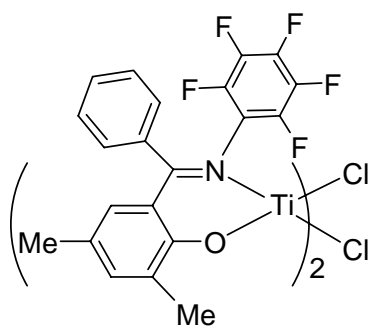
In 2001, Coates reported a fluorinated bis(phenoxyimine) titanium complexes **23**, which is an efficient initiator for the polymerization of living *syndio*-PP, activated by MAO.<sup>154</sup> Subsequent report by Fujita depicted that a similar complex **24** is also an efficient pre-catalyst towards the living *syndio*-PP polymerization, and **24** is found to be 10 times more active than its non-fluorinated derivative, providing highly syndiotactic PP with rrrr of 0.96 and  $T_m$  of 148 °C.<sup>146</sup> Upon activation by MAO, a trimethylsilyl substituted FI complex **25** is also a living pre-catalyst for *syndio*-PP polymerization, and a *syndio*-PP material with  $T_m$  of 156 °C was obtained.<sup>155</sup>

Two types of co-catalysts were used to activate these FI pre-catalysts, MAO and  $\text{Al}(i\text{-Bu})_3/[\text{Ph}_3\text{C}][\text{B}(\text{C}_6\text{F}_5)_4]$  (**26**). It is believed that a similar putative mono-cationic active species is generated as typical metallocenes. The free  $\text{AlMe}_3$  in MAO tends to act as a reducing agent to form less or non-reactive centers at lower oxidation states, especially for titanium. When free  $\text{AlMe}_3$  is removed in MAO, higher activity was observed. If  $\text{Al}(i\text{-Bu})_3/26$  is used as co-catalysts, dramatically different polymerization behavior is observed, producing PPs with higher  $M_n$  and narrower regioselectivity.<sup>42</sup>

By changing  $R_1$ ,  $R_2$  and  $R_3$ , fine-tuning of the initiator greatly influences the polymerization activity and its stereo- and regio-selectivity. A bulkier  $R_1$  tends to

afford a polymer with higher molecular weight. The non-bonding steric interaction between R<sub>1</sub> and the metal center narrowed the active site pocket, thus discouraging a potential 6-membered ring transition state for β-hydride transfer to monomer. This side reaction is competing with the four-membered ring transition state, which propagation occurs. The bulkiness of R<sub>2</sub> also affects polymerization activity, comonomer incorporation ability and the stereoregularity. A FI catalyst bearing a larger R<sub>2</sub> group usually has lower α-olefin incorporation with ethylene. Also, R<sub>2</sub> influences the stereoregularity in syndioselective propylene polymerization. Since R<sub>3</sub> is relatively far away from the metal center, the influence is not significant.<sup>42</sup>

In 2004, Fujita reported a zirconium and hafnium FI catalysts with extremely high isoselectivity, *iso*-PP with mmmm% of 0.97 and melting temperature as high as 165.1 °C is obtained.<sup>156</sup> The *iso*-PP obtained has broad polydispersity (PDI = 2.99), though. This is a catalyst with R<sub>1</sub> = cyclohexyl, R<sub>2</sub> = adamantyl and R<sub>3</sub> = methyl. It was reported that the propagation goes via *primary* insertion; the fluxional inversion of the chirality is blocked by the bulky adamantyl group.



**27**

**Figure 11. Modified FI pre-catalyst for living *iso*-PP polymerization developed by Coates.**

Late 2004, Coates<sup>43</sup> published a paper regarding to the *iso*-PP prepared by bis(phenoxyimine) catalyst **27**, an extra phenol substituent adjacent to the N was employed. When activated by MAO, **27** is an active pre-catalyst for the living *iso*-PP polymerization at  $-20\text{ }^{\circ}\text{C}$ . Narrow polydispersity ( $\text{PDI} < 1.17$ ) was reported for the PP obtained. The *iso*-PP has a  $T_m$  of  $96.4\text{ }^{\circ}\text{C}$ . A  $\text{mmmr}:\text{mmrr}:\text{mrrm} = 2:2:1$  indicates the enantiomorphic site control of the polymerization, while a  $\sigma$  value of 91% is obtained from the pentad analysis. Less than 5% head-to-head or tail-to-tail misinsertion was detected for the *iso*-PP obtained. No termination or chain-transfer side reaction was detected for the *iso*-PP obtained. No termination or chain-transfer side reaction was detected as the system is living. A *iso*-PP-*co*-(PP-*random*-PE) diblock is prepared by sequential addition of the monomer. This is the first group 4 metal catalyst that polymerizes *iso*-PP in a living and isoselective fashion. At higher polymerization temperature, lower enantiofacial selectivity is observed along with a lower  $T_m$  for the material.

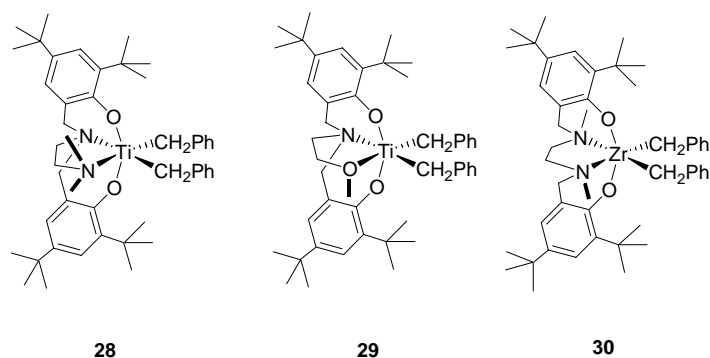


**Figure 12.** Amine bis(phenoxy) catalysts for living polymerizations.

In late 2000, Kol group reported a group 4 living  $\alpha$ -olefin Ziegler-Natta catalytic system based on amine bis(phenoxy) ligand, commonly referred to as ONDO (D: extra donor) ligand.<sup>157</sup> Typical complexes, **28** – **30**, are shown in Figure 12.

Activated by  $B(C_6F_5)_3$  (**31**) at room temperature, **28** is an active catalyst for the living polymerization of 1-hexene ( $M_n = 14\ 000$ , and PDI = 1.18). Upon activation by  $B(C_6F_5)_3$ , a  $C_s$ -symmetric pre-catalyst **29** proved to be living for an extended period of time, and the synthesis of PH-*b-co*-PO with narrow polydispersity (1.2) was possible.<sup>158,159</sup>

The presence of the extra donor arm suppresses the  $\beta$ -hydride elimination side reactions. Later, an auxiliary THF ligand was connected to the amino arm, as shown in Figure 13. With this pendant donor, the titanium complex shows extraordinary livingness up to 6 days at ambient temperature for 1-hexene polymerization, upon activation of **31**.<sup>160</sup> By changing the THF donor to furan, a 10 fold increase in activity is obtained for the titanium derivative, with the increase of termination rate as well.<sup>161</sup>

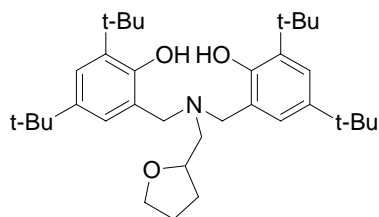


**Figure 13.** The amine bis(phenolate) THF ligand.

A  $C_2$ -symmetric complex **30** was proven to be active towards living 1-hexene polymerization at room temperature, after activated by **31**. More importantly, high isoselectivity of the initiator was confirmed by NMR analysis of the *iso*-PH obtained (>95%).

For a common metallocene, such as  $Et(Ind)_2ZrCl_2$ , neutral initiator has an electron count of 16. For most of the post-metallocene initiators, lower electron counts are observed. A summary is listed in Table 1. McConville's system has an electron

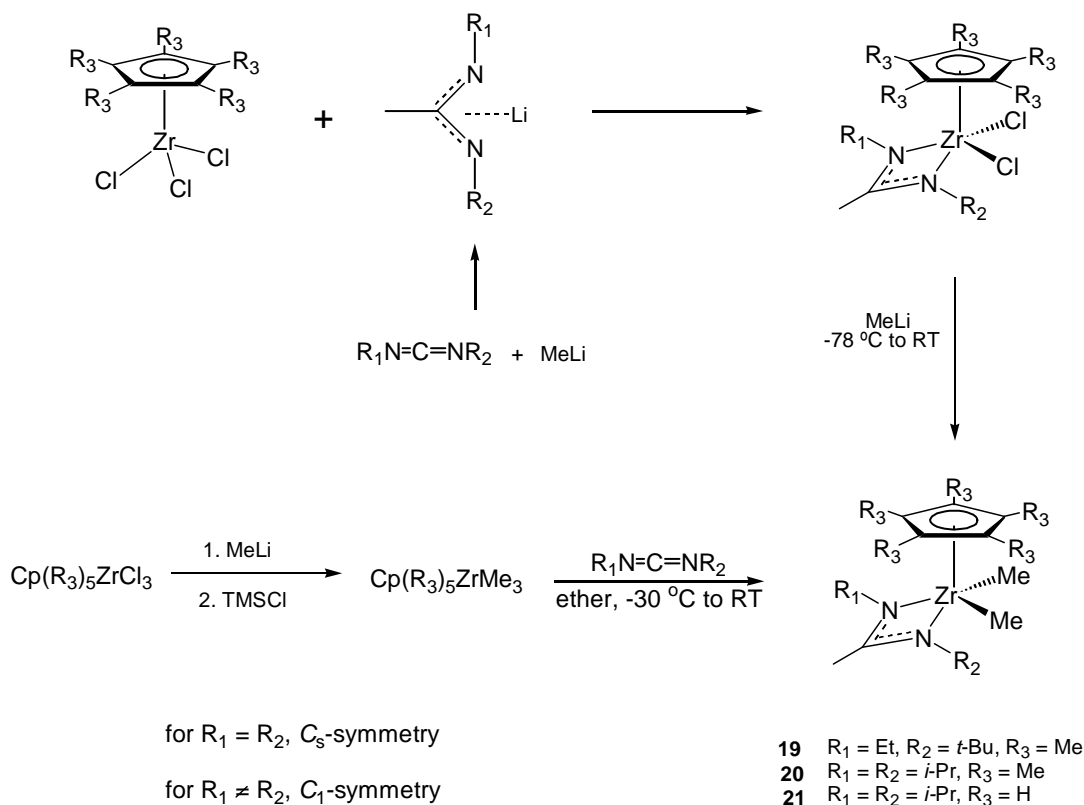
count as low as 8. This could be part of the reason for the unusual polymerization properties for the post-metallocene initiators.<sup>154</sup>

**Table 1. Typical electron count for metallocene and post-metallocene catalysts.**

<b>Neutral initiator</b>	<b>Electron count</b>
Et(Ind) <sub>2</sub> ZrMe <sub>2</sub>	16
McConville	8
Schrock NNN, NON	10
CGC Ikeda	12
Sita amidinate	14
Fujita/Coates FI	10-12
Kol	10-12

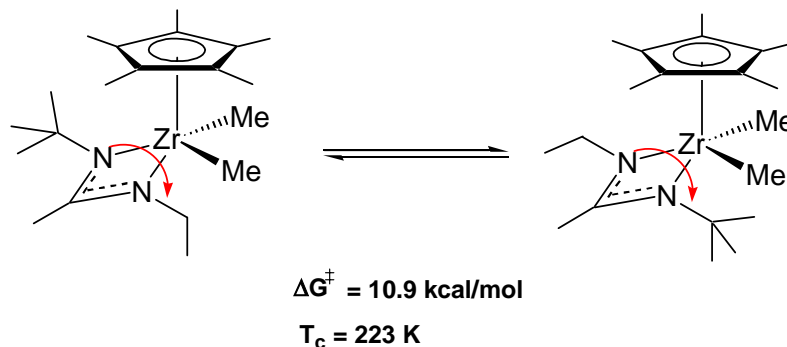
#### **1.4 Sita System: More Detailed Picture**

In Sita group, a novel Ziegler-Natta zirconium amidinate based pre-catalyst has been reported.<sup>125</sup> Activated by **18** or **26** in chlorobenzene at -10 °C, a C<sub>1</sub>-symmetric pre-catalyst **19** produced poly(1-hexene) in living fashion. In addition, this is the very first catalytic system that polymerizes  $\alpha$ -olefin both isospecific and in living fashion. A variety of  $\alpha$ -olefins have been polymerized, such as 1-pentene, 1-octene and higher olefins. The catalyst polymerizes  $\alpha,\omega$ -nonconjugated dienes as well; 1,6-hexadiene can be polymerized to form poly(methylene cyclopentane) (PMCP). Due to its living feature of the catalyst, a PH-*co-b*-PMCP diblock was successfully synthesized, while the diblock shows unique properties, such as microphase separation.<sup>124</sup>



**Scheme 16. General synthetic routes for amidinate based catalysts.**

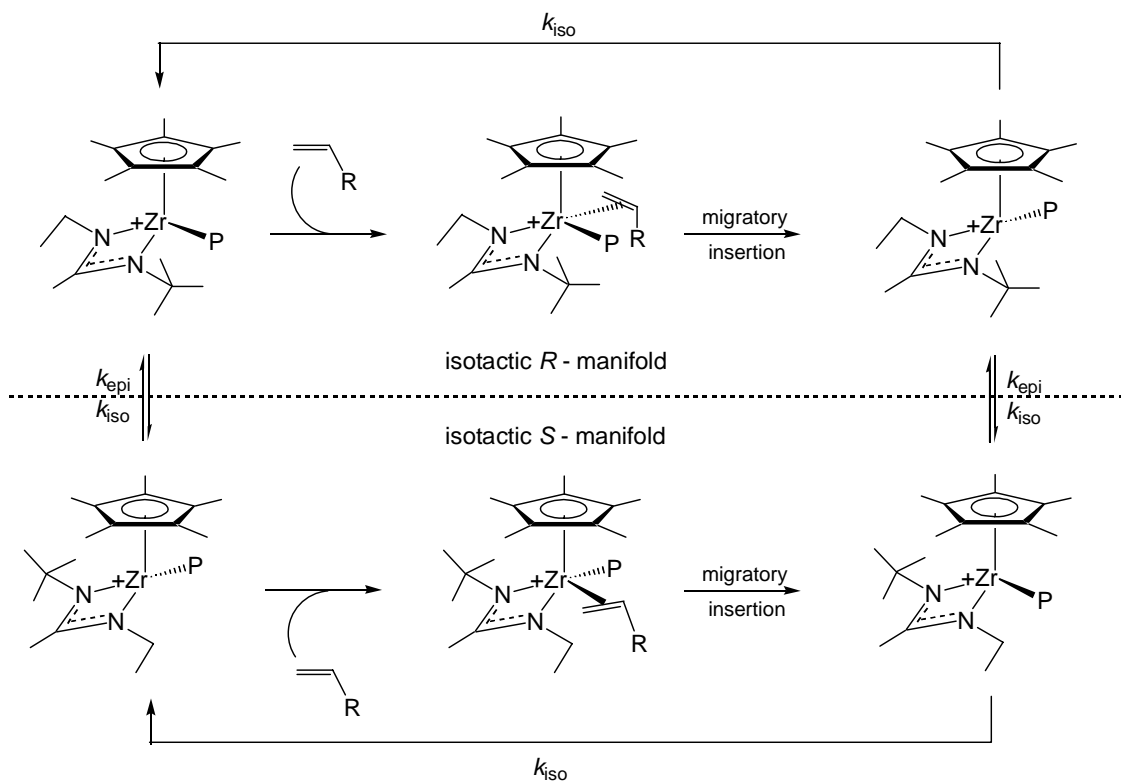
Also, a Cp derivative  $C_5$ -symmetric  $(\eta^5\text{-C}_5\text{H}_5)\text{ZrMe}_2[\text{N}(i\text{-Pr})\text{C}(\text{Me})\text{N}(i\text{-Pr})]$  (**21**) pre-catalyst polymerizes bulky monomers such as vinyl cyclohexane (VCH) in a living fashion, upon activation by **18**. A wide range of catalysts can be made via one-pot-two-step synthesis from readily available  $(\eta^5\text{-C}_5\text{Me}_5)\text{ZrCl}_3$  and carbodiimides with high yields as shown in Scheme 16. In addition, the catalyst can be obtained by salt elimination, followed by methylation, as shown in the top route of Scheme 16.



**Scheme 17. Configurational instability of the neutral pre-catalyst.**

The polyolefins produced by  $C_1$ -symmetric catalyst are isotactic. For 1-hexene, the first initiation step has an enantiofacial selectivity higher than 95%, and after the initiation, the insertion is *stereospecific* and no misinsertion was observed.<sup>162</sup>

The configurational instability of the zirconium amidinate complexes was well documented, as shown in Scheme 17, while the cationic zirconium amidinate is configurationally stable. For  $C_2$ -symmetric catalyst **19**, upon demethylation by **18**, two enantiomers are generated, referring to as R manifold and S manifold. Both manifolds produce isotactic polymer chain at the present of monomer at  $-10^\circ\text{C}$ . It is believed that the polymerization was carried out via a one-site model, as shown in Scheme 18. After *each* migratory insertion, the polymer chain swings back to the *t*-Bu side. The site isomerization is much faster than the propagation, which is also much faster than any chain transfer to monomer or termination ( $R_{\text{iso}} \gg R_p \gg R_{\text{epi}}, R_t$ ). No  $\beta$ -hydride elimination was detected by NMR analysis of the polymers obtained. Narrow polydispersity and expected molecular weight were obtained for all the polymerizations. Also, molecular weight increases linearly proportional to the consumption of the monomer. In the case of  $R_1 = R_2$ , a  $C_s$  symmetry catalyst **20** also polymerizes 1-hexene in a living fashion, but atactic polyolefins are generated.



**Scheme 18. The origin of stereospecificity of amidinate based zirconium initiator.**

Another unique property of this cyclopentadienyl zirconium amidinate complex is the extreme stability of its alkyl zirconium cations; no  $\beta$ -hydride elimination is observed at  $-10\text{ }^{\circ}\text{C}$ , while for most of the metallocenes cations,  $\beta$ -hydride elimination is a major side reaction. Different alkyl zirconium complexes were synthesized with a variety of ligand sets as mechanistic models for the polymerization.<sup>163</sup>

## Chapter 2 Methyl Group Degenerative Transfer Ziegler-Natta Polymerization

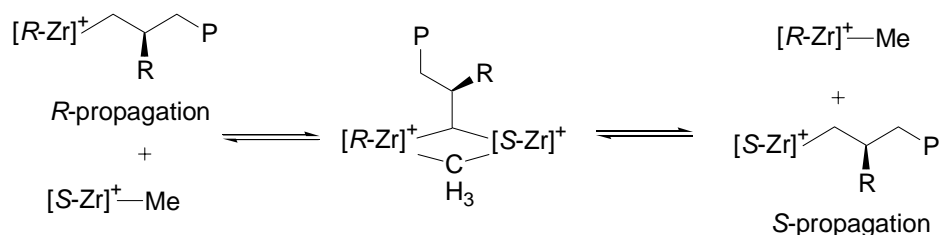
### MeDeT<sup>164</sup>

#### 2.1 Background

As mentioned in chapter 1, the pentamethylcyclopentadienyl zirconium amidinate complex,  $(\eta^5\text{-C}_5\text{Me}_5)\text{ZrMe}_2[\text{N}(t\text{-Bu})\text{C}(\text{Me})\text{N}(\text{Et})]$  (**19**), is an effective pre-catalyst for the stereospecific living Ziegler-Natta polymerization<sup>165</sup> of 1-hexene when activated by stoichiometric amount of the co-catalyst,  $[\text{PhNHMe}_2][\text{B}(\text{C}_6\text{F}_5)_4]$  (**18**).

It is also observed that cation  $\{(\eta^5\text{-C}_5\text{Me}_5)\text{ZrMe}[\text{N}(t\text{-Bu})\text{C}(\text{Me})\text{NEt}]\} [\text{B}(\text{C}_6\text{F}_5)_4]$  (**32**) exists as a dimeric di-cation with bridging methyl groups in the solid state.<sup>166</sup> As shown in Scheme 19, in solution, rapid methyl, polymeryl group exchange occurs between a living polymer derived from **32** and either **32** itself, or structurally related cationic initiators.<sup>103</sup> No polymer, polymer chain exchange was observed in this system though.

Since the four-membered intermediate in Scheme 19 is di-cationic, a mono-cationic derivative should be easier to form due to less repulsion between two zirconium species. Question rises that whether the formation of mono-cationic methyl-bridged intermediate is facile or not.



**Scheme 19. Methyl, polymeryl groups exchange between cationic species**

## 2.2 Degenerative Transfer Ziegler-Natta Polymerization

When a substoichiometric amount of **18** was used to activate the pre-catalyst **19**, a mixture of cationic initiator **32** and neutral pre-catalyst **19** were generated. Upon addition of 200 equivalents of 1-hexene, PH with narrow polydispersity was obtained at  $-10\text{ }^{\circ}\text{C}$  for 4 h. By keeping **18** and monomer concentration as constants, the amount of **19** (1 to 4 equivalents compared to **18**) was varied and polymerizations were carried out. As shown in Figure 15, the weight average molecular weight  $M_w$  is inversely proportional to the total zirconium concentration, instead of only those zirconium centers been activated by **18**. This suggests that all the zirconium centers, whether initially activated or not, are identical at the time scale of monomer propagation. Further more, whatever the ratio of **19**:**18** is, polymers with very narrow polydispersities ( $<1.07$ ) were obtained, which indicates each polymerization is living. More importantly, as shown in Figure 14, atactic polymer microstructure is confirmed by NMR analysis of the polymers obtained, and no olefin end group was detected. As shown in Fig. 14 (top), NMR spectrum of the polymer obtained from the full activation shows six sharp singlets for *iso*-PH, while for half activation polymerization, a broad peak around 33.0 to 35.0 ppm is observed. This region

represents C3 carbon for the 1-hexene units, which shows significant influence by different relative configuration of the C2 stereocenters.

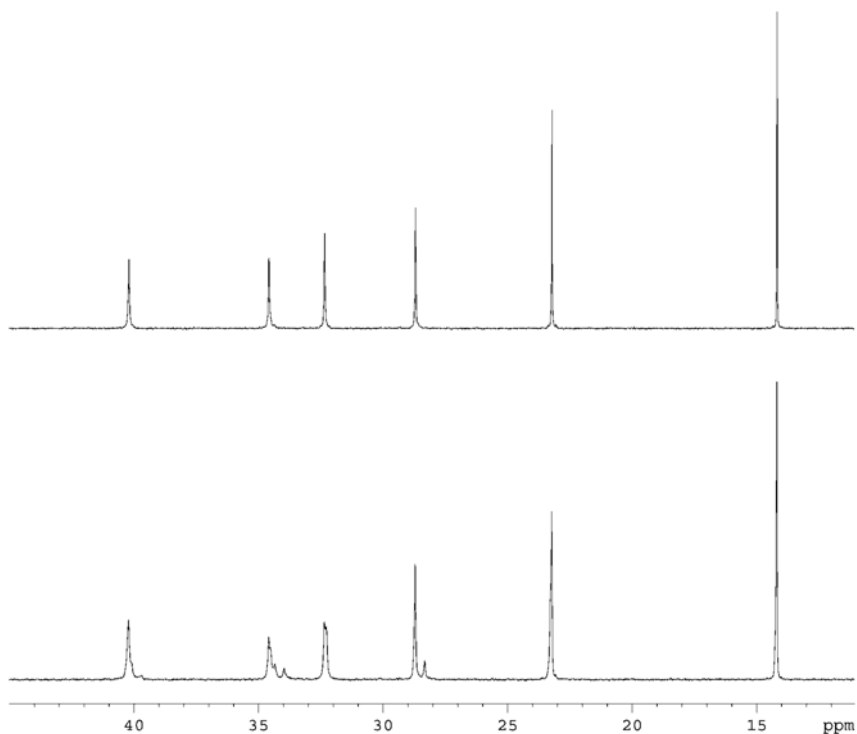


**Figure 14.**  $^{13}\text{C}$   $\{^1\text{H}\}$  NMR (100 MHz,  $\text{CDCl}_3$ , 25 °C) of PH obtained from pre-catalyst 19, a), stoichiometric activation (up), *iso*-PH and b), half activation (bottom) with 19 : 18 = 2:1, *a*-PP.

The result is of great significance, since polymer was obtained even at an activation percentage of 25%. The great excess of the neutral species does not inhibit the polymerization at all.

The fact that alkyl group exchange between different cationic species<sup>103</sup> and all the zirconium centers are active, along with the narrow polydispersities for all the polymers obtained, led us to propose a methyl group degenerative transfer (MeDeT) mechanism, a polymerization that is reversibly deactivated by degenerative transfer

based on methyl group exchange between an active cationic propagating species and a dormant neutral species according to equations 2-4.

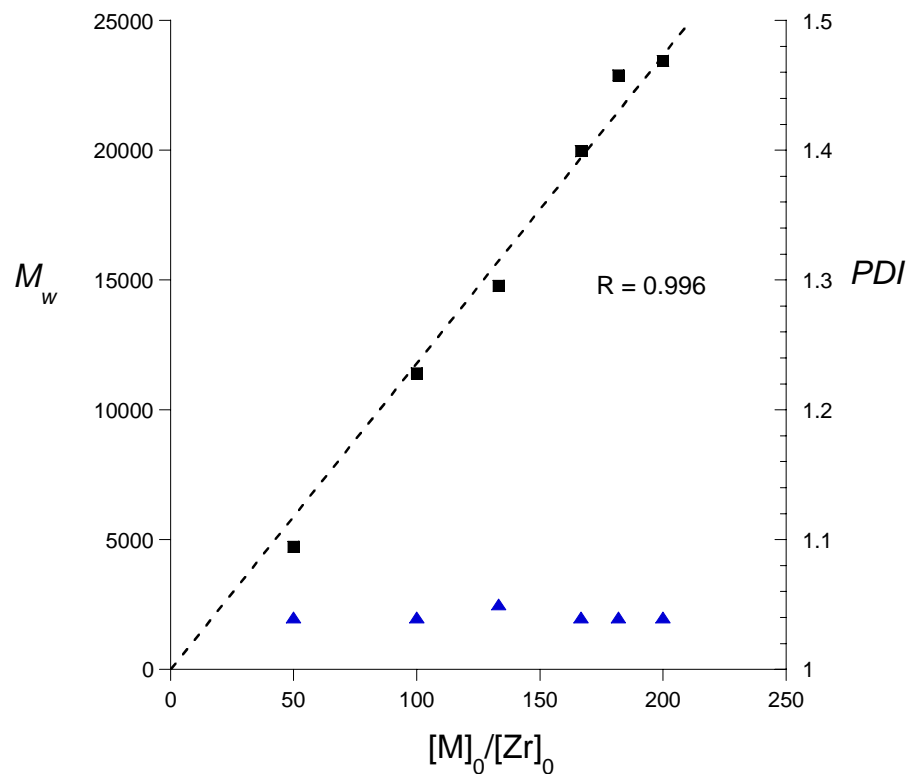
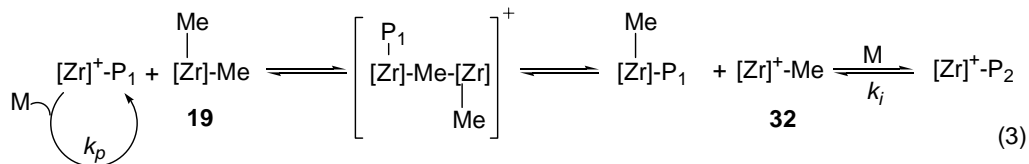
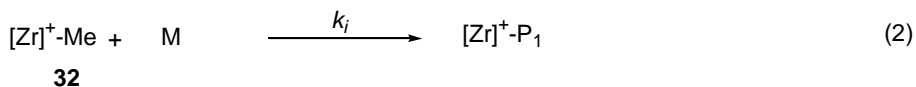
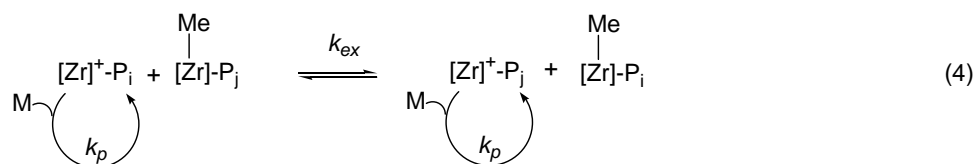


Figure 15. Dependence of PH  $M_w$  (■) and PDI values (▲) on  $[1\text{-hexene}]_0/[Zr]_0$  at constant.  $[1\text{-hexene}]_0 = 0.50\text{ M}$  and  $[18]_0 = 2.5\text{ mM}$ .

### Initiation



### Degenerative Transfer & Propagation

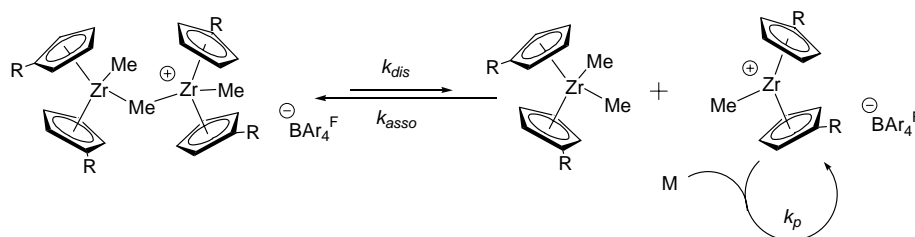


**Scheme 20. Proposed Mechanism for Methyl group Degenerative Transfer Polymerization.**

In more detail, equations 2 and 3 are the initiation steps. First, one equivalent of monomer inserts into **32**, which is the traditional initiation. Subsequently, a cationic species can dimerize with the neutral **19**, then dissociate to form polymeryl methyl zirconium and reform **32**, which can also insert monomer and initiate polymerization. In the case of **19:18** = 2:1, (a 1:1 ratio of **19** and **32**), after initiation, **32** can either undergo olefin insertion ( $k_p$ ), or rapid methyl group exchange ( $k_{ex}$ ) with **19**. For this system, if the rates of these reactions obey the rule:  $R_{ex}, R_i \gg R_p$ , degenerative transfer polymerization occurs, with a 1:1 ratio of active  $[\text{Zr}]-\text{P}$  (P: polymer chain) cation and dormant  $\text{Me}-[\text{Zr}]-\text{P}$  in solution, while  $R_i \gg R_p$  is an essential criterion for living polymerization to ensure the narrow polydispersity.<sup>167</sup>

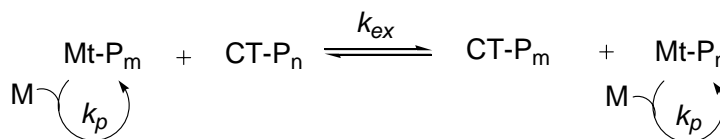
This is far from given. Marks and co-workers found that the polymerization using their cationic methyl group dimeric system provided a broader PDI compared to the

mononuclear system, probably due to the slow exchange rate between cationic and neutral species.<sup>168</sup> Schrock found their homogeneous living Ziegler-Natta system dies when substoichiometric co-catalyst is used, probably because the methyl-bridged dimer is too strong to dissociate.<sup>169</sup> It seems that all the parameters of this amidinate-based system are of the proper magnitude for MeDeT living Ziegler-Natta polymerization to occur.



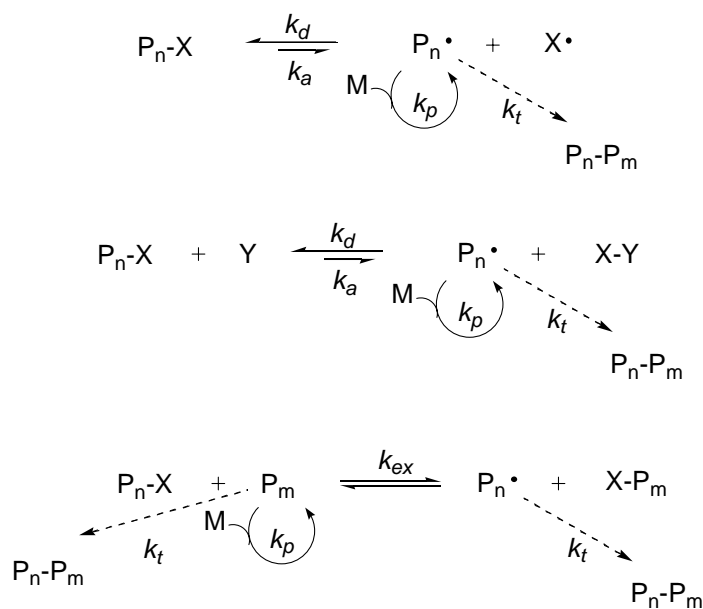
**Scheme 21.** Slow dissociation of the monocationic Zr-Me-Zr dimer reported by Marks.

The concept of degenerative transfer has been well documented in radical polymerizations. Generally speaking, in degenerative transfer, a dormant species reacts in a bimolecular way with the propagating species, deactivating the latter and simultaneously activating the former. This process requires less concentration of the active species, thus minimizes the bimolecular disproportionation side reactions. The great success of living/controlled free radical polymerization relies on this mechanism. The basic scheme of degenerative transfer is shown in scheme 22, while CT is originally the chain transfer reagent for radical polymerization. In MeDeT polymerization, no chain transfer reagent is required, while CT can be the active center itself.



**Scheme 22.** Basic mechanism of degenerative transfer polymerization

Degenerative transfer shares the same basic idea of at least three controlled / living radical polymerizations (CRP): nitroxide<sup>170</sup> or cobalt<sup>108</sup> mediated controlled radical polymerization, atom transfer radical polymerization (ATRP<sup>171-173</sup>) and reversible addition-fragmentation transfer radical polymerization (RAFT<sup>174</sup>). In these systems, a deactivated propagating species can be re-activated by reversible homolytic or heterolytic cleavage of a weak chain end, a covalent bond via redox process, or re-distribution of the chain end to a propagating chain. Degenerative transfer controlled radical polymerization was first reported by Matyjaszewski, where alkyl iodides were employed.<sup>175</sup> A Fe and Zn based coordination degenerative transfer ethylene polymerization was reported by Gibson and co-workers in 2005.<sup>176</sup>



**Scheme 23. Brief mechanisms for different systems controlled radical polymerizations.**

### 2.3 Mechanistic Studies

$^1\text{H}$  NMR (400 MHz,  $-10\text{ }^\circ\text{C}$ ,  $\text{C}_6\text{D}_5\text{Cl}$ ) studies of different ratios of **19:18** (from 1 : 0 to 10 : 1) were first carried out. Detailed spectra are shown in Figure 16. For each ratio, only one set of peaks was observed, which could be assigned as the time average chemical shifts of the cationic **32** (top) and neutral species **19** (bottom). For the  $\text{NCH}_2\text{CH}_3$  protons in **32**, due to the configurationally stability of the amidinate ligand, it should be two doublets of quartets (shows multiplet in the spectrum since two chemical shifts are quite close). While for the neutral pre-catalyst **19**, a quartet was observed because of the dynamic configuration of the amidinate. With the different ratio of **19** and **32**, the shape of  $\text{NCH}_2\text{CH}_3$  peak changes from one set of two doublets of quartets to quartets with the addition of more **19**. This indicates that the exchange between the dormant and the active species is much faster than the NMR time scale (cf.  $>10^5\text{ s}^{-1}$ ). In addition, this number is extremely large compared to the  $R_p$  ( $R_p = k_p[\text{monomer}]$ ) obtained under pseudo first-order polymerization conditions, i.e.,  $k_p = 0.266\text{ M}^{-1}\text{ s}^{-1}$  (*vide infra*) and  $[\text{monomer}] = 0.5\text{ M}$ , which means the exchange between the dormant and the active species is several orders of magnitude faster than monomer insertion.

Müller and co-workers have reported detailed mathematical model about the effect on polydispersity by the kinetic parameters.<sup>177</sup> Also, based on the calculation from Goto,<sup>178</sup> the influence of conversion on polydispersity of living polymerization could be represented as equation 5, if other side reactions are negligible. ( $\rho$  : conversion):

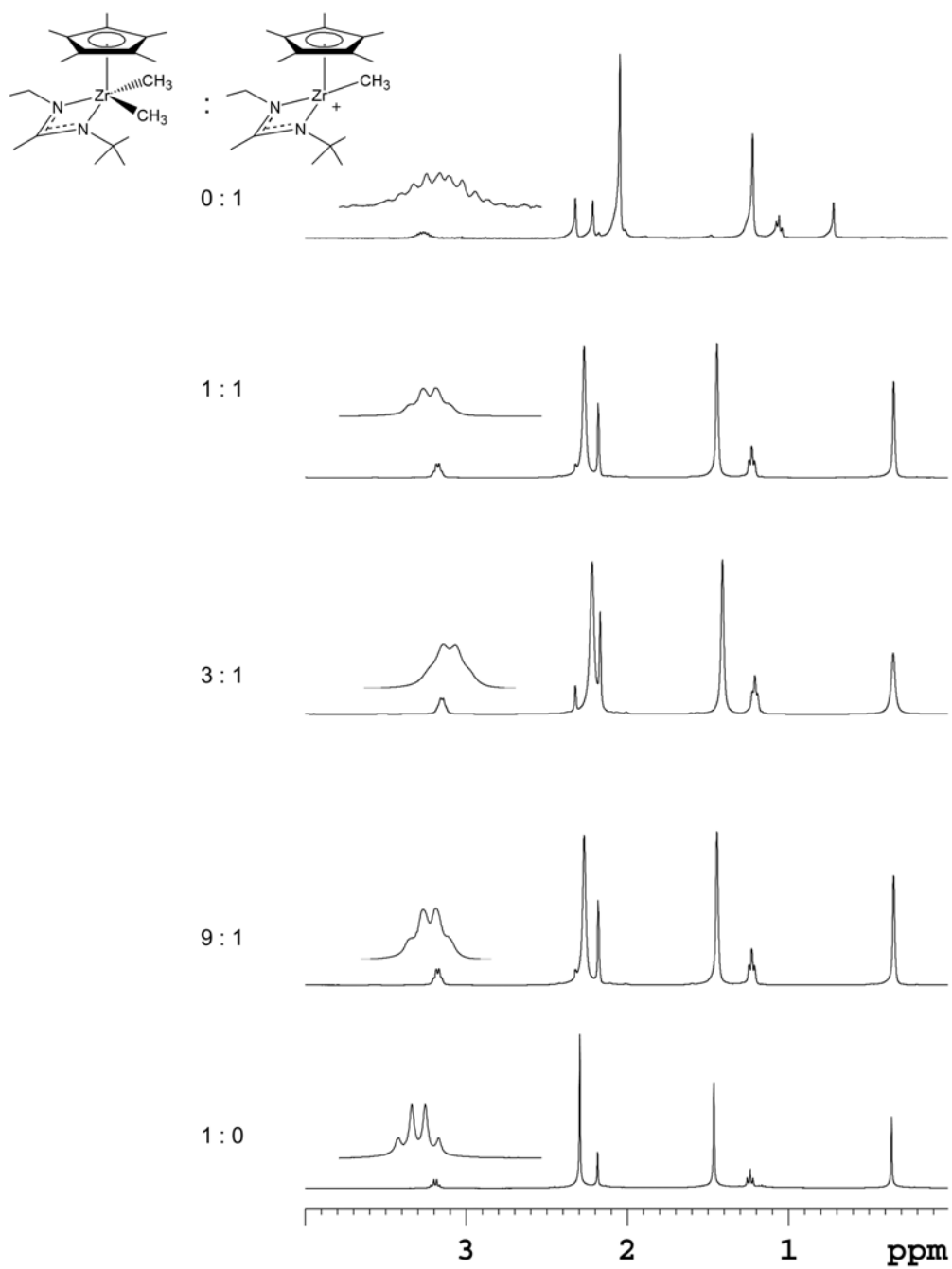


Figure 16.  $^1\text{H}$  NMR spectra (400 MHz,  $\text{C}_6\text{D}_5\text{Cl}$ ,  $-10^\circ\text{C}$ ) of 19 and 32 mixtures with various ratios. At the top: pure cationic 32 and at the bottom: pure neutral 19.

$$\text{PDI} = \frac{M_w}{M_n} = 1 + \left(\frac{2}{\rho} - 1\right) \frac{2k_p}{k_{ex}} \quad (5)$$

Since the value of  $k_p/k_{ex}$  is extremely small, in this case, PDI should be very close to 1, which is consistent with the experiment results. Also, the narrow polydispersities for all the PH samples obtained at different ratios of **19** : **18** show that  $R_i$  is faster than  $R_p$ , which indicates the system meets the essential criteria for living polymerization.

In conclusion, the extreme fast methyl group exchange is essential for the living degenerative transfer Ziegler-Natta polymerization to occur, while  $R_{ex}$  is much faster than  $R_p$ , along with an extreme fast initiation. The loss of stereospecificity will be discussed later.

## 2.4 Kinetic Analysis

Since all the polymerizations are living, kinetic parameters are quite simple. Kinetic experiments were carried out, and  $k_p$  could be simply extracted out based on equation 6.

$$\frac{d[M]}{dt} = k_p[Zr][M]$$

$$\ln \frac{[M]_0}{[M]_t} = k_p[Zr]t \quad (6)$$

while  $[Zr]_0$  is the initial cationic zirconium concentration, which equals the borate **18** concentration;

$t$ : polymerization time, in seconds;

$[M]_0$ : initial monomer concentration, in M;

$[M]_t$ : monomer concentration at certain time, in M.

Termination is negligible in living polymerization, compared to the propagation. Based on the definition of living polymerization, it is not clear that under what definition a termination is negligible. On the other hand, living polymerization does not mean immortal polymerization; a very small amount of polymer chain termination is acceptable. When kinetic experiments are carried out at least 3 to 4 half-life long, it was observed that termination *does influence* the kinetic parameters. Without considering the chain termination, an error as big as 20% for  $k_p$  could be observed based on our observation.<sup>179</sup>

To obtain more precise kinetic parameters, elimination side reaction is to be considered, while first it is assumed that  $\beta$ -hydride elimination is the only termination pathway and the rate of the termination only depends on the concentration of the active species  $[Zr]$  due to its unimolecular nature. The decreasing of active species is described in equation 7.

$$\frac{d[Zr]}{dt} = -k_t[Zr] \quad (7)$$

$$\ln \frac{[M]_0}{[M]_t} = \frac{k_p}{k_t} [Zr]_0 (e^{-k_t t} - 1)$$

where  $k_t$  is the rate constant of the termination due to  $\beta$ -hydride elimination.

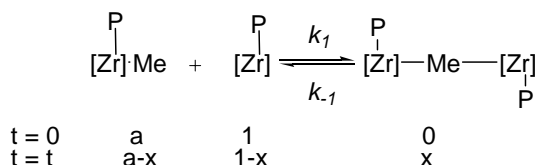
Based on the MacLaurin approximation,  $e^x = 1 + \sum_1^{\infty} \frac{x^n}{n!} \approx 1 + x + \frac{x^2}{2} + \frac{x^3}{6}$

$$\ln \frac{[M]_0}{[M]_t} = \frac{k_p}{k_t} [Zr]_0 (e^{-k_t t} - 1) \doteq \frac{k_p}{k_t} [Zr]_0 \left(1 - k_t t + \frac{(k_t t)^2}{2} - 1\right)$$

$$\ln \frac{[M]_0}{[M]_t} \doteq k_p [Zr]_0 t - \frac{k_p k_t}{2} [Zr]_0 t^2 \quad (8)$$

In addition, an equilibrium model is proposed, while the methyl-bridged monocationic dimer will decrease the concentration of the propagating species, thus decreasing the polymerization rate. If the dimer dissociation/association is considered as equilibrium, kinetic equations could be employed.

Assume an excess equivalent of neutral initiator is used; the efficient cation concentration  $1-x$  could be represented as equation 9, and the  $k_{p(eff)}$  can be described as  $k_{p(eff)} = k_p \cdot (1-x)$ .



$$\text{then } K = \frac{k_1}{k_{-1}} = \frac{x}{(a-x)(1-x)}$$

$$1-x = \frac{1-a - \frac{1}{K} + \sqrt{(a+1 + \frac{1}{K})^2 - 4a}}{2}, \quad (9)$$

$K$ : equilibrium constant

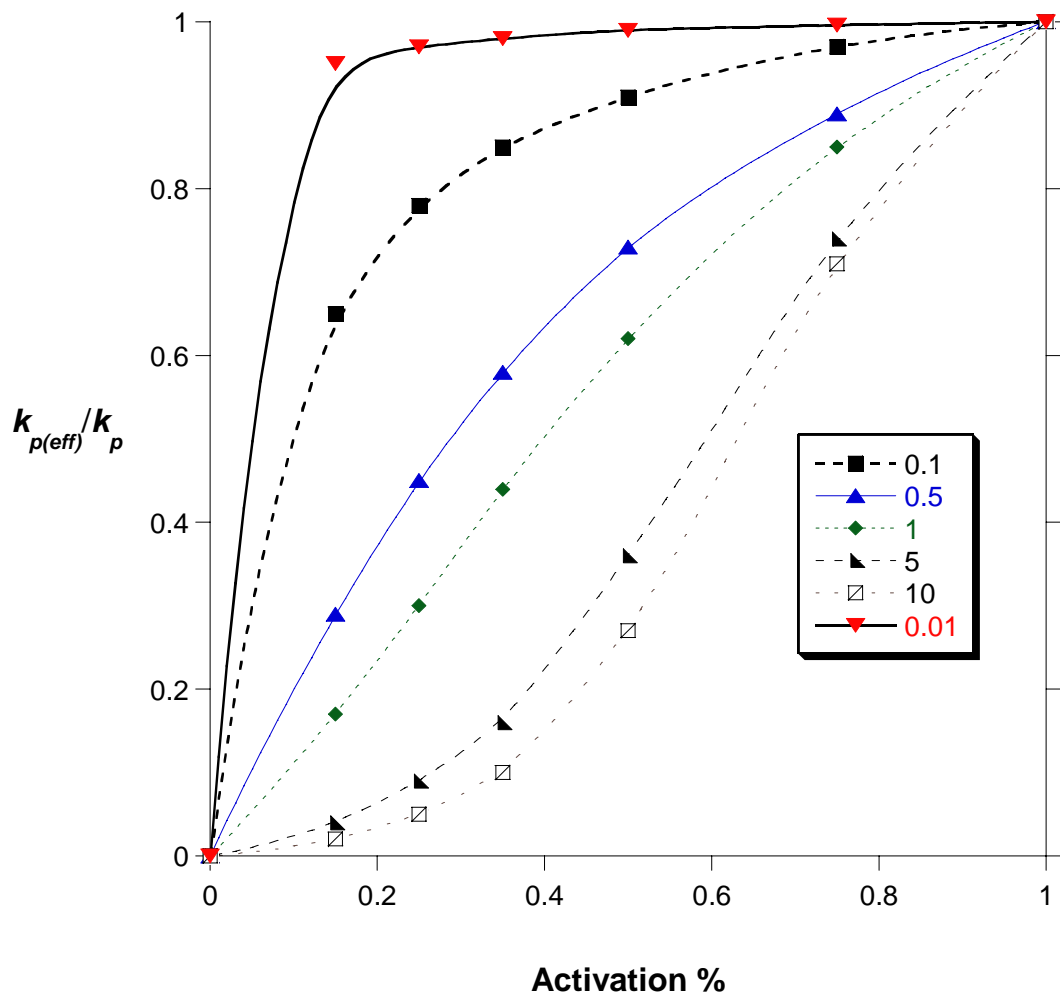


Figure 17. Typical simulation plot based on equilibrium. Equilibrium constants are shown in the insets of the figure.

Figure 17 shows a simulated  $k_{p(\text{eff})}/k_p$  vs. activation based on equation 9, with an equilibrium constant ranged from 0.01 to 10.

Monomer concentration can be measured by GC, with the polymerization solvent chlorobenzene as the internal standard. From the plot of  $\ln([M]_0/[M]_t)$  vs. time, which fits the polynomial equation,  $y = a + bx + cx^2$ ,  $b$  and  $c$  are obtained. Based on equation 8,

$$b = k_p[\text{Zr}]_0 \text{ and } c = \frac{k_p k_t [\text{Zr}]_0}{2}$$

Detailed kinetic data of polymerizations at different activation percentage is shown in table 2.

**Table 2. Kinetic summary of MeDeT.**

Activation %	$k_p$ ( $s^{-1}M^{-1}$ )	$k_t$ ( $s^{-1}$ )	$R^2$
5	NP	NA	NA
15	0.085	$2.12 \times 10^{-5}$	0.995
25	0.189	$4.03 \times 10^{-5}$	0.999
35	0.164	$2.93 \times 10^{-5}$	0.997
50	0.151	$0.80 \times 10^{-5}$	0.998
75	0.201	$5.77 \times 10^{-5}$	0.996
100	0.266	$2.61 \times 10^{-5}$	0.997

NP: No polymerization activity.

First, a dramatic difference between  $k_p$  and  $k_t$  is observed. For a typical 1-hexene polymerization at the monomer concentration  $[M]_0$  of 0.5 M, at the 50% activation MeDeT,

$$\frac{\text{Rate of propagation}}{\text{Rate of termination}} = \frac{k_p [M][Zr]}{k_t [Zr]} = \frac{k_p [M]}{k_t} = \frac{0.151 \times 0.5}{0.80 \times 10^{-5}} = 0.944 \times 10^4,$$

the rate of propagation is about four orders of magnitude faster than the rate of termination. The large deviation obtained for  $k_t$  is believed to stem from the subtle change of the polymerization temperatures.

From the plot of  $\ln([M]_0/[M]_t)$  vs. time, as shown in Fig. 18,  $k_p$  drops dramatically from full activation to 75% (from 0.266 to 0.201  $s^{-1}M^{-1}$ ), while  $k_p$  stays almost within experimental error at the range of 25 to 75% activation region. A sudden drop to 0.085  $s^{-1}M^{-1}$  was observed at very low activation (15%), while no polymer was

obtained for 5% activation. A dramatic decrease of  $k_{p(\text{eff})}$  can be observed for a small  $K$  value, such as 0.01, based on the simulation.

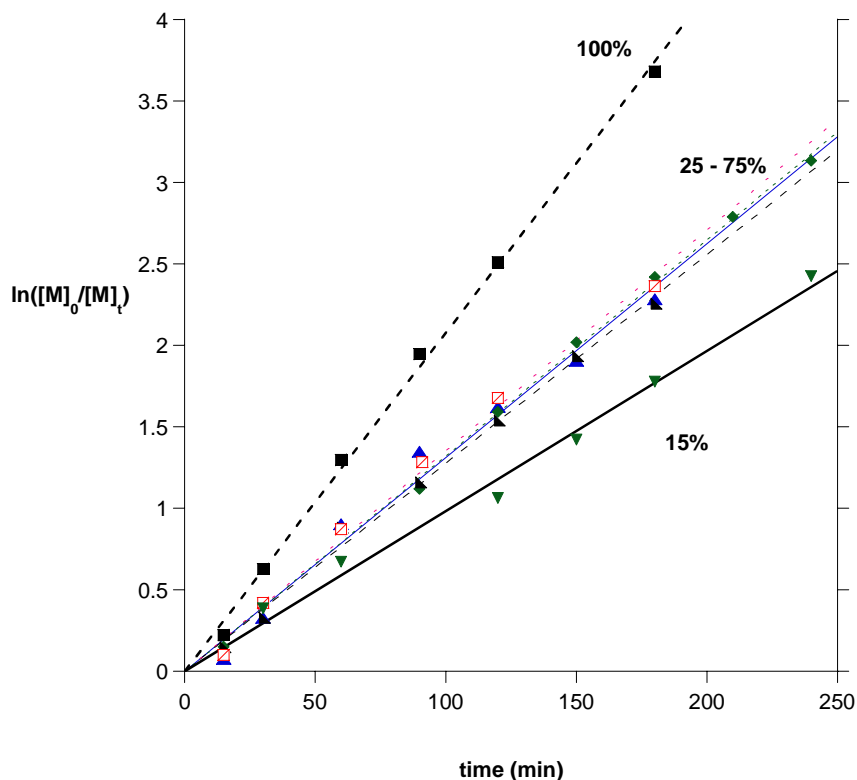
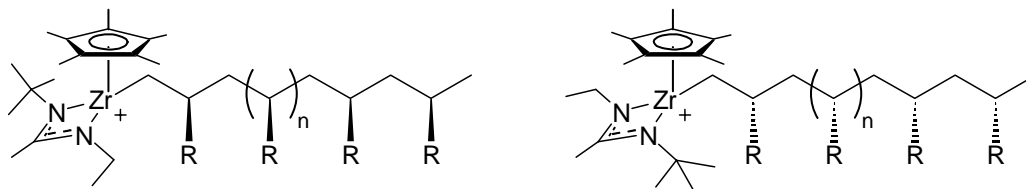


Figure 18. Kinetic plot for different percentage activation. Linear curve fit only for guide of eye.

The experimental data does not fit the simulation well, while the mechanism of MeDeT could be much more complicated than expected. It is possible that there are more processes involved. It was found recently that with a bulkier initiator, such as  $[\text{Zr}](i\text{-Bu})$  cation, even at 5% activation, polymer was obtained. Kinetic study with bulkier initiator is under investigation.

## 2.5 Origin of the Loss of Stereospecificity

The origin of loss of stereocontrol during MeDeT polymerization is of great interest. It is known that the stereocontrol for the conventional homogeneous polymerization of **32** under full activation conditions stems from a one-site model mechanism (*vide supra*). There are two enantiomeric propagating species, the *R* manifold and the *S* manifold. At full activation, both species generate enantiotopic isotactic polymer chain. Specifically, as shown in scheme 24, an *R* zirconium manifold will polymerize an *R* isotactic chain, while a *S* zirconium manifold will generate a *S* isotactic chain. If these two manifolds, under certain conditions, scramble each other, or the amidinate ligand changes its coordination configuration, atactic polyolefins will be generated even though each monomer insertion is still isospecific.



**Scheme 24. Two enantiotopic propagating species and their isotactic polymer chains**

This process that amidinate ligand changes its coordination configuration is generally referred as amidinate ring flipping.<sup>180</sup> Amidinate ring flipping is a unique property for these amidinate zirconium complexes. It is also known that ring flipping is a facile process for a variety of dimethyl pre-catalysts and alkyl methyl zirconium complexes<sup>162</sup>, but the ring flipping of alkyl chloro-zirconium and alkyl zirconium cation is extremely slow. A hypothesis is proposed based on the fact that alkyl

groups are electron-donating groups, while chloride is an electron-withdrawing group. A chloro-zirconium species or a cationic species, which has an electron deficient metal center, will pull the amidinate ligand closer to the zirconium. This shorter distance between the ligand and the metal is most likely the reason why there's no amidinate ring flipping for a cationic propagating species. Bond lengths from X-ray crystal analysis support this hypothesis, while the *i*-Bu methyl compound has the longest Zr-N bond length, and the cationic zirconium has a 0.13 Å shorter bond length, as shown in Figure 19.

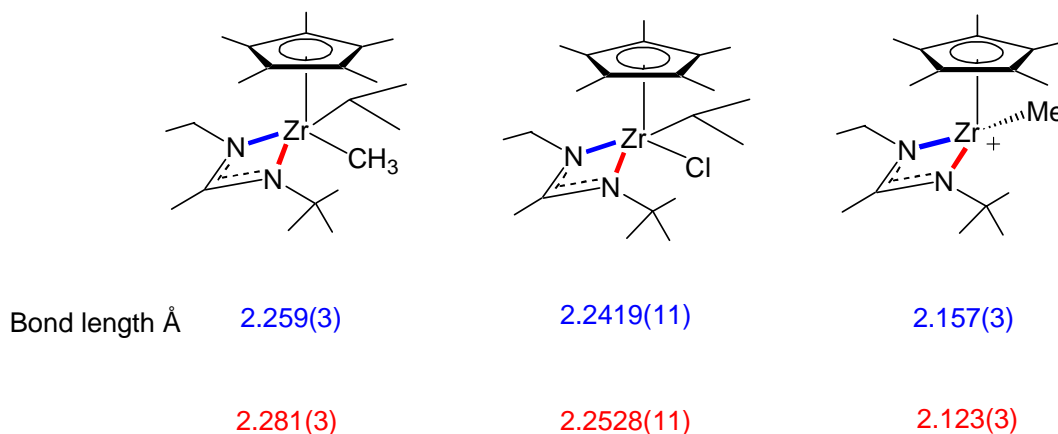
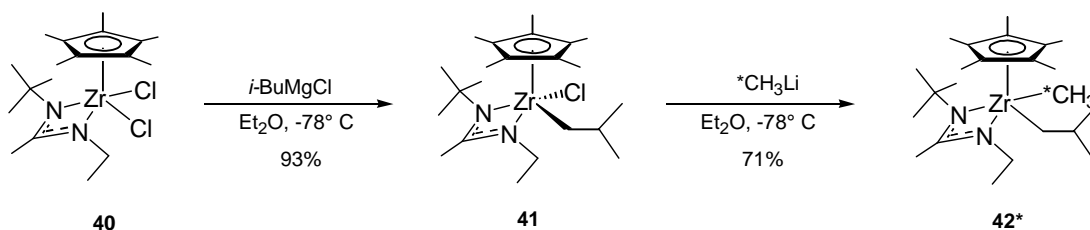


**Figure 19. Bond lengths for three different zirconium species.**

To determine the rate of the ring flipping of alkyl methyl zirconium complexes, a 2D  $^{13}\text{C}\{^1\text{H}\}$  EXSY (EXchange SpectroscopY) NMR<sup>181-184</sup> experiment was carried out. EXSY NMR determines slow exchange between two species of which the chemical shifts can be resolved by NMR, and EXSY is typically used to determine chemical exchange before line broadening occurs. Also, by integrating the cross peaks, an exchange rate can be obtained based on equation:  $d_{2opt} \approx \frac{1}{T_1^{-1} + k_{AB} + k_{BA}}$ ,

where  $d_2$  is the optimized mixing time,  $T_1$  is the spin-lattice relaxation time and  $k_{AB}$ ,  $k_{BA}$  are the rate constants for the exchange.

The *i*-Bu methyl zirconium complex **42** was selected because it is a mimic of the first insertion product of  $\alpha$ -olefin into the cationic zirconium center, and it is stable towards  $\beta$ -hydride elimination of the *i*-Bu group at low temperature.  $^{13}\text{C}$  labeled  $[\text{Zr}]$ - $^{13}\text{CH}_3$  **42\*** was made as shown in Scheme 25. In the  $^{13}\text{C}$  NMR spectrum (100 MHz,  $\text{C}_6\text{D}_6$ , 298K), two resonances assignable to the diastereotopic Zr-Me methyl groups are present as two well-resolved  $^{13}\text{C}$  NMR singlets,  $\text{Me}_a$  and  $\text{Me}_b$ , at 48.3 ppm and 44.1 ppm, respectively.



**Scheme 25. Preparation of alkyl methyl amidinate zirconium alkyl complex.**

2D  $^{13}\text{C}\{^1\text{H}\}$  EXSY NMR spectrum of **42\*** is shown in Figure 20. Exchange between  $\text{Me}_a$  and  $\text{Me}_b$  was observed according to the presence of the cross peaks. By integrating four major peaks, equilibrium constant between  $\text{Me}_a$  and  $\text{Me}_b$  ( $K$  value) of 4.0 is obtained. At 263K, value for  $k_1$  and  $k_{-1}$  were determined as  $0.6\text{ s}^{-1}$  and  $2.5\text{ s}^{-1}$ , respectively. This number, if compared to the  $k_p$  obtained under pseudo first-order polymerization conditions<sup>125</sup>, i.e.,  $k_p = 0.266\text{ M}^{-1}\text{ s}^{-1}$ , is at least two orders of magnitude bigger than the rate of propagation, based on the monomer concentration of 2.5 mM, which is the maximum concentration for most the polymerizations been carried out.

$$\frac{R_{ex}}{R_p} = \frac{k_{ex}[Zr]}{k_p[M][Zr]} = \frac{k_{ex}}{k_p[M]} = \frac{0.6 \times 80\%}{0.266 \times 2.5 \times 10^{-3}} = 721$$

In other words, between two consecutive monomer insertions, there are hundreds of ring flips, which with no doubt will scramble the stereospecificity of the second insertion. This amidinate ring flipping is obviously a reasonable mechanism for the loss of stereo control.

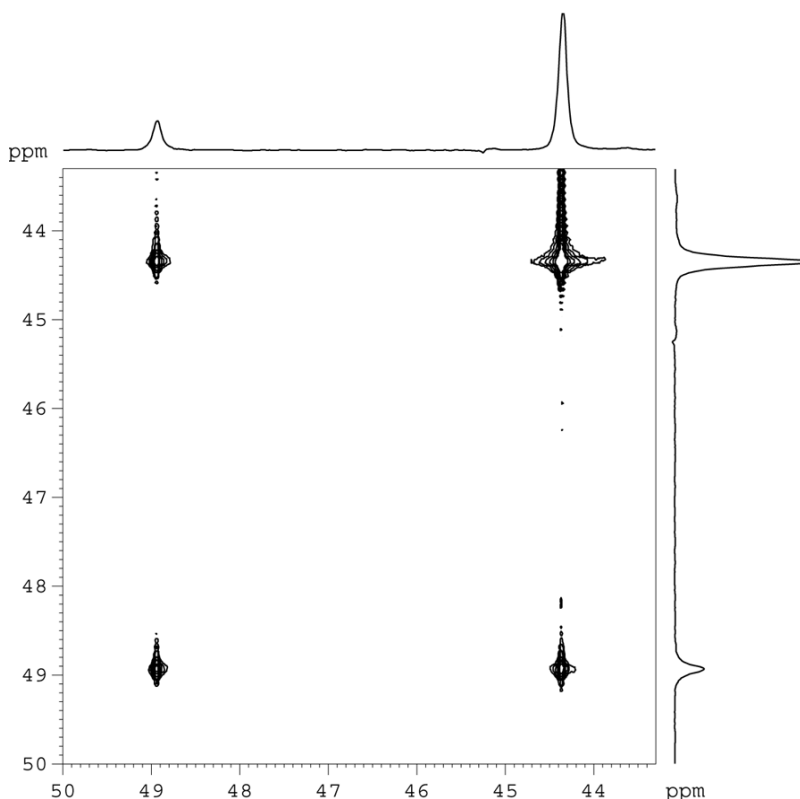
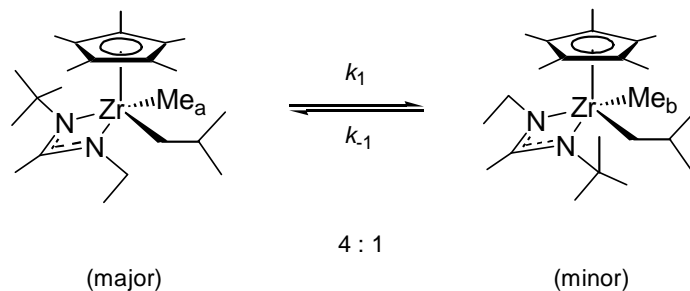
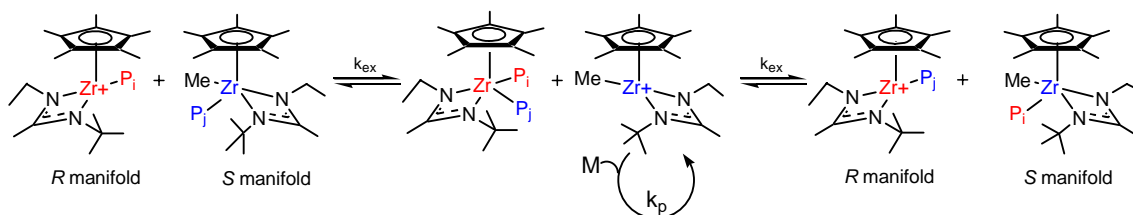


**Figure 20.** 2D  $^{13}\text{C}\{^1\text{H}\}$  EXSY NMR (125 MHz, chlorobenzene- $d_5$ ,  $-10\text{ }^\circ\text{C}$ ) spectrum of the diastereotopic methyl resonances for 42\*  $\text{Me}_a / \text{Me}_b$  mixture obtained with a mixing time of 400 ms<sup>185</sup>, a variety of mixing time from 200 ms to 800 ms were carried out for the calculation of rate constants.

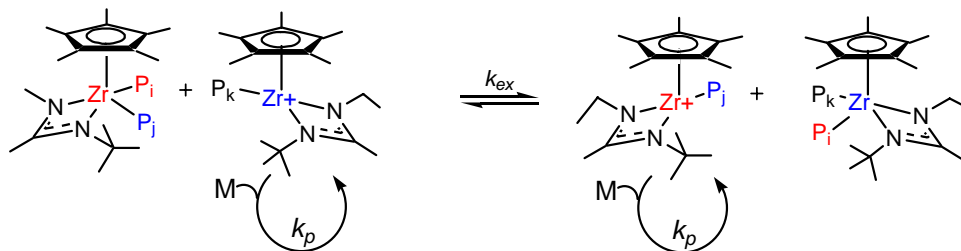


**Scheme 26. Metal centered epimerization of alkyl methyl compound 42. Me<sub>a</sub> is favored due to less interactions between the *i*-Bu group and the *t*-Bu group.**



**Scheme 27. Possible mechanism for the loss of stereo-control during MeDeT.**

An alternative mechanism is proposed based on polymer chain exchange. As shown in Scheme 27, if polymeryl chain exchange occurs between the *R* and *S* manifolds, **32** will be a possible intermediate or byproduct by the polymeryl chain exchange at the beginning of the polymerization. A degenerative transfer between Zr(P<sub>i</sub>)(P<sub>j</sub>) and Zr(P<sub>k</sub>) happens if polymeryl chain exchange is much faster than the propagation, and P<sub>i</sub>, P<sub>j</sub>, P<sub>k</sub> will have the same block length due to the fast exchange. Also, it is reasonable to assume that a di-polymeryl zirconium species has facile amidinate ring flipping based on the aforementioned electronic effects. The proposed polymer chain transfer degenerative transfer is shown in scheme 28.

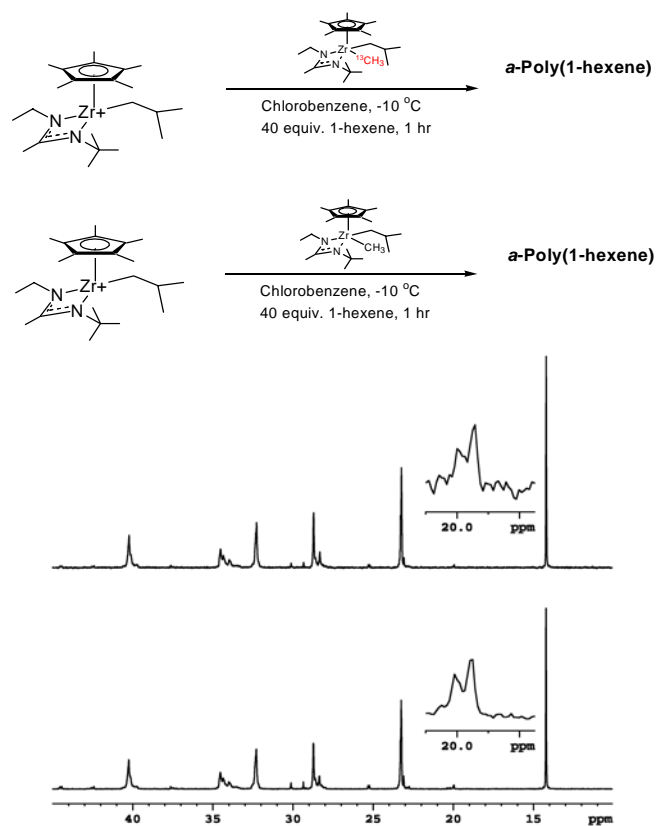


**Scheme 28. Degenerative transfer based on polymeryl chain transfer**

To differentiate the mechanisms of degenerative transfer, an experiment was designed with  $^{13}\text{C}$ -labeled **42** (**42\***), which is an efficient initiator for polymerization after chemoselective demethylation by **18**.

If degenerative transfer occurs through polymer chain transfer, a  $^{13}\text{C}$  labeled methyl group from the initiator **42\*** will be incorporated into 1/6 of the end groups of the polymer based on Scheme 27.

First, an equal molar ratio of **42** and **18** were employed to generate an *i*-Bu zirconium cation. To this cation solution, another equivalent of **42** or **42\*** was added before 40 equivalents of 1-hexene were introduced.  $^{13}\text{C}\{^1\text{H}\}$  NMR spectra of the two polymers obtained are nearly identical. NMR insets in Scheme 29 show the end group region of the PHs obtained. No  $^{13}\text{C}$  enriched methyl end group was observed, which rules out the polymeryl chain exchange postulation. Having two bulky polymer chains on the same zirconium center is unlikely due to the strong steric interactions.



Scheme 29.  $^{13}\text{C}$  labeled polymerization experiment to rule out the polymeryl chain transfer postulation,  $^{13}\text{C}$  NMR spectra for the labeled experiment (top), and non-labeled (bottom).

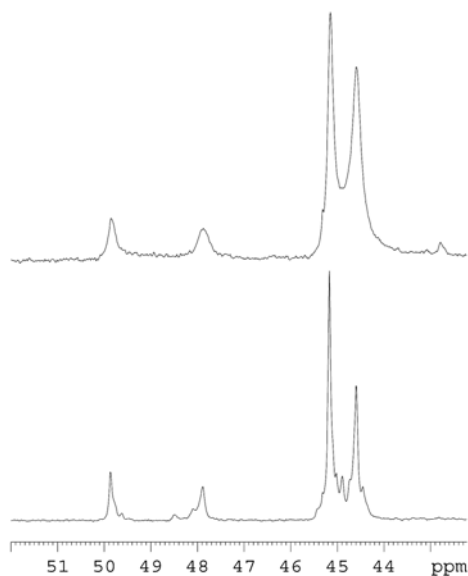
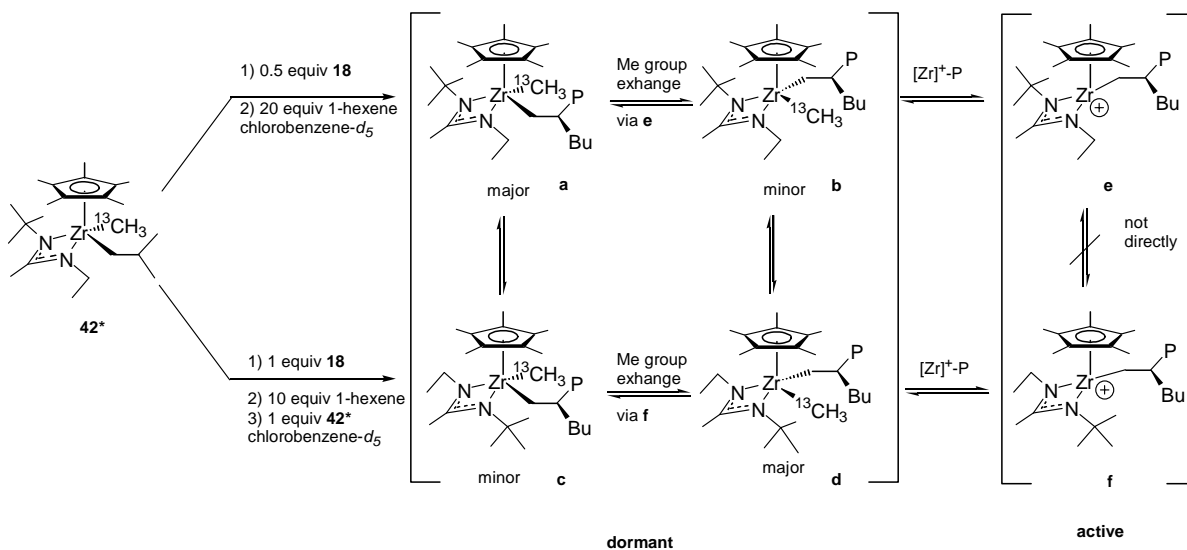


Figure 21. Partial  $^{13}\text{C}\{^1\text{H}\}$  NMR (125 MHz, chlorobenzene- $d_5$ ,  $-10\text{ }^\circ\text{C}$ ) spectra of methyl, polymeryl dormant species a-d prepared according to (a) upper reaction sequence of Scheme 32 (atactic) and (b) lower reaction sequence of Scheme 32 (isotactic).

To a half activated **42\*** mixture at  $-10\text{ }^{\circ}\text{C}$ , 10 equivalents of 1-hexene were added to generate an active species with 10 DP *atactic* polymeryl chain attached, four  $^{13}\text{C}$  labeled methyl resonances, two major and two minor, between 44 and 50 ppm, were observed as shown in Figure 21a. A similar spectrum is shown in Figure 21b, by polymerizing 10 equiv of 1-hexene using one equivalent of fully activated **42**, followed by the addition of 1 equivalent of **42\***, where an *isotactic* polymeryl chain was generated instead. These four peaks are assigned as the four possible diastereomers in Scheme 30. The narrower resonances in Figure 21b are most likely from the isotactic chains instead of atactic counterparts of Figure 21a.



**Scheme 30. Proposed mechanism for loss of stereo-control during MeDeT. For a and b, P = *a*-poly(1-hexene) chain, and for c and d, P = *iso*-poly(1-hexene) chain.**

It is important to notice that: a) diastereomeric dormant end groups are produced and exist during MeDeT and b) formation of a neutral methyl, polymeryl zirconium end group results in rapid metal-centered epimerization.

At  $-10\text{ }^{\circ}\text{C}$ , a 2D  $^{13}\text{C}\{^1\text{H}\}$  EXSY experiment was carried out which reveals all four diastereomers are exchanging with each other, according to the cross peaks observed in the NMR spectrum shown in Figure 22. This is solid evidence for the methyl exchange and metal-centered epimerization. Either mechanism itself will generate only two diastereomers.

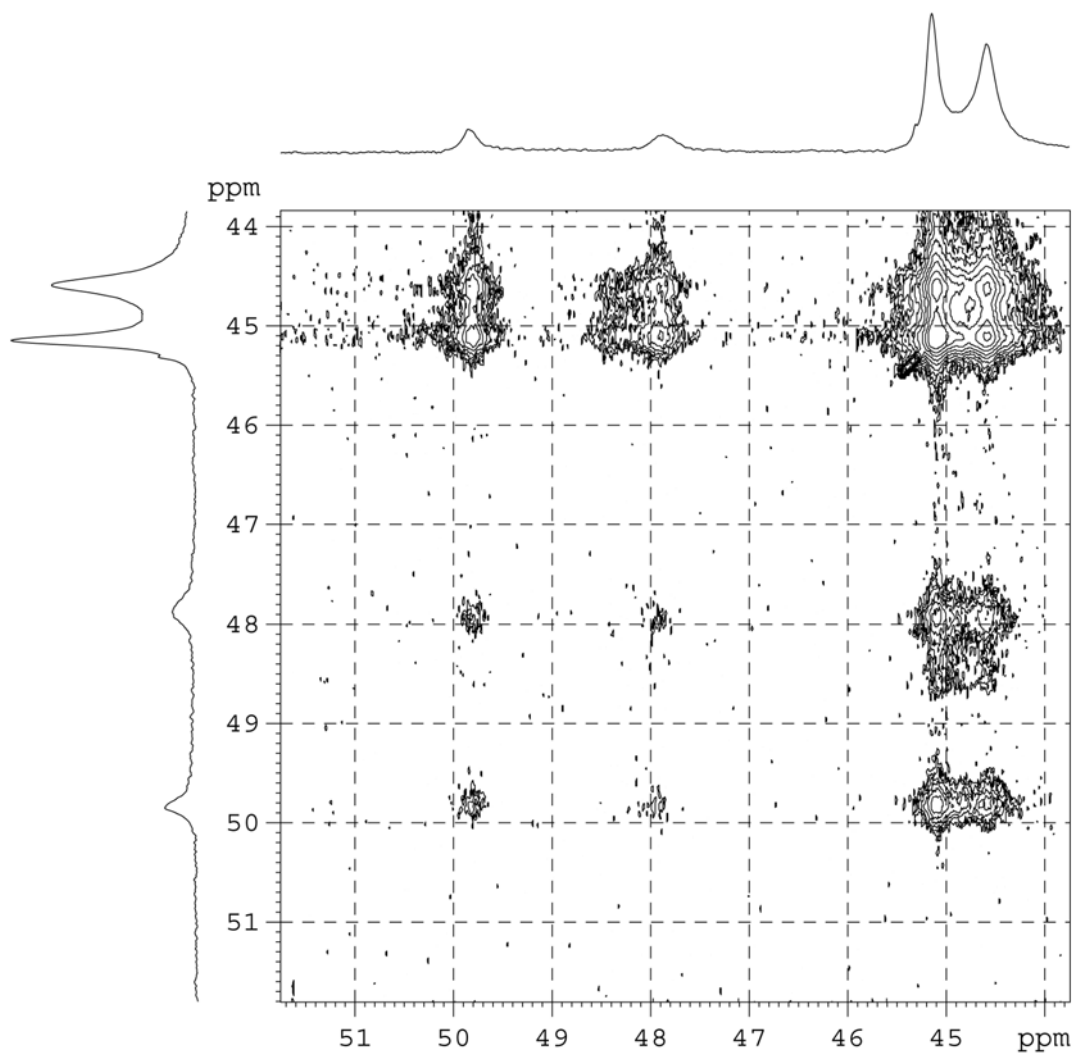


**Figure 22.** 2D  $^{13}\text{C}\{^1\text{H}\}$  EXSY NMR (125 MHz, chlorobenzene- $d_5$ ,  $-10\text{ }^{\circ}\text{C}$ ) spectrum of methyl, polymeryl dormant species a-d of Scheme 30 and Figure 21a recorded with a mixing time of 100 ms.

Another NMR experiment was designed and carried out to prove that the methyl group exchange is the indirect pathway for metal-centered epimerization of the active cationic polymeryl species. First, it is known that the polymeryl cationic species is configurationally stable at  $-10\text{ }^{\circ}\text{C}$  for extended periods of time (*vide supra*). As shown in Figure 23, at  $-10\text{ }^{\circ}\text{C}$ , 10 equivalents of  $^{13}\text{C}$ -1-dodecene<sup>186</sup> was added to 1 equivalent of **32** and after 10 min, a distinguishable peak at 83 ppm was observed, which is assigned as the first methylene carbon of the cationic polymer (**I**) species, adjacent to the zirconium. Upon the addition of 1 equivalent of **42**, immediately followed by chemoselective demethylation using 1 equivalent of **18**, a new resonance at 86 ppm was observed. This new peak is believed to have resulted from methyl group exchange from the neutral **42** to **I**, epimerization of the polymeryl methyl neutral **I**, followed by demethylation to provide **II**. These two diastereoisomers cannot be generated by cationic or neutral species alone by any means.

In conclusion, when substoichiometric co-catalyst **18** is used to activate the pre-catalyst **19**, MeDeT polymerization occurs. The MeDeT polymerization maintains its living character, but loses the stereocontrol of the fully activated polymerization. The lost of stereospecificity is due to the unique facile amidinate ring-flipping at its dormant state.

## 2.6 Synthesis of Multi-Stereoblocks

Since polymer obtained via MeDeT is atactic, and a great loss of stereocontrol of the initiator was observed during 1-hexene polymerizations even at 90% activation. At 50% activation, i.e., **19**: **18** = 2: 1, as shown in Fig. 14 (bottom), an *a*-PH is

obtained, at most with a %mm triad content of about 45-50% (cf., %mm = 25% for pure atactic polymer).

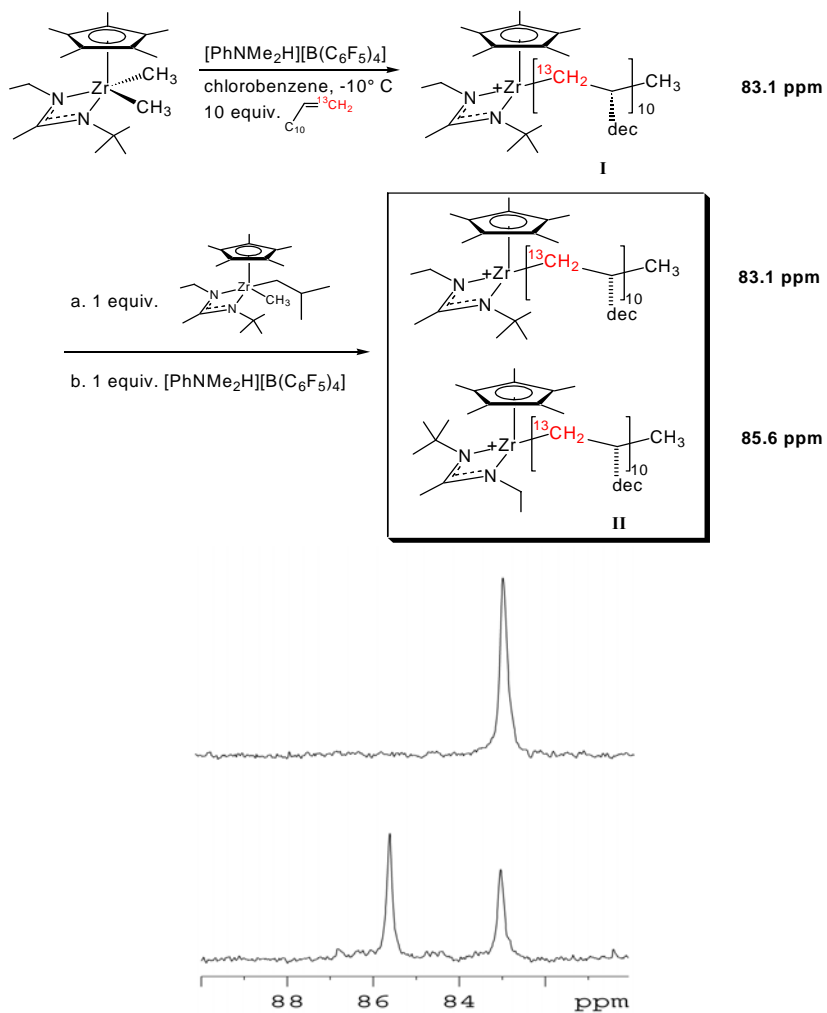


**Figure 23.**  $^{13}\text{C}\{^1\text{H}\}$  NMR (100 MHz, chlorobenzene- $d_5$ ,  $-10^\circ\text{C}$ ) spectrum of (a), upper, I and (b) lower, after addition of 1 equivalents of 42 followed by addition of 1 equivalent of 18.

Since MeDeT is still a living system, it is very promising to use this process for atactic-isotactic stereoblock simply by turning “on” or “off” degenerative transfer, by adding a half equivalent of **18** to the pre-catalyst **19** for the “on” state and applying the full amount for the “off” state.

To prove this concept, 50 equivalents of 1-hexene, based on the concentration of **18**, were polymerized at  $-10\text{ }^{\circ}\text{C}$  under MeDeT conditions by half activated **32**, which was generated at a **19:18** ratio of 2:1. This produced a living *a*-PH chain with DP of 50. After all the monomer had been consumed, 1 more equivalents of **18** was added to fully activate the zirconium species, followed by 50 more equivalents of 1-octene introduced all at once. After the reaction was quenched and polymer purified, NMR and GPC data showed an *a*-PH-*b*-*iso*-PO stereoblock with  $M_n$  of 12 400 (cf.,  $M_{n(\text{calc})} = 9\ 800$ )<sup>187</sup> and PDI of 1.04. The inverse gated  $^{13}\text{C}\{^1\text{H}\}$  NMR is shown in Figure 24, in which the ratio of 1-hexene to 1-octene block was determined to be very close to 1:1.

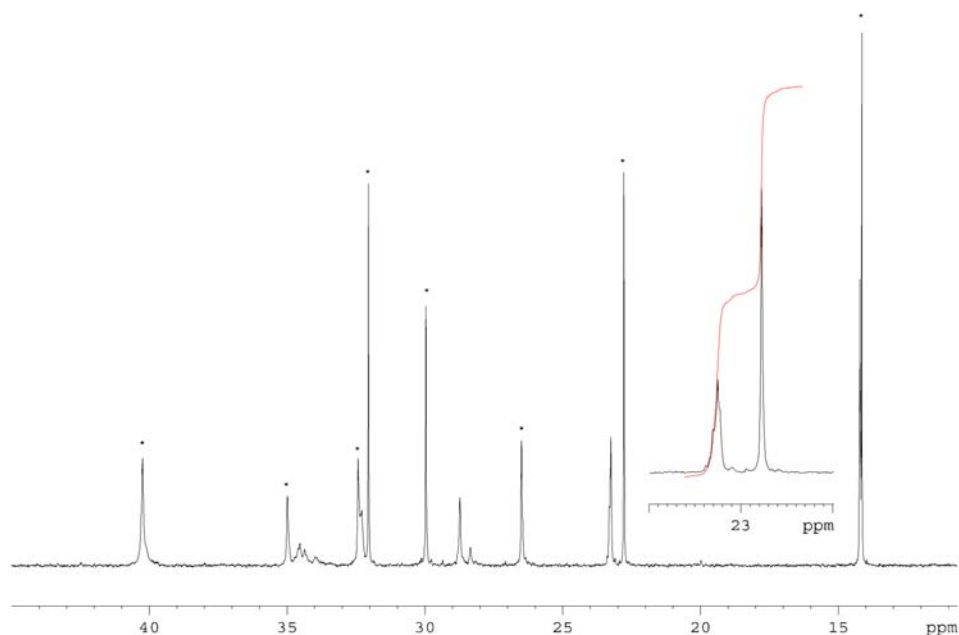


**Figure 24. Inverse-gated  $^{13}\text{C}\{^1\text{H}\}$  NMR (100 MHz, chloroform- $d_1$ , 298K) spectrum of *a*-poly(1-hexene)-*block-iso*-poly(1-octene).  $^{13}\text{C}$  NMR resonances for the isotactic poly(1-octene) block are marked with an asterisk (\*)**

The same procedure could be used to make a variety of diblock copolymers, such as an *a-iso*-PH stereoblock. It is very easy to switch from MeDeT conditions to conventional conditions by adding additional **18**, similar to the copolymerization

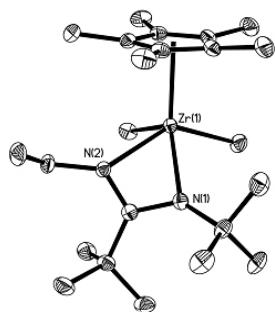
described above. However, it will be more difficult to make copolymers beginning with an isotactic sequence. In this case, a methylating reagent is necessary to turn “on” MeDeT. Most importantly, after methyl group transfer, the remnants of the methylating reagent should either be inert to the polymerization or can be fully removable from the polymerization system.

A heterogeneous zirconium dimethyl pre-catalyst<sup>188</sup> **57** (*vide infra*) certainly serves this need. Based on the degenerative transfer mechanism, when **57** is added to a fully cationic polymeryl zirconium condition (which makes isotactic polymer chain), methyl group exchange from **57** to the homogeneous **32** occurs. Since it is possible to filter the solid-supported beads away from the polymerization system, under a complicated setup to keep the low temperature during the filtration, the fully cationic polymeryl zirconium solution (isotactic) is converted to MeDeT conditions, in which atactic polymer chain will be generated. To prove this methodology, *iso*-PO-*b-a*-PH was synthesized. GPC and NMR data showed the correct tacticity for each block and narrow PDI (1.08) was observed. To further utilize this methodology, we have also successfully prepared a stereotriblock copolymer, an *a*-PH-*b-iso*-PO-*b-a*-PH ( $M_n = 17\ 900$ , PDI = 1.07). Inverse-gated  $^{13}\text{C}\{^1\text{H}\}$  NMR spectra verified the correct block length of 1-hexene and 1-octene segments.

In conclusion, it is theoretically possible to make an infinite variety of narrow PDI stereoblock copolymers via living polymerization, by turning on or off the MeDeT conditions. However the difficulty involved in the filtration under low temperature and the complication due to the heterogeneous nature of the methylating reagent make this process impractical.

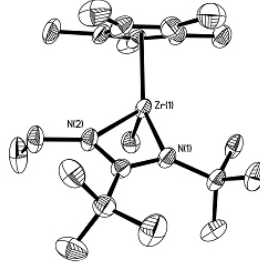
To circumvent the need for filtration, an innocent bystander, who serves as the methylating reagent, is needed to turn on MeDeT conditions. Compound **34**, based on the crystal structure, has a very large fold angle ( $36.1^\circ$ ), which is defined as the N-C-N-Zr biplane angle along with the amidinate zirconium planes. A much smaller angle was observed for **19**.

Compound **34** is chemoselective demethylated by **18** to form **35**. The crystal structure of the cation **35** shows a much smaller fold angle ( $3.1^\circ$ ). By releasing one methyl group, the strain of **34** has been greatly released. As we know<sup>189</sup>, **35** shows no activity towards 1-hexene polymerization even at elevated temperatures. Half an equivalent of **34** was added as the methylating reagent to a fully activated **32** solution. When 200 equivalent of 1-hexene was then added to the **34** / **32** mixture, an  $\alpha$ -PH of narrow polydispersity is obtained ( $M_n = 23\ 500$  and PDI of 1.06) with 98% yield, further NMR analysis confirmed that the polymer obtained is atactic.



34

$C_{Et}-N(2)-Zr(1)$   $131.4(2)^\circ$   
 Fold angle  $34.7^\circ$



35

$C_{Et}-N(2)-Zr(1)$   $140.4(2)^\circ$   
 Fold angle  $3.8^\circ$

To prove the concept that stereoblock polyolefin can be synthesized by using MeDeT and **34** as the methylating reagent to turn “on” MeDeT from a fully activated system. An *iso*-PO-*a*-PH-*iso*-PO-*a*-PH-*iso*-PO pentablock has been successfully synthesized, by changing the activation conditions (MeDeT on: 50% activation, and

MeDeT off: 100% activation) alternatively with two different monomers for each stage. Co-catalyst **18** and methylating reagent **34** were successfully used to change the polymerization conditions.

Detailed inverse gated  $^{13}\text{C}\{^1\text{H}\}$  NMR and GPC (Figure 25) were carried out for each aliquot and the final bulk polymer. Narrow PDI was detected for each aliquot, and the integration of PH and PO segments for each block indicates the expected block length for the pentablock, as shown in Figure 26. To our best knowledge, this is the first well-defined polyolefin stereoblock ever synthesized.

**Table 3. GPC data for each block aliquot and the final pentablock.**

Block	$M_w^{190}$	PDI
1	7 800	1.06
2	12 000	1.07
3	18 300	1.07
4	23 400	1.08
5	28 500	1.08

Subsequently, a series of sterically hindered zirconium derivatives (**36** – **39**) were prepared to test the potential ability as methylating reagents. A competent methylating reagent should be: 1). Have no polymerization activity, 2). Have negligible interaction or minor interaction with the propagating species. Based on the results of **34**, great steric hindrance (such as a big fold angle as described) will facilitate the liberating of the methyl group. An ideal candidate is a compound that will give up a methyl group and immediately decompose, or in other words, a “suicide” methylating reagent.

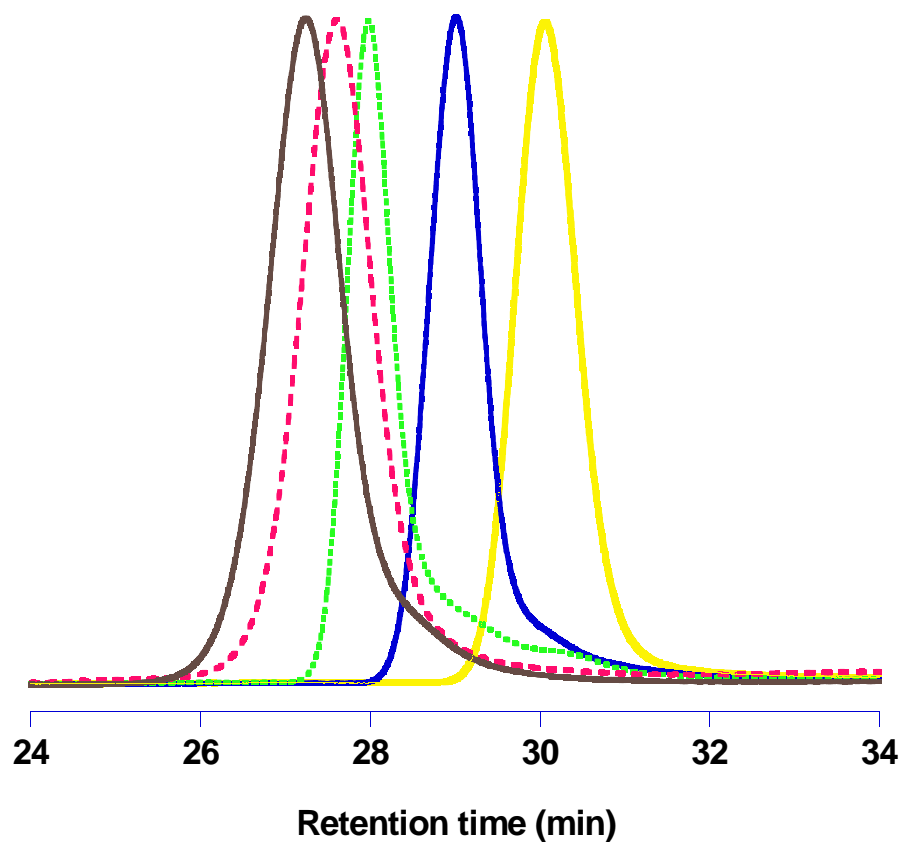
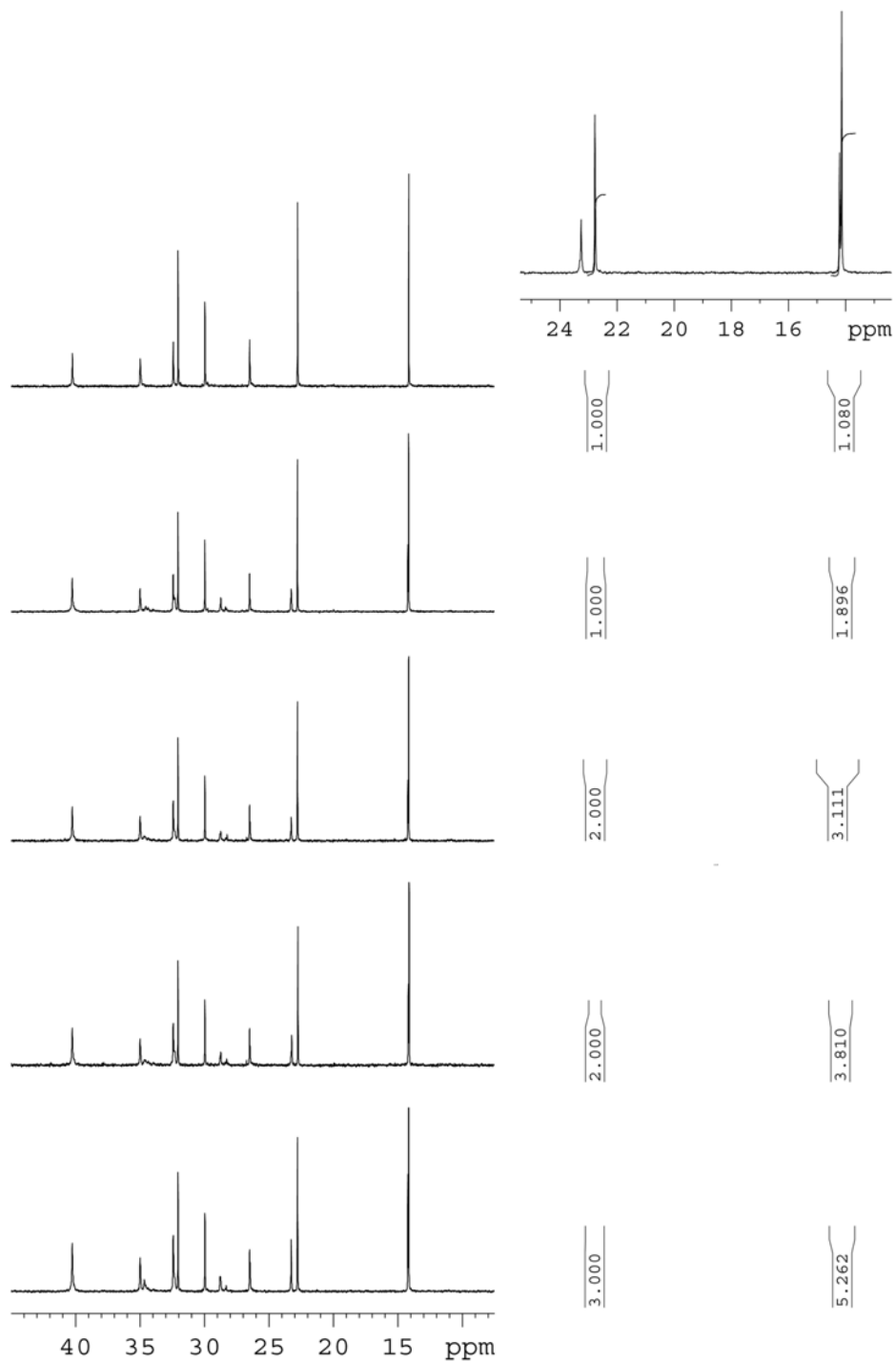
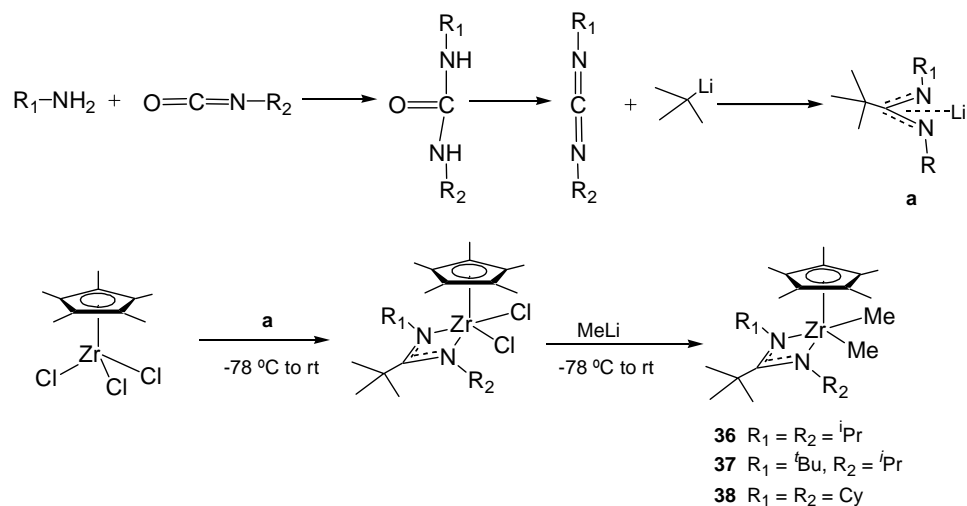


Figure 25. GPC trace for aliquots of the pentablock. From left to right are the 1<sup>st</sup> block to the bulk pentablock.

Compound **34**, **36** - **38** were synthesized based on Scheme 31, started with the synthesis of lithium amidinate (**a**) obtained from alkyl lithium and carbodiimides. Compound **39** was made via one-pot-two-step amidinate insertion into a Zr-C bond, which is the standard synthetic route for **19** synthesis.<sup>124</sup> *tert*-butyl *neo*-pentyl carbodiimide was used, which in turn, could be synthesized from *tert*-butyl amine and *neo*-pentyl isocyanate.



**Figure 26. Inverse gated  $^{13}\text{C}\{^1\text{H}\}$  NMR (100 MHz,  $\text{CDCl}_3$ , 25 °C) spectra for aliquots of the pentablock and the integration of PH and PO peaks.**



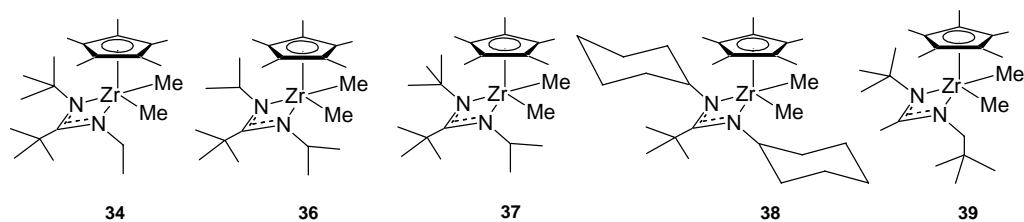
**Scheme 31. General reaction scheme to make *t*-Bu amidinate derivatives.**

Each compound was employed for 1-hexene polymerization, upon activation by **18**. Typically, the polymerization was carried out at  $-10\text{ }^\circ\text{C}$  for 5 h or longer, with a  $[\text{Zr}]$  of  $2.5 \times 10^{-3}\text{ M}$ , and  $[\text{1-hexene}]$  of  $0.5\text{ M}$ . The detailed results are shown in Table 4.

**Table 4. Polymerization results for different potential methylating reagents.**

Compound	Time (h)	$M_n$	PDI	Yield
<b>36</b>	10	N.P.	NA	NA
<b>37</b>	18	1376	1.21	<5%
<b>38</b>	20	N.P.	NA	NA
<b>39</b>	5	N.P.	NA	NA

N.P.: No polymer obtained.



**Scheme 32. Potential methylating reagent to turn on MeDeT.**

Besides **34**, compound **39**, with fewer steps involved in the synthesis from carbodiimide, does not have polymerization activity towards 1-hexene.<sup>191</sup> Compound **36** has no activity as well, while a sterically bulkier complex **37** shows minimum activity for 1-hexene polymerization upon activation by **18**, less than 20 insertions were observed for 18 h. When introduced to a fully activated polymerization system, **36**, **39** both liberate methyl group and turn on the MeDeT conditions.

## 2.7 Hafnium MeDeT<sup>192</sup>

It is also of great interest whether MeDeT can be expanded to other metals, such as hafnium. First, questions arise as to whether a hafnium analogue of **19** is an active pre-catalyst for the polymerization of  $\alpha$ -olefins, and if so, whether it will polymerize in a living fashion. Not surprisingly,  $(\eta^5\text{-C}_5\text{Me}_5)\text{HfMe}_2[\text{N}(t\text{-Bu})\text{C}(\text{Me})\text{N}(\text{Et})]$  (**43**) can be synthesized via the conventional carbodiimide insertion into a Hf-C bond with moderate yield (58%), when  $\text{R}_1 = \text{Et}$  and  $\text{R}_2 = t\text{-Bu}$ .<sup>193</sup>

Upon activation by **18** at  $-10\text{ }^\circ\text{C}$ , **43** is an active pre-catalyst that polymerizes 1-hexene in living and stereospecific fashion. Kinetic analysis was carried out and  $\ln([\text{M}]_0/[\text{M}]_t)$  vs. time is shown in Figure 27. A strict first order linear plot is obtained and a  $k_p$  of  $3.5 \times 10^{-3}\text{ M}^{-1}\text{s}^{-1}$  can be extracted from the plot.<sup>194</sup> NMR and GPC analysis of the final product from the kinetic analysis proved an *iso*-PH with  $M_n$  of 18 600, and PDI of 1.08. Compared to the zirconium pre-catalyst **19**, with a  $k_p$  of  $0.266\text{ M}^{-1}\text{s}^{-1}$ , *the hafnium derivative polymerizes 1-hexene at least 70 times slower than the zirconium analogue*. This similar rate attenuation of polymerization from Zr to Hf is observed in most metallocenes.

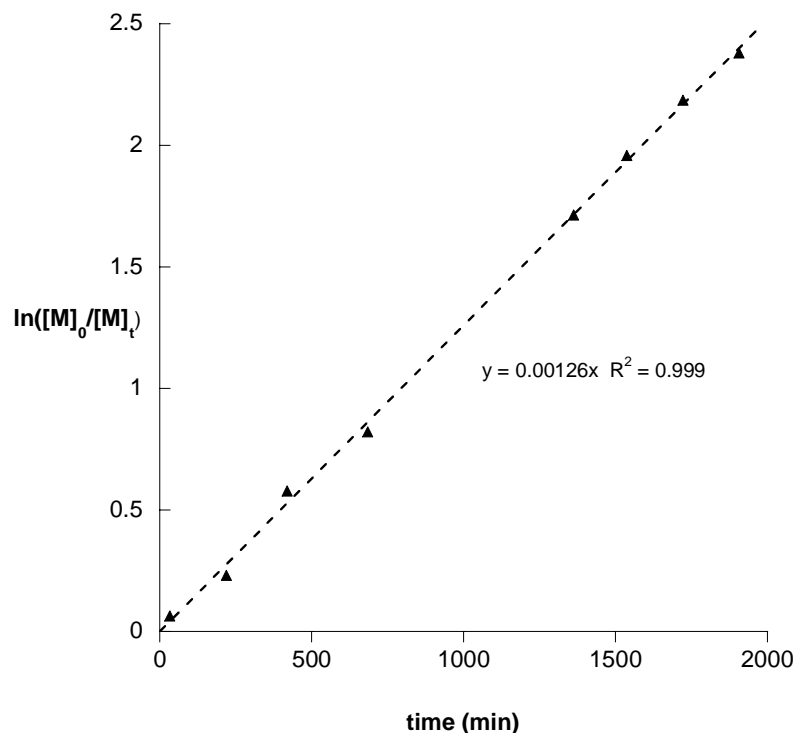


**Figure 27. Kinetic analysis of fully activated Hafnium 1-hexene polymerization system.**

To check whether MeDeT happens for hafnium, similar  $^1\text{H}$  NMR experiments were carried out. A 2:1 mixture of **43** and **18** provides only a single set of exchanged broadened peaks. Polymerization by **43** was also carried out, using a substoichiometric amount of **18** and 200 equivalents of 1-hexene. After 64 h, a 71% yield of *a*-PH with a  $M_n$  of 11 600 and a PDI of 1.27 was obtained (cf. lower molecular weight is due to partial consumption of the monomer). No vinyl end group was detected in  $^1\text{H}$  NMR for the polymer obtained, which indicates the lack of  $\beta$ -hydride elimination during the polymerization even after 64 h. The broader polydispersity probably stems from a larger  $k_p/k_{ex}$  value for hafnium system, since a symmetric peak with unnoticeable tailing was shown in GPC. The exchange between the neutral **43** and its cation is extremely fast based on the NMR spectra. With a

longer polymer chain attached,  $k_{ex}$  could be dramatically decreased, thus influencing the  $k_p/k_{ex}$  value.

Kinetic analysis under half activation revealed a first-order linear relationship between  $\ln([M]_0/[M]_t)$  vs. time, which indicates the living character of the polymerization. The similar mechanism is shown in Figure 28.

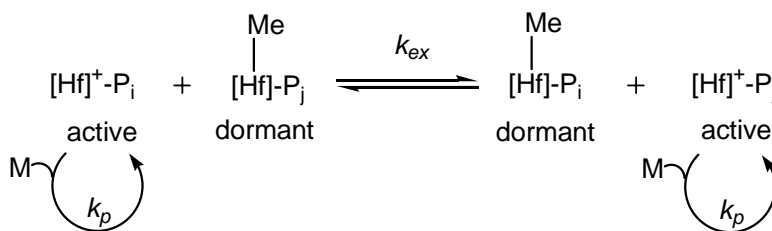


**Figure 28. MeDeT mechanism for hafnium polymerization**

Also, similar to zirconium MeDeT, a detailed kinetic analysis of different activations were carried out and a plot of  $\ln([M]_0/[M]_t)$  vs. time is shown in Figure 29 and Table 5. All of the polymerizations are living according to the kinetic data ( $R^2$  of 0.995 is obtained for each plot). 2<sup>nd</sup> order polynomial curve fitting was employed for  $k_p$  determination. However,  $k_t$  value was not able to be determined due to the experimental error and an extremely small value of  $k_t$ .

A decrease of rate constant can be observed from 100% to 75%. The rate of polymerization drops very slowly from 75% to 20%, and dramatically decreases when the activation percentage drops to 10%. This is very similar to the zirconium MeDeT described previously.

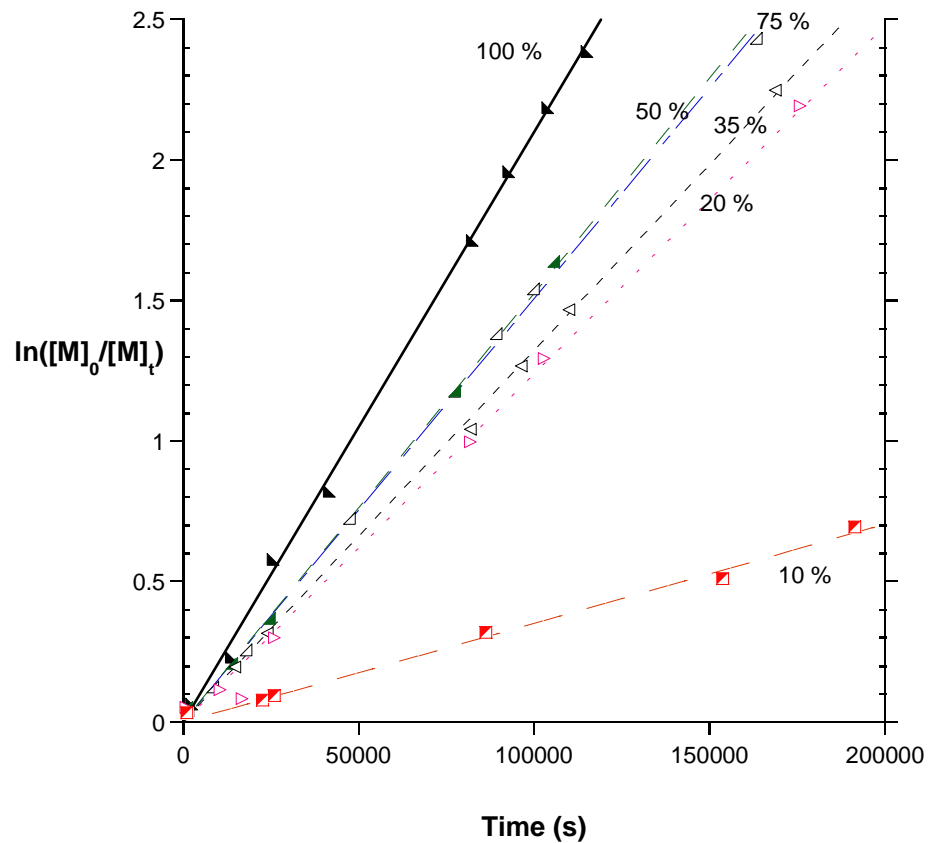


Figure 29. Different percentage activation for hafnium polymerizations.

Table 5. Rate constants for different percentage activation of 43.

Activation %	$k_p$ ( $s^{-1}M^{-1}$ )
100	$3.46 \times 10^{-3}$
85	$2.93 \times 10^{-3}$
50	$2.96 \times 10^{-3}$
35	$2.78 \times 10^{-3}$
20	$2.74 \times 10^{-3}$
10	$0.65 \times 10^{-3}$

## 2.8 Conclusions

Upon activation with a substoichiometric amount of co-catalyst **18**, living methyl group degenerative transfer polymerization of  $\alpha$ -olefins is observed for zirconium pre-catalyst **19**. The exchange between an active species and a dormant species is at least  $10^4$  faster than the propagation under typical polymerization conditions. The great loss of stereoselectivity is due to a metal centered epimerization of the propagating species via a facile amidinate ring flipping. NMR evidence unambiguously proves the MeDeT mechanism. Stereoblock polymers were polymerized and microstructure characterized. Also, a hafnium based living MeDeT polymerization is observed.

## 2.9 Experimental

Manipulations were performed under an inert atmosphere of dinitrogen using standard Schlenk techniques or a Vacuum Atmospheres glovebox. Dry, oxygen-free solvents were employed throughout. Diethyl ether ( $\text{Et}_2\text{O}$ ), tetrahydrofuran (THF), toluene and pentane were distilled from sodium / benzophenone (with a few milliliters of triglyme being added to the pot in the case of pentane). Benzene- $d_6$  was likewise vacuum transferred from NaK alloy prior to being used for NMR spectroscopy. Chlorobenzene- $d_5$  was vacuum transferred from  $\text{CaH}_2$  prior to being used for NMR spectroscopy. For alkylations, *i*-BuMgCl in  $\text{Et}_2\text{O}$  and MeLi in  $\text{Et}_2\text{O}$  were purchased from Aldrich. NMR spectra were recorded on Bruker 400 MHz / 500 MHz instruments using benzene- $d_6$  or chlorobenzene- $d_5$  as the solvent. Elemental analyses were performed by Midwest Microlab, Inc.

GPC analyses were performed using a Waters GPC system equipped with a column oven and differential refractometer both maintained at 40° C and four columns (Waters Ultrastyrigel 500 Å, Waters Styragel HR3, Waters Styragel HR4, and Shodex K-806M) also maintained at 40° C. THF was used as the eluant at a flow rate of 1.1 mL/min.  $M_n$  and  $M_w/M_n$  values were obtained using the Waters GPC software and seven different polystyrene standards (Polymer Laboratories).

**Preparation of  $(\eta^5\text{-C}_5\text{Me}_5)\text{ZrMe}_2[\text{N}(t\text{-Bu})\text{C}(\text{Me})\text{NEt}]$  (19).** To a solution of  $(\eta^5\text{-C}_5\text{Me}_5)\text{ZrCl}_3$  (4.00 g, 12.0 mmol) in 400 mL of  $\text{Et}_2\text{O}$  at  $-78^\circ\text{C}$ , was added 24.9 mL (39.6 mmol) of MeLi in  $\text{Et}_2\text{O}$ . After slowly warming to  $-10^\circ\text{C}$  within 2 h, the reaction was quenched with 0.2 mL of chlorotrimethylsilane. The solution was then cooled back to  $-30^\circ\text{C}$  and 1.548 g (12.0 mmol) of *tert*-butyl ethyl carbodiimide in 40 mL of  $\text{Et}_2\text{O}$  was added via cannula within 2 h. The reaction was allowed to stir for an additional 2 h at  $-10^\circ\text{C}$ . Upon removal of the volatiles *in vacuo*, the crude material was recrystallized from pentane at  $-35^\circ\text{C}$  to provide 3.89 g (81.6% yield) of the desired product. For **19**:  $^1\text{H}$  NMR (400 MHz, benzene- $d_6$ ):  $\delta$  2.86 (q,  $J = 7.2$  Hz, 2H), 2.01 (s, 15H), 1.70 (s, 3H), 1.16 (s, 9H), 0.90 (t,  $J = 7.2$  Hz, 3H), 0.23 (s, 6H) Anal. Calcd. for  $\text{C}_{20}\text{H}_{38}\text{N}_2\text{Zr}$ : C 60.39, H 9.63, N 7.04; Found: C 60.54, H 9.61, N 7.03.

**Preparation of  $(\eta^5\text{-C}_5\text{Me}_5)\text{ZrCl}_2[\text{N}(t\text{-Bu})\text{C}(t\text{-Bu})\text{NEt}]$  (33).** At  $0^\circ\text{C}$ , to a solution of *t*-BuN=C=NEt (0.253 g, 2.00 mmol) in 60 mL of  $\text{Et}_2\text{O}$ , 1.40 mL of *t*-BuLi (1.50 M in pentane, from Aldrich) was added via a syringe. The reaction was stirred for 3 h. This clear solution was then transferred via cannula into a flask with  $(\eta^5\text{-C}_5\text{Me}_5)\text{ZrCl}_3$  (0.666 g, 2.00 mmol) in 40 mL of  $\text{Et}_2\text{O}$  at  $-78^\circ\text{C}$ . The mixture was stirred for 12 h,

then volatiles removed *in vacuo*. The residue was extracted with toluene, filtered through a short pad of Celite, and all volatiles removed *in vacuo*. Yellow powder was obtained (0.72 g, 82 %). For **33**,  $^1\text{H}$  NMR (400 MHz, benzene- $d_6$ ):  $\delta$  3.39 (q,  $J = 7.2$  Hz, 2H,  $\text{CH}_2\text{CH}_3$ ), 2.04 (s, 15H,  $\text{C}_5\text{Me}_5$ ), 1.37 (s, 9H), 1.20 (s, 9H). 1.09 (t,  $J = 7.2$  Hz, 3H,  $\text{CH}_2\text{CH}_3$ ). Anal. Calcd. for  $\text{C}_{21}\text{H}_{38}\text{Cl}_2\text{N}_2\text{Zr}$ : C 51.04, H 7.76, N 5.55; Found: C 51.23, H 7.77, N 5.43, 180.1.

**Preparation of  $(\eta^5\text{-C}_5\text{Me}_5)\text{ZrMe}_2[\text{N}(t\text{-Bu})\text{C}(t\text{-Bu})\text{N}(\text{Et})]$  (**34**).** To a solution of **33** (0.72 g, 1.5 mmol) in 100 mL of  $\text{Et}_2\text{O}$  at  $-78$  °C, was added 1.93 mL (3.15 mmol) of MeLi in  $\text{Et}_2\text{O}$ . After slowly warming to RT within 2 h, the reaction was stirred for an additional hour before quenching with excess chlorotrimethylsilane, after which the volatiles were removed *in vacuo*. Extraction in pentane and filtration through a thin pad of Celite afforded a yellow solution, which upon concentration and cooling to  $-35$  °C afforded yellow crystals (0.46 g, 70%). For **34**:  $^1\text{H}$  NMR (400 MHz, benzene- $d_6$ ):  $\delta$  3.18 (q,  $J = 7.2$  Hz, 2H,  $\text{CH}_2\text{CH}_3$ ), 1.99 (s, 15H,  $\text{C}_5\text{Me}_5$ ), 1.35 (s, 3H,  $\text{CMe}_3$ ), 1.25 (s, 9H,  $\text{CMe}_3$ ), 1.05 (t,  $J = 7.2$  Hz, 3H,  $\text{CH}_2\text{CH}_3$ ), 0.08 (s, 6H,  $\text{ZrMe}_2$ ).  $^{13}\text{C}$   $\{^1\text{H}\}$  NMR (benzene- $d_6$ , 100 MHz, 298K):  $\delta$  180.1, 119.3, 55.8, 43.7, 40.7, 40.5, 34.4, 31.4, 19.1, 12.1. Anal. Calcd. for  $\text{C}_{23}\text{H}_{44}\text{N}_2\text{Zr}$ : C 62.79, H 10.10, N 6.37; Found: C 62.89, H 10.41, N 6.12.

**Preparation of  $(\eta^5\text{-C}_5\text{Me}_5)\text{ZrMe}_2[\text{R}_1\text{NC}(t\text{-Bu})\text{NR}_2]$  (**36-38**).** Same procedures were followed as the synthesis of **34**. Diisopropyl carbodiimide and dicyclohexenyl carbodiimide were purchased from Aldrich and used without further purification. *t*-butyl *i*-propyl carbodiimide was synthesized as reported.<sup>195</sup> For **36a**: 4.16 (dq, 2H), 2.05 (s, 15H), 1.27 (bm, 12H), 1.08 (s, 9H). For **37a**:  $\delta$  4.17 (m, 1H), 2.10(s, 15H),

1.44 (d, 3H), 1.41 (s, 9H), 1.24 (d, 3H), 1.22 (s, 9H). For **38a**:  $^1\text{H}$  NMR (400 MHz, benzene- $d_6$ ):  $\delta$  3.83 (m, 2H), 2.41 (m, 2H), 2.23 (m, 2H), 2.07 (s, 15H), 1.77 (m, 4H), 1.64 (m, 2H), 1.48 (m, 2H), 1.33 (m, 2H), 1.27-1.07 (m, 6H), 1.17 (s, 9H). For **36**:  $^1\text{H}$  NMR (400 MHz, benzene- $d_6$ ):  $\delta$  4.15 (dq, 2H), 2.00 (s, 15H), 1.18 (s, 9H), 1.12-1.11 (bm, 12H), 0.47 (s, 6H). For **38**:  $^1\text{H}$  NMR (400 MHz, benzene- $d_6$ ),  $\delta$  3.78 (m, 2H), 2.02 (s, 15H), 1.70-1.52 (m, 10H), 1.27 (s, 9H), 1.13 (m, 6H), 0.50 (s, 6H).

**Preparation of  $(\eta^5\text{-C}_5\text{Me}_5)\text{ZrMe}_2[\text{N}(t\text{-Bu})\text{C}(\text{Me})\text{N-CH}_2(t\text{-Bu})]$  (**39**).** Same procedures were carried out as the synthesis of **19**, while *t*-butyl neopentyl carbodiimide was used instead. Yield, 78%. For **39**:  $^1\text{H}$  NMR (400 MHz, benzene- $d_6$ ),  $\delta$  2.91 (s, 2H), 2.02 (s, 15H), 1.79 (s, 3H), 1.19 (s, 9H), 0.86 (s, 9H), 0.28 (s, 6H).

**Preparation of  $(\eta^5\text{-C}_5\text{Me}_5)\text{ZrCl}_2[\text{N}(t\text{-Bu})\text{C}(\text{Me})\text{N}(\text{Et})]$  (**40**).** At 0 °C, to a solution of *t*-BuN=C=NEt (0.253 g, 2.00 mmol) in 60 mL of Et<sub>2</sub>O, 1.31 mL of MeLi (1.60 M in Et<sub>2</sub>O) was added via a syringe. The reaction was stirred for 3 h. This clear solution was then transferred via cannula into a flask with  $(\eta^5\text{-C}_5\text{Me}_5)\text{ZrCl}_3$  (0.666 g, 2.00 mmol) in 40 mL of Et<sub>2</sub>O at -78 °C. The mixture was stirred for 12 h, and then volatiles removed *in vacuo*. The residue was extracted with toluene, filtered through a short pad of Celite, and all volatiles removed *in vacuo*. Yellow powder was obtained (0.84 g, 96 %). The compound is very clear and no further purification was required. For **40**:  $^1\text{H}$  NMR (400 MHz, benzene- $d_6$ ):  $\delta$  3.05 (q,  $J=7.2$  Hz, 2H,  $\text{CH}_2\text{CH}_3$ ), 2.06 (s, 15H,  $\text{C}_5\text{Me}_5$ ), 1.49 (s, 3H,  $\text{CCH}_3$ ), 1.23 (s, 9H,  $\text{CMe}_3$ ). 0.94 (t,  $J = 7.2$  Hz, 3H,  $\text{CH}_2\text{CH}_3$ ).  $^{13}\text{C}$   $\{^1\text{H}\}$  NMR (benzene- $d_6$ ):  $\delta$  173.2 ( $\text{CCH}_3$ ), 125.4 ( $\text{C}_5\text{Me}_5$ ), 54.3 ( $\text{CMe}_3$ ), 43.6 ( $\text{CH}_2\text{CH}_3$ ), 31.9 ( $\text{C}_5\text{Me}_5$ ), 16.8 ( $\text{CH}_2\text{CH}_3$ ), 15.5 ( $\text{CCH}_3$ ), 12.9 ( $\text{CMe}_3$ ).

Anal. Calcd. for C<sub>18</sub>H<sub>32</sub>Cl<sub>2</sub>N<sub>2</sub>Zr: C 49.28, H 7.37, N 6.39; Found: C 49.57, H 7.18, N 6.09.

**Preparation of ( $\eta^5$ -C<sub>5</sub>Me<sub>5</sub>)ZrCl(*i*-Bu)[N(*t*-Bu)C(Me)NEt] (41).** To a solution of 2.62 g (6.0 mmol) of **40** in 200 mL of Et<sub>2</sub>O at -78° C was added 2.8 mL (6.1 mmol) of 2.21 M *i*-BuMgCl in Et<sub>2</sub>O. After slowly warming to room temperature, the reaction mixture was stirred for an additional hour before the reaction was quenched with excess chlorotrimethylsilane, after which the volatiles were removed *in vacuo*. Extraction in toluene and filtration through a thin pad of Celite afforded a yellow solution, which upon concentration and cooling to -35° C afforded yellow crystals (2.55 g, 93%). For **41**, <sup>1</sup>H NMR: (benzene-*d*<sub>6</sub>, 400 MHz, 25 °C)  $\delta$  2.81 (dq, <sup>2</sup>*J* = 14.3Hz, <sup>3</sup>*J* = 7.2Hz, 1H), 2.67 (dq, <sup>2</sup>*J* = 14.3Hz, <sup>3</sup>*J* = 7.2Hz, 1H), 2.20 (nonet, <sup>3</sup>*J* = 6.4Hz, 1H), 2.00 (s, 15H), 1.71 (s, 3H), 1.33 (s, 9H), 1.32 (d, <sup>3</sup>*J* = 6.4Hz, 3H), 1.15 (d, <sup>3</sup>*J* = 6.4Hz, 3H), 0.83 (t, <sup>3</sup>*J* = 7.2Hz, 3H), 0.73 (dd, <sup>2</sup>*J* = 13.5Hz, <sup>3</sup>*J* = 6.4Hz, 3H), 0.01 (dd, <sup>2</sup>*J* = 13.5Hz, <sup>3</sup>*J* = 6.4Hz, 3H). <sup>13</sup>C {<sup>1</sup>H} NMR:  $\delta$ 173.7, 122.1, 77.9, 54.0, 43.2, 32.1, 30.9, 29.0, 27.9, 18.3, 15.9, 12.6. Anal. Calcd. for C<sub>22</sub>H<sub>41</sub>ClN<sub>2</sub>Zr: C 57.40, H 9.00, N 6.09; Found: C 57.36, H 8.90, N 5.89.

**Preparation of ( $\eta^5$ -C<sub>5</sub>Me<sub>5</sub>)ZrMe(*i*-Bu)[N(*t*-Bu)C(Me)N(Et)] (42):** To a solution of 0.55 g (1.2 mmol) of **41** in 40 mL of Et<sub>2</sub>O at -78° C was added 0.9 mL (1.2 mmol) of 1.38M MeLi in Et<sub>2</sub>O. After slowly warming to RT, the reaction mixture was stirred for an additional hour before the reaction was quenched with excess chlorotrimethylsilane, after which the volatiles were removed *in vacuo*. Extraction in pentane and filtration through a thin pad of Celite afforded a yellow solution, which

upon concentration and cooling to  $-35^{\circ}\text{C}$  afforded yellow crystals (0.37 g, 71%). For **42**:  $^1\text{H}$  NMR: (benzene- $d_6$ , 400 MHz,  $25^{\circ}\text{C}$ )  $\delta$  2.97 (dq,  $^2\text{J}=14.3\text{Hz}$ ,  $^3\text{J}=7.2\text{Hz}$ , 1H), 2.75 (dq,  $^2\text{J}=14.3\text{Hz}$ ,  $^3\text{J}=7.2\text{Hz}$ , 1H), 2.20 (m, 1H), 1.98 (s, 15H), 1.80 (s, 3H), 1.27 (d,  $^3\text{J}=6.4\text{Hz}$ , 3H), 1.20 (d,  $^3\text{J}=6.4\text{Hz}$ , 3H), 1.19 (s, 9H), 0.88 (t,  $^3\text{J}=7.2\text{Hz}$ , 3H), 0.41 (dd,  $^2\text{J}=13.1\text{Hz}$ ,  $^3\text{J}=6.4\text{Hz}$ , 3H), -0.25 (dd,  $^2\text{J}=13.1\text{Hz}$ ,  $^3\text{J}=6.4\text{Hz}$ , 3H). Anal. Calcd. for  $\text{C}_{23}\text{H}_{44}\text{N}_2\text{Zr}$ : %C

**Preparation of  $(\eta^5\text{-C}_5\text{Me}_5)\text{HfMe}_2[\text{N}(t\text{-Bu})\text{C}(\text{Me})\text{NEt}]$  (**43**).** To a suspension of 1.0 g (2.4 mmol) of  $(\eta^5\text{-C}_5\text{Me}_5)\text{HfCl}_3$  in 30 mL of  $\text{Et}_2\text{O}$ , 4.54 mL of MeLi (1.6 M in  $\text{Et}_2\text{O}$ ) were added at  $-35^{\circ}\text{C}$ . The mixture was allowed to warm gradually to room temperature, and stirred for an additional hour before 370  $\mu\text{L}$  (2.4 mmol) of 1-*tert*-butyl-3-ethylcarbodiimide was added. The reaction was allowed to stir overnight, then all volatiles removed in vacuo. Extraction in pentane and filtration through a thin pad of Celite afforded a white solution, which upon concentration and cooling to  $-40^{\circ}\text{C}$  afforded white crystals (0.66 g, 58%). For **43**:  $^1\text{H}$  NMR (400 MHz, benzene- $d_6$ ):  $\delta$  2.85 (q, 2H), 1.99 (s, 15H), 1.59 (s, 3H), 1.09 (s, 9H), 0.84 (t, 3H), -0.04 (s, 6H).  $^{13}\text{C}$   $\{^1\text{H}\}$  NMR (100 MHz, benzene- $d_6$ ):  $\delta$  172.9, 118.4, 52.5, 51.6, 40.7, 32.0, 17.0, 15.3, 11.4. Anal. Calcd. for  $\text{C}_{20}\text{H}_{38}\text{HfN}_2$ : C 49.53, H 7.90, N 5.78; Found: C 49.21, H 7.72, N 5.48.

**Preparation of  $\{(\eta^5\text{-C}_5\text{Me}_5)\text{Zr}(i\text{-Bu})[\text{N}(t\text{-Bu})\text{C}(\text{Me})\text{N}(\text{Et})]\}[\text{B}(\text{C}_6\text{F}_5)_4]$  cation:** To 31mg (3.9  $\mu\text{mol}$ ) of **42** was added a solution of 17 mg (3.7  $\mu\text{mol}$ ) of **18** in 0.9 mL of  $\text{C}_6\text{D}_5\text{Cl}$  to provide a clear, deep yellow solution.  $^1\text{H}$  NMR: (500 MHz,  $-10^{\circ}\text{C}$ )  $\delta$  3.05 (dq,  $^2\text{J} = 13.2\text{Hz}$ ,  $^3\text{J} = 6.8\text{Hz}$ , 1H), 3.04 (dq,  $^2\text{J} = 13.2\text{Hz}$ ,  $^3\text{J} = 6.8\text{Hz}$ , 1H), 1.99 (s, 3H), 1.87 (s, 15H), 1.61 (dd,  $^2\text{J} = 12.2\text{Hz}$ ,  $^3\text{J} = 3.7\text{Hz}$ , 1H), 1.16 (d,  $^3\text{J} = 5.5$ , 3H), 1.02

(s, 9H), 0.98 (d,  $^3J = 5.5\text{Hz}$ , 3H), 0.91 (t,  $^3J = 6.8\text{Hz}$ , 3H), 0.77 (dd,  $^2J = 12.2\text{Hz}$ ,  $^3J = 7.2\text{Hz}$ , 1H), -0.25 (m, 1H).

**$^1\text{H}$  NMR studies for mixture of **19** and **32**** (in the case of 1:1 ratio): To a small vial with 23.2 mg of **26** (25.1  $\mu\text{mol}$ ), was added a solution of 20.0 mg of **19** in 0.7 mL of chlorobenzene- $d_5$  at  $-10\text{ }^\circ\text{C}$ . The bright yellow solution was then transferred to a 5 mm NMR tube kept at  $-10\text{ }^\circ\text{C}$  cold bath. NMR spectrum was recorded at  $-10\text{ }^\circ\text{C}$  right after the generation of the cation. NMR spectra of different **19:32** ratio were carried out at the similar manner, by varying the amount of **19** used. (See Figure 16 for details.)

**General procedure for 1-hexene polymerizations:** All polymerizations were carried out inside a refrigerator with magnetic stirrer plate housed in a dinitrogen golvebox. Polymerization temperature was set to  $-10\text{ }^\circ\text{C}$  unless otherwise mentioned. Vials of 20 to 50 mL volume were used as polymerization reactor.

**MeDeT Kinetic analysis (Polymerization of 1-hexene):** To a solution of 40 mg (50  $\mu\text{mol}$ ) of **19** in 12 mL of chlorobenzene at  $-10\text{ }^\circ\text{C}$  was added a solution of 20 mg (50  $\mu\text{mol}$ ) of **18** in 8 mL of chlorobenzene also at  $-10\text{ }^\circ\text{C}$ , to produce a clear yellow solution. At this time 842 mg (10 mmol) of 1-hexene, pre-cooled to  $-10\text{ }^\circ\text{C}$ , was added all at once and the resulting mixture was allowed to stir for 2 h at  $-10\text{ }^\circ\text{C}$ , after which time, it was rapidly quenched by the addition of acidic methanol. The volatiles were then removed *in vacuo*, and the crude material was purified through

precipitation of a toluene solution into a large volume of acidic methanol. The final pure material was collected and dried overnight at 60 °C/0.01 mmHg. Polymerizations of 1-hexene using other [19]/[18] ratios were conducted in an identical manner by varying only the amount of **19** that was used.

**Synthesis of *a*-PH-*b*-*iso*-PO:** Using the standard polymerization procedure from above, 420 mg (5 mmol) of 1-hexene was polymerized using a [19]/[18] ratio of 2.0. After 2 h, an aliquot was removed for NMR and GPC analysis. Then, an additional 40 mg (50 μmol) of **18** was added, allowed to gestate for 5 min, and 560 mg (5 mmol) of 1-octene (pre-cooled to –10 °C) was added all at once. After another 3 h at –10 °C, the reaction was rapidly quenched by the addition of acidic methanol. The volatiles were then removed *in vacuo*, and the crude material was purified through precipitation of a toluene solution into a large volume of acidic methanol. The final pure material was collected and dried overnight at 60 °C/0.01 mmHg. Yield: 0.87 g (88%).

**Polymeryl cation <sup>13</sup>C NMR studies:** At –10 °C, 5 mg of **42** (11 μmol) was dissolved in 0.6 g of C<sub>6</sub>D<sub>5</sub>Cl. The solution was added to 9 mg (11 μmol) of **18** at –10 °C. The yellow solution was then added to 5 mg of **42\*** (11 μmol), and then added to 20 mg of 1-hexene (0.23 mmol). The solution was rapidly transferred to a 5 mm NMR tube. NMR was recorded at –10 °C (125 MHz).

**2D-<sup>13</sup>C NMR EXSY of <sup>13</sup>CH<sub>3</sub>-labeled **42\***:** NMR was recorded at –10 °C in C<sub>6</sub>D<sub>5</sub>Cl. The mixing time was varied from 0.2s to 0.8s.

**Preparation of 1-<sup>13</sup>C-1-dodecene.** To 3.89 g of Ph<sub>3</sub>P<sup>13</sup>CH<sub>3</sub>I (9.60 mmol) in 40 mL of THF at room temperature, 4.62 mL of *n*-BuLi (9.60 mmol) in ether was added slowly. The mixture was stirred for 30 min, then 1.635 g of undecyl aldehyde (9.60 mmol) in 10 mL of THF was added via a syringe. After stirring for 2 h, 5 mL of saturated NH<sub>4</sub>Cl solution was used to quench the reaction, followed by washing with saturated NH<sub>4</sub>Cl 3 times (30 mL each). Diethyl ether was used for extraction, then the organic layer dried by MgSO<sub>4</sub>. The crude product was vacuum transferred to remove the byproduct triphenylphosphine oxide, after all the volatiles were removed *in vacuo*. Crude yield 1.265 g (77.8 %). The product was finally vacuum transferred from NaK alloy prior to polymerization studies.

**1-Dodecene studies** (Figure 23):

1). At -10 °C, 10 mg of **19** (0.025 mmol) was dissolved in 0.6 g of C<sub>6</sub>D<sub>5</sub>Cl and the solution was cooled to -10 °C. The solution was then added to 20 mg (0.025 mmol) of **18** at -10 °C. The yellow solution was then added to 43 mg (0.25 mmol) of 1-<sup>13</sup>C-1-dodecene at -10 °C. The mixture was rapidly transferred to a 5 mm NMR tube. <sup>13</sup>C{<sup>1</sup>H} NMR (125 MHz) was recorded at -10 °C.

2). Zirconium polymeryl cation was generated same procedure as above. To the polymeryl cation solution, 11 mg (0.025 mmol) of **42** was introduced and the mixture was mixed for 2 min, then 20 mg (0.025 mmol) of **18** was added at -10 °C. The mixture was rapidly transferred to a 5 mm NMR tube. <sup>13</sup>C{<sup>1</sup>H} NMR (125 MHz) was recorded at -10 °C.

**Experiment to exclude polymer chain transfer MeDeT mechanism.**

1). At  $-10\text{ }^{\circ}\text{C}$ , 20 mg (0.045 mmol) of **42** was dissolved in 20 mL of chlorobenzene. To the solution, 19 mg of **18** (0.023 mmol) was added at  $-10\text{ }^{\circ}\text{C}$  followed with 153 mg of 1-hexene (1.82 mmol). The mixture was allowed to stir for 1 hr at  $-10\text{ }^{\circ}\text{C}$ , then the polymerization was quenched with acidic methanol. The polymer was purified by precipitation in a large quantity of methanol, followed by drying *in vacuo*. Yield: 88.0 %

2). Same polymerization was carried out, except **42\*** was used instead of non-labeled compound. Yield 92 %.

**Experiment of the 4 distinguish exchanging species in DT (Figure 21 and Scheme 30):**

1). At  $-10\text{ }^{\circ}\text{C}$ , 5 mg of  $^{13}\text{C}$  labeled **42** (0.011 mmol) was dissolved in 0.6 g of  $\text{C}_6\text{D}_5\text{Cl}$ . The solution was added to a vial with 9 mg (0.011 mmol) of **18** at  $-10\text{ }^{\circ}\text{C}$ . The yellow solution was then added to 5 mg of **42** (0.011 mmol), and then added to 20 mg of 1-hexene (0.23 mmol). The solution was rapidly transferred to a 5 mm NMR tube.  $^{13}\text{C}\{^1\text{H}\}$  NMR (125 MHz) was recorded at  $-10\text{ }^{\circ}\text{C}$ .

2). At  $-10\text{ }^{\circ}\text{C}$ , 10 mg of **42** (0.023 mmol) was dissolved in 0.6 g of  $\text{C}_6\text{D}_5\text{Cl}$ . The solution was added to a vial with 19 mg (0.023 mmol) of **18** at  $-10\text{ }^{\circ}\text{C}$ . The yellow solution was then added to 20 mg of 1-hexene (0.23 mmol). The solution was kept at  $-10\text{ }^{\circ}\text{C}$  for 30 min, then 10 mg of **42\*** ( $^{13}\text{CH}_3\text{-Zr}$  labeled) (0.023 mmol) was added at  $-10\text{ }^{\circ}\text{C}$ . The mixture was quickly transferred to a 5 mm NMR tube.  $^{13}\text{C}\{^1\text{H}\}$  NMR (125 MHz) was recorded at  $-10\text{ }^{\circ}\text{C}$ .

**NMR of  $\{(\eta^5\text{-C}_5\text{Me}_5)\text{HfMe}[\text{N}(t\text{-Bu})\text{C}(\text{Me})\text{N}(\text{Et})]\}\text{[B}(\text{C}_6\text{F}_5)_4\text{]}$ :** To a suspension of 18 mg (20  $\mu\text{mol}$ ) of **43** in 0.5 mL of chlorobenzene- $d_5$ , a solution of 20  $\mu\text{mol}$  of **18** in 0.2 mL of chlorobenzene- $d_5$  was added at  $-10\text{ }^\circ\text{C}$ . The clear yellow solution was then transferred to a 5mm NMR tube kept at a  $-10\text{ }^\circ\text{C}$  cold bath. Spectrum was taken at 400 MHz NMR at  $25\text{ }^\circ\text{C}$ .  $^1\text{H}$  NMR (400 MHz, chlorobenzene- $d_5$ ,  $25\text{ }^\circ\text{C}$ ):  $\delta = 3.06$  (dq, 1H,  $^2J = 12.8\text{ Hz}$ ,  $^3J = 7.2\text{ Hz}$ ,  $\text{CH}_2\text{CH}_3$ ), 3.02 (dq, 1H,  $^2J = 12.8\text{ Hz}$ ,  $^3J = 7.2\text{ Hz}$ ,  $\text{CH}_2\text{CH}_3$ ), 1.96 (s, 3H,  $\text{CMe}$ ), 1.79 (s, 15H,  $\text{C}_5\text{Me}_5$ ) 0.88 (s, 9H,  $\text{CMe}_3$ ), 0.72 (t, 3H,  $^2J = 7.2\text{ Hz}$ ,  $\text{CH}_2\text{CH}_3$ ), 0.14 (s, 3H,  $\text{HfMe}$ ).

**Kinetic analysis of 1-hexene polymerization using 43:** To a solution of 120.2 mg (150  $\mu\text{mol}$ ) of **18** in 16.25 mL of chlorobenzene at  $-10\text{ }^\circ\text{C}$ , was added a solution of 72.8 mg (150  $\mu\text{mol}$ ) of **43** in 5 mL of chlorobenzene at  $-10\text{ }^\circ\text{C}$ . To this mixture, 2.53 g of 1-hexene was added all at once. Aliquots were quenched with silica gel after different time intervals over the next 31 hours. 1-Hexene concentrations were measured by GC using the polymerization solvent chlorobenzene as the internal standard.

**Polymerization of 1-hexene under 100% activation conditions using 43:** To a solution of 48.0 mg (60  $\mu\text{mol}$ ) of **18** in 8 mL of chlorobenzene at  $-10\text{ }^\circ\text{C}$ , was added a solution of 29.1 mg (60  $\mu\text{mol}$ ) of **43** in 2mL of chlorobenzene at  $-10\text{ }^\circ\text{C}$ . To this mixture 1.01 g (12 mmol) of 1-hexene was added all at once and resulting mixture was allowed to stir for 31 h at  $-10\text{ }^\circ\text{C}$ , after which time it was rapidly quenched by the addition of acidic methanol. The volatiles were then removed under vacuum, and the crude material was purified through precipitation of a toluene solution into a large

volume of acidic methanol. The final pure material was collected and dried overnight at 60 °C/0.01 mmHg.  $M_n$  18 610, PDI 1.08, yield 0.90g (90%).

Polymerization of 1-hexene under DT conditions (50% activation): To a solution of 24.0 mg (30  $\mu$ mol) of **43** in 8 mL of chlorobenzene, was added a solution of 29.1 mg (60  $\mu$ mol) of **18** in 2 mL of chlorobenzene at -10 °C. To this mixture, 1.01 g (12 mmol) of 1-hexene was added all at once and the resulting mixture was allowed to stir for 64 h at -10 °C, after which time it was rapidly quenched by the addition of acidic methanol. The volatiles were removed in vacuo and the crude material was purified through precipitation of a toluene solution into a large volume of acidic methanol. The final pure material was collected and dried overnight at 60 °C/0.01 mmHg.  $M_n$ : 11 600, PDI: 1.27, yield 0.72 (71 %)

**Kinetic analysis of 1-hexene polymerization under DT conditions:** To a solution of 36.1 mg (45  $\mu$ mol) of **18** in 5.75 mL of chlorobenzene at -10 °C, was added a solution of 43.7 mg (90  $\mu$ mol) of **43** in 2 mL of chlorobenzene at -10 °C. To this mixture, 1.515 g (18 mmol) of 1-hexene was added all at once. Aliquots were quenched with silica gel after different time intervals over the next 30 h. 1-Hexene concentrations were detected by GC. Total initial volume of the polymerization was 10 mL. Different percentage activation kinetic experiments were carried out by the same manner, by varying the initial amount of **43**.

## Chapter 3 Chloride Group Degenerative Transfer Ziegler-Natta Polymerization

### ChloDeT

#### 3.1 Background

As described in Chapter 2, methyl group degenerative transfer (MeDeT) living Ziegler-Natta polymerization occurs when pre-catalyst **19** is activated by a substoichiometric amount of the co-catalyst **18**. Due to the dynamic configuration of the neutral polymeryl methyl zirconium, the loss of the metal chirality leads to the loss of stereospecificity of the polymerization. The methyl group exchange ( $R_{ex}$ ) is much faster than the monomer propagation ( $R_p$ ), which is critical for the narrow polydispersity observed in all the MeDeT polymerizations. Also, the metal center epimerization ( $R_{epi}$ ) is faster than the propagation, thus a nearly atactic polyolefin is obtained.

The MeDeT process can decrease the amount of co-catalyst required for the polymerization, at the expense of a slightly decreased polymerization rate. Also, with a lower concentration of the active species in solution, certain microstructures that cannot be generated by fully activated Ziegler-Natta polymerization systems would be possible, i.e., comb polymers, or star polymers as shown in Figure 30. For comb polymers, if all the branches have a cationic propagating species, and each propagating center has a bulky non-coordinating borate counteranion, the local environment will be unfavorable due to the steric and electronic interactions. One solution is the application of degenerative transfer to lower the cationic concentration.

Since MeDeT only gives atactic polyolefin, question arises that whether a stereospecific degenerative transfer exists.

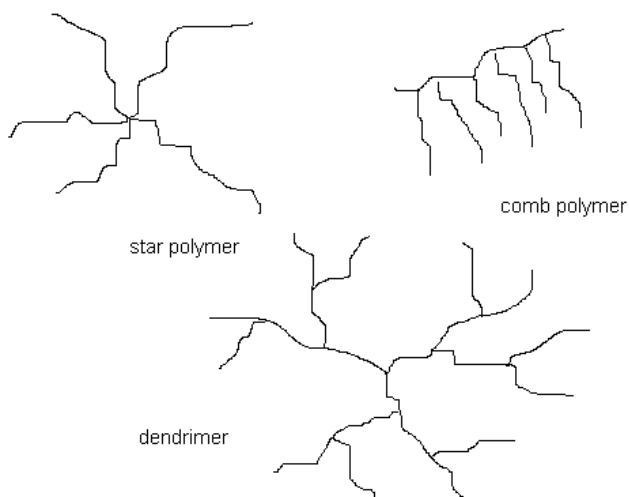


**Figure 30. Polymers with Different microstructures.**

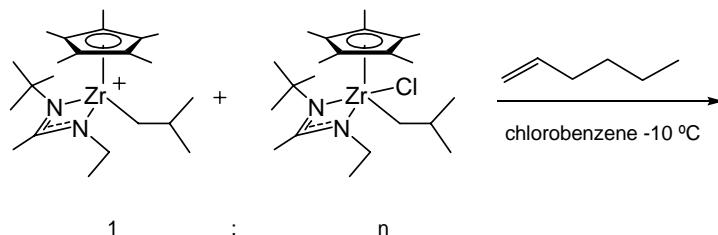
An alkyl chloro amidinate zirconium is configurationally stable. The short bond length between the amidinate ligand and the metal center blocks the potential epimerization of the ligand. Also, chloride bridged zirconium complexes have been observed independently by different research groups.<sup>162,196-198</sup> All these factors led us to explore the feasibility a chloride group degenerative transfer (ChloDeT) polymerization, though a zirconium chloride bond is considered to be much stronger than a zirconium methyl bond.

### **3.2 Stereospecific Degenerative Transfer Living Polymerization**

To test the hypothesis, a polymerization using **42** as the pre-catalyst, activated by **18** was carried out. With a 1:1:1 ratio of **41:42:18** at  $-10\text{ }^{\circ}\text{C}$ , a 1:1 molar ratio of zirconium cation and an alkyl chloride neutral species were generated. 4 h after 200

equivalents of 1-hexene were introduced, PH with  $M_n$  of 13 300 and PDI of 1.05 was obtained with 95% yield (cf. 200 DP PH typically gives a  $M_n$  of 22 000 to 24 000 based on polystyrene standards run under the GPC setting). First, compared to the polymerization without alkyl chloride **41**, a polymer with only half the  $M_n$  was obtained with 95% yield. Second, the narrow polydispersity of the polymer indicates all the zirconium centers are active, though 50% of the zirconium centers were neutral initially.

As shown in Scheme 33, by keeping the amount of **42** and **18** as constants and varying the amount of **41**, polymerizations were carried out. Detailed data and  $M_n$  vs. [Zr] plot is shown in Table 6 and Figure 31.



**Scheme 33. ChloDeT polymerization using *i*-Bu derivatives **42**.**

**Table 6.  $M_n$  and PDI results for different zirconium concentration.**

$[M]_0/[41 + 42]$	$M_n$	PDI
50	5 600	1.05
80	10 500	1.04
100	13 300	1.05
120	14 000	1.04
160	20 600	1.04
200	23 800	1.03

Similar to MeDeT, for each polymerization with a different ratio of (**41** + **42**) : **18**, a narrow polydispersity was obtained. This indicates that all the polymerizations are living under different neutral alkyl chloride zirconium concentrations. Second, it suggests that a chloride group degenerative transfer is possible and the chloride exchange between two zirconium species is much faster than the monomer propagation.

Since all the zirconium species involved are configurationally stable, no epimerization occurs during the polymerization, which means theoretically, an *iso*-PH should be obtained. <sup>13</sup>C {<sup>1</sup>H} NMR of the polymer obtained shows six sharp singlets, which confirms the isotactic microstructure of the PH. Also, no vinyl end groups were observed in the <sup>1</sup>H NMR spectrum of the polymer as the polymerization is living.

<sup>1</sup>H NMR studies of the zirconium cations were carried out. First, the neutral *i*-butyl chloro zirconium **41** NMR is detected at -10 °C in *C*<sub>6</sub>*D*<sub>5</sub>*Cl*. As shown in the top of Figure 32, two distinguishable peaks are assignable to the methylene protons (3.09 and 3.28 ppm) adjacent to the amidinate nitrogen (NCH<sub>2</sub>CH<sub>3</sub>), due to the lack of amidinate flipping. An equal molar amount of co-catalyst **18** is used to activate **42**, the fully activated cation spectrum is shown in the middle of Figure 32. Two peaks are observed for the methylene (NCH<sub>2</sub>CH<sub>3</sub>) protons, again. If one equivalent of **41** is added to the fully activated cation, only one set of peaks is observed, which is the time average of the species in the mixture. This indicates the extremely fast exchange on the NMR time scale between the cation and **41**. Based on the equation<sup>178</sup> PDI =

$$\frac{M_w}{M_n} = 1 + \left(\frac{2}{p} - 1\right) \frac{2k_p}{k_{ex}}, \text{ narrow polydispersity is expected for all the polymers.}^{199}$$

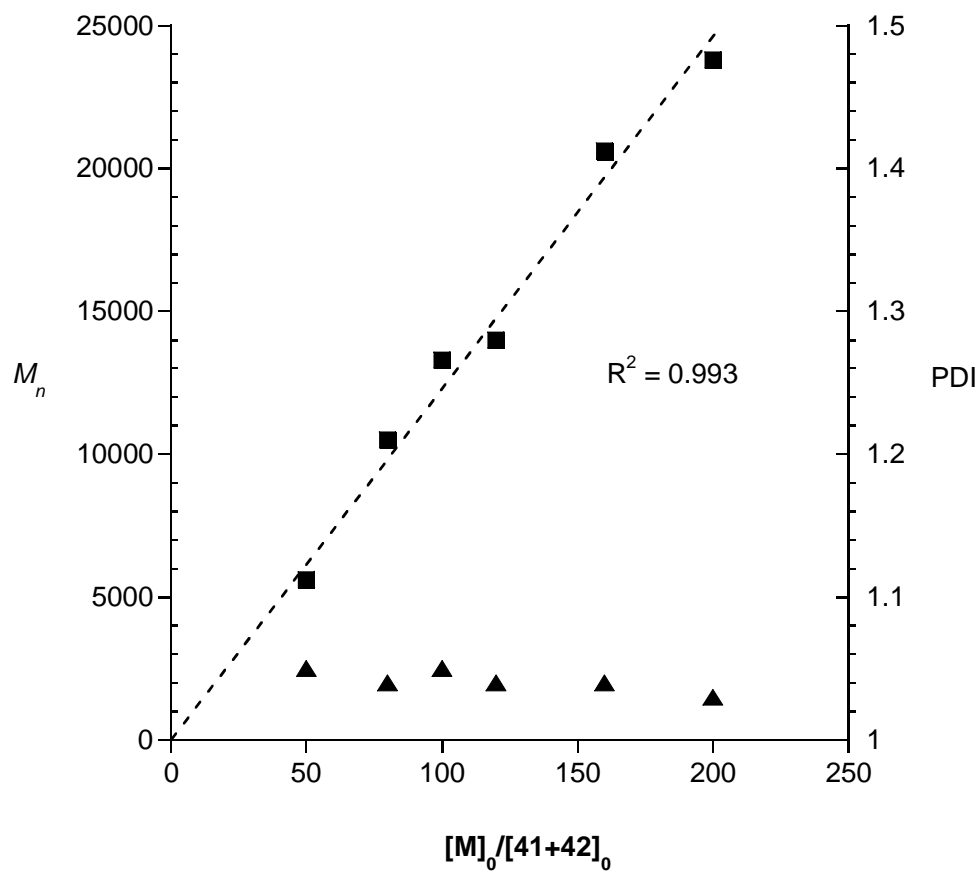
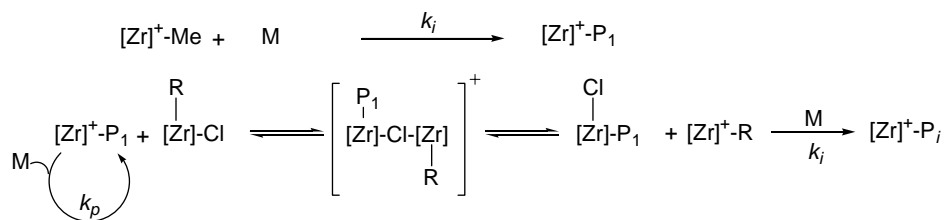
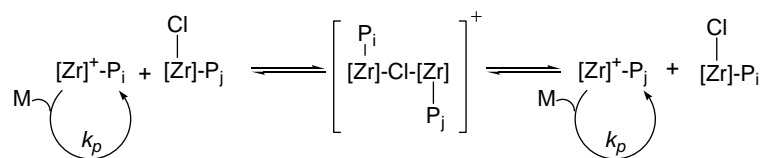


Figure 31. Dependence of poly(1-hexene)  $M_n$  (■) and PDI (▲) values on  $[M]_0/[Zr]_{total}$  at constant  $[M]_0 = 0.50$  M and  $[18] = 2.5$  mM.

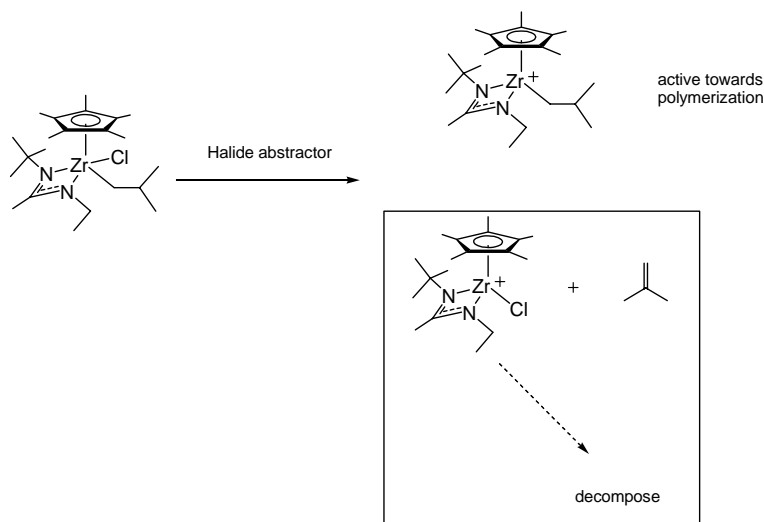
### Initiation



### Chloro-Bridged Degenerative Transfer & Propagation



Scheme 34. Chloride group degenerative transfer polymerization mechanism.



Scheme 35. Potential reactions for halide abstraction, counteranion borate omitted for clarity.

### 3.3 Halide Abstraction Reagents

To further the applications of ChloDeT, a halide abstractor is highly desirable. Attempt to use  $\text{SbCl}_5$ ,  $\text{AlCl}_3$ ,  $\text{K}[\text{B}(\text{C}_6\text{F}_5)_4]$ ,  $\text{Ag}[\text{B}(\text{C}_6\text{F}_5)_4]$ ,  $\text{Li}[\text{B}(\text{C}_6\text{F}_5)_4]$ ,  $\text{Na}[\text{BAR}^{\text{F}}_4]$

<sup>200</sup>, Tl[BAr<sup>F</sup><sub>4</sub>], [Me<sub>4</sub>N][BAr<sup>F</sup><sub>4</sub>] and [Me<sub>4</sub>N][BAr<sup>F</sup><sub>4</sub>] all failed. None of these salts are strong enough to pull the chloride off from the zirconium. One promising candidate is **26**. While **26** does abstract the chloride, but also pulls the alkyl group off from the zirconium. A polymerization using **41** as the initiator, activated by **26** gives a PH with  $M_n$  of 48 400 and PDI of 1.11, when 200 equivalents of monomer is used. This suggests that a large amount of **41** is initially deactivated by pulling  $\beta$ -hydrogen off from the *i*-Bu group, as shown in Scheme 35.

Considering the strong Si-Cl bond,<sup>201</sup> a silylium perfluorophenyl borate [Et<sub>3</sub>Si][B(C<sub>6</sub>F<sub>5</sub>)<sub>4</sub>] (**44**) was tested. For 200 equivalents of 1-hexene, a 2:1 ratio of **41:44** at -10 °C provided an *iso*-PH with  $M_n$  and PDI values of 24 000 and 1.02, respectively, which are very close to the expected values. Unfortunately, halide abstraction via **44** is not chemospecific, either. Compound **44** tends to react with a very small amount of *i*-Bu group as shown in Scheme 35.

Attempts to use **58** gave very promising results, since no alkyl abstraction is observed. But the heterogeneous nature of the halide abstraction reaction and the complicated process of filtration of **58** off from the polymerization system at low temperature greatly limit the application of **58** as an ideal halide abstraction reagent.

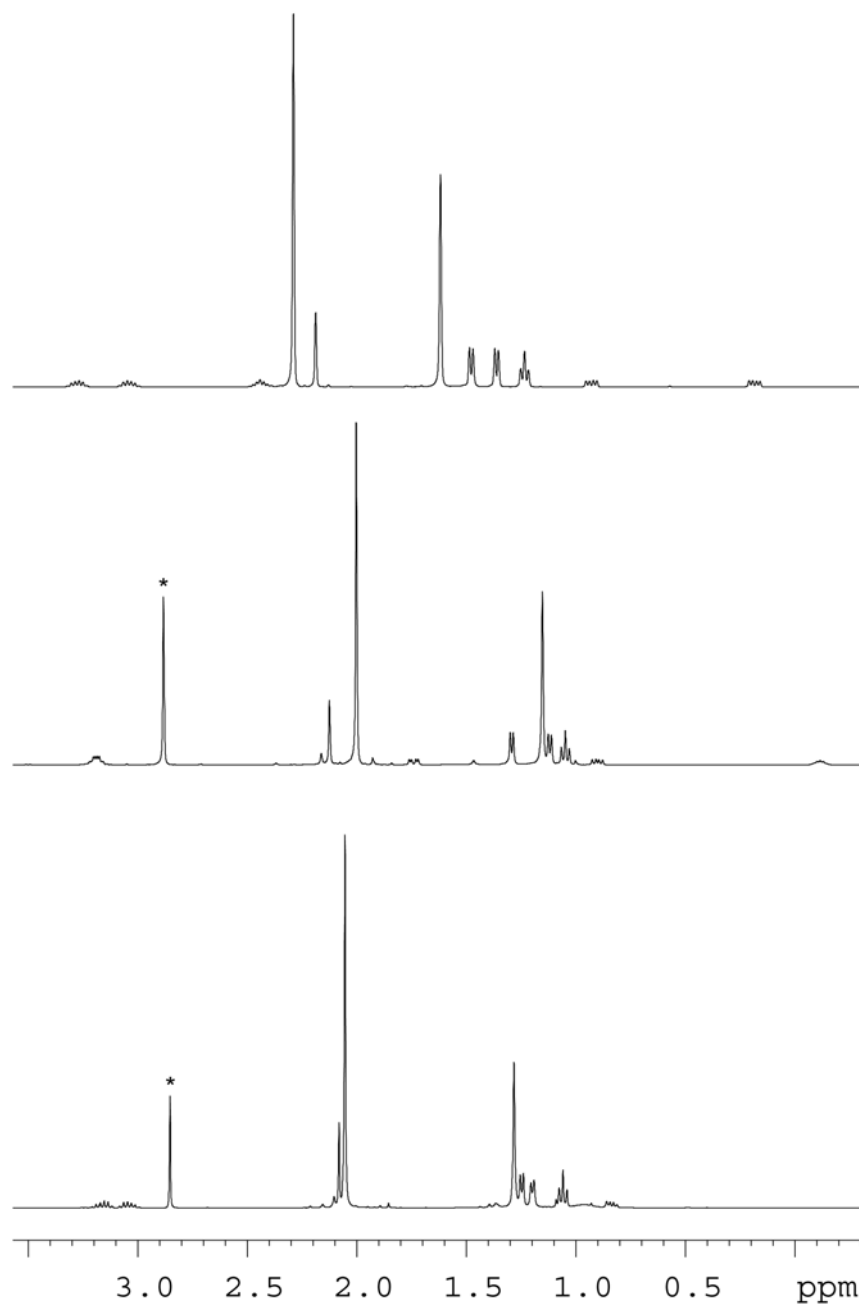


**Figure 32.**  $^1\text{H}$  NMR (400 MHz, chlorobenzene- $d_5$ ,  $-10\text{ }^\circ\text{C}$ ) spectra of 41 (top), 1:1 of 42:18 (middle) and a 1:1:1 mixture of 41, 42 and 18 (bottom). The peaks with asterisks are  $\text{PhNMe}_2$ .

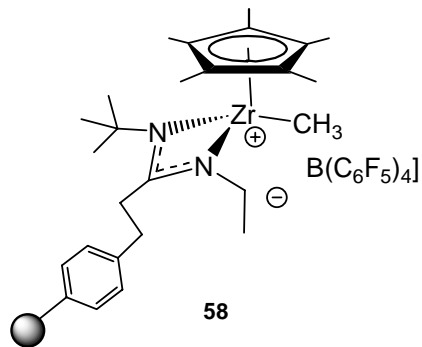
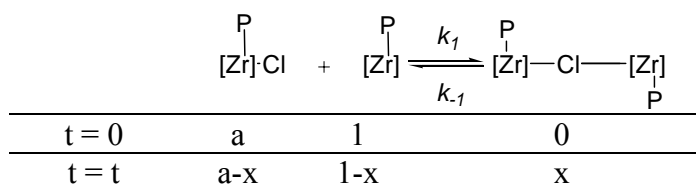


Figure 33. Potential de-chloro reagent

### 3.4 Kinetic of ChloDeT

Similar to MeDeT, detailed kinetic studies were carried out with different percentage of activation, from 10% to 100%. The rate constants of  $k_p$  and  $k_t$  for different activation are shown in Table 7. A very similar trend is observed compared to the MeDeT. First, for each activation, a linear plot indicates the living nature of the polymerization.<sup>202</sup> Polymerization rate decreases with lower activation. At 50% activation,  $k_p$  decreases only 9%, while for MeDeT, a 42% decrease was observed.



$$\text{then } K = \frac{k_1}{k_{-1}} = \frac{x}{(a-x)(1-x)}$$

$$1-x = \frac{1-a - \frac{1}{K} + \sqrt{(a+1 + \frac{1}{K})^2 - 4a}}{2}, \quad (9)$$

$K$ : equilibrium constant

Based on equation 9, similar simulation as MeDeT<sup>203</sup> was carried out, and as shown in Figure 34. A best fit with  $K$  of 0.13 and the observed rate constant under different activation was shown in Figure 34.  $K$  of 0.13 indicates the disfavor of chloride-bridged dimer in the polymerization solution since  $K = k_1/k_{-1}$ .

**Table 7. Different rate constants of polymerization under different activations%**

Activation %	[ <b>41</b> ] <sub>0</sub> (mM)	$k_p$ (s <sup>-1</sup> M <sup>-1</sup> )	$k_t$ (s <sup>-1</sup> )	R <sup>2</sup>
100	0	0.256	2.52 10 <sup>-5</sup>	0.999
50	1.56	0.255	4.14 10 <sup>-5</sup>	0.991
36	2.72	0.239	3.88 10 <sup>-5</sup>	0.991
25	4.68	0.199	3.01 10 <sup>-5</sup>	0.997
18	7.12	0.153	1.12 10 <sup>-5</sup>	0.994
10	14.04	0.098	2.32 10 <sup>-5</sup>	0.995

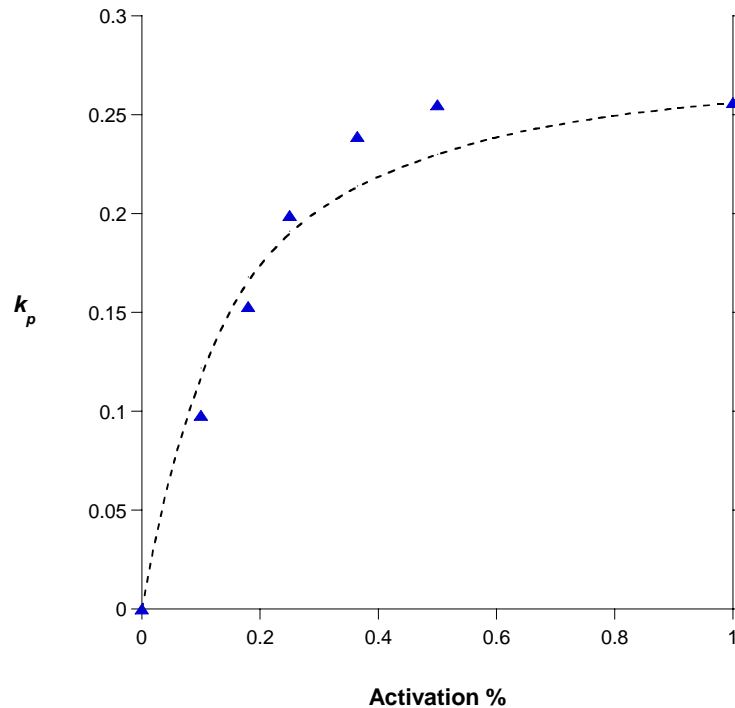


Figure 34.  $k_{\text{obs}}$  vs. percentage activation, dotted line is the simulation with  $K = 0.13$ .

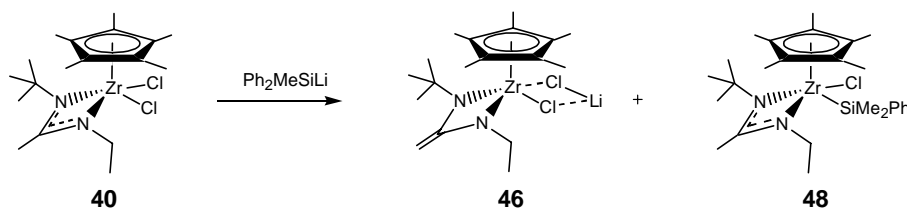
### 3.5 Applications of ChloDeT

The advantage of ChloDeT vs. regular polymerization is the lower concentration of the active species during the polymerization. Similar to living/controlled radical polymerization,<sup>170-173,204</sup> lower concentration of the propagating species lowers possibility of the potential disproportionation and other side reactions.

As mentioned before, the serious electrostatic interaction for a comb polymer will slow down, or even shut down the polymerization, if each branch has one cationic propagating center. Since chloride exchange between the dormant species and the active species is extremely fast, for a star polymer, or comb polymer, there's no need to activate all the propagating centers if ChloDeT applied. Based on the kinetic data, mere 20% activation still maintains 50% activity.

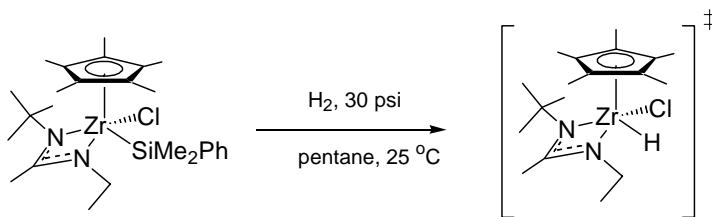
To prove the concept, a dinuclear zirconium chloride **50** is synthesized by hydrozirconation of 1,5-hexadiene, of which the methodology was developed by our group (see appendix for details).<sup>205</sup>

The transient hydrido-chloride zirconium shown in Scheme 37 is generated *in situ* by hydrogenolysis of Zr-Si bond when dimethylphenylsilyl zirconium (**48**) was charged with 30 psi of hydrogen. Compound **48** was generated by salt elimination between **40** and PhMe<sub>2</sub>SiLi in Et<sub>2</sub>O. It is worth noting that a 1:2 molar ratio of deprotonation (*vide infra*) vs. substitution was observed, if the reaction is carried out in THF. The polarity and the coordination ability of the solvent could be a possible explanation.



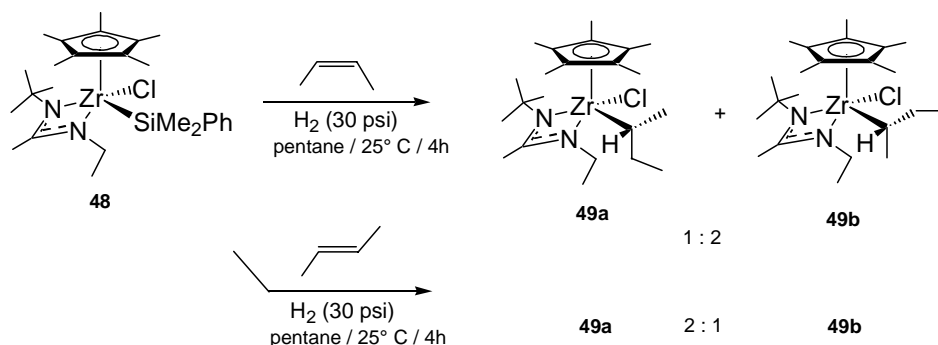
Solvent	Product ratios	
THF	67	: 33
Et <sub>2</sub> O	0	: 100

**Scheme 36. Deprotonation vs. substitution**



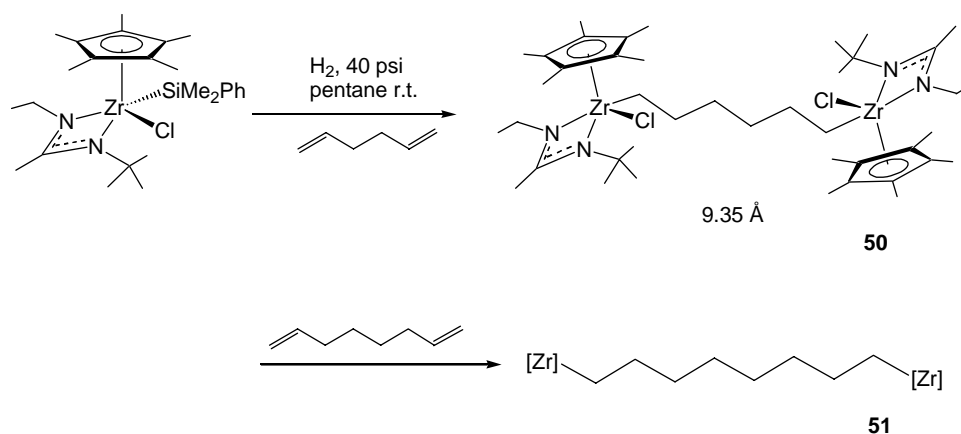
**Scheme 37. Hydrogenolysis of Zr-Si bond.**

The hydridochloride is very reactive and has similar reactivity as the Schwartz reagent.<sup>206-208</sup> In the presence of external or internal olefins, the hydride and zirconium can be added to a double bond via *cis* insertion.

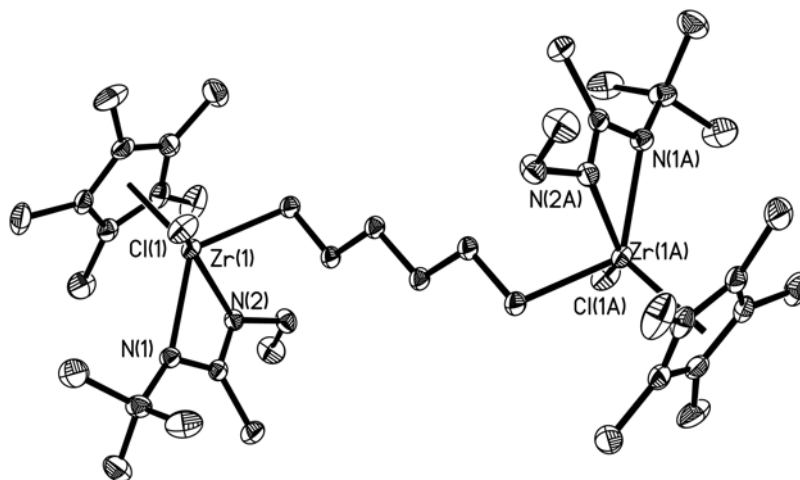


**Scheme 38. Examples of the hydrozirconation of pro-chiral substrates.**

A crystal structure of the dimer **50** is shown in Figure 35. The model complex **50** has an *i* symmetry, and the distance between two zirconium centers is 9.35 Å. Complex **51**, with longer linker, a  $C_8$  unit was prepared using the same methodology. But unfortunately, attempts to grow single crystals suitable for X-ray diffraction failed for an accurate distance between two zirconium centers.



**Scheme 39. Synthesis of the dinuclear initiators**



$$\text{Zr(1)-Zr(1A)} = 9.35 \text{ \AA}$$

Figure 35. X-ray structure of the dinuclear initiator.

The polymerization of 1-hexene was carried out using **50** as the pre-catalyst when half activated by **44** as the co-catalyst. When 400 equivalents of 1-hexene was used and a PH with slight high  $M_n$  of 53 800 and PDI of 1.16 (a theoretical  $M_n$  of 44 000 is expected<sup>209</sup>.) was obtained. Unfortunately, the GPC trace shows that the polymer is bi-modal, which means there are at least two propagating species involved. A potential explanation is that co-catalyst **44** is not a chemospecific halide abstraction reagent, and a small amount of the dimer may possibly be deactivated as shown in Scheme 40. Also, potential  $\beta$ -hydride elimination will take part of the propagating centers out of the polymerization, thus increase the molecular weight. The  $\beta$ -hydride elimination of the **50** generates a zirconium hydride and a 5-hexenyl zirconium species, which undergoes cyclization<sup>124</sup> to form a methylene cyclopentane intermediate.<sup>210</sup> This cationic intermediate is proven to be an active initiator for further 1-hexene polymerization.

Since the dimer is 50 % activated, statistically, there is 25% chance for the initiator to be di-cationic. The electronic and steric interactions between the non-coordinate counteranions and the two propagating centers could be the driving force of the  $\beta$ -hydride elimination.

To minimize these negative effects, a model complex **52** was synthesized, which is a dinuclear zirconium methyl initiator with a C<sub>6</sub> linkage, synthesized by methylating of compound **50**. When 25% of the initiator was activated by **18**, polymerization of 200 equivalents of 1-hexene produced a PH with  $M_n$  of 21 400 and PDI of 1.09, and a yield of 60%. However, GPC trace shows a bi-modal pattern, though the application of **52** circumvented the possibility of any alkyl abstraction by **44**.

Similar experiment with C<sub>8</sub> linkage shows almost identical result. These results indicate that the side reaction shown in Scheme 40 is inevitable, probably due to the limited distance and strong interaction between two zirconium species. This suggests that to make a star polymer by coordination polymerization, the propagating cationic centers on the branches should have a distance long enough to prevent the possible  $\beta$ -hydride elimination prompt by interaction between the cationic centers. Compared to radical, cationic/anionic polymerizations, where a bulky counteranion is not necessary, Ziegler-Natta polymerization may not be the ideal way to make star polymers or comb polymers, but the benefit of ultimate stereo control for Ziegler-Natta polymerization is *irreplaceable*. Some potential cores for these polymers are shown in Figure 36, and the application of these rigid cores is under further investigation.

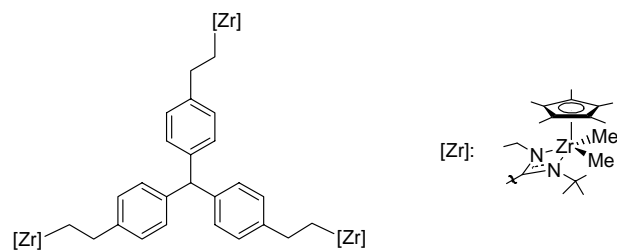
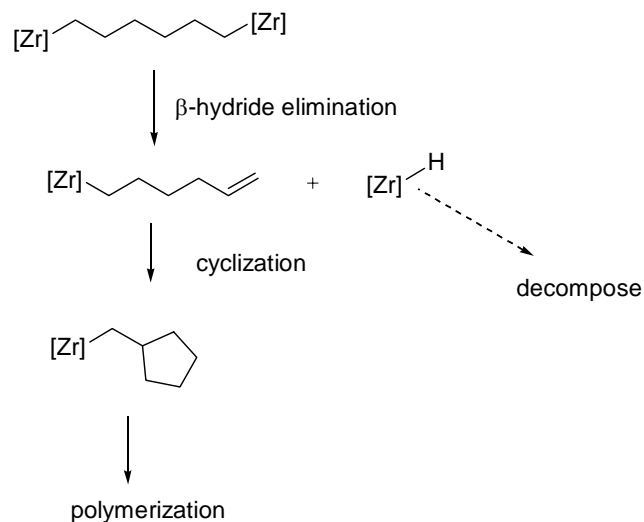


**Figure 36. Potential core for a tri-arm star polymer.**



**Scheme 40. Potential mechanism for the dimer initiator polymerization.**

### 3.6 Conclusion

A living chloride group degenerative transfer Ziegler-Natta polymerization ChloDeT is discovered. Similar to MeDeT, an extremely fast exchange between the dormant and the active species is observed. For all different dormant to active ratios, living polymerizations with narrow polydispersity polymer were observed. The dimerization of the active species and the dormant species are under equilibrium, with an equilibrium constant  $K$  of 0.13, indicating the system disfavors the formation of the dimer during the propagation. Silylium borate **44** was used as an efficient, but not chemospecific, halide abstractor. Finally, ChloDeT is applied to the synthesis of a

two-arm PH, of which the polymerization core **50** was generated from hydrozirconation of 1,5-hexadiene. However, attempt to synthesize a well-defined two-arm polymer was not successfully, probably due to the  $\beta$ -hydride eliminations prompted by the strong interactions between the cationic propagating centers.

### 3.7 Experimental

**Polymerization of 1-hexene** (in the case where  $[M]_0/[41 + 42] = 100:1$ ): To a solution of 20 mg (25  $\mu$ mol) of **18** in 6 mL of chlorobenzene at  $-10$  °C was added a solution of 11 mg (25  $\mu$ mol) of **42** in 4 mL of chlorobenzene also at  $-10$  °C, followed by 11.5 mg (25  $\mu$ mol) of **41**. After 5 min, 0.421 g (5.0 mmol) of 1-hexene, pre-cooled to  $-10$  °C, was added all at once and the resulting mixture was allowed to stir for 4 h at  $-10$  °C, after which time it was rapidly quenched by the addition of methanol. The volatiles were then removed *in vacuo*, and the crude material was purified through precipitation of a toluene solution into a large volume of acidic methanol. The final pure material (0.40 g, yield 95 %,  $M_n = 13,300$ , PDI = 1.05) was collected and dried overnight at  $60$  °C/0.01 mmHg. Polymerizations of 1-hexene using other  $[M]_0/[Zr]_{total}$  ratios were conducted in an identical manner by varying only the amount of **41** that was used.

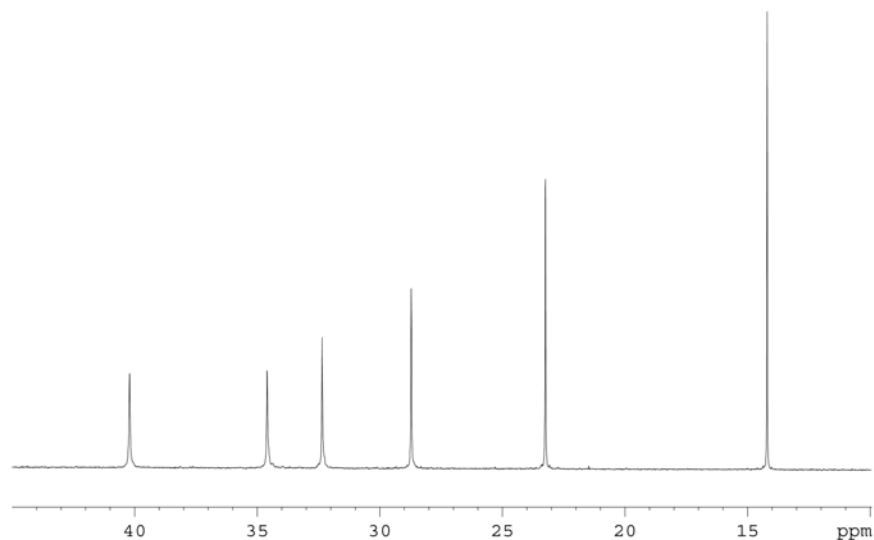


**Figure 37.**  $^{13}\text{C}\{^1\text{H}\}$  NMR (100 MHz, chloroform-*d*, 25 °C) spectrum of PH prepared using [1-hexene]<sub>0</sub>/[41+ 42] = 100 : 1.

**Polymerization of 1-hexene activated by 44:** Compound **44** is synthesized based on the literature.<sup>201</sup> To a solution of 9.8 mg (12.5 μmol) of **50** in 2 mL of chlorobenzene at -10 °C was added a solution of 11.5 mg (25 μmol) of **41** in 8 mL of chlorobenzene at -10 °C. After 5 min, 0.421 g (5.0 mmol) of 1-hexene, pre-cooled to -10 °C, was added all at once and the resulting mixture was allowed to stir for 8 h at -10 °C, after which time it was rapidly quenched by the addition of methanol. The volatiles were then removed *in vacuo*, and the crude material was purified through precipitation of a toluene solution into a large volume of acidic methanol. The final pure material (0.37 g, 86 %,  $M_n = 24,100$ , PDI = 1.02) was collected and dried overnight at 60 °C/0.01 mmHg.

**Polymerization of 1-hexene using 50 activated by [Et<sub>3</sub>Si][B(C<sub>6</sub>F<sub>5</sub>)<sub>4</sub>] (44):** To a solution of 9.8 mg (12.5 μmol) of **50** in 1 mL of chlorobenzene at -10 °C was added a solution of 11.1 mg (12.5 μmol) of **44** in 4 mL of chlorobenzene at -10 °C. After 5

min, 0.421 g (5.0 mmol) of 1-hexene, pre-cooled to  $-10\text{ }^{\circ}\text{C}$ , was added all at once and the resulting mixture was allowed to stir overnight at  $-10\text{ }^{\circ}\text{C}$ , after which time it was rapidly quenched by the addition of methanol. The volatiles were then removed *in vacuo*, and the crude material was purified through precipitation of a toluene solution into a large volume of acidic methanol. The final pure material (0.40 g, 95 %,  $M_n = 53\ 800$ , PDI = 1.16) was collected and dried overnight at  $60\text{ }^{\circ}\text{C}/0.01\text{ mmHg}$ .

**Kinetic study of ChloDeT** (in the case when  $[\mathbf{41}]_0 = 1.56\text{ mM}$ ): To a solution of 50.1 mg (62.5  $\mu\text{mol}$ ) of **18** in 25 mL of chlorobenzene at  $-10\text{ }^{\circ}\text{C}$  was added a solution of 24.8 mg (62.5  $\mu\text{mol}$ ) of **42** in 10 mL of chlorobenzene at  $-10\text{ }^{\circ}\text{C}$ . A solution of 28.8 mg (62.5  $\mu\text{mol}$ ) of **41** in 5 mL of chlorobenzene was then added. To this yellow solution, a mixture of 1.05 g (12.5 mmol) of 1-hexene was added all at once at  $-10\text{ }^{\circ}\text{C}$ . Aliquots were quenched with silica gel after 15 min and every 30 min thereafter.

**Table 8. Full activation kinetic data.**

Time (min)	$[\mathbf{M}]_t/[\mathbf{M}]_0$	$\ln([\mathbf{M}]_0/[\mathbf{M}]_t)$
15	0.8597	0.151
30	0.5719	0.559
60	0.2612	1.343
90	0.1460	1.924
120	0.0898	2.410
150	0.0488	3.020
180	0.0296	3.520
210	0.0155	4.167

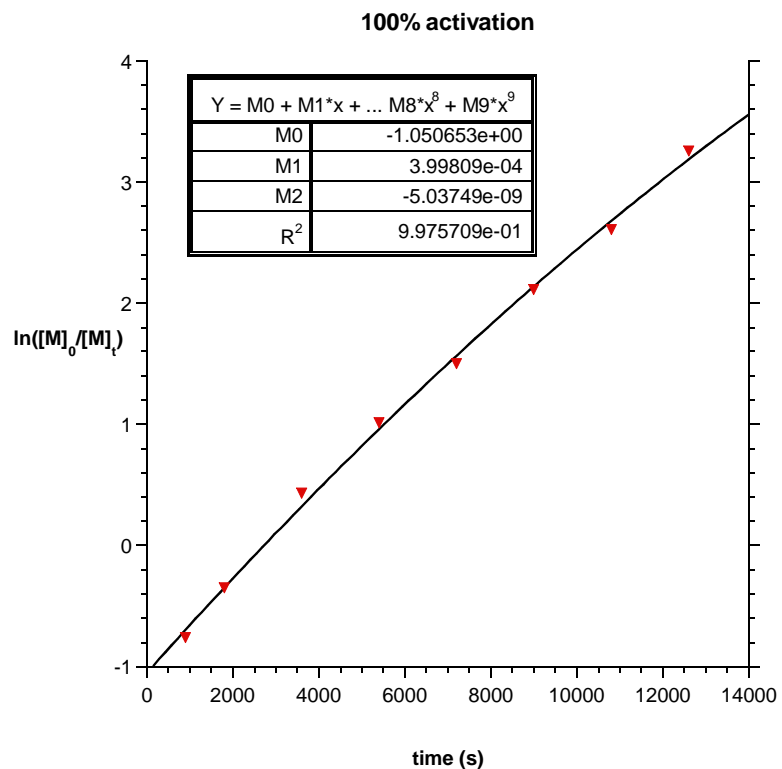


**Figure 38. Full activation ChloDeT kinetic**

**Table 9. 50% activation kinetic data.**

Time (min)	$[M]_t/[M]_0$	$\ln([M]_0/[M]_t)$
15	0.7654	0.2674
30	0.5709	0.5605
60	0.3239	1.1273
90	0.1563	1.8560
120	0.0957	2.3465
150	0.0623	2.7758

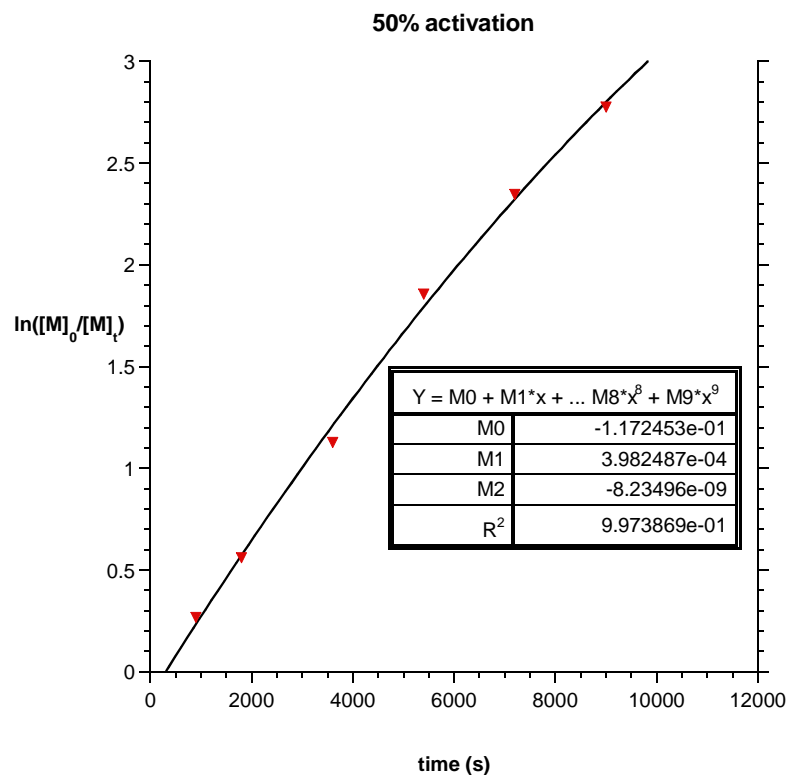


**Figure 39. 50% activation ChloDeT kinetic.**

**Table 10. 36.5% activation kinetic data.**

Time (min)	$[M]_t/[M]_0$	$\ln([M]_0/[M]_t)$
15	0.8884	0.1183
33	0.5162	0.6613
60	0.3711	0.9913
105	0.1438	1.9393
142	0.0837	2.4805
190	0.0428	3.1512

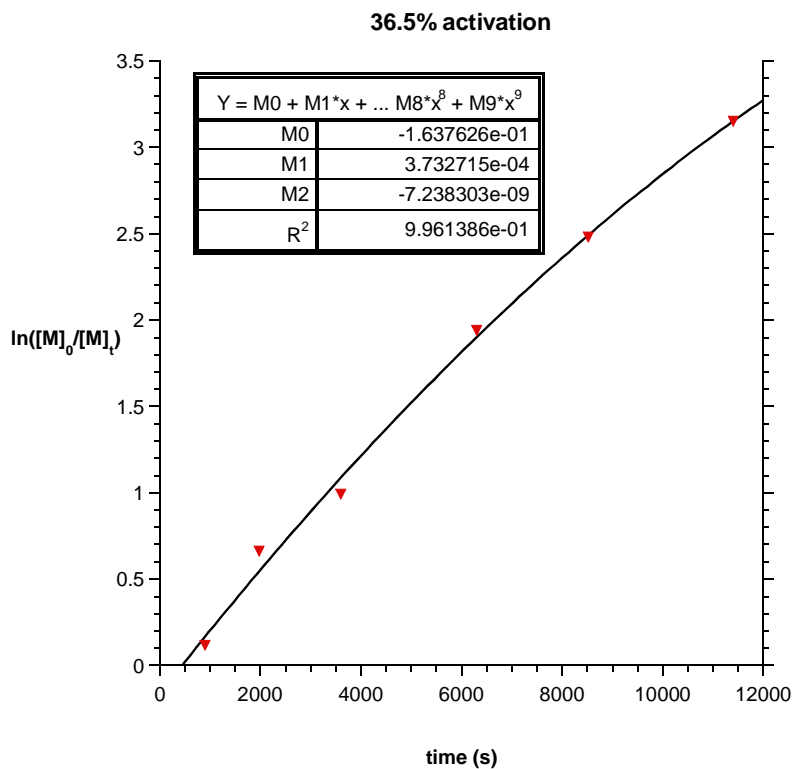


**Figure 40. 36.5% activation ChloDeT kinetic.**

**Table 11. 25% activation kinetic data.**

Time (min)	$[M]_t/[M]_0$	$\ln([M]_0/[M]_t)$
15	0.8080	0.2132
33	0.6227	0.4737
60	0.3894	0.9431
90	0.2287	1.4753
120	0.1481	1.9100
171	0.0745	2.597

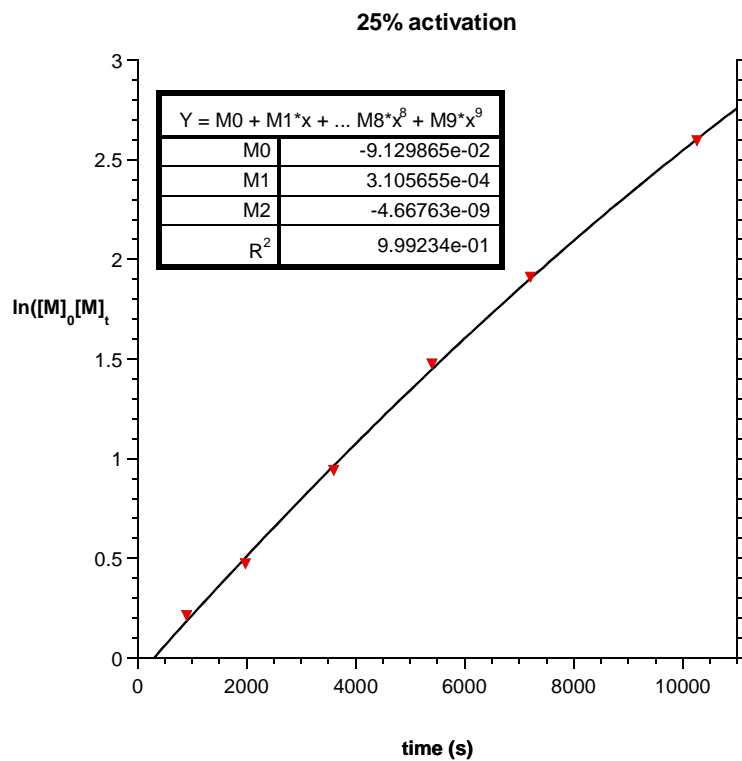


**Figure 41. 25% activation ChloDeT kinetic.**

**Table 12. 18% activation kinetic data.**

Time (min)	$[M]_t/[M]_0$	$\ln([M]_0/[M]_t)$
33	0.6213	0.4759
60	0.4939	0.7054
90	0.2909	1.1235
120	0.1920	1.6503
180	0.0930	2.3751

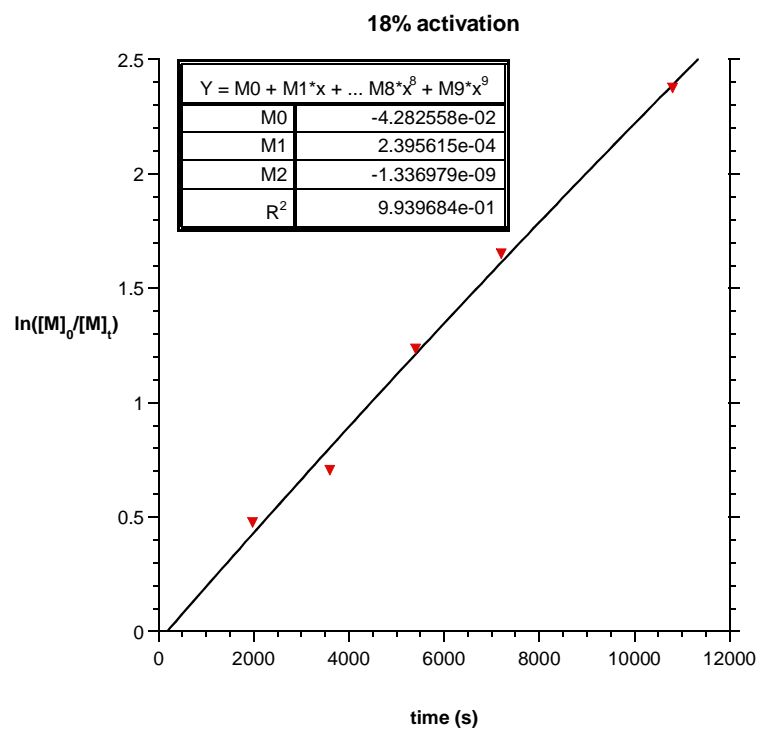


**Figure 42. 18% activation ChloDeT kinetic.**

**Table 13. 10% activation kinetic data.**

Time (min)	$[M]_t/[M]_0$	$\ln([M]_0/[M]_t)$
60	0.7459	0.2932
120	0.4900	0.7133
180	0.2770	1.2837
305	0.1463	1.9220
427	0.0797	2.5295

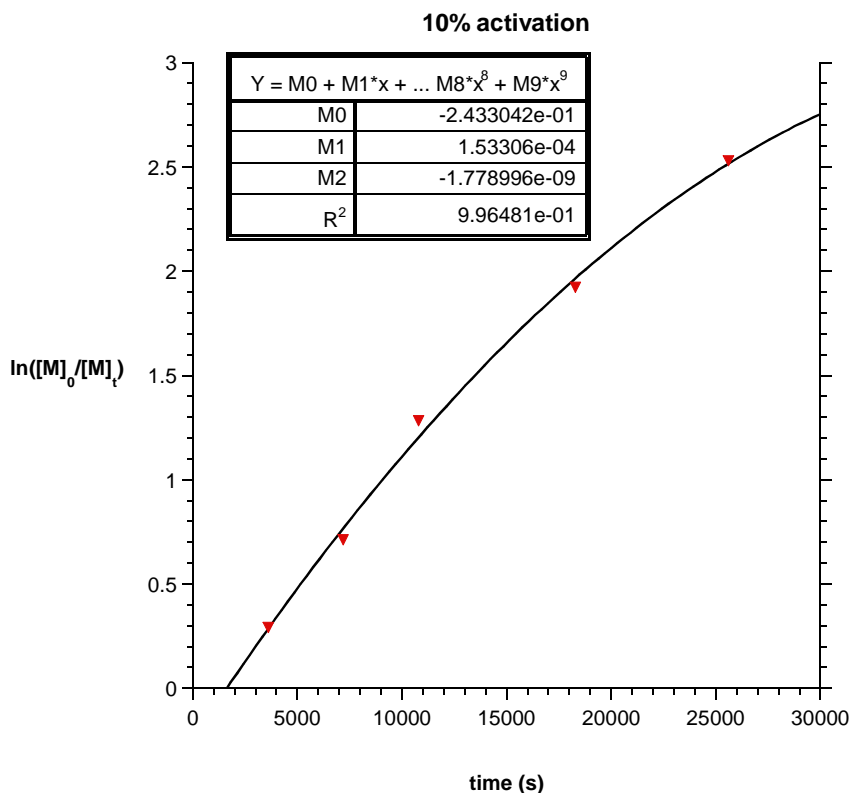


**Figure 43. 10% activation ChloDeT kinetic.**

**Preparation of  $\{(\eta^5\text{-C}_5\text{Me}_5)\text{ZrCl}[\text{N}(t\text{-Bu})\text{C}(\text{Me})\text{N}(\text{Et})]\}_2(\text{CH}_2)_6$  (**50**):** In a 100 mL Schlenk tube fitted with a gas tight Kontes Teflon valve, 0.81 g (1.50 mmol) of **48** was dissolved in 25 mL of pentane and 62 mg (0.75 mmol) of 1,5-hexadiene was added, and then the tube sealed. After removal from the glove box, the tube was pressurized with H<sub>2</sub> (40 psi) and then sealed once more. The mixture was shaken for 2 days and the volatiles removed *in vacuo*. Yellow powder was obtained (0.61 g, 91%). Upon recrystallization at -30 °C in THF, yellow crystals suitable for X-ray analysis were obtained. For **50**: <sup>1</sup>H NMR (400 MHz, 25 °C): δ 2.89 (m, NCH<sub>a</sub>H<sub>b</sub>CH<sub>3</sub>, 2H), 2.62 (m, NCH<sub>a</sub>H<sub>b</sub>CH<sub>3</sub> 1H), 2.13 (m, ZrCH<sub>2</sub>CH<sub>a</sub>CH<sub>b</sub>, 2H), 2.02 (s, C<sub>5</sub>Me<sub>5</sub>, 30H), 1.79 (s, CCH<sub>3</sub>, 6H), 1.69 (m, ZrCH<sub>2</sub>CH<sub>a</sub>CH<sub>b</sub>, 2H), 1.58 (m, ZrCH<sub>2</sub>CH<sub>2</sub>CH<sub>2</sub>, 4H), 1.35 (s, NC(CH<sub>3</sub>)<sub>3</sub>, 18H), 0.85 (t, J=7.2 Hz, NCH<sub>2</sub>CH<sub>3</sub>, 6H), 0.60 (m, ZrCH<sub>a</sub>CH<sub>b</sub>, 2H), 0.27

(m, ZrCH<sub>a</sub>CH<sub>b</sub>, 2H). Anal. Calcd. for C<sub>42</sub>H<sub>76</sub>N<sub>4</sub>Cl<sub>2</sub>Zr<sub>2</sub>: %C 56.52, %H 8.81, %N 6.28; Found %C 56.46, %H 8.57, %N 5.92.

**Preparation of  $\{(\eta^5\text{-C}_5\text{Me}_5)\text{ZrCl}[\text{t-BuNC}(\text{Me})\text{NEt}]\}_2(\text{CH}_2)_6$  (**52**):** In a 100 mL Schlenk tube fitted with a gas tight Kontes teflon valve, 0.81 g (1.50 mmol) of **50** was dissolved in 25 mL of pentane and 62 mg (0.75 mmol) of 1,5-hexadiene was added, and then the tube sealed. After removal from the glove box, the tube was pressurized with H<sub>2</sub> (40 psi) and then sealed once more. The mixture was shaken for 2 days and the volatiles removed *in vacuo*. Yellow powder was obtained (0.61 g, 91%). Upon recrystallization at -30 °C in THF, yellow crystals suitable for X-ray analysis were obtained. For **52**: <sup>1</sup>H NMR (400 MHz, 25 °C): δ 2.89 (m, NCH<sub>a</sub>H<sub>b</sub>CH<sub>3</sub>, 2H), 2.62 (m, NCH<sub>a</sub>H<sub>b</sub>CH<sub>3</sub> 1H), 2.13 (m, ZrCH<sub>2</sub>CH<sub>a</sub>CH<sub>b</sub>, 2H), 2.02 (s, C<sub>5</sub>Me<sub>5</sub>, 30H), 1.79 (s, CCH<sub>3</sub>, 6H), 1.69 (m, ZrCH<sub>2</sub>CH<sub>a</sub>CH<sub>b</sub>, 2H), 1.58 (m, ZrCH<sub>2</sub>CH<sub>2</sub>CH<sub>2</sub>, 4H), 1.35 (s, NC(CH<sub>3</sub>)<sub>3</sub>, 18H), 0.85 (t, J=7.2 Hz, NCH<sub>2</sub>CH<sub>3</sub>, 6H), 0.60 (m, ZrCH<sub>a</sub>CH<sub>b</sub>, 2H), 0.27 (m, ZrCH<sub>a</sub>CH<sub>b</sub>, 2H). Anal. Calcd. for C<sub>42</sub>H<sub>76</sub>N<sub>4</sub>Cl<sub>2</sub>Zr<sub>2</sub>: %C 56.52, %H 8.81, %N 6.28; Found %C 56.46, %H 8.57, %N 5.92.

## Chapter 4 Heterogeneous Living Ziegler-Natta Polymerization of $\alpha$ -olefins

### 4.1 Background

Right after Ziegler and Natta's discovery of the ethylene and propylene polymerization, the heterogeneous polymerization ethylene and propylene was commercialized. The polymerization catalysts were immobilized onto  $\text{MgCl}_2$  or  $\text{SiO}_2$  supported systems with  $\text{TiCl}_3$  as the initiator.<sup>211</sup>

Within last 50 years, as the development of homogeneous catalysts with higher activity, better stereocontrol, the parallel demand for heterogeneous catalyst is increasing at the same time. The slurry and gas phase process is widely used in industry and is a very matured technology. The advantages of a solid-supported system are multifold, among which are 1) excellent polymer morphology and 2) polyolefins with high bulk density and 3) low reactor fouling. Silica and alumina based solid supports are typically used. Recently, clay,<sup>212</sup> polymers, heteropolyacids,<sup>212</sup> cyclodextrin,<sup>213</sup> polysiloxanes<sup>214</sup> are reported as new materials.

Due to the high activity and exceptional microstructure control for metallocene catalysts, the potential to immobilize them onto solid supports is of great commercial interest.

There are three different ways for a catalyst to be immobilized. First, which is most commonly used by industry, the co-catalyst, such as MAO is deposited onto solid supports. This is typically done after a pre-treatment of the solid support, such as calcinations up to 600 °C to remove residual moisture and excess hydroxyl groups. The solid support is typically a porous material with enormous surface area. An

example<sup>215</sup> is the commercial available IOLA<sup>TM</sup> from W. R. Grace shown in Figure.43. IOLA is a porous inorganic oxide with an average bead diameter of 10-30  $\mu\text{m}$ . High activity and excellent morphology is typically seen within this type of solid-supported activator.

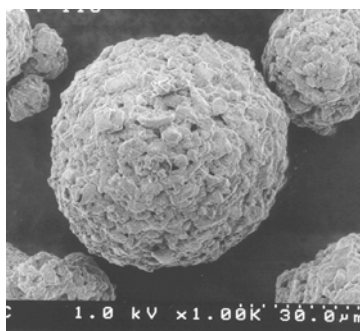


**Figure 44. IOLA solid supported activator.**

The second category is physically depositing the initiator onto a porous solid support; with no chemical linkage involved. The advantage is the less complicated process to immobilize the initiator, with the compensation of the potential loss of the polymer chain from the solid support during polymerization. Woo and coworkers<sup>216</sup> employed zeolites as the supporting materials. Certain zeolites have a cage with fixed diameter, which can trap metallocenes with certain size. Different zeolites with various diameters can be used for different metallocenes to suppress the loss of polymer chains from the solid supports.

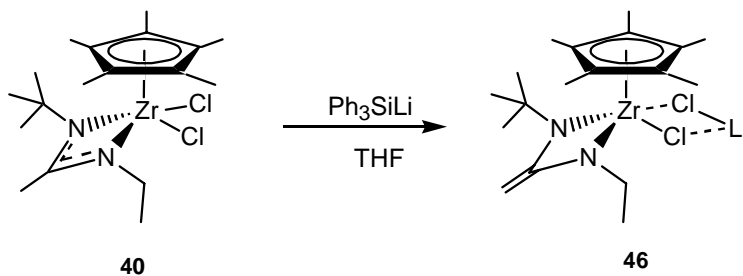
The last method is to chemically link the initiator to the solid-support. This greatly attenuates the loss of polymer chain during polymerization. An advantage of this method is that the system is mechanistically much less complicated compared to the first two methods. The drawback is the possibility of altering the chemical environment of the active species, since the initiator is chemically linked to the solid

support. Compared to other methods, moderate activity is commonly observed for this method, though.

#### 4.2 Deprotonation of Zirconium Amidinate<sup>217</sup>

For the amidinate based zirconium system, to anchor the initiator to solid supports, a chemical linkage is most desired due to its simplicity described previously. For **19**, the distal position shows great potential. It is far away from the zirconium center and the cyclopentadienyl ligand, which means altering the distal position will most likely have the least influence on the polymerization ability of the initiator. However, the distal position has no functional group, which can react with other functional groups to link the initiator to a solid support.

Fortunately, an interesting result indicates that the distal methyl group is acidic and prone to be deprotonated. A slight excess of  $\text{Ph}_3\text{SiLi}\cdot(\text{THF})_3$  with **40** in THF produces a purple colored ate-complex  $[(\eta^5\text{-C}_5\text{Me}_5)\text{ZrCl}\{\text{N}(t\text{-Bu})\text{C}(\text{CH}_2)\text{NEt}\} \text{LiCl}]$  (**46**) exclusively.



**Scheme 41. Deprotonation of the distal methyl group by a sterically hindered base.**

For compound **46**,  $^1\text{H}$  NMR in  $\text{C}_6\text{D}_6$  is shown in Figure 45. A broad peak is observed at 3.5 ppm, representing the methylene protons at the distal position. A geminal coupling for an external olefin typically ranges from  $-4$  to  $4$  Hz.<sup>218</sup> The

$^2J(^1\text{H}-^1\text{H})$  coupling of these two protons is smaller than the observable line width.<sup>219</sup> Also, the  $^{13}\text{C}-^1\text{H}$  HSQC NMR spectrum, with a  $^{13}\text{C}$  NMR resonance at 55.6 ppm shows a  $^1J(^{13}\text{C}-^1\text{H})$  of 157 Hz (cf.  $^1J_{\text{CH}} = 156.4$  Hz for ethylene).

It is observed that this ate-complex can lose LiCl to form a dimeric complex in aprotic polar coordinating solvents like  $\text{Et}_2\text{O}$ . Suitable dark orange crystals were obtained for single crystal diffraction analysis. The crystal structure of **46** is shown in Figure 46. Of interest, the C11-C12 bond length of 1.332(8) Å suggests full double bond character. Also atom C12 is trigonal coplanar, determined by the sum of the bond angles about this atom,  $\Sigma\text{C}_{12}$  of 360°.

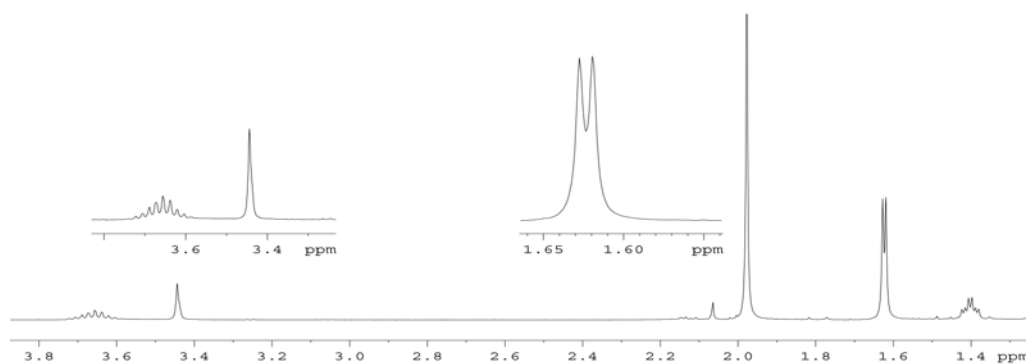


**Figure 45.**  $^1\text{H}$  NMR spectrum (400 MHz,  $\text{C}_6\text{D}_6$ , 25 °C) of **46**.

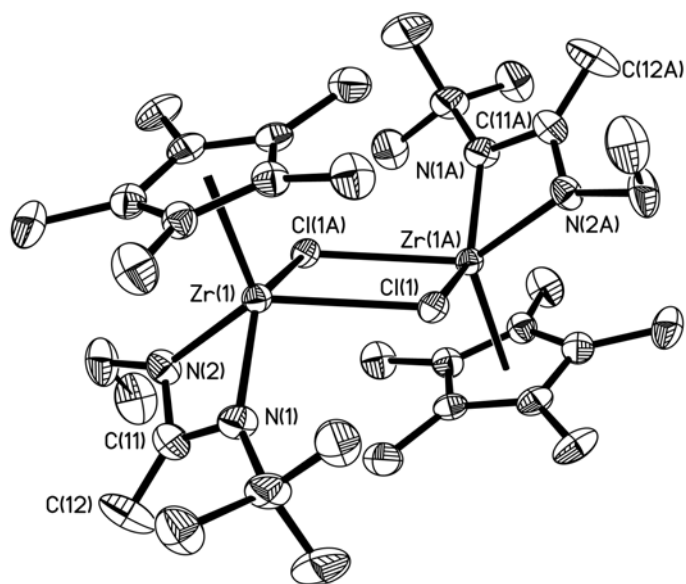


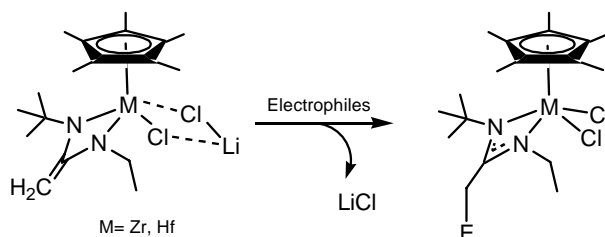
**Figure 46.** Molecular structure (30% thermal ellipsoids) of **46**. Hydrogen atoms have been removed for clarity.

### 4.3 Reaction with Electrophiles

The formation of this diamino zirconium complex **46** is very similar to the formation of enolate deprotonated by bases of the  $\alpha$ -carbon in carbonyl groups. Similarly to enolates, compound **46** is very reactive toward electrophiles. Using various electrophiles, successful transformations to make new zirconium amidinates were carried out based on Scheme 42. Most of the reactions proceed rapidly without side reactions based on NMR analysis.

There are only few synthetic methodologies exist to incorporate amidinate to a metal center, which include: 1). salt elimination using alkali metal amidinates with metal halides,<sup>220,221</sup> 2). carbodiimide insertion into a metal-carbon bond,<sup>180,222</sup> 3). reaction between a silyl substituted amidinate with metal halides.<sup>189</sup> The on-site

functionalization of **46** can produce a wide variety of zirconium amidinates, with readily available precursors.



Electrophiles = (a)  $\text{PhCH}_2\text{Cl}$ , (b)  $\text{CH}_2\text{Cl}_2$ , (c)  $\text{Me}_2\text{SiCl}_2$ , (d)  $\text{PhCOCl}$

**Scheme 42. Nucleophilic substitution reaction of 46.**

Hafnium derivatives ( $\eta^5\text{-C}_5\text{Me}_5$ ) $\text{HfCl}_2[\text{N}(t\text{-Bu})\text{N}(\text{Me})\text{N}(\text{Et})]$  (**53**) can also be deprotonated by sterically hindered bases.  $\text{KN}(\text{TMS})_2$  is used instead, due to the slow reaction rate of  $\text{Ph}_3\text{SiLi}$  with **53**. A variety of electrophiles were successfully attached to the distal position. To our great satisfaction, single crystals suitable for X-ray diffraction analysis were obtained from the nucleophilic substitution of the hafnium derivative, and some of the examples are shown in Figure 47.

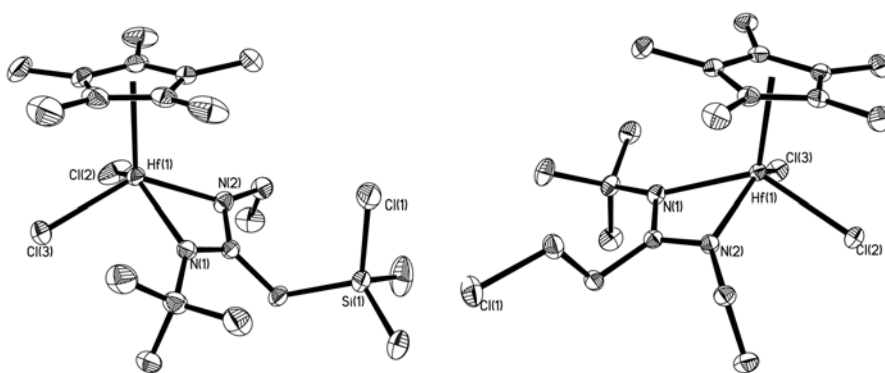
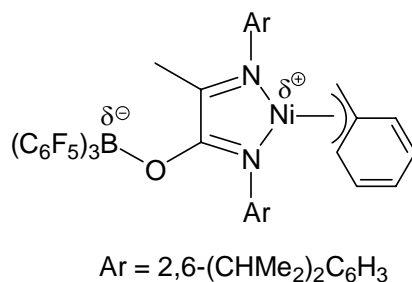


**Figure 47. Molecular structure (30% thermal ellipsoids) of the nucleophile addition reaction product of the hafnium derivative towards  $\text{Me}_2\text{SiCl}_2$  (left) and  $\text{Me}_3\text{SiCl}$  (right). Hydrogen items have been removed for the sake of clarity.**

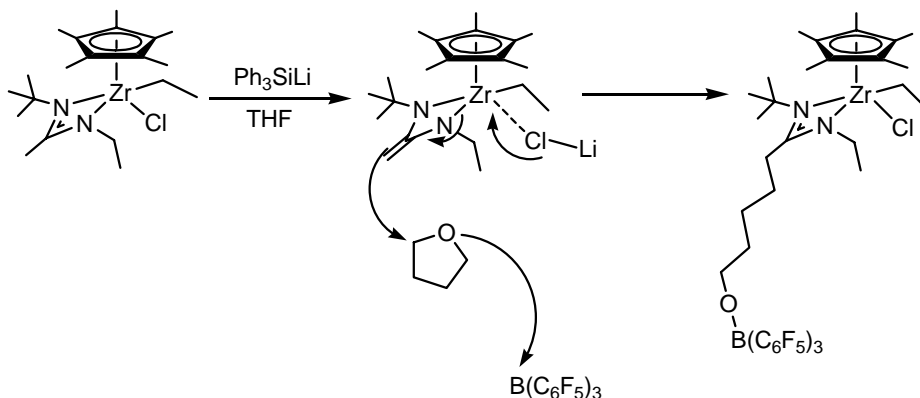
Among all the electrophiles, two are of great interest. First candidate is **31**. Borane is commonly used as a co-catalyst to activate zirconocene initiators (*vide supra*). However, it is not as strong as borate activator such as **18** or **26** due to different activation mechanisms. The  $\text{MeB}(\text{C}_6\text{F}_5)_3$  anion is considered to be smaller than the  $\text{B}(\text{C}_6\text{F}_5)_4$  anion. The closer coordination between the borate anion  $\text{MeB}(\text{C}_6\text{F}_5)_3$  and the zirconium cation could thus decrease the polymerization activity. Bazan and coworkers discovered that **31** can be used to remove electron density for a nickel atom from the opposite direction where monomer inserts, in doing so, a zwitterionic active species was first obtained.<sup>223</sup> The counteranion borate does not block the incoming monomer, as shown below.



**Scheme 43. Zwitterionic initiator remotely activated by  $\text{B}(\text{C}_6\text{F}_5)_3$ .**

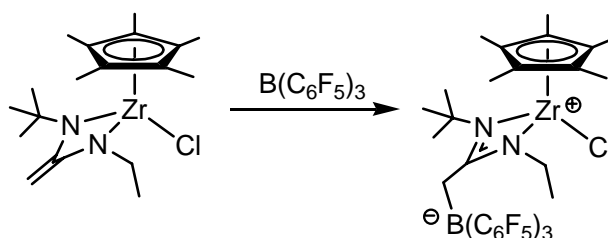
Since **19** is an effective initiator for the living Ziegler-Natta polymerization of  $\alpha$ -olefins, a remote activation of the initiator from the distal position by **31** seems reasonable. The first attempt to make the zwitterionic complex failed when 1 equivalent of **31** was added to a THF solution of an ethyl derivative of **46** ( $\eta^5$ - $\text{C}_5\text{Me}_5$ )Zr(Et)[N(*t*-Bu)C(CH<sub>2</sub>)N(Et)](LiCl). (**47**) The purple color changed to light yellow rapidly, and light yellow crystals were obtained after the reaction solution was concentrated and recrystallized at  $-35$  °C in THF. Single crystal **54** was subjected to X-ray analysis. Compound **54** was confirmed as the product of an electrophilic

addition via THF ring-opening, as shown in Scheme 44. Compound **46** is so reactive that it reacts with the large excess of THF before it reacts with borane. Similar reaction happens when **46** is dissolved in methylene chloride, and a compound with 2-chloro-ethylene tail was observed.



**Scheme 44.** Electrophilic addition via THF ring-opening to produce **54**.

To prevent the ring opening of THF, diethyl ether ( $\text{Et}_2\text{O}$ ) was used as the solvent instead. Compound **46** was first generated in THF by the deprotonation of  $\text{Ph}_3\text{SiLi}$  and solvent removed *in vacuo*.  $\text{Et}_2\text{O}$  was added and the purple powder **46** was re-dissolved. After the addition of a slight excess of **31**, the color faded to light yellow. The mixture was kept at  $-30\text{ }^\circ\text{C}$  for recrystallization to afford the desired product. Light yellow crystals of **55** suitable for X-ray analysis were obtained and the crystal structure is shown in Figure 48.



**Scheme 45.** Formation of the zwitterionic zirconium species **55**.

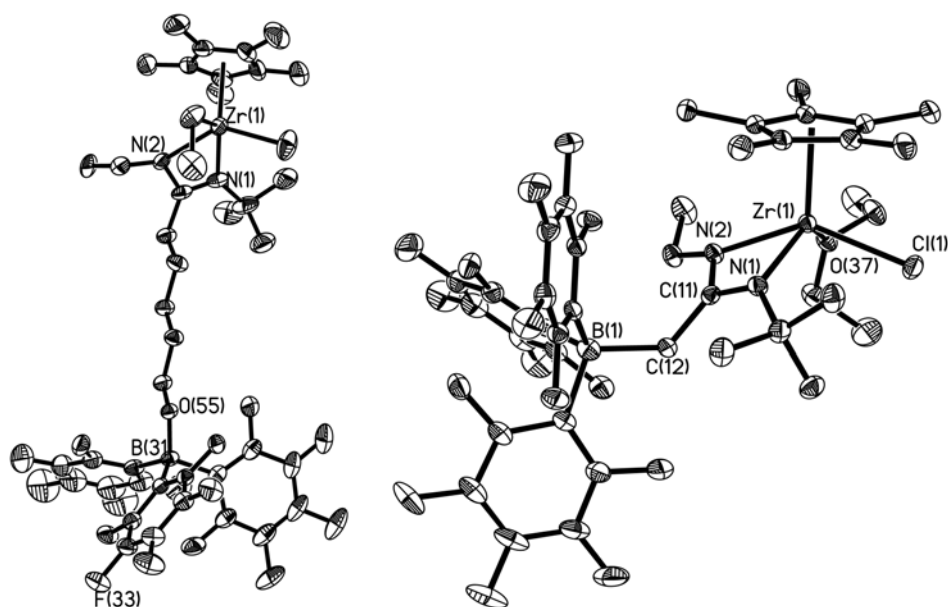


**Figure 48. Molecular structure of 54 (left) and 55 (right). Hydrogen atoms removed for clarity.**

The crystal structure confirmed a zwitterionic zirconium complex with one equivalent of diethyl ether coordinated to the cationic zirconium. It should be noted that the electronic environment of the zirconium of **55** is very similar to that used for Ziegler-Natta living polymerization, except for the chlorine vs. methyl substitution. Attempts to methylate **55** failed, probably due to the instability of this zwitterionic complex.

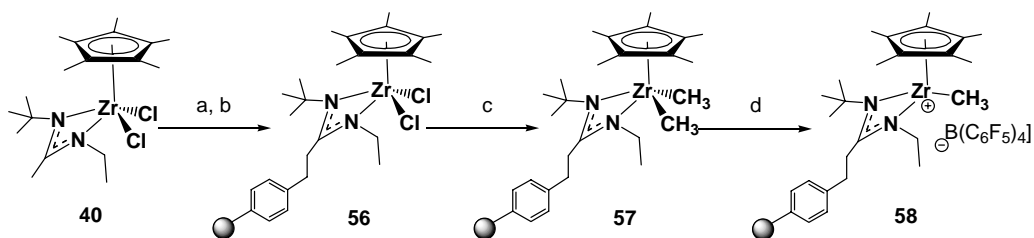
So far, we have demonstrated that **46** is very reactive towards a variety of electrophiles, and many new amidinate zirconium complexes have been successfully synthesized along with hafnium derivatives. Most of the examples shown in Scheme 42 have no practical interests for Ziegler-Natta polymerization, but provide routes to several new amidinates that are not available by conventional synthetic methodologies.

#### 4.4 Preparation of the Solid-Supported Initiator<sup>224</sup>

Another interesting electrophile is methylene chloride, while a CH<sub>2</sub>Cl group is attached to **46** successfully. This provides a potential means to anchor the initiator to a solid support with chloro end groups.

To investigate this concept, commercially available chloromethylated polystyrene beads (Bio-Rad, Bio-beads<sup>TM</sup> S-X1 200-400 mesh, 1.36 mmol g<sup>-1</sup>) were used as the “electrophile” to react with **46** in toluene at ambient temperature. The beads contain -CH<sub>2</sub>Cl end groups with known concentration. The detailed reaction is shown in Scheme 46. First, nucleophilic substitution was carried out after the deprotonation of **40**; the chloro end group reacts with **46** and the zirconium was connected to the beads. Methylation by MeLi then converts **56** to dimethyl-zirconium solid-supported pre-catalyst **57**. A color change can be observed from pure white (color of the polystyrene beads) to pale yellow (**56**), to off white (**57**).

No direct analysis method has been developed yet, but elemental analysis has been used as an indirect way. The beads have no nitrogen content (N%) before the reaction with **46**. Based on multiple values of N% from elemental analysis, it can be established that the extent of conversion of the initial polystyrene beads to **57** in these three steps is in the range of 40 –50 % (0.54 – 0.68 mmol g<sup>-1</sup>). Orange beads can be obtained by chemoselective demethylation using **18** as the co-catalyst in chlorobenzene at –10 °C to give the solid supported active species **58**.



**Scheme 46.** The synthesis of solid-supported initiator **62**. Reagents and conditions: a)  $\text{Ph}_3\text{SiLi}\cdot(\text{THF})_3$ , THF, 25 °C, 2 h; b) Bio-beads<sup>TM</sup> S-X1, toluene, 2 h; c) MeLi, Et<sub>2</sub>O, -78 °C to 25 °C, 3 h; d) **18**, chlorobenzene, -10 °C, 5 min.

#### 4.5 Living Polymerization of 1-Hexene

The solid-supported catalyst **58** was tested for  $\alpha$ -olefin polymerization. Data for polymerization of 1-hexene is shown in Figure 49. A linear curve was obtained with  $M_w$  and polymer yield, by carrying out separate polymerization experiments with fixed amount of **58** and fixed initial concentration of 1-hexene (0.5 M in chlorobenzene) at -10 °C for varied periods of polymerization time.

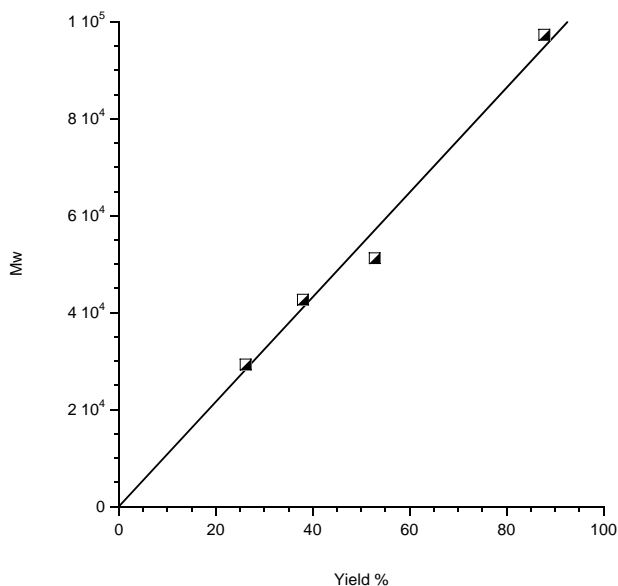


**Figure 49.** Dependence of  $M_w$  for *iso*-PH on yield of isolated polymers.

First, all polymers obtained from these separate polymerizations are of narrow polydispersity.  $^1\text{H}$  and  $^{13}\text{C}\{^1\text{H}\}$  NMR spectra of the polymer samples show no vinyl end groups, which indicates the lack of  $\beta$ -hydride elimination from the zirconium propagating centers occurred during the polymerization, even after 24 h. These results are consistent with the criteria of living Ziegler-Natta polymerization.<sup>225,226</sup> In addition, all the polymers obtained were proven to be isotactic, which means this heterogeneous catalyst preserves the living and stereospecific characters of the homogeneous analogue. This confirms the initial hypothesis that the alternation of the distal position does not significantly influence the chemical environment of the initiator.

Also, due to the living character of **58**, narrow polydispersity, tunable chain block length copolymers can be made by consecutive addition of monomers. It should be noted first that the rate of propagation is slower than the homogeneous catalyst under the same monomer concentration, which is reasonable due to the heterogeneous nature of the polymerization. The advantage to use heterogeneous catalysts to make block polymers is that the residue monomer for the previous block can be easily removed by filtration, while for homogeneous system, it takes long time for full conversion since the rate of polymerization decreases dramatically as monomer been consumed, and the decreasing follows the equation

$$R_p = k_p[\text{Zr}][\text{M}] = k_p[\text{Zr}][\text{M}]_0 e^{-[\text{Zr}]_0 k_p t}$$

To make a block copolymer, first, 90 equiv of 1-hexene were added to a mixture of **58** in chlorobenzene at  $-10\text{ }^\circ\text{C}$ , and after 8 h of polymerization, a portion of 1-octene (90 equiv) were added. The polymerization was quenched with methanol after 3

more hours. After precipitation from acidic methanol, a polymer with  $M_n$  of 23 700, PDI of 1.07 was obtained in 84 % yield (the workup is more involved than the homogeneous version, which can be the reason for a lower yield.). No vinyl end groups were observed in  $^1\text{H}$  NMR. An inverse gated  $^{13}\text{C}\{^1\text{H}\}$  NMR spectrum showed that both blocks are isotactic, and almost 1:1 ratio of the 1-hexene and 1-octene blocks integration, which is consistent with the ratio of the monomer equivalents. GPC traces are shown in Figure 51.

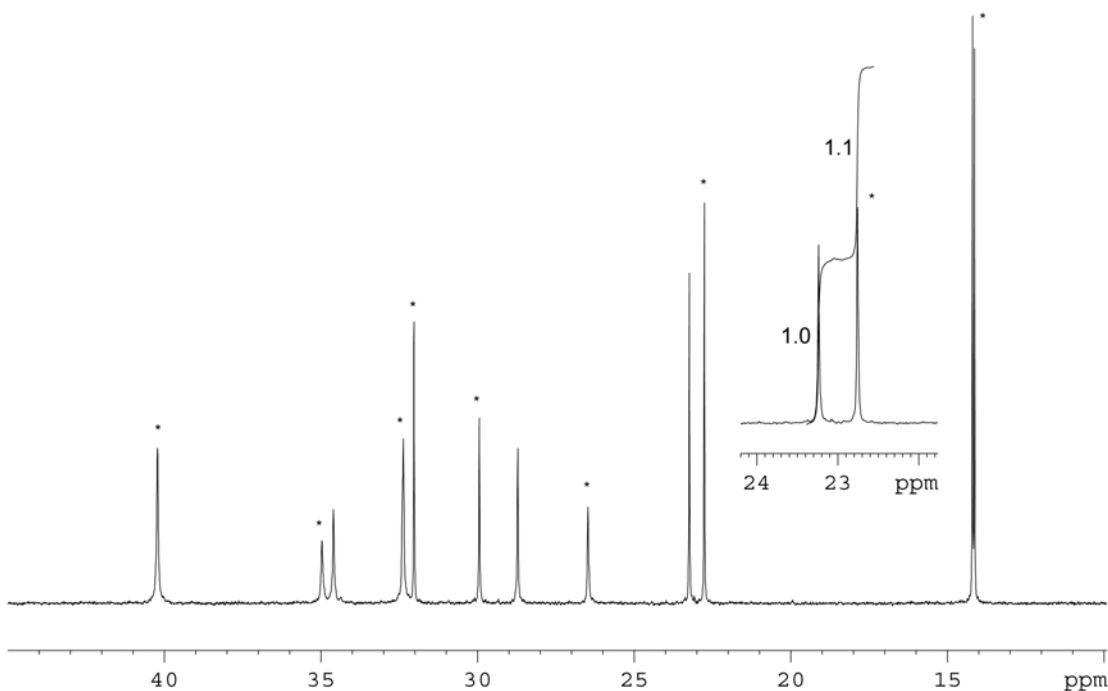


**Figure 50.** Inverse-gated  $^{13}\text{C}\{^1\text{H}\}$  NMR (100 MHz,  $\text{CDCl}_3$ , 25 °C) spectrum of *iso*-PH-*b*-PO block copolymer. Resonances for the PO block are marked with an asterisk (\*).

To the best of our knowledge, this is the first example of a heterogeneous stereospecific living Ziegler-Natta polymerization catalyst of  $\alpha$ -olefins.

Several experiments showed other unique properties of this immobilized initiator **58**. First, unlike the homogeneous cationic species, which decomposes slowly at  $-10$

°C, **58** can be preserved at –10 °C almost in infinite periods. **58** also shows incredible stability at room temperature; for example, after 10 days, the beads still keep 93 % activity for 1-hexene, and 55 % after 20 days. Even after 20 days, the polymer obtained from the polymerization still has the same narrow polydispersity and isotacticity, which indicates the remaining active centers have not changed. Second, by immobilizing the catalyst to the solid-support, less polar solvents, like toluene, can be used for polymerization (cf.,  $M_n = 70,000$ , PDI = 1.10, yield = 78 %, 24 h), while for the homogeneous catalyst **19**, no polymer was obtained under the same conditions, probably because of the tighter ion pair.<sup>227</sup>

#### 4.6 Conclusions

On-site chemoselective functionalization was developed by deprotonating of the distal position of **40** using sterically hindered bases, such as  $\text{Ph}_3\text{SiLi}$ ,  $\text{KN}(\text{TMS})_2$ . The enolate product is **46** very reactive towards electrophiles. A variety of nucleophilic addition reactions were carried out and new types of amidinate zirconium complexes were synthesized with high yield. Also, this methodology was applied to the preparation of heterogeneous  $\alpha$ -olefin initiator on chemically modified polystyrene resins Bio-beads. The heterogeneous initiator **58** polymerizes 1-hexene and 1-octene in a living and stereospecific fashion. This is the first example of living stereospecific Ziegler-Natta polymerization of  $\alpha$ -olefins.

#### 4.7 Experimental

**Preparation of  $[(\eta^5\text{-C}_5\text{Me}_5)\text{ZrCl}_2\{\text{N}(t\text{-Bu})\text{C}(\text{CH}_2)\text{NEt}\}]^-\text{Li}^+$  (**46**).** To a solution of **18** (1.32 g, 3.0 mmol) in 60 mL of THF, 1.40 g (3.0 mmol) of  $\text{Ph}_3\text{SiLi}\cdot(\text{THF})_3$ <sup>228</sup>

was added and the reaction was stirred for 2 h. All the volatiles were removed *in vacuo* and the residue was washed with 200 mL of pentane to provide a crude product, which was recrystallized from diethyl ether at  $-30\text{ }^{\circ}\text{C}$  to afford **46** as a purple powder (0.72 g, 60 % yield). For **46**:  $^1\text{H}$  NMR (400 MHz, THF- $d_8$ ):  $\delta$  ppm 3.46 (br m, 2H,  $\text{CH}_2\text{CH}_3$ ), 2.91 (s, 1H,  $\text{C}=\text{CH}_a\text{H}_b$ ), 2.89 (s, 1H,  $\text{C}=\text{CH}_a\text{H}_b$ ), 2.22 (s, 15H,  $\text{C}_5\text{Me}_5$ ), 1.49 (s, 9H,  $\text{CMe}_3$ ) 1.29 (t,  $J=6.8$  Hz, 3H,  $\text{CH}_2\text{CH}_3$ ).  $^{13}\text{C}$   $\{^1\text{H}\}$  NMR (THF- $d_8$ ):  $\delta$  ppm 152.8 ( $\text{C}=\text{CH}_2$ ), 123.9 ( $\text{C}_5\text{Me}_5$ ), 55.8 ( $\text{CMe}_3$ ), 55.6 ( $\text{C}=\text{CH}_2$ ), 43.3 ( $\text{CH}_2\text{CH}_3$ ), 32.4 ( $\text{CMe}_3$ ), 16.7 ( $\text{CH}_2\text{CH}_3$ ), 12.9 ( $\text{C}_5\text{Me}_5$ ). Anal. Calcd. for  $\text{C}_{18}\text{H}_{31}\text{ZrN}_2\text{Cl}_2\text{Li}$ : C 48.63, H 7.04, N 6.30; Found: C 48.11, H 7.04, N 6.06.

**General procedure for the nucleophilic addition of 46.** To a freshly made **46** (0.44 g, 1.0 mmol) in 20 mL of toluene, benzyl chloride (0.15 g, 1.2 mmol) was added at room temperature. The mixture was stirred for 1 h, then volatiles removed *in vacuo*. The residue was extracted with pentane, the extracts filtered through a short pad of Celite, and then all the volatiles removed *in vacuo*. Pale yellow powder was obtained (0.42 g, 72%). Attempt to recrystallization failed. Reaction of methylene chloride, dichlorodimethylsilane, benzoyl chloride were carried out as the same procedure of benzyl chloride. The hafnium derivative is done in the same manner.

**Preparation of the Solid-supported pre-catalyst 57.** To a solution of **40** (1.76 g, 4.00 mmol) in 50 mL of THF at room temperature, was added 1.958 g (4.2 mmol) of  $\text{Ph}_3\text{SiLi}\cdot(\text{THF})_3$  and the reaction was stirred for 2 h. All the volatiles were removed *in vacuo* and 100 mL of toluene was added. To the red solution, 2.94 g of white polystyrene beads (Bio-Rad, Bio-beads<sup>TM</sup> S-X1, chloromethylated 200 - 400 mesh, 1.36 mmol/g) was added and the mixture was allowed to stir for 3 h, then the slurry

was filtered. To the yellow solid, 70 mL of Et<sub>2</sub>O was added and the mixture was cooled down to – 78 °C, followed by MeLi (8.36 mmol) in 6.48 mL of Et<sub>2</sub>O via a syringe. The reaction mixture was allowed to warm to room temperature in 3 h, then the mixture was filtered and the beads (4.20 g) were dried *in vacuo*. Anal. Found: C 77.25, H, 8.02; N, 1.57; Cl, 5.51.

**Activation of the solid-supported pre-catalyst 57.** To a –10 °C mixture of **57** (0.548 g) in 20 mL of chlorobenzene, was added a solution of 0.4 g (0.5 mmol) of [PhNHMe<sub>2</sub>][B(C<sub>6</sub>F<sub>5</sub>)<sub>4</sub>] in 10 mL of chlorobenzene pre-cooled to –10 °C. After 5 min, the mixture was filtered and the orange beads **58** generated were washed thoroughly with cold chlorobenzene. The beads were then dried *in vacuo* and kept at –10 °C. Anal. Found: C, 66.41; H, 5.57; N, 1.14; F, 18.19.

For polymerization, the entire procedure was conducted at –10 °C with magnetic stirring within a low temperature refrigerator housed within a glove box and all reagents and solutions were pre-cooled to this temperature prior to being used.

**General procedure for polymerization of 1-hexene by solid-supported catalyst 58.** To a slurry of **58** (79.4 mg) in 10 mL of chlorobenzene, was added all at once 0.84 g (10.0 mmol) of 1-hexene. The resulting mixture was allowed to stir for a period of time, after which time, it was rapidly quenched by the addition of MeOH. All volatiles were removed *in vacuo*, and the crude material was extracted by toluene from the beads. Polymer was obtained after precipitation of the toluene solution into a large volume of acidic methanol. The final pure material was collected and dried overnight at 60 °C/0.01 mmHg.

**General procedure for the shelf-time experiment of catalyst 58.** Catalyst **58** was prepared as described previously and stored at room temperature ( ~ 25 °C) inside the glove box. At predetermined days, polymerization was carried out by this “aged” catalyst.

**Polymerization of *iso*-PH-*b*-*iso*-PO block copolymer using 58.** 1-hexene (0.358 g, 4.25 mmol) was added all at once to 110 mg of **58** in 20 mL of chlorobenzene. The mixture was stirred for 3 h, then 0.477 g (4.25 mmol) of 1-octene was added. The mixture was stirred for an additional 3 h. The polymerization was quenched with MeOH. After removal of volatiles, the polymer was extracted with chloroform from the beads, then purified by precipitation of a toluene solution into a large volume of acidic MeOH. The final pure polymer was collected and dried overnight at 60 °C/0.01 mmHg. Yield: 0.70 g (84%),  $M_n = 23,700$ , PDI = 1.07.

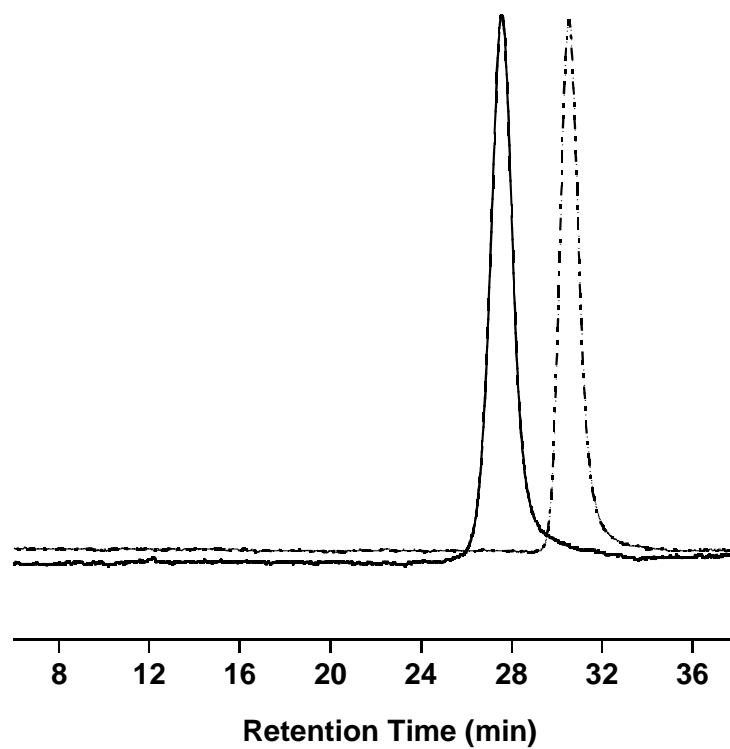


Figure 51. GPC trace of *iso*-poly(1-hexene)-*b-iso*-poly(1-octene) block copolymer ( $M_n$  23 700, PDI 1.07) (Solid line), and an aliquot of the *iso*-poly(1-hexene) block formed before addition of 1-octene monomer ( $M_n$  8 500, PDI 1.05) (dashed line).

## Chapter 5 Living 1-Butene and Propylene Polymerization

### 5.1 Background

Living degenerative transfer polymerization is a unique approach to polymers with intriguing microstructures. As described previously, isotactic and atactic PH can be obtained by simply turning off or turn on the MeDeT polymerization. By switching between the two states during polymerization, a well-defined stereoblock polymer can easily be achieved, when an elegantly designed methylating reagent such as **34** is employed. As PH has very limited commercial applications, it is only used as a propylene model, mainly because it is easy to weight and handle. Both isotactic and atactic PH are non-crystalline polymer materials. *iso*-PB is a semi-crystalline material, and is widely used as a blend component to improve the properties of other polyolefins, such as polyethylene, polypropylene and PE-PP thermoplastic elastomers. Also, PB has excellent creep resistance, impact resistance and exceptional elastic recovery. Technically, 1-butene has a boiling point of  $-6.3$  °C, and is practical to weight as a liquid at low temperature.

In addition, propylene is one of the most widely used olefin monomers in industry and polypropylene is among the highest productivity of any man-made plastics. Fifty years after the discovery of Ziegler-Natta polymerization, hundreds of catalytic systems have been reported with different activities, stereo selectivity, while a living isotactic polymerization was only recently reported in 2004 by Coates.<sup>43</sup> In our lab, preliminary data<sup>229</sup> shows the ability to polymerize ethylene and propylene. At room temperature, polymerization with **19** provided polypropylene with a low  $M_n$  value of

2860 and *PDI* of 1.73, no vinyl end group due to  $\beta$ -hydride elimination was observed, though. A preliminary NMR analysis of the PP obtained shows high isotactic contents.

## 5.2 Polymerization of 1-Butene Stereoblock

Polymerizations of 1-butene were carried out. First, under full activation condition, an isotactic poly(1-butene) with a  $M_n$  of 32 300 and *PDI* of 1.09 was obtained. No vinyl end groups were observed in  $^1\text{H}$  NMR, which indicates the polymerization of 1-butene is living.  $^{13}\text{C}$   $\{^1\text{H}\}$  NMR spectrum is shown in Figure 52 (top), from which four narrow singlets are observed. Degenerative transfer (50% activation) polymerization of 1-butene also provided a polymer with narrow polydispersity (1.08), and four broad peaks were observed in the  $^{13}\text{C}$   $\{^1\text{H}\}$  NMR, confirming the atactic microstructure of the polymer. *iso*-PB is crystalline, with a distinguishable sharp  $T_m$  (94 °C) in DSC, while *a*-PB is amorphous, oily and tacky.

A 1:1 *a-iso*-PB diblock is made by first polymerizing under 50% activated DT condition, followed by full activation. Also, as described in Chapter 2, **34** was used to synthesize poly(1-butene) *iso:a:iso* stereoblock, by simply turning on and turning off MeDeT conditions. A detailed synthetic scheme is shown in Scheme 47, and well-defined 25:150:25 DP *iso:a:iso*-PB is obtained.

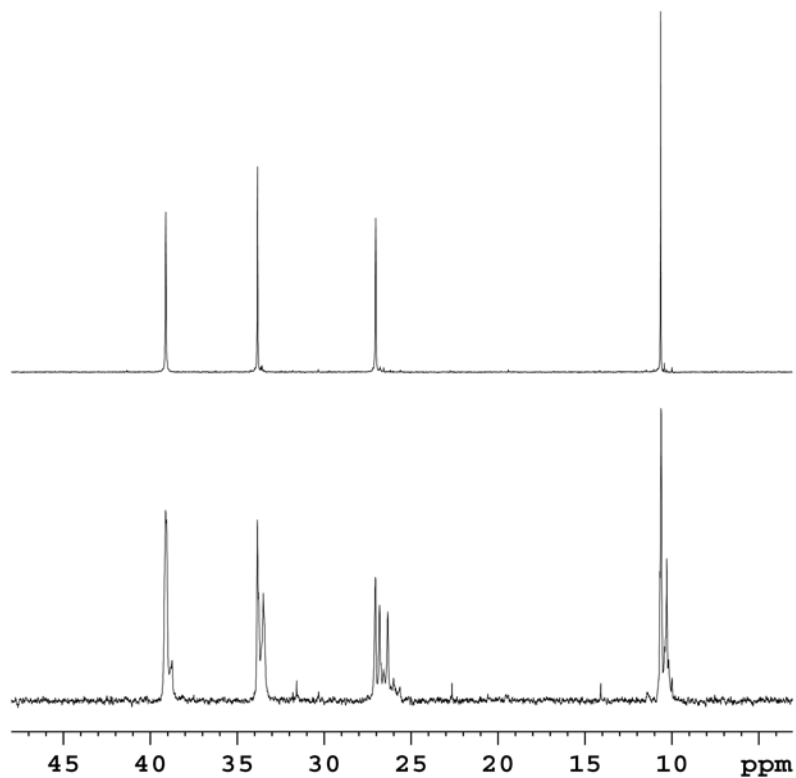
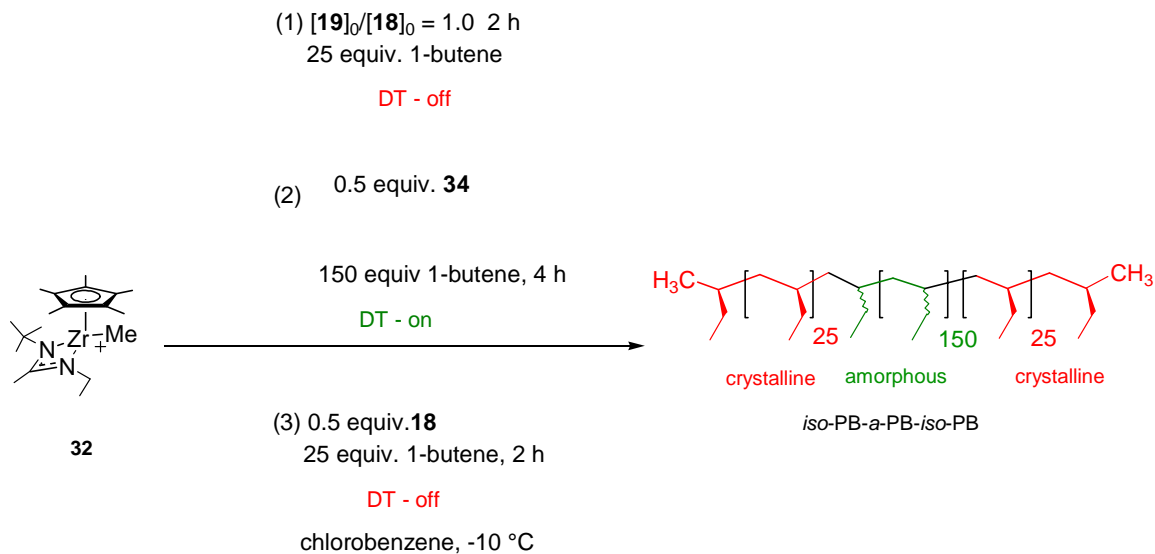


Figure 52.  $^{13}\text{C} \{^1\text{H}\}$  NMR (100 MHz,  $\text{CDCl}_3$ , 25 °C) spectra for *iso*-PB (top), and *a*-PB (bottom).



Scheme 47. Synthesis of *iso-a-iso*-PB.

To study structure/property relationships, phase sensitive tapping mode AFM (ps-tm AFM) was used to examine *iso*-PB as well as *iso-a*-PB. Both samples were

prepared by spin casting of a 1.0% wt solution in toluene on a silicon wafer. AFM images were observed before and after annealing at 120 °C for 12 h, followed by slowly cooling down to room temperature. Both height and phase maps are shown below.

*iso*-PB shows very high crystallinity, both before and after annealing. As shown in Figure 54, a hexagonal crystal is observed for the sample after annealing. For *iso*-*a*-PB stereoblock, fiber-like crystallites are observed as shown in Figure 55. It is still hard to determine the fiber is real or just the edge of lamella structure. This phase separation is considered to be from the crystalline *iso*-PB block and the amorphous *a*-PB block.

After annealing, small balls as shown in Figure 56 were observed. These beads are probably due to the repulsion between polymer and the wafer surface. Within the beads, crystalline fiber-like structure was buried by soft dark amorphous matrix.

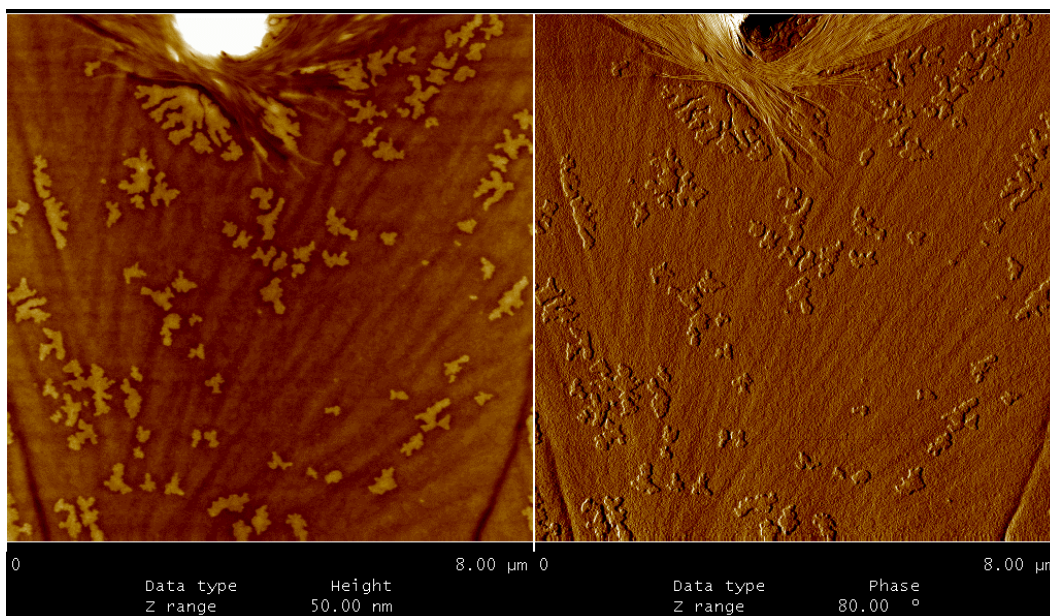


**Figure 53. AFM height and phase maps for *iso*-PB before annealing.**

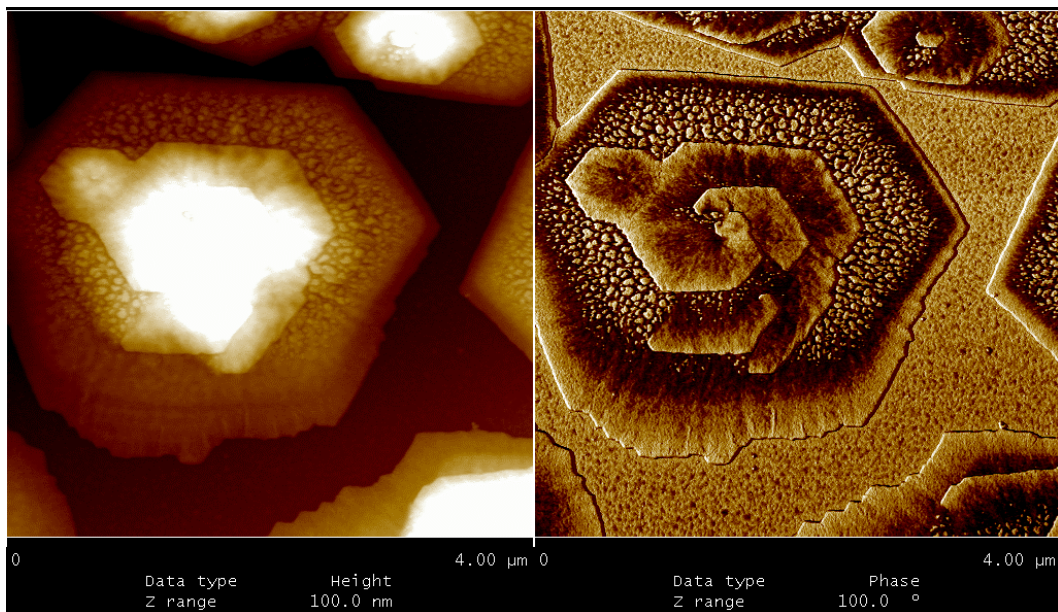


**Figure 54. AFM height and phase maps for *iso*-PB after 120 °C annealing and cooling down slowly.**

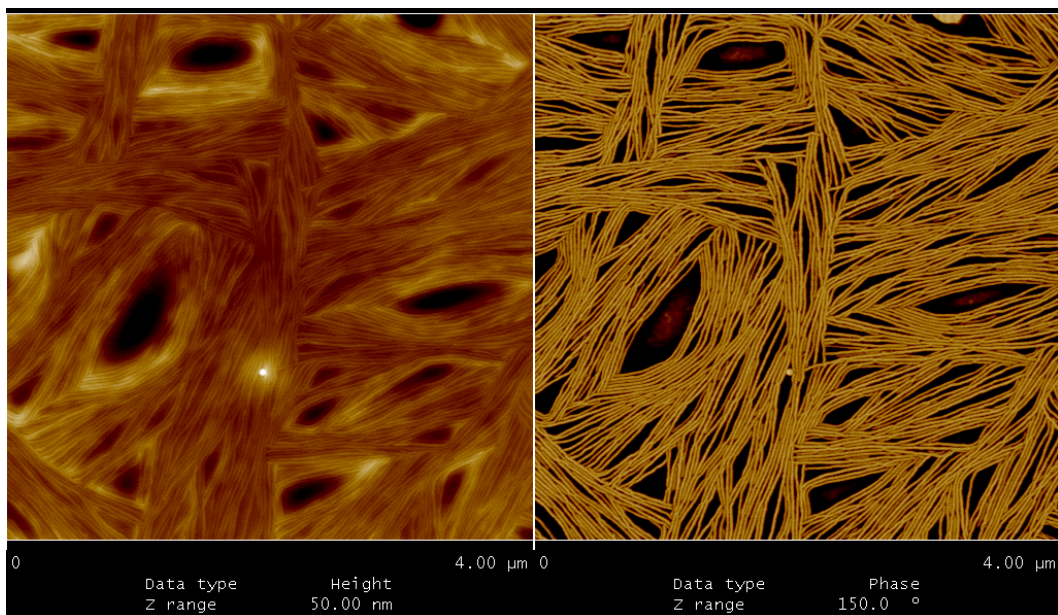


**Figure 55. AFM height and phase maps for *iso-a*-PB before annealing.**

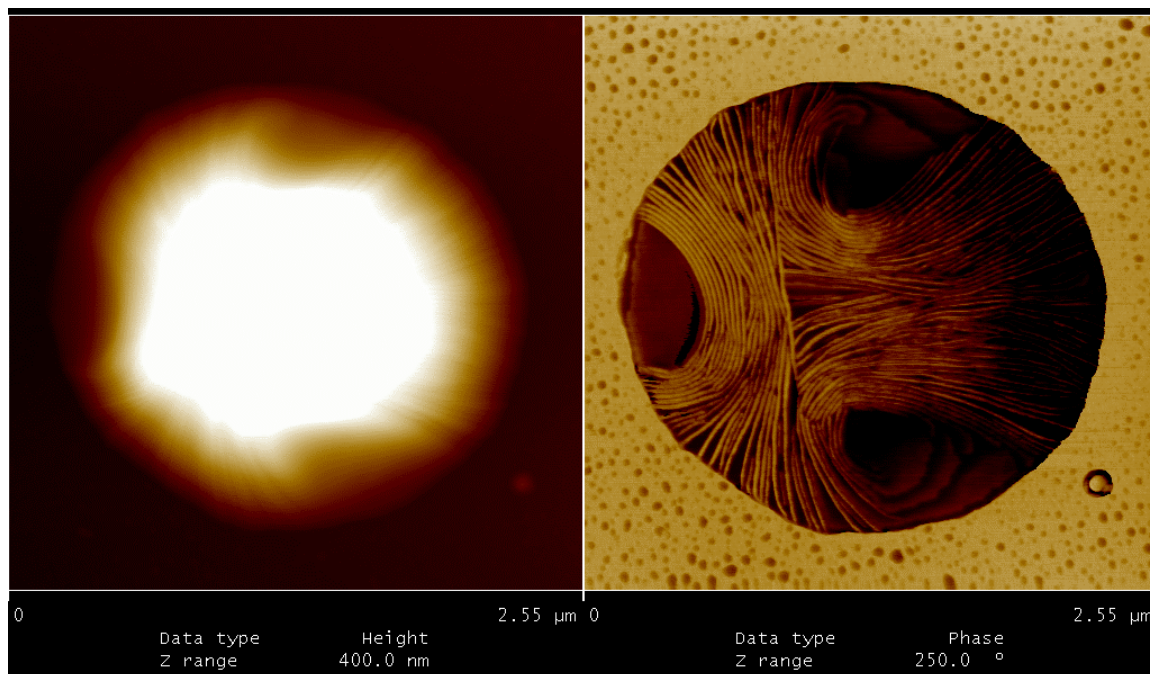


**Figure 56. AFM height and phase maps for *iso-a*-PB after 120 °C annealing and slowly cooling down to room temperature.**

### 5.3 Polypropylene Polymerization

A special setup was designed for the polymerization of propylene (see Figure 57 for detail). The polymerization vessel and the cold well are kept in the glove box, since the catalyst is air and moisture sensitive. An immersion cooler provides the cold source and metal shots (copper coated lead, or stainless steel beads) are used to transfer the cold. The cold well is isolated in an insulated bucket to keep the temperature. Below the cold well, outside the glove box, a super magnetic bar is attached to a speed variable electronic motor for stirring. Propylene (polymerization grade, Matheson Trigas, Inc) is purified by passing through a columns filled with Q5 (purchased from Engelhand Crop.), which is regenerated by heating up to 200 °C under 5% hydrogen forming gas, and a column filled with molecular sieve (5 Å), which is heated up to 400 °C under vacuum for 3 h before use.

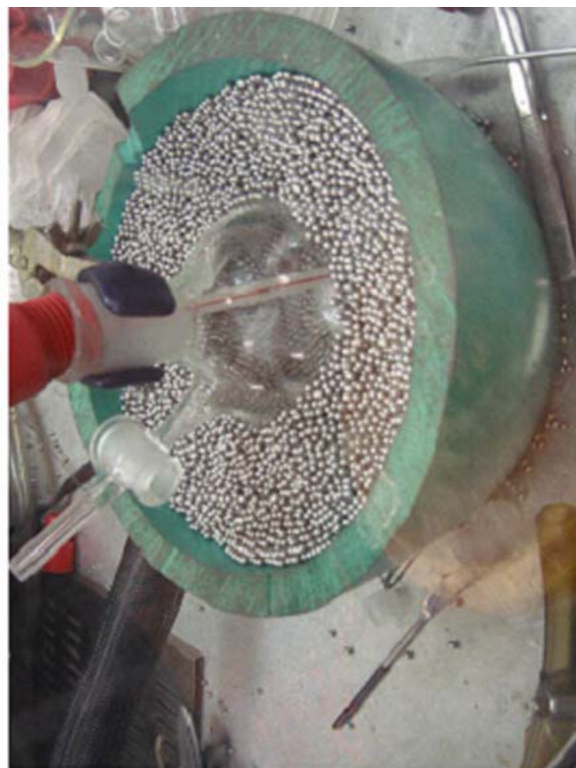
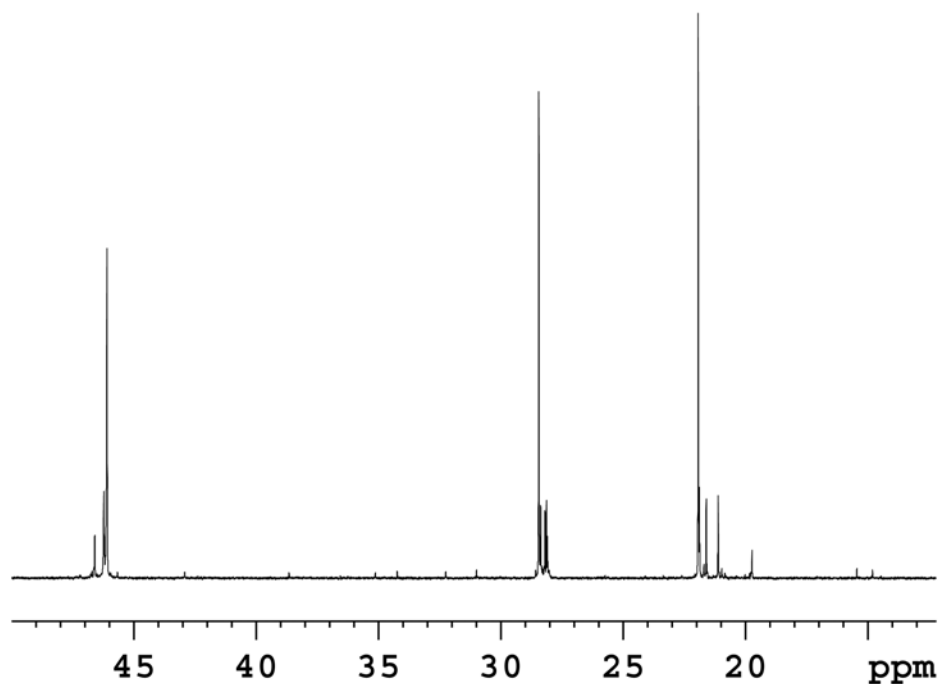


Figure 57. Polypropylene polymerization setup.

First, at  $-10\text{ }^{\circ}\text{C}$ , in a 250 mL Schlenk flask with an egg shape stirrer bar, was added 20 mL of chlorobenzene, and pressurized with 5 psi propylene. After 20 min, a solution of zirconium cation generated by equal molar ratio of **19** : **18**, was introduced all at once. The monomer pressure was kept at 5 psi throughout the polymerization. After 30 min, the yellow solution turned light opaque. A white powder was obtained after the methanol quenched solution precipitated in a large amount of acidic methanol. The powder was dried overnight at  $60\text{ }^{\circ}\text{C}$  under 0.01 mmHg.



**Figure 58.**  $^{13}\text{C}\{^1\text{H}\}$  (100 MHz,  $\text{C}_2\text{D}_2\text{Cl}_4$ ,  $70\text{ }^{\circ}\text{C}$ ) NMR spectrum of *iso*-PP.

This white powder was subjected to  $^{13}\text{C}\{^1\text{H}\}$  NMR analysis at  $70\text{ }^{\circ}\text{C}$ . A  $^{13}\text{C}\{^1\text{H}\}$  NMR spectrum is shown in Figure 58. Three major peaks were observed, representing the methine, methylene and methyl groups in polypropylene. The methyl group region of 23 to 19 ppm is the main region for detailed microstructure

analysis. An expanded NMR spectrum is shown in Figure 59 (bottom). The major peak at 21.8 ppm is assigned to the mmmmmmm nonad, while other peaks are assigned to mmmm, mmmr mmrr and mrrm as shown in Figure 46. An integration ratio [mmmr]: [mmrr]: [mrrm] of 2 : 2 : 1 was detected, indicative of the enantiomorphic site control mechanism. mmmm% of was detected by integration, too. Based on the enantiomorphic site control equation:<sup>230</sup>

$$\text{mmmm}\% = 5\sigma^4 - 10\sigma^3 + 10\sigma^2 - 5\sigma + 1$$

a  $\sigma$  value of 94% was obtained, which means the incoming monomer has 94% chance to choose the right enantioface for insertion. This is not the best  $\sigma$  value in metallocene PP polymerization, but certainly is the best among the living propylene polymerization.<sup>43</sup>

A very small amount of secondary insertion was observed by NMR, the peaks are marked with \* in Figure 59. It is very curious that only one set of 2,1 regio-error insertion peaks is observed, or in other words, the 2,1 regio misinsertion also has very high enantioface selectivity.<sup>43,231-233</sup> The polymer end group *iso*-propyl (marked + in Figure 60) can also be clearly identified by NMR analysis. No GPC data is available since *iso*-PP is not soluble enough in THF for low temperature GPC analysis.

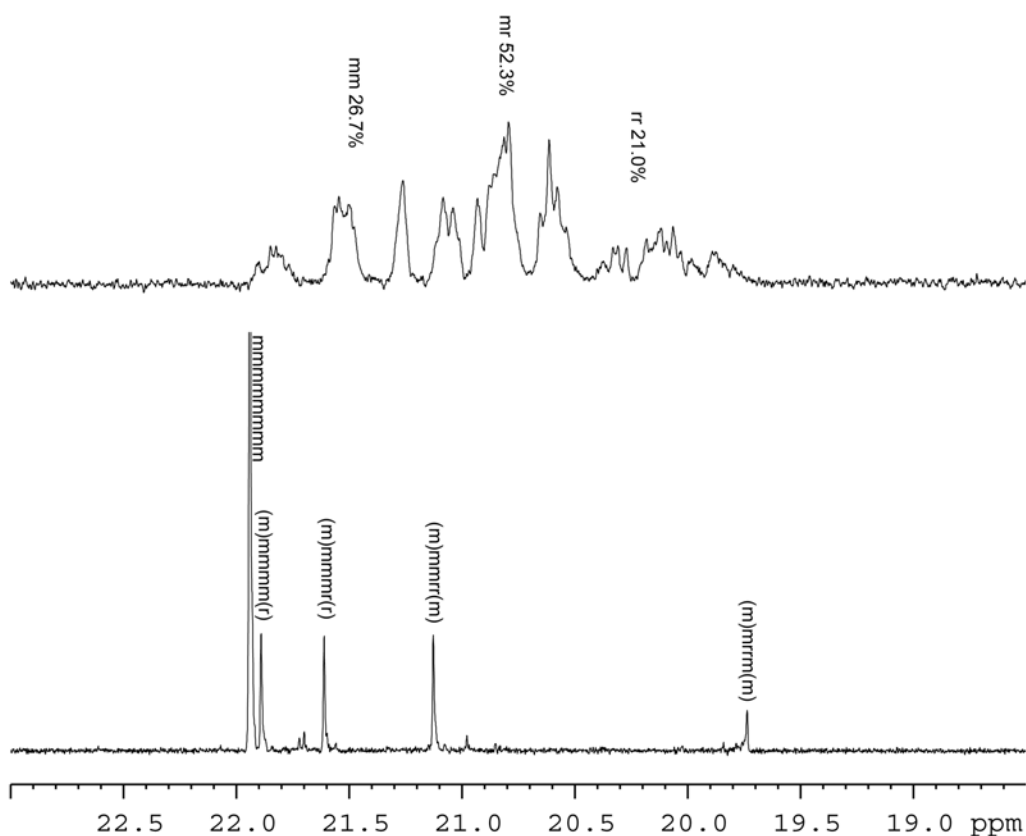


Figure 59. 125 MHz  $^{13}\text{C}\{^1\text{H}\}$  NMR ( $\text{C}_2\text{D}_2\text{Cl}_4$ , 70 °C) spectra of *a*-PP and *iso*-PP methyl region.

With a substoichiometric amount of borate **18**, similar polymerization of propylene under degenerative transfer condition was carried out. An oily, tacky material was obtained after 170 min of polymerization.  $M_n$  of 25 500 and PDI of 1.11 were determined by GPC.  $^1\text{H}$  NMR shows no vinyl end groups from  $\beta$ -hydride elimination/transfer, which suggests the living nature of the polymerization. Also,  $^{13}\text{C}\{^1\text{H}\}$  NMR shows dramatically different results compared with the full activation polymerization. Broad peaks between 22.5 and 19.0 ppm indicates the polymer is atactic, furthermore, the integration of different region give a mm (22.5 – 21.2 ppm):

mr (21.2 – 20.5 ppm) : rr (20.5 – 19.0) ratio of 26.7 : 52.3 : 21.0. An “ideal” atactic PP has a mm : mr : rr of 25 : 50 : 25 based on statistical model.

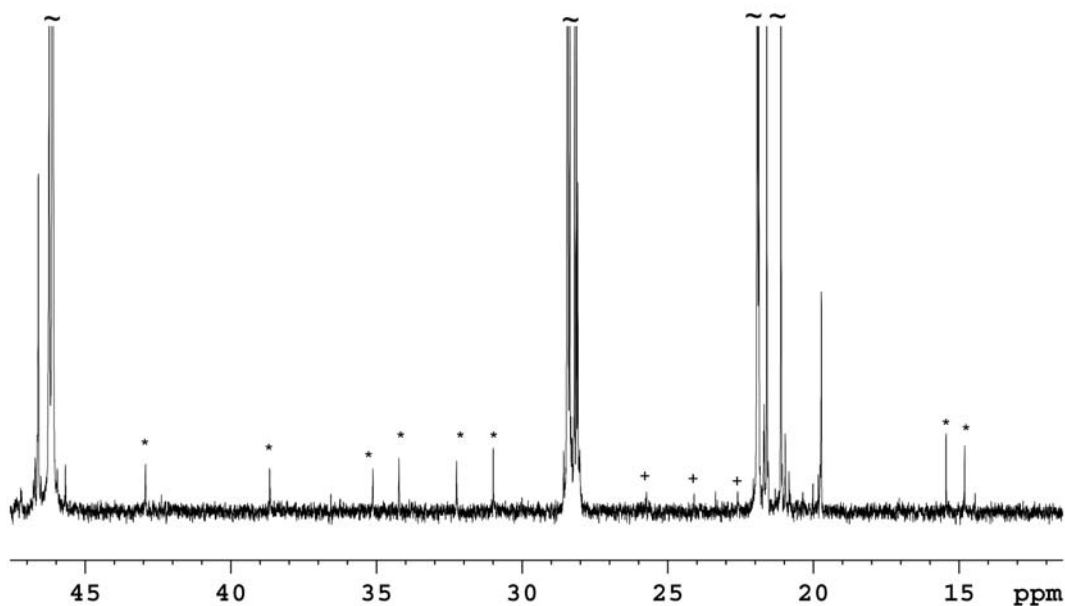


Figure 60. 125 MHz  $^{13}\text{C}\{^1\text{H}\}$  NMR spectrum ( $1,2\text{-C}_2\text{D}_2\text{Cl}_4$  at 70 °C) of *iso*-PP sample. \* indicates 2,1 regioerror insertion and + represents *iso*-propyl polymer end groups. The 2,1 insertion errors are stereospecific since only one set of NMR peaks has been observed.

#### 5.4 Kinetic Analysis

Since neither *a*-PP nor *iso*-PP shows noticeable termination, it suggests both polymerizations are living. Further evidence is required, such as a linear increase of molecular weight with polymerization time, when monomer concentration is kept as a constant. The kinetic analysis of degenerative transfer (50% activation)

polymerization was carried out by taking aliquots during a 6 h polymerization. The aliquots were then subjected to GPC analysis; detailed data is shown in Table 14.

**Table 14. Kinetic data for *a*-PP polymerization**

Time (min)	$M_n$	$M_w$	PDI
48	8100	9100	1.132
102	11700	13000	1.115
155	15500	17600	1.136
215	19400	21800	1.123
289	24200	27100	1.122
362	27000	30400	1.125

For all the aliquots, narrow polydispersity were observed<sup>234</sup>. Even after 6 h of the polymerization, a PP with 1.125 *PDI* is obtained. The plot of  $M_n$  vs. time is shown in Figure 61.

The increase of the degree of polymerization (DP) equals the rate of polymerization per zirconium center, thus we can have:

$$\frac{dDP}{dt} = \frac{R_p}{[Zr]} = \frac{k_p[Zr][M]}{[Zr]} = k_p[M]$$

$$DP = \frac{M_n}{M_1} \quad M_1 \text{ is the molecular weight for one monomer, which is 42}$$

g/mol for propylene.

$$\frac{dM_n}{dt} = M_1 \cdot k_p[M] \frac{[Zr]_t}{[Zr]_0} \quad \text{if zirconium concentration changes during the}$$

polymerization..

$$M_n \approx M_1 \cdot k_p[M]t - M_1 \cdot k_p \frac{k_t}{2} t^2$$

For a 2<sup>nd</sup> order polynomial fitting equation<sup>235</sup>

$$y = a + bx + cx^2$$

$$\frac{b}{c} = \frac{k_t}{k_t^2/2} = \frac{2}{k_t} \text{ and } k_t = \frac{2c}{b} \quad (10)$$

$$k_p = \frac{b}{M_1 \cdot [M]} \quad (11)$$

while [M] is the monomer concentration (see experimental for more detail).

If the polymerization is a living system, the increase of molecular weight is proportional to the polymerization time. Linear curve fits well and gives a R<sup>2</sup> of 0.992. If termination is considered and assumed to be a unimolecular process, the same kinetic model could be used as Chapter 2. A 2<sup>nd</sup> order polynomial fitting was used and an R<sup>2</sup> of 0.998 is obtained. The kinetic equation is shown as equation 12:

$$M_n = 3940.9 + 1.3993t - 1.503 \times 10^{-5} t^2 \quad (12)$$

The constant 3940.9 in equation 12 directly related to the systematic error by using polystyrene as the standard for GPC analysis, which was observed in poly(1-hexene) polymerization, too.

Propylene concentration of 0.129 M at -10 °C and 5psi in chlorobenzene was carefully determined by weighing the difference of a 50 mL flask equipped with a kontas TFPE seal, before and after the flask been charged with 5 psi propylene dipped in a -10 °C cold bath for 30 min. From eq 10 – 12,  $k_t$  of  $2.15 \times 10^{-5} \text{ s}^{-1}$  and  $k_p$  of  $0.258 \text{ M}^{-1} \text{ s}^{-1}$  are obtained. Based on the calculation, at the beginning of the polymerization,

$$\frac{R_p}{R_t} = \frac{k_p [Zr][M]}{k_t [Zr]} = \frac{k_p [M]}{k_t} = \frac{0.258 \text{ M}^{-1} \text{ s}^{-1} \times 0.129 \text{ M}}{2.15 \times 10^{-5} \text{ s}^{-1}} = 1548, \text{ } R_p \text{ is 1500 times faster}$$

than the rate of termination. Since the rates are not related to the zirconium

concentration, even a very small amount of propagating centers die during the polymerization, the relative rate between  $R_p$  and  $R_t$  will be a constant. One important factor that will change the rate is the temperature, which will change the intrinsic values of  $k_p$  and  $k_t$ . Also, the monomer concentration will influence the relative rate at different temperature; and higher monomer concentration attenuates the termination. Based on relative rates, termination could be considered as negligible. However, more accurate value will be obtained with the consideration of the “negligible” termination.

This again suggests the very small amount of termination does influence the kinetic data, and it must be considered in all the cases.

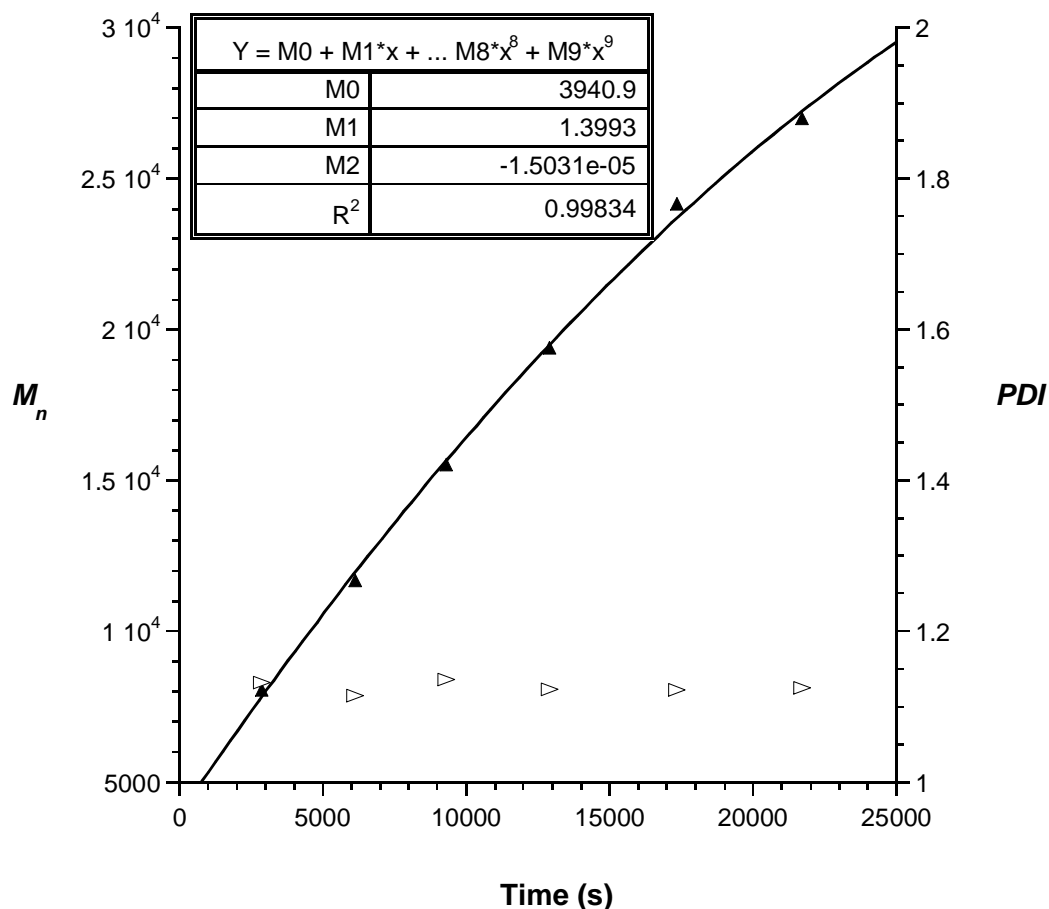


Figure 61. Kinetic plot of *a*-PP polymerization. ▼ represents number average molecular weight, and the hollow triangle represents polydispersity index.

A similar kinetic<sup>236</sup> investigation was completed for *iso*-PP polymerization. Due to the poor solubility of *iso*-PP in chlorobenzene, an atactic sequence was first polymerized before the *iso*-PP polymerization under MeDeT conditions. The long atactic block ( $M_n < 20\ 000$ ) helps the propagating polymer chain to stay in the solution quite successfully. After the synthesis of the *a*-PP block, all the propagating centers were activated, and polymerization was carried out under non-DT conditions. A kinetic experiment of 200 min polymerization after the *a*-PP block was carried out. The detailed data is shown in Table 15.

**Table 15. Kinetic data of *iso*-PP polymerization.**

Time (min)	$M_n$	$M_w$	$PDI$
10	20 000	22 600	1.13
43	24 200	28 200	1.167
72	27 300	32 100	1.178
104	30 900	36 800	1.193
134	35 300	42 100	1.192
160	38 500	45 800	1.191
199	42 000	50 000	1.189

Similar to the *a*-PP polymerization, all the aliquots have narrow polydispersities, which indicates the living nature of the polymerization.  $M_n$  vs. time plot is shown in Figure 62. A 2<sup>nd</sup> order polynomial curve fit gives a  $R^2$  of 0.997.

$$M_n = 18624 + 2.124t - 1.156 \times 10^{-6}t^2 \quad (13)$$

Based on eq 10, 11,  $k_t$  of  $1.08 \times 10^{-5} \text{ s}^{-1}$  and  $k_p$  of  $0.392 \text{ M}^{-1}\text{s}^{-1}$  are obtained. Also, in this case,  $\frac{R_p}{R_t} = \frac{k_p[\text{Zr}][\text{M}]}{k_t[\text{Zr}]} = \frac{k_p[\text{M}]}{k_t} = \frac{0.392 \text{ M}^{-1}\text{s}^{-1} \times 0.129 \text{ M}}{1.08 \times 10^{-5} \text{ s}^{-1}} = 4682$ , which means

the termination is negligible based on the relative rate. If termination was not considered in the kinetic model, and a linear curve fit was used for  $M_n$  vs. time plot, a kinetic equation  $M_n = 18914 + 1.979t$  with an  $R^2$  of 0.997 can be obtained. This is an error of 6.8%, compared to the one where termination is considered. Since most of the polymerization is carried out for hours, even the termination is negligible based on the relative rates, it should be considered in the kinetic analysis for more accurate rate constants.

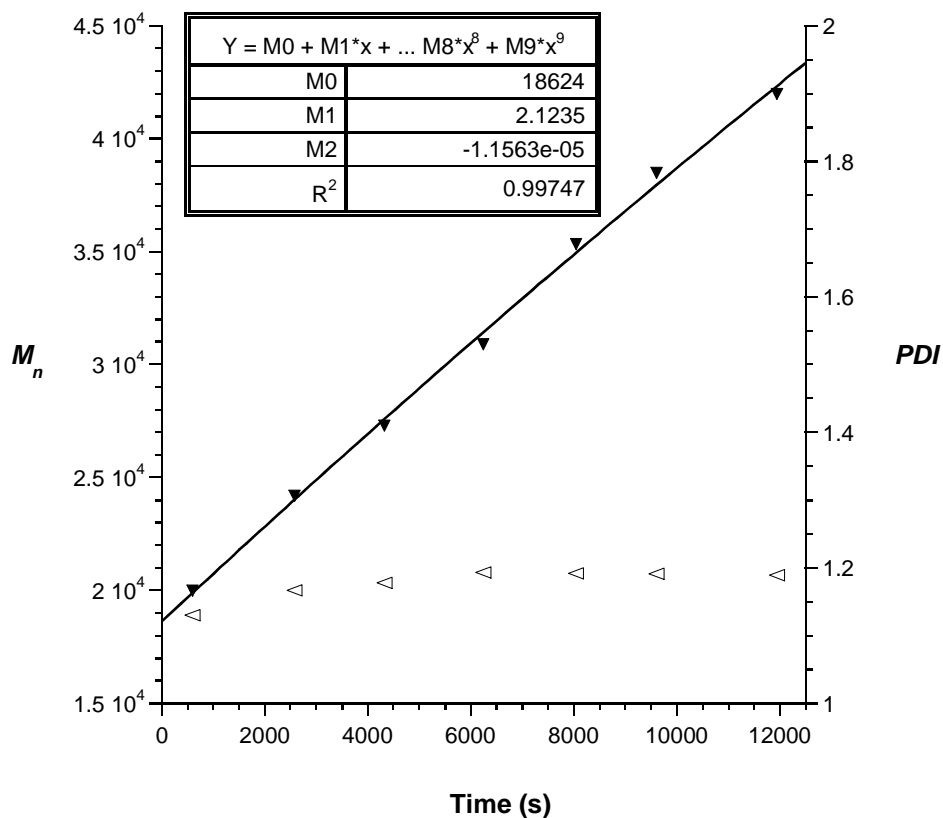


Figure 62. Kinetic data for *iso*-PP polymerization. ▼ represents number average molecular weight, and the hollow triangle represents polydispersity index.

## 5.5 Methylating Reagents

Now with a novel catalytic system, which polymerizes propylene in a living fashion and is capable of both *iso*-PP and *a*-PP polymerization under full/partial activation, well-defined stereo-diblock polymer such as *a-iso*-PP is first accessible. As described in Chapter 2, a series of zirconium complexes were designed as methylating reagents to turn on MeDeT after the propagating species were fully activated by **18**. First, **34** was used. As expected, *a*-PP with narrow polydispersity was obtained when a 2:1 ratio of **32** and **34** (under a 50% activation DT condition) was used for the polymerization. Significant tailing in the GPC trace of higher molecular weight *sb*-PPs caused us to re-investigate the activity of **34** towards

propylene polymerization, though **34** was proven to be inactive for 1-hexene polymerization under a variety of conditions. Surprisingly, a significant amount of *a*-PP was polymerized after 15 h polymerization with a fully activated **34** cation in chlorobenzene at  $-10\text{ }^{\circ}\text{C}$ . Sterically demanding derivatives, such as **36** – **38** also show propylene activity.

This result indicates that 1-hexene is not a perfect model for propylene polymerization, though it is much easier to handle. 1-Hexene is bulkier than propylene, and during polymerization, the pendant *n*-butyl group could interfere with the ligand set, while the methyl group from propylene is much smaller. Even if a very small amount of 1-hexene could insert into the metal center of **34**, the bulky *n*-butyl can block the incoming monomers, thus shut down the polymerization. It is important to understand that any polymerization results for a certain catalyst towards higher  $\alpha$ -olefins cannot be directly extrapolated to propylene or ethylene.

Fortunately, polymerization of propylene using fully activated compound **39**<sup>191</sup> shows no polypropylene activity after 15 h. Also, a 2:1 ratio of **32** to **39** produces *a*-PP, which indicates the ability of **39** to act as an efficient methylating reagent.

## 5.6 Synthesis of PP Stereoblocks

Once an efficient methylating reagent is in hand, it is straightforward to make PP stereoblocks simply by turning MeDeT ‘on’ or ‘off’. Unfortunately, a stereoblock starting with an isotactic sequence is not successful due to the poor solubility of polymer in chlorobenzene at low temperature. A relatively long block of *a*-PP is necessary as the initial block to facilitate the solubility of the polymer.

Based on the kinetic data obtained for *a*-PP and *iso*-PP polymerization, a tunable block length could be obtained by adjusting the polymerization time for each block. To prove the concept, a diblock (*a-iso*), triblock (*a-iso-a*) and a tetrablock (*a-iso-a-iso*) were polymerized with similar molecular weight and isotactic content. GPC was used to determine the molecular weight and  $^{13}\text{C}$   $\{^1\text{H}\}$  NMR was used to determine the *iso*:*a* block ratio. Since a pure *iso*-PP generated from full activation conditions has a 73% distribution at the chemical shift range from 22.0 to 21.7 ppm, which is the mmmm region, and for *a*-PP generated from 50% activation, a negligible amount of mmmm between 22.0 to 21.7 ppm was detected. This region is used to calculate the actual ratio for each block in the *sb*-PPs. For each stereoblock, GPC and NMR were used to characterize the aliquots. Detailed data is shown in Table 16 to Table 18.

*a-iso* diblock



**Table 16. Detailed data for *a-iso*-PP diblock**

Time (h)	4	2
$M_n$	31 500	54 100
$M_w$	35 400	62 600
Calcd %	56	44
GPC %	53	47
NMR %	54	46

*a-iso-a* triblock



**Table 17. Detailed data for *a-iso-a*-PP triblock polymerization**

Time (h)	2	1	2
$M_n$	19 600	41 300	51 500
$M_w$	22 000	47 300	60 500
Calcd %	28	44	28
GPC %	30	43	27
NMR %	33	41	26

*a-iso-a-iso* tetrablock



**Table 18. Detailed data for *a-iso-a-iso*-PP polymerization.**

Time (h)	2	1	2	1
$M_n$	17 500	27 600	38 100	47 100
$M_w$	20 800	33 600	46 600	55 900
caclcd %	28	22	28	22
GPC %	30	22	26	22
NMR %	25	18	31	27

For all the aliquots and the final products, the block length percentages from GPC and NMR analysis fit the calculated number quite well. By controlling the polymerization time and zirconium activation percentage, well-defined stereoblock

*sb*-PPs are produced. This is so far the first example of *sb*-PPs that have been synthesized with the controlled block sequence, block length, tacticity and controlled molecular weight by a Ziegler-Natta polymerization system.

*sb*-PP was reported to be a good candidate of the thermoplastic elastomer. However, none *sb*-PP reported have full control over the polymer microstructure, such as tacticity, molecular weight, etc. Typically, one catalyst can only produce one type of elastomers, and the ability to adjust the elastomer is very limited to monomer pressure, polymerization temperature, etc. Most of the *sb*-PPs are mixtures of different microstructures and can be solvent fractionated. Now with the full control over the microstructure, a wide variety of *sb*-PPs could be easily obtained.

The strength of an elastomer is believed to stem from the physical linkage of the crystalline domain, while the elastomeric property is from the chain entanglement within the amorphous matrixes. Also, molecular weight is critical for the physical properties of *sb*-PP. A significant degree of polymerization is necessary for the chain entanglement to give substantive elastomeric properties. *sb*-PPs with higher molecular weights (150000 – 200000) were synthesized with approximate isotactic content of 40%. A significant amount of *sb*-PPs were obtained by scale-up the polymerization to 200 mL with the same zirconium concentration. Molecular weight and isotactic content data are shown in Table 19.

**Table 19. 3 high molecular weight *sb*-PPs.**

<i>sb</i> -PP	$M_n$	PDI	iso%
<i>a-iso</i> -PP	162 100	1.20	41
<i>a-iso-a</i> -PP	167 500	1.19	39
<i>a-iso-a-iso</i> -PP	172 500	1.19	37

Dumbbell specimens were cut from *sb*-PP sheets prepared by pressing the sample at 140 °C in a hotplate at a pressure around 1000 psi. All the *sb*-PPs specimens were then subjected to tensile test based on the ASTM 412 - 98a. DSC analysis was also carried out.

First, all three *sb*-PP samples show excellent elongation-to-break, up to 1500%, which is among the best reported in the literature.<sup>100</sup> *a-iso-a-is*-PP has the lowest elongation, but has the largest value in stress. *a-iso-a*-PP has the best elongation with low stress. Diblock *a-iso*-PP is the one with both moderate stress and elongation. All materials have excellent recovery after 300% elongation and good to excellent recovery after break, which is shown in Table 20. The detailed correlation between the *sb*-PP microstructure and the elastomeric properties is yet well understood. But the *iso*-PP as the crystalline domain and *a*-PP as the soft amorphous matrix is believed to be essential.

Also, *a-iso-a-iso*-PP tetrablock is subjected to a 10 cycle 300% elongation test. The specimen is first stretched to 300% elongation, then the stress released back to the point where stress is zero. The test is repeated for 10 cycles and the strain stress curve is shown in Figure 63. As the plot shows, the first cycle shows a significant

stress difference between stretch and release of the specimen. After the initial deformation, the curves are almost identical, which indicates an excellent recovery.

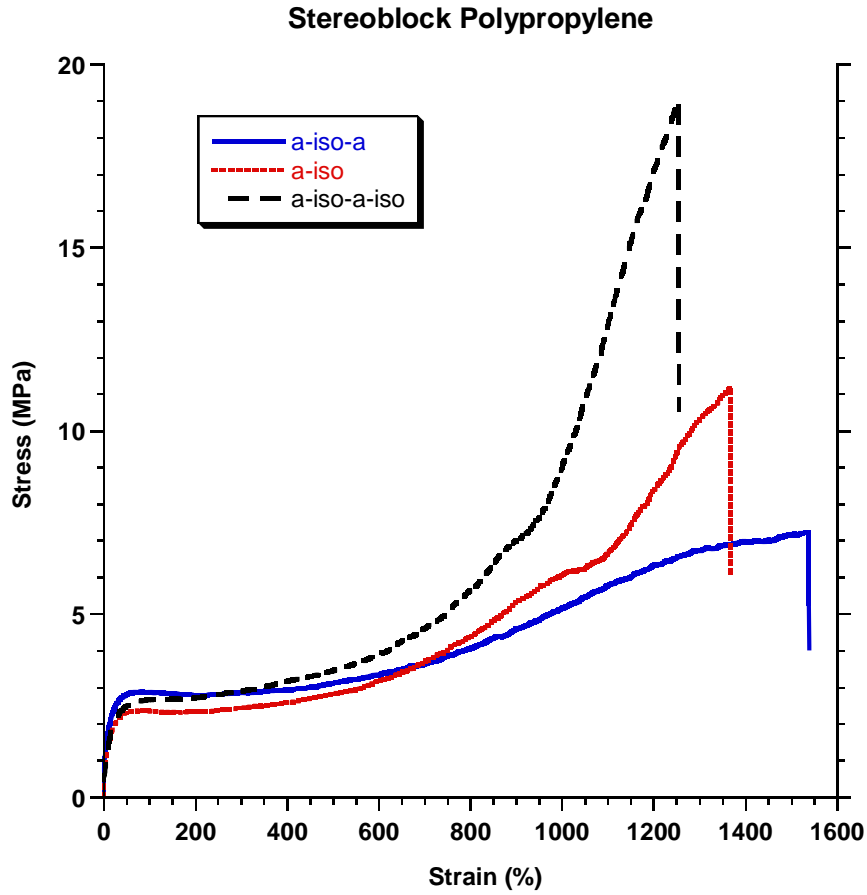


Figure 63. Tensile test results for three *sb*-PPs<sup>237</sup>.

Table 20. Analysis data for tensile test of *sb*-PPs

<i>sb</i> -PP	Recovery after break	Recovery after 300% elongation
<i>a-iso</i> -PP	84.1	81.8
<i>a-iso-a</i> -PP	69.5	69.5
<i>a-iso-a-iso</i> -PP	90.9	87.6

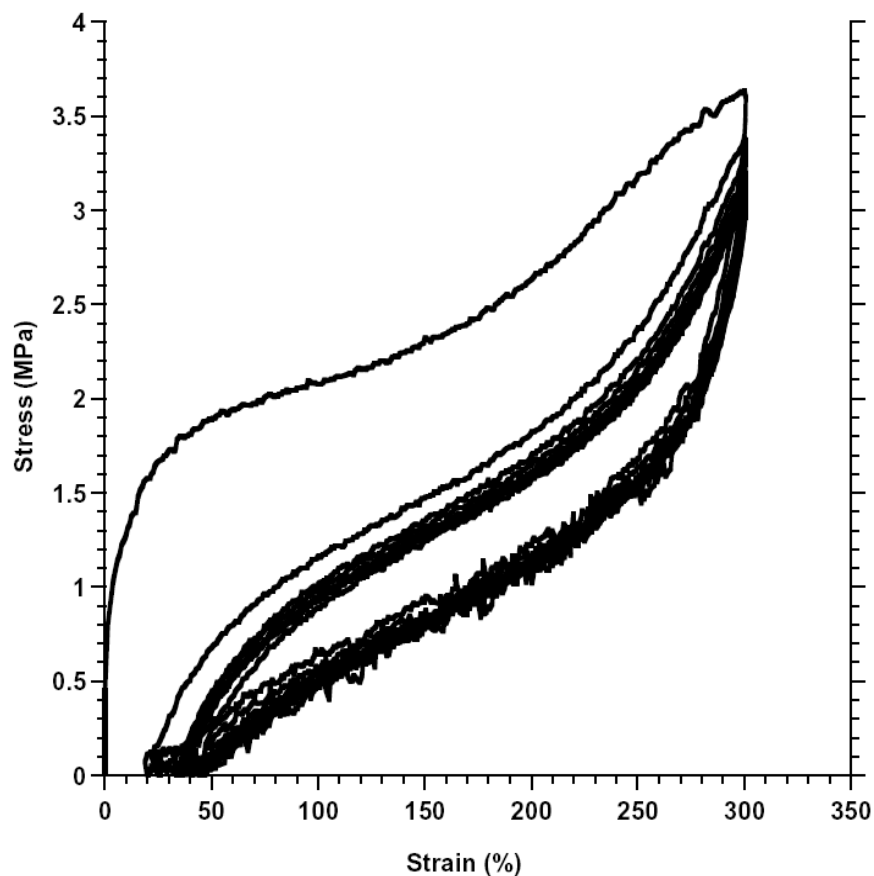


Figure 64. Ten cycle 300% elongation test for *a-iso-a-iso-PP* sample.

DSC analysis of these three samples gave similar patterns, with a single sharp  $T_m$  and  $T_c$ . All the  $T_m$  ( $\sim 110$  °C) and  $T_c$  ( $\sim 65$  °C) are very close. *a-iso-a-iso-PP* tetrablock shows a slightly lower  $T_c$  (58 °C), which probably due to the shorter *isotactic* block length. An *iso-PP* generated by **32** has a  $T_m$  of 112.3°C and  $T_c$  of 79.4°C, while *a-PP* shows no distinguishable melting point or crystalline temperature.

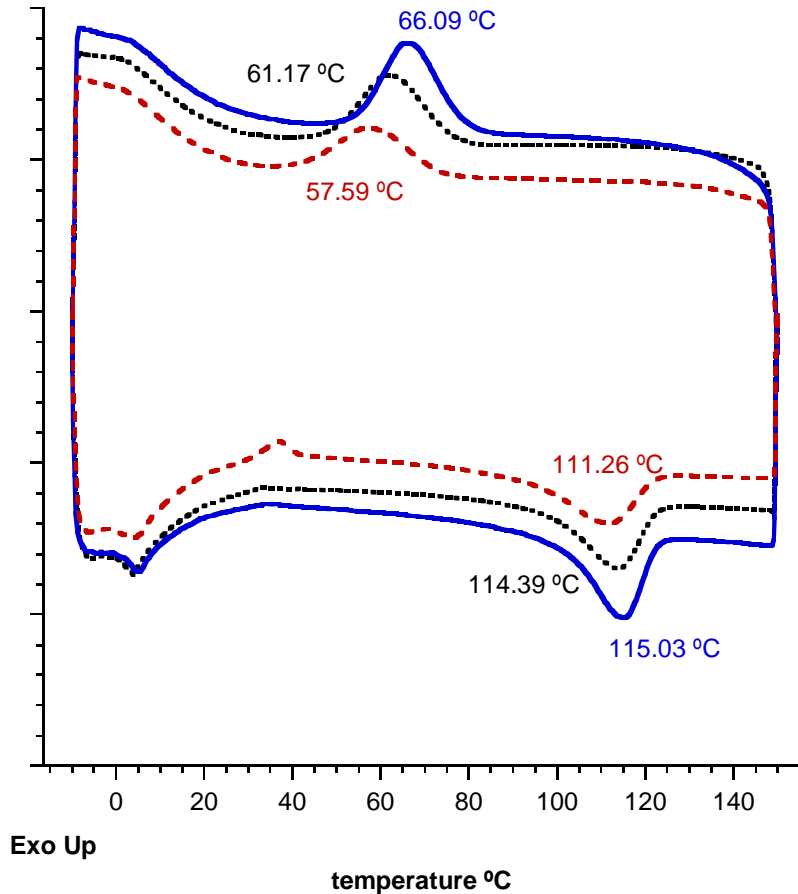


Figure 65. DSC curves for three *sb*-PPs, *a-iso-a* (solid line), *a-iso* (dotted line ) and *a-iso-a-iso* (dashed line)

Phase-sensitive tapping mode atomic force microscope (ps-tm AFP) was employed to analysis these samples<sup>238</sup> in an attempt to relate the physical properties of the *sb*-PP with its microstructure. First, a film of an average thickness of 200  $\mu\text{m}$  was prepared on the surface of amorphous carbon. The film was annealed at 120 °C for 15 h then slowly cooled down to room temperature. Figure 66 shows the phase images of an *iso*-PP, an *sb*-PP film and a super thin film of the *sb*-PP. The *iso*-PP film shows a well-organized lamella crystalline structure, along with small individual crystallites, which is very common for pure *iso*-PP. The image of the *sb*-PP shows

microphase-separation with long crystalline “fibers” crossing each other, though it could also be lamella because AFM only shows the surface image. A super-thin film was obtained after spin cast of a 0.5% wt solution in the carbon surface. Bright crystallite similar to *iso*-PP was observed, all surrounded by dark soft atactic domains. Surprisingly, all three *sb*-PPs show very similar patterns. This probably could be explained that all of the *sb*-PPs have significantly long isotactic blocks to crystallize and have long enough atactic matrixes.

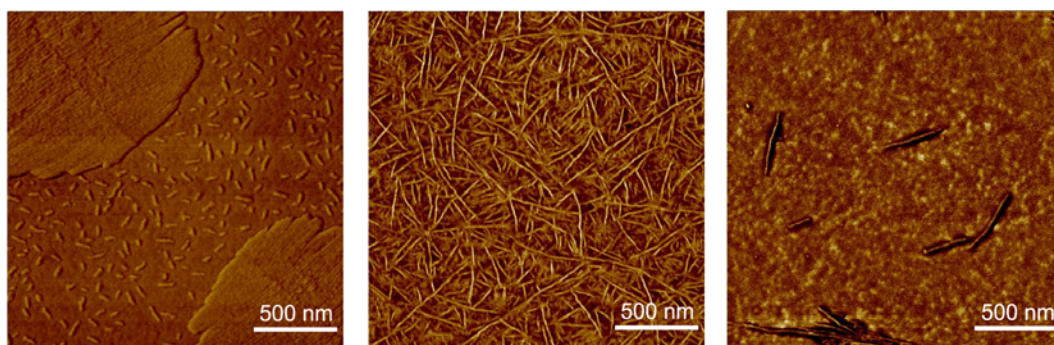


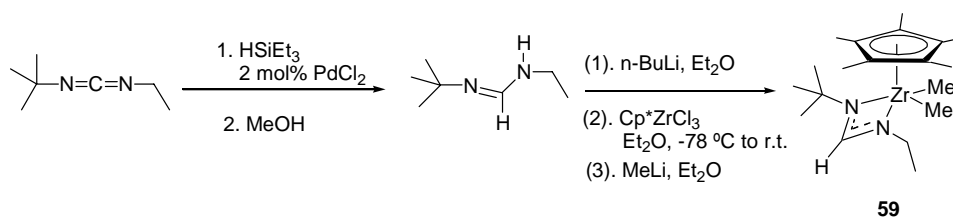
Figure 66. ps-tm AFM phase maps for thin films on amorphous carbon. a) *iso*-PP (left); b) *iso-a-iso*-PP (middle) and c) a thin film of b (right).

## 5.7 Polypropylene Produced by Formamidinate Zirconium Complex

A **19** derivative ( $\eta^5$ -C<sub>5</sub>Me<sub>5</sub>)ZrMe<sub>2</sub>[N(*t*-Bu)C(H)NEt]<sup>189</sup> (**59**) with proton in the distal position was synthesized based on Scheme 48. A stable cation  $\{(\eta^5$ -C<sub>5</sub>Me<sub>5</sub>)ZrMe [N(*t*-Bu)C(H)NEt]}\{B(C<sub>6</sub>F<sub>5</sub>)<sub>4</sub>\} (**60**) was generated by demethylation using **18** or **26** as the co-catalyst at -10 °C. As shown in Figure 67, <sup>1</sup>H NMR spectrum of **60** shows a broad NCH<sub>2</sub>CH<sub>3</sub> peak, which indicates the configurational instability of the formamidinate ligand even at -10 °C.

Compound **59** was subjected to 1-hexene polymerization under full activation conditions, upon activation by **18**. For a 2 h polymerization with 200 equivalents of

1-hexene, a polymer with  $M_n$  of 20 100, polydispersity of 1.59 and 45% yield was obtained. Longer polymerization time does not increase the molecular weight. NMR analysis of the polymer shows no olefin end group for the polymer, which indicates the  $\beta$ -hydride elimination is not a major termination pathway. Also, *a*-PH microstructure was confirmed by NMR analysis.



**Scheme 48. Synthetic route for 58.**

The *a*-PH is produced due to the dynamic configuration of the formamidinate ligand of cation **60**. On the other hand, the ring flipping is not very fast or the NMR spectrum of  $NCH_2CH_3$  region will appear as a quartet (*vide supra*).

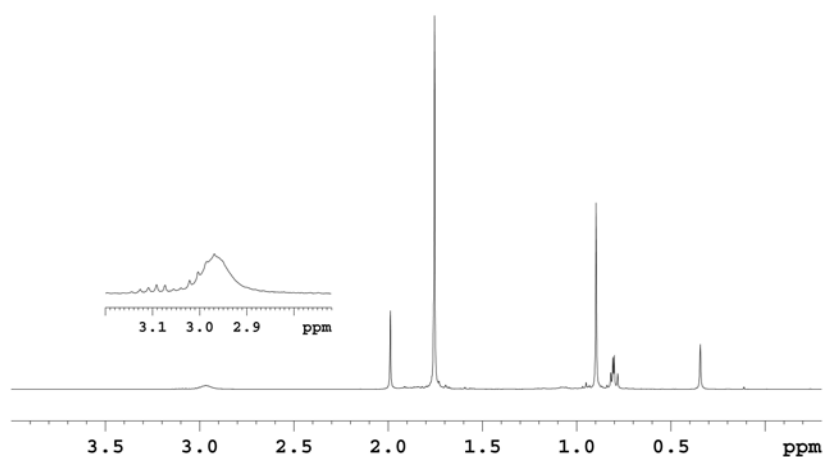
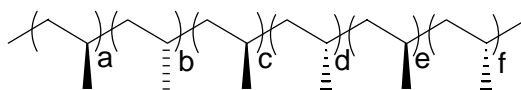


**Figure 67.  $^1\text{H}$  NMR (400 MHz,  $C_6D_5Cl$ ,  $-10\text{ }^\circ\text{C}$ ) spectrum of 60.**

This unique property of **60** can be used to synthesize intriguing microstructure polypropylenes, such as isotactic stereoblock, if the rate of the amidinate ring flipping and the rate of propagating could be controlled. Propylene polymerization was carried out by **60** under full activation conditions. For a 130 min polymerization under 5 psi continuous propylene pressure, PP with  $M_n$  of 98 000, and polydispersity of 1.15 was obtained. This is very surprising. First, a much faster polymerization rate was observed. This is probably due to the more open coordinating site compared to **32**. Second, a rather narrow PDI was obtained, while 1.59 was observed for 1-hexene polymerization.  $^1\text{H}$  NMR of the polymer shows no olefin end group. All these results indicate the propylene polymerization via **60** is *living*, while inferior activity was observed for 1-hexene polymerization.



**Scheme 49. an isotactoc polypropylene stereoblock.**

$^{13}\text{C}$   $\{^1\text{H}\}$  NMR spectrum of the polypropylene obtained is shown in Figure 68. The spectrum does not show very high isoselectivity. But several peaks with isolated r are of great interests. These peaks represent the amidinate ring flipping during propagation. Among the major peaks are the mmmmmmm iso peak, and misinsertion followed by self-correction (such as 21.1 ppm), which shows a mrrm sequence.

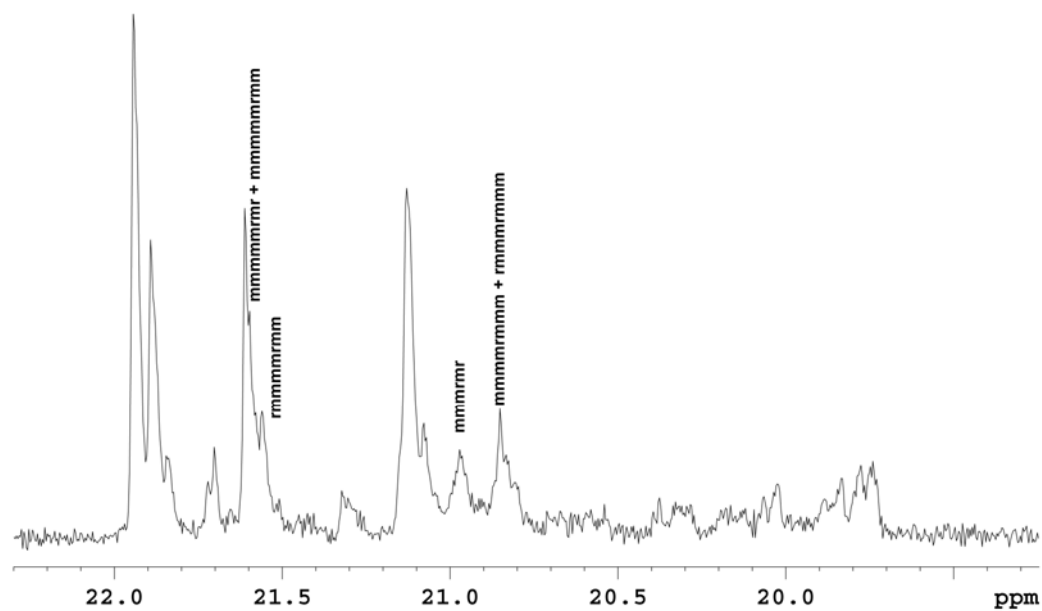


**Figure 68. Methyl region  $^{13}\text{C}$   $\{^1\text{H}\}$  NMR (125 MHz,  $\text{C}_2\text{D}_2\text{Cl}_4$ , 70 °C) spectrum of polypropylene sample obtained from **60**.**

The polymer obtained by **60**, theoretically, should have the similar microstructure compared to the crystalline fraction reported by the oscillating catalyst designed by Waymouth<sup>86</sup>, based on the *rac-rac* mechanism proposed by Busico<sup>98,239</sup> recently (*vide supra*). By precisely controlling the relative rate of propagating and ligand epimerization, a stereoblock with expected block lengths can be obtained. A system of higher  $\sigma$  value with dynamic amidinate property is under investigation.

## 5.8 Conclusions

Living Ziegler-Natta polymerization of propylene with high isoselectivity was successful by using **19** as an efficient initiator, activated by a stoichiometric amount of **18** co-catalyst. When a substoichiometric amount of **18** is used, *a*-PP was obtained instead via the MeDeT mechanism. A zirconium derivative **39** is employed as a methylating reagent, while itself remaining inactive towards propylene

polymerization. By varying the polymerization conditions between MeDeT and full activation, well-defined *sb*-PPs were synthesized for the first time, with full control over molecular weight, tacticity, block sequence and block length, in a living fashion. The designed *sb*-PP shows good to excellent elastomeric properties, with an ultimate elongation up to 1500% and 91% recovery after 300% elongation.

## 5.9 Experimental

**Preparation of  $t\text{-BuN}=\text{C}(\text{H})\text{-NH}(\text{Et})\text{SiEt}_3$ :** To a mixture of 10.1 g (80.0 mmol) of  $t\text{BuN}=\text{C}=\text{NEt}$ , 11.1 g (95.4 mmol) of triethylsilane was added with 0.24 g (1.35 mmol, 1.6 mol%) of  $\text{PdCl}_2$  and the Schlenk tube was sealed. The mixture was heated at 150 °C overnight. After cooling to room temperature, vacuum distillation (85 °C at 4 mmHg) provided a light yellow liquid (11.6 g, 61%).  $^1\text{H}$  NMR (400 MHz, benzene- $d_6$ , 25 °C):  $\delta$  7.57 (s, 1H), 3.26 (q,  $^3\text{J} = 6.8$  Hz, 2H), 1.28 (s, 9H), 1.18 (t,  $^3\text{J} = 6.8$  Hz, 3H), 0.90 (t,  $^3\text{J} = 7.6$  Hz, 9H), 0.59 (q,  $^3\text{J} = 7.6$  Hz, 6H).

**Preparation of  $t\text{-BuN}=\text{C}(\text{H})\text{-CH}_2\text{Et}$ :** To 11.6 g (47.8 mmol) of freshly distilled  $t\text{BuN}=\text{C}(\text{H})\text{-NH}(\text{Et})\text{SiEt}_3$  was added 1.8 g (56.3 mmol) of methanol. The mixture was kept for 1 h. Vacuum distillation provided 5.0 g (81 %) of colorless liquid.  $^1\text{H}$  NMR (400 MHz,  $\text{CDCl}_3$ , 25 °C):  $\delta$  7.40 (s, 1H), 3.16 (q,  $^3\text{J} = 7.2$  Hz, 2H), 1.18 (s, 9H), 1.10 (t,  $^3\text{J} = 7.2$  Hz, 3H).

**Preparation of  $(\eta^5\text{-C}_5\text{Me}_5)\text{ZrCl}_2[\text{N}(t\text{-Bu})\text{C}(\text{H})\text{N}(\text{Et})]$ .** At -30 °C, to a solution of  $t\text{BuN}=\text{C}(\text{H})\text{-NH}(\text{Et})$  (1.03 g, 8.00 mmol) in 100 mL of  $\text{Et}_2\text{O}$ , 2.81 mL of *n*-BuLi (2.90 M in hexane, 8.16 mmol) was added via a syringe. The reaction was allowed to warm up to room temperature within 3 h. This clear solution was then transferred via

cannula into a flask with  $(\eta^5\text{-C}_5\text{Me}_5)\text{ZrCl}_3$  (2.66 g, 8.00 mmol) in 250 mL of  $\text{Et}_2\text{O}$  at  $-78^\circ\text{C}$ . The mixture was allowed warm up slowly and stirred for 12 h, then volatiles removed *in vacuo*. The residue was extracted with toluene, filtered through a short pad of Celite afforded a yellow solution, which upon concentration and cooling to  $-35^\circ\text{C}$  afforded yellow crystals (2.49 g, 73.2%).  $^1\text{H}$  NMR (400 MHz, benzene- $d_6$ ):  $\delta$  7.98 (s, 1H), 3.06 (q,  $^3\text{J} = 7.2$  Hz, 2H), 2.03 (s, 15H), 1.12 (s, 15H), 0.96 (d,  $^3\text{J} = 7.2$  Hz, 3H). Anal. Calcd. for  $\text{C}_{17}\text{H}_{30}\text{Cl}_2\text{N}_2\text{Zr}$ : C 48.09, H 7.12, N 6.60; Found: C 48.19, H 7.02, N 6.36.

**Preparation of  $(\eta^5\text{-C}_5\text{Me}_5)\text{ZrMe}_2[\text{N}(t\text{-Bu})\text{C}(\text{H})\text{NEt}]$  **59**:** To a solution of  $(\eta^5\text{-C}_5\text{Me}_5)\text{ZrCl}_2[t\text{-BuNC}(\text{H})\text{NEt}]$  (0.30 g, 0.71 mmol) in 20 mL of  $\text{Et}_2\text{O}$  at  $-78^\circ\text{C}$ , was added 1.10 mL (14.3 mmol) of MeLi in  $\text{Et}_2\text{O}$ . After slowly warming to room temperature within 1 h, the reaction was stirred for an additional hour before quenching with excess chlorotrimethylsilane, after which the volatiles were removed *in vacuo*. Extraction in pentane and filtration through a thin pad of Celite afforded a light yellow solution, which upon concentration and cooling to  $-35^\circ\text{C}$  afforded off-white crystals (0.19 g, 70%).  $^1\text{H}$  NMR (400 MHz, benzene- $d_6$ ):  $\delta$  8.25 (s, 1H), 2.91 (q,  $^3\text{J} = 7.2$  Hz, 2H), 1.99 (s, 15H), 1.07 (s, 9H), 0.94 (t,  $^3\text{J} = 7.2$  Hz, 3H), 0.26 (s, 6H).  $^{13}\text{C}$  NMR (100 MHz, benzene- $d_6$ ,  $25^\circ\text{C}$ ): 165.2, 120.5, 46.1, 32.1, 23.0, 18.7, 14.9, 12.3. Anal. Calcd. for  $\text{C}_{19}\text{H}_{36}\text{N}_2\text{Zr}$ : C 59.46, H 9.48, N 7.30; Found: C 59.20, H 9.33, N 7.21.

### **Polymerization under DT conditions**

**General procedure:** To a solution of 10.0 mg (0.013 mmol) **18** in 0.5 mL of chlorobenzene at  $-10^\circ\text{C}$  was added 10.0 mg (0.025 mmol) of **19** in 0.5 mL of

chlorobenzene at -10 °C. This solution was then rapidly added to a 50 mL Schlenk flask charged with 20 mL of chlorobenzene at -10 °C, which was previously pressurized to 5 psi with propylene and stirred for 10 minutes. The flask was then repressurized and the pressure maintained for 2 hours while stirring before quenching with 1 mL of acidic methanol. The volatiles were then removed *in vacuo* and the crude polymeric material was purified through precipitation of a hot toluene solution into a large volume of acidic methanol. The final pure polypropylene was collected and dried overnight at 60 °C (0.01 mmHg).

**Kinetics experiment under DT conditions:** The polymerization was carried out in the same manner as the general procedure, while 20.0 mg (0.05 mmol) of **19** and 20.0 mg (0.025 mmol) of **18** were used and the total solution volume was 35 mL. Aliquots were quenched with methanol after 48 min and 5 more points were collected within the next 5 h. Polypropylene samples were purified and GPC data was collected.

**Polymerization under non-DT conditions.**

General procedure conducted in an identical manner to DT condition, but an equal molar ratio of **19** to **18** were used.

**Kinetics under non-DT condition:** In order to circumvent solubility issues, the kinetics of isotactic propagation were determined by first synthesizing an atactic polypropylene block under DT conditions using 20.5 mg (0.051 mmol) **19** and 21.2 mg (0.026 mmol) **18** in 10 mL chlorobenzene for 2 hours. The solution was then

diluted to 60 mL total volume and the reaction was switched to non-DT conditions by fully activating the system with a second portion of 21.2 mg of **18**. Aliquots were quenched with acidic methanol at 10 min. from full activation and approximately every 30 min. thereafter for 3 h.

**Synthesis of *a*-iso-PP stereoblock diblock:** Under non-DT conditions, a polymerization was carried out using 25.0 mg (0.063 mmol) **19** and 25.2 mg (0.031 mmol) **18** in 100 mL chlorobenzene for 30 h. At this point the reaction was switched to non-DT by the addition of a second portion of 25.2 mg (0.031 mmol) of **18** in ~ 0.5 mL chlorobenzene for 10 h, after which the reaction was quenched with ~1 mL of acidic methanol, the volatiles were removed *in vacuo* and the crude polymeric material was purified through precipitation of a hot toluene solution into a large volume of acidic methanol. The final pure polypropylene was collected and dried overnight at 60 °C (0.01 mmHg). Yield: 5.70 g.  $M_n = 162\ 100$ , PDI = 1.20. Detailed  $^{13}\text{C}$  { $^1\text{H}$ } NMR proved the total iso:a ratio of the diblock to be 41:59.

**Synthesis of *a*-iso-*a*-PP stereoblock triblock:** Under non-DT conditions, a polymerization was carried out using 25.0 mg (0.063 mmol) **19** and 25.2 mg (0.031 mmol) **18** in 100 mL chlorobenzene for 15 h. At this point the reaction was switched to non-DT by the addition of a second portion of 25.2 mg (0.031 mmol) of **18** in ~ 0.5 mL chlorobenzene for 10 h, after which the reaction was returned to DT by the addition of 13.8 mg (0.031 mmol) **39** for another 15 h. The reaction was then quenched with ~1 mL of acidic methanol, the volatiles were removed *in vacuo* and

the crude polymeric material was purified through precipitation of a hot toluene solution into a large volume of acidic methanol. The final pure polypropylene was collected and dried overnight at 60 °C (0.01 mmHg). Yield: 6.92 g.  $M_n = 167\,500$ , PDI = 1.19. Detailed  $^{13}\text{C} \{^1\text{H}\}$  NMR proved the total *iso:a* ratio of the triblock to be 39:61.

**Synthesis of *a-iso-a-iso*-PP stereoblock tetrablock:** Under non-DT conditions, a polymerization was carried out using 36.0 mg (0.063 mmol) **19** and 25.2 mg (0.031 mmol) **18** in 100 mL chlorobenzene for 15 h. At this point the reaction was switched to non-DT by the addition of a second portion of 25.2 mg (0.031 mmol) of **18** in ~ 0.5 mL chlorobenzene for 5 h, after which the reaction was returned to DT by the addition of 13.8 mg (0.031 mmol) **39** for another 15 h. The reaction was then returned to non-DT by a final addition of 25.2 mg (0.031 mmol) **18** in ~ 0.5 mL chlorobenzene for 5 h before being quenched with ~1 mL of acidic methanol. The volatiles were removed *in vacuo* and the crude polymeric material was purified through precipitation of a hot toluene solution into a large volume of acidic methanol. The final pure polypropylene was collected and dried overnight at 60 °C (0.01 mmHg). Yield: 6.54 g.  $M_n = 172\,500$ , PDI = 1.19. Detailed  $^{13}\text{C} \{^1\text{H}\}$  NMR proved the total *iso:a* ratio of the tetrablock to be 37:63.

**Tensile test for polypropylene stereoblock triblocks:** The materials were compression molded at 135 °C into 0.5 mm-thick sheets from which dumbbell were cut using the ASTM D638-5 cutter. The testing was conducted on an Instron model

3345 tensile tester equipped with pneumatic grips and extensometer at an extension rate of 2 in/min. Recovery after break and recovery after 300% elongation were calculated as defined in the ASTM D412 method.

**DSC analysis conditions for the *sb*-PPs:** A temperature rate of 10 °C/min was applied. The sample was heated up to 220 °C and kept isothermal for 20 min under nitrogen atmosphere before the analysis to erase any possible heat history. Scan temperature was ranged from -10 °C to 150 °C, and repeated at least 2 times. Identical curves were observed for each sample. 8 – 10 mg of sample was used.

Kinetic model for PP polymerizations:

$$[\text{Zr}]_0 \frac{dM_n}{dt} = M_1 \cdot R_p = M_1 \cdot k_p [\text{M}] [\text{Zr}]_t$$

$$\frac{dM_n}{dt} = M_1 \cdot k_p [\text{M}] \frac{[\text{Zr}]_t}{[\text{Zr}]_0}$$

while for unimolecular 1<sup>st</sup> order decomposition of the zirconium cation:

$$\ln \frac{[\text{Zr}]_0}{[\text{Zr}]_t} = k_t \cdot t$$

$$\frac{[\text{Zr}]_t}{[\text{Zr}]_0} = e^{-k_t \cdot t}$$

$$\frac{dM_n}{dt} = M_1 \cdot k_p [\text{M}] e^{-k_t \cdot t}$$

$$dM_n = M_1 \cdot k_p [\text{M}] e^{-k_t \cdot t} dt$$

$$M_n = M_1 \cdot \frac{k_p}{k_t} [\text{M}] (e^{-k_t \cdot t} - 1) \approx M_1 \cdot \frac{k_p [\text{M}]}{k_t} (1 + k_t t - \frac{k_t^2}{2} t^2 - 1) = M_1 \cdot \frac{k_p [\text{M}]}{k_t} (k_t t - \frac{k_t^2}{2} t^2)$$

$$M_n \approx M_1 \cdot k_p [\text{M}] t - M_1 \cdot k_p \frac{k_t}{2} t^2$$

For a 2<sup>nd</sup> order polynomial fitting equation  $y = a + bx + cx^2$

$$\frac{b}{c} = \frac{k_t}{k_t^2/2} = \frac{2}{k_t} \quad \text{and} \quad k_t = \frac{2c}{b}$$

$$k_p = \frac{b}{M_1 \cdot [\text{M}]}$$

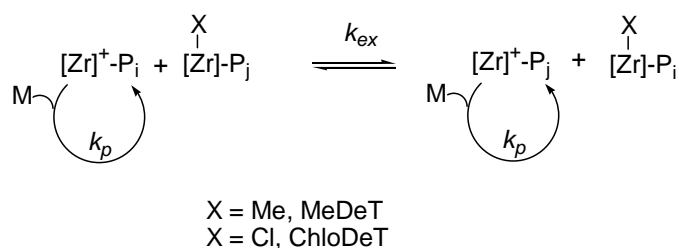
$M_1$  : molecular weight of a monomer

$[\text{M}]$ : monomer concentration, which is 0.129 M at -10 °C at 5 psi.

## Chapter 6 Conclusions

A degenerative transfer (DT) living Ziegler-Natta polymerization system based on pentamethyl cyclopentadienyl amidinate zirconium **19** has been studied in detail. Compound **19** is an efficient initiator for polymerizations of  $\alpha$ -olefins and propylene in a living and stereospecific fashion, upon activation by a *stoichiometric* amount of **18**. With a *substoichiometric* amount of **18**, degenerative transfer living Ziegler-Natta polymerization occurs. The extremely fast interconversion between an active cationic zirconium species and a dormant neutral zirconium species via a methyl group (MeDeT) or chloride group (ChloDeT) is essential for degenerative transfer to occur ( $R_{ex} \gg R_p$ ). Detailed mechanistic studies and kinetic analysis were carried out.

Under MeDeT polymerization conditions, atactic polyolefins are produced due to the configuration instability of the amidinate ligand at its dormant state, and the dramatic rate difference between epimerization and propagation ( $R_{epi} \gg R_p$ ). The configurational stability of all the species involved in ChloDeT ensures the stereospecific property of the polymerization.



**Scheme 50. Mechanism of Degenerative Transfer Polymerization.**

Methylating reagents such as **34** and **39** were designed and synthesized to change the polymerization conditions of a fully activated system to degenerative transfer conditions. Adding co-catalyst and methylating reagents alternatively to a

polymerization system produces well-defined stereoblock polyolefins. For the first time, an stereoblock polyolefin with controlled block length, block tacticity and block placement within the polymer backbone can be synthesized.

Also, living stereospecific propylene polymerization was carried out by **32**. A mmmm of 73% and a  $\sigma$  value of 94% was determined, which is the best among living polypropylene polymerizations reported to date, while under degenerative transfer conditions, atactic polypropylene was produced. Applying the same methodology, stereoblock polypropylene was synthesized with controlled block length, block tacticity for the first time. Preliminary data shows excellent elastomeric properties for the *sb*-PPs synthesized.

On the other hand, pre-catalyst **19** was chemically immobilized to polystyrene based solid support material via deprotonation and nucleophilic addition reactions on the distal position of **40**. Heterogeneous catalyst **58** polymerizes  $\alpha$ -olefins in a living and stereospecific fashion. Also, a long shelf time was observed for an activated initiator **58** at room temperature. This is the first living Ziegler-Natta stereospecific catalyst been reported to date.

## References

- (1) Ziegler, K.; Holzkamp, E.; Breil, H.; Martin, H. *Angew. Chem., Int. Ed.* **1955**, *67*, 426-426.
- (2) Natta, G.; Pino, P.; Corradini, P.; Danusso, F.; Mantica, E.; Mazzanti, G.; Moraglio, G. *J. Am. Chem. Soc.* **1955**, *77*, 1708-1710.
- (3) American Plastic Council, 2004 review.
- (4) Natta, G. *Makromol. Chem.* **1955**, *16*, 213-237.
- (5) Natta, G. *Angew. Chem., Int. Ed.* **1956**, *68*, 393-403.
- (6) Natta, G. *Chem. Ind.* **1957**, 1520-1530.
- (7) Natta, G.; Pino, P.; Mazzanti, G.; Giannini, U. *J. Am. Chem. Soc.* **1957**, *79*, 2975-2976.
- (8) Blomenhofer, M.; Ganzleben, S.; Hanft, D.; Schmidt, H.-W.; Kristiansen, M.; Smith, P.; Stoll, K.; Mader, D.; Hoffmann, K. *Macromolecules* **2005**, *38*, 3688-3695.
- (9) Shoshany, H.; Shoshany, A. In *U.S. Pat. Appl. Publ.*; (Israel). US, 2005, p 5 pp.
- (10) Rojo, E.; Fernandez, M.; Pena, J. J.; Pena, B.; Munoz, M. E.; Santamaria, A. *Polym. Eng. Sci.* **2004**, *44*, 1792-1799.
- (11) Zanchetta, N.; Mohseen, S. In *U.S. Pat. Appl. Publ.*; (USA). US, 2004, p 11 pp., Cont.-in-part of U.S. Pat. Appl. 2003 203,145.
- (12) Getlichermann, M.; Cogneau, P. In *Eur. Pat. Appl.*; (Performance Roof Systems S.A. En Abrege P.R.S., Belg.). Ep, 2001, p 16 pp.

- (13) McNally, T.; Fawcett, A. H.; McNally, G. M.; Andrews, F.; Clarke, J. *Annual Technical Conference - Society of Plastics Engineers* **1998**, *56th*, 2486-2491.
- (14) Arlman, E. J. *J. Catal.* **1964**, *3*, 89.
- (15) Arlman, E. J.; Cossee, P. *J. Catal.* **1964**, *3*, 99.
- (16) Cossee, P. *J. Catal.* **1964**, *3*, 80.
- (17) Cossee, P. *Tetrahedron lett.* **1960**, *17*, 12.
- (18) Hillman, M.; Weiss, A. J.; Hahne, R. M. A. *Radiochimica Acta* **1969**, *12*, 200-2.
- (19) Breslow, D. S.; Newburg, N. R. *J. Am. Chem. Soc.* **1957**, *79*, 5072-3.
- (20) Breslow, D. S.; Newburg, N. R. *J. Am. Chem. Soc.* **1959**, *81*, 81-6.
- (21) Long, W. P.; Breslow, D. S. *J. Am. Chem. Soc.* **1960**, *82*, 1953-1957.
- (22) James C. W. Chien, B.-P. W. *J. Polym. Sci. Part A: Polym. Chem.* **1988**, *26*, 3089-3102.
- (23) Kaminsky, W.; Kuelper, K.; Brintzinger, H. H.; Wild, F. R. W. P. *Angew. Chem.* **1985**, *97*, 507-8.
- (24) Kaminsky, W. *Stud. in Surf. Sci. and Catal.* **1986**, *25*, 293-304.
- (25) Kaminsky, W.; Miri, M. H. *Homogeneous Heterog. Catal., Proc. Int. Symp. Relat. Homogeneous Heterog. Catal., 5th* **1986**, 327-41.
- (26) Kaminsky, W.; Hahnsen, H. *Adv. Polyolefins, [Proc. ACS Int. Symp.]* **1987**, 361-71.
- (27) Kaminsky, W.; Steiger, R. *Polyhedron* **1988**, *7*, 2375-81.

- (28) Andresen, A.; Cordes, H. G.; Herwig, J.; Kaminsky, W.; Merck, A.; Mottweiler, R.; Pein, J.; Sinn, H.; Vollmer, H. J. *Angew. Chem.* **1976**, *88*, 689-90.
- (29) Schneider, M. J.; Suhm, J.; Muelhaupt, R.; Prosenc, M.-H.; Brintzinger, H.-H. *Macromolecules* **1997**, *30*, 3164-3168.
- (30) Herwig, J.; Kaminsky, W. *Poly. Bull. (Berlin, Germany)* **1983**, *9*, 464-9.
- (31) Kaminsky, W.; Miri, M.; Sinn, H.; Woldt, R. *Makromol. Chem., Rapid Commun.* **1983**, *4*, 417-21.
- (32) Smith, J. A.; Brintzinger, H. H. *J. Organomet. Chem.* **1981**, *218*, 159-167.
- (33) Smith, J. A.; Von Seyerl, J.; Huttner, G.; Brintzinger, H. H. *J. Organomet. Chem.* **1979**, *173*, 175-85.
- (34) Diamond, G. M.; Jordan, R. F.; Petersen, J. L. *Organometallics* **1996**, *15*, 4045-4053.
- (35) Christopher, J. N.; Diamond, G. M.; Jordan, R. F.; Petersen, J. L. *Organometallics* **1996**, *15*, 4038-4044.
- (36) Diamond, G. M.; Jordan, R. F.; Petersen, J. L. *Organometallics* **1996**, *15*, 4030-4037.
- (37) Diamond, G. M.; Jordan, R. F.; Petersen, J. L. *J. Am. Chem. Soc.* **1996**, *118*, 8024-8033.
- (38) Diamond, G. M.; Rodewald, S.; Jordan, R. F. *Organometallics* **1995**, *14*, 5-7.
- (39) Resconi, L.; Cavallo, L.; Fait, A.; Piemontesi, F. *Chem. Rev.* **2000**, *100*, 1253-1345.

- (40) Kawamurakuribayashi, H.; Koga, N.; Morokuma, K. *J. Am. Chem. Soc.* **1992**, *114*, 2359-2366.
- (41) Yoshida, T.; Koga, N.; Morokuma, K. *Organometallics* **1996**, *15*, 766-777.
- (42) Makio, H.; Fujita, T. *Bull. Chem. Soc. Jpn* **2005**, *78*, 52-66.
- (43) Mason, A. F.; Coates, G. W. *J. Am. Chem. Soc.* **2004**, *126*, 16326-16327.
- (44) Ewen, J. A. *J. Am. Chem. Soc.* **1984**, *106*, 6355.
- (45) Kaminsky, W.; Wild, F.; Kulper, K.; Brintzinger, H. *Angew. Chem., Int. Ed. Engl.* **1985**, *24*, 507.
- (46) Busico, V.; Cipullo, R.; Monaco, G.; Vacatello, M.; Bella, J.; Segre, A. L. *Macromolecules* **1998**, *31*, 8713-8719.
- (47) Busico, V.; Cipullo, R.; Vacatello, M.; Segre, A. L. *Abstracts of Papers of the American Chemical Society* **1997**, *213*, 290-POLY.
- (48) Busico, V.; Cipullo, R. *Prog. Polym. Sci.* **2001**, *26*, 443-533.
- (49) Ewen, J. A.; Elder, M. J.; Jones, R. L.; Haspeslagh, L.; Atwood, J. L.; Bott, S. G.; Robinson, K. *Makromol. Chem.-Macromol. Symp.* **1991**, *48-9*, 253-295.
- (50) Ewen, J. A.; Jones, R. L.; Razavi, A.; Ferrara, J. D. *J. Am. Chem. Soc.* **1988**, *110*, 6255-6256.
- (51) Volkis, V.; Shmulinson, M.; Averbuj, C.; Lisovskii, A.; Edelman, F. T.; Eisen, M. S. *Organometallics* **1998**, *17*, 3155-3157.
- (52) Busico, V.; Cipullo, R. *J. Am. Chem. Soc.* **1994**, *116*, 9329-9330.
- (53) Leclerc, M. K.; Brintzinger, H. H. *J. Am. Chem. Soc.* **1995**, *117*, 1651-1652.
- (54) Busico, V.; Caporaso, L.; Cipullo, R.; Landriani, L.; Angelini, G.; Margonelli, A.; Segre, A. L. *J. Am. Chem. Soc.* **1996**, *118*, 2105-2106.

- (55) Leclerc, M. K.; Brintzinger, H. H. *J. Am. Chem. Soc.* **1996**, *118*, 9024-9032.
- (56) Busico, V.; Brita, D.; Caporaso, L.; Cipullo, R.; Vacatello, M.  
*Macromolecules* **1997**, *30*, 3971-3977.
- (57) Resconi, L. *J. Mol. Catal. A, Chem.* **1999**, *146*, 167-178.
- (58) Karol, F. J.; Kao, S. C.; Wasserman, E. P.; Brady, R. C. *New J. Chem.* **1997**,  
*21*, 797-805.
- (59) Abrams, M. B.; Yoder, J. C.; Loeber, C.; Day, M. W.; Bercaw, J. E.  
*Organometallics* **1999**, *18*, 1389-1401.
- (60) Yoder, J. C.; Bercaw, J. E. *J. Am. Chem. Soc.* **2002**, *124*, 2548-2555.
- (61) Harney, M. B.; Keaton, R. J.; Sita, L. R. *J. Am. Chem. Soc.* **2004**, *126*, 4536-  
4537.
- (62) Fierro, R.; Yu, Z.; Rausch, M. D.; Dong, S.; Alvares, D.; Chien, J. C. W. *J.*  
*Polym. Sci., Part A: Polym. Chem.* **1994**, *32*, 661-73.
- (63) Mallin, D. T.; Rausch, M. D.; Lin, Y. G.; Dong, S.; Chien, J. C. W. *J. Am.*  
*Chem. Soc.* **1990**, *112*, 2030-1.
- (64) Natta, G. *J. Poly. Sci.* **1959**, *34*, 531-549.
- (65) Chien, J. C. W.; Llinas, G. H.; Rausch, M. D.; Lin, G. Y.; Winter, H. H.;  
Atwood, J. L.; Bott, S. G. *J. Am. Chem. Soc.* **1991**, *113*, 8569-70.
- (66) Babu, G. N.; Newmark, R. A.; Cheng, H. N.; Llinas, G. H.; Chien, J. C. W.  
*Macromolecules* **1992**, *25*, 7400-2.
- (67) Llinas, G. H.; Dong, S. H.; Mallin, D. T.; Rausch, M. D.; Lin, Y. G.; Winter,  
H. H.; Chien, J. C. W. *Macromolecules* **1992**, *25*, 1242-53.
- (68) Gauthier, W. J.; Collins, S. *Macromolecules* **1995**, *28*, 3779-86.

- (69) Gauthier, W. J.; Corrigan, J. F.; Taylor, N. J.; Collins, S. *Macromolecules* **1995**, *28*, 3771-8.
- (70) Llinas, G. H.; Day, R. O.; Rausch, M. D.; Chien, J. C. W. *Organometallics* **1993**, *12*, 1283-1288.
- (71) Collette, J. W.; Ovenall, D. W.; Buck, W. H.; Ferguson, R. C. *Macromolecules* **1989**, *22*, 3858-3866.
- (72) Collette, J. W.; Tullock, C. W.; Macdonald, R. N.; Buck, W. H.; Su, A. C. L.; Harrell, J. R.; Mulhaupt, R.; Anderson, B. C. *Macromolecules* **1989**, *22*, 3851-3858.
- (73) Miyake, S.; Okumura, Y.; Inazawa, S. *Macromolecules* **1995**, *28*, 3074-3079.
- (74) Giardello, M. A.; Eisen, M. S.; Stern, C. L.; Marks, T. J. *J. Am. Chem. Soc.* **1995**, *117*, 12114-12129.
- (75) Giardello, M. A.; Eisen, M. S.; Stern, C. L.; Marks, T. J. *J. Am. Chem. Soc.* **1993**, *115*, 3326-3327.
- (76) Deng, H.; Winkelbach, H.; Taeji, K.; Kaminsky, W.; Soga, K. *Macromolecules* **1996**, *29*, 6371-6376.
- (77) Guerra, G.; Cavallo, L.; Moscardi, G.; Vacatello, M.; Corradini, P. *Macromolecules* **1996**, *29*, 4834-4845.
- (78) Fierro, R.; Chien, J. C. W.; Rausch, M. D. *J. Polym. Sci., Part A, Polym. Chem.* **1994**, *32*, 2817-2824.
- (79) Esteb, J. J.; Bergeron, M.; Dormady, C. N.; Chien, J. C. W.; Rausch, M. D. *J. Organomet. Chem.* **2003**, *675*, 97-104.

- (80) Esteb, J. J.; Chien, J. C. W.; Rausch, M. D. *J. Organomet. Chem.* **2003**, *688*, 153-160.
- (81) Thomas, E. J.; Rausch, M. D.; Chien, J. C. W. *Organometallics* **2000**, *19*, 4077-4083.
- (82) Thomas, E. J.; Chien, J. C. W.; Rausch, M. D. *Macromolecules* **2000**, *33*, 1546-1552.
- (83) Rieger, B.; Jany, G.; Fawzi, R.; Steimann, M. *Organometallics* **1994**, *13*, 647-653.
- (84) Kukral, J.; Lehmus, P.; Klinga, M.; Leskela, M.; Rieger, B. *Eur. J. Inorg. Chem.* **2002**, 1349-1356.
- (85) Dietrich, U.; Hackmann, M.; Rieger, B.; Klinga, M.; Leskela, M. *J. Am. Chem. Soc.* **1999**, *121*, 4348-4355.
- (86) Coates, G. W.; Waymouth, R. M. *Science* **1995**, *267*, 217-219.
- (87) Dreier, T.; Erker, G.; Frohlich, R.; Wibbeling, B. *Organometallics* **2000**, *19*, 4095-4103.
- (88) Kravchenko, R.; Masood, A.; Waymouth, R. M. *Organometallics* **1997**, *16*, 3635-3639.
- (89) Petoff, J. L. M.; Bruce, M. D.; Waymouth, R. M.; Masood, A.; Lal, T. K.; Quan, R. W.; Behrend, S. J. *Organometallics* **1997**, *16*, 5909-5916.
- (90) Kimura, K.; Takaishi, K.; Matsukawa, T.; Yoshimura, T.; Yamazaki, H. *Chem. Lett.* **1998**, 571-572.
- (91) Kravchenko, R.; Masood, A.; Waymouth, R. M.; Myers, C. L. *J. Am. Chem. Soc.* **1998**, *120*, 2039-2046.

- (92) Lee, G. Y.; Xue, M.; Kang, M. S.; Kwon, O. C.; Yoon, J. S.; Lee, Y. S.; Kim, H. S.; Lee, H.; Lee, I. M. *J. Organomet. Chem.* **1998**, *558*, 11-18.
- (93) Lin, S.; Hauptman, E.; Lal, T. K.; Waymouth, R. M.; Quan, R. W.; Ernst, A. *B. J. Mol. Catal. A-Chem.* **1998**, *136*, 23-33.
- (94) Witte, P.; Lal, T. K.; Waymouth, R. M. *Organometallics* **1999**, *18*, 4147-4155.
- (95) Wang, W.; Fan, Z. Q.; Feng, L. X.; Li, C. H. *Eur. Polym. J.* **2005**, *41*, 83-89.
- (96) Lin, S.; Waymouth, R. M. *Acc. Chem. Res.* **2002**, *35*, 765-773.
- (97) Busico, V.; Cipullo, R.; Segre, A. L.; Talarico, G.; Vacatello, M.; Castelli, V. *V. A. Macromolecules* **2001**, *34*, 8412-8415.
- (98) Busico, V.; Castelli, V. V. A.; Aprea, P.; Cipullo, R.; Segre, A.; Talarico, G.; Vacatello, M. *J. Am. Chem. Soc.* **2003**, *125*, 5451-5460.
- (99) Wilmes, G. M.; France, M. B.; Lynch, S. R.; Waymouth, R. M. In *224th National Meeting of the American Chemical Society* Boston, MA, 2002.
- (100) Chien, J. C. W.; Iwamoto, Y.; Rausch, M. D.; Wedler, W.; Winter, H. H. *Macromolecules* **1997**, *30*, 3447-3458.
- (101) Chien, J. C. W.; Iwamoto, Y.; Rausch, M. D. *J. Polym. Sci., Part A: Polym. Chem.* **1999**, *37*, 2439-2445.
- (102) Lieber, S.; Brintzinger, H. H. *Macromolecules* **2000**, *33*, 9192-9199.
- (103) Jayaratne, K. C.; Sita, L. R. *J. Am. Chem. Soc.* **2001**, *123*, 10754-10755.
- (104) Matyjaszewski, K., Müller A. Macromolecular Nomenclature Note No. 12, [www.polyacs.org/nomcl/mnn12.html](http://www.polyacs.org/nomcl/mnn12.html)

- (105) Hadjichristidis, N.; Pitsikalis, M.; Pispas, S.; Iatrou, H. *Chem. Rev.* **2001**, *101*, 3747-3792.
- (106) Ramireddy, C.; Tuzar, Z.; Prochazka, K.; Webber, S. E.; Munk, P. *Macromolecules* **1992**, *25*, 2541-2545.
- (107) Fayt, R.; Forte, R.; Jacobs, C.; Jerome, R.; Ouhadi, T.; Teyssie, P.; Varshney, S. K. *Macromolecules* **1987**, *20*, 1442-1444.
- (108) Wayland, B. B.; Poszmik, G.; Mukerjee, S. L.; Fryd, M. *J. Am. Chem. Soc.* **1994**, *116*, 7943-7944.
- (109) Aoshima, S.; Higashimura, T. *Macromolecules* **1989**, *22*, 1009-1013.
- (110) Higashimura, T.; Aoshima, S.; Sawamoto, M. *Makromol. Chem.-Macromol. Symp.* **1988**, *13-4*, 457-471.
- (111) Sawamoto, M.; Okamoto, C.; Higashimura, T. *Macromolecules* **1987**, *20*, 2693-2697.
- (112) *tele* means far, and *chele* means claw, in Greek
- (113) Lamberti, M.; Mazzeo, M.; Pappalardo, D.; Zambelli, A.; Pellecchia, C. *Macromol. Symp.* **2004**, *213*, 235-251.
- (114) Doi, Y.; Ueki, S.; Keii, T. *Macromolecules* **1979**, *12*, 814-819.
- (115) Liang, L. C.; Schrock, R. R.; Davis, W. M.; McConville, D. H. *J. Am. Chem. Soc.* **1999**, *121*, 5797-5798.
- (116) Baumann, R.; Davis, W. M.; Schrock, R. R. *J. Am. Chem. Soc.* **1997**, *119*, 3830-3831.
- (117) Schrock, R. R.; Baumann, R.; Reid, S. M.; Goodman, J. T.; Stumpf, R.; Davis, W. M. *Organometallics* **1999**, *18*, 3649-3670.

- (118) Liang, L. C.; Schrock, R. R.; Davis, W. M. *Organometallics* **2000**, *19*, 2526-2531.
- (119) Mehrkhodavandi, P.; Schrock, R. R. *Abstracts of Papers of the American Chemical Society* **2002**, *224*, U502-U502.
- (120) Mehrkhodavandi, P.; Schrock, R. R.; Pryor, L. L. *Organometallics* **2003**, *22*, 4569-4583.
- (121) Schrock, R. R.; Adamchuk, J.; Ruhland, K.; Lopez, L. P. H. *Organometallics* **2003**, *22*, 5079-5091.
- (122) Matsui, S.; Mitani, M.; Saito, J.; Tohi, Y.; Makio, H.; Tanaka, H.; Fujita, T. *Chem. Lett.* **1999**, 1263-1264.
- (123) Coates, G. W.; Hustad, P. D.; Reinartz, S. *Angew. Chem., Int. Ed.* **2002**, *41*, 2236-2257.
- (124) Jayaratne, K. C.; Keaton, R. J.; Henningsen, D. A.; Sita, L. R. *J. Am. Chem. Soc.* **2000**, *122*, 10490-10491.
- (125) Jayaratne, K. C.; Sita, L. R. *J. Am. Chem. Soc.* **2000**, *122*, 958-959.
- (126) Keaton, R. J.; Jayaratne, K. C.; Henningsen, D. A.; Koterwas, L. A.; Sita, L. R. *J. Am. Chem. Soc.* **2001**, *123*, 6197-6198.
- (127) Keaton, R. J.; Jayaratne, K. C.; Sita, L. R. *Abstracts of Papers of the American Chemical Society* **2001**, *221*, U648-U648.
- (128) Sita, L. R.; Jayaratne, K. C.; Keaton, R. J.; Henningsen, D. A. *Abstracts of Papers of the American Chemical Society* **2001**, *222*, U552-U553.

- (129) Sita, L. R.; Keaton, R. J.; Jayaratne, K. C.; Kissounko, D. A.; Zhang, Y. H. *Abstracts of Papers of the American Chemical Society* **2002**, 224, U502-U502.
- (130) Hagihara, H.; Shiono, T.; Ikeda, T. *Macromolecules* **1998**, 31, 3184-3188.
- (131) Hasan, T.; Ioku, A.; Nishii, K.; Shiono, T.; Ikeda, T. *Macromolecules* **2001**, 34, 6152-6152.
- (132) Nishii, K.; Shiono, T.; Ikeda, T. *Macromol. Rapid Commun.* **2004**, 25, 1029-1032.
- (133) Tshuva, E. Y.; Goldberg, I.; Kol, M.; Goldschmidt, Z. *Inorg. Chem. Commun.* **2000**, 3, 611-614.
- (134) Ittel, S. D.; Johnson, L. K.; Brookhart, M. *Chem. Rev.* **2000**, 100, 1169-1203.
- (135) Scollard, J. D.; McConville, D. H. *J. Am. Chem. Soc.* **1996**, 118, 10008-10009.
- (136) Scollard, J. D.; McConville, D. H.; Payne, N. C.; Vittal, J. J. *Macromolecules* **1996**, 29, 5241-5243.
- (137) Uozumi, T.; Tsubaki, S.; Jin, J. Z.; Sano, T.; Soga, K. *Macromol. Chem. Phy.* **2001**, 202, 3279-3283.
- (138) Tsubaki, S.; Jin, J.; Ahn, C. H.; Sano, T.; Uozumi, T.; Soga, K. *Macromol. Chem. Phy.* **2001**, 202, 482-487.
- (139) Hitoshi Hagimoto, T. S., Tomiki Ikeda, *Macromol. Rap. Commun.* **2002**, 23, 73-76.
- (140) Mehrkhodavandi, P.; Schrock, R. R.; Bonitatebus, P. J. *Abstracts of Papers of the American Chemical Society* **2000**, 220, U463-U463.

- (141) Mehrkhodavandi, P.; Schrock, R. R. *J. Am. Chem. Soc.* **2001**, *123*, 10746-10747.
- (142) Keaton, R. J.; Jayaratne, K. C.; Fettinger, J. C.; Sita, L. R. *J. Am. Chem. Soc.* **2000**, *122*, 12909-12910.
- (143) Not as PI probably due to the "fe-no-ki-shi i-mi-n" pronunciation of phenoxyimine in Japanese.
- (144) Matsugi, T.; Kojoh, S.; Fujita, T.; Kashiwa, N. *Kobunshi Ronbunshu* **2002**, *59*, 410-414.
- (145) Matsugi, T.; Matsui, S.; Kojoh, S.; Takagi, Y.; Inoue, Y.; Nakano, T.; Fujita, T.; Kashiwa, N. *Macromolecules* **2002**, *35*, 4880-4887.
- (146) Saito, J.; Mitani, M.; Onda, M.; Mohri, J. I.; Ishi, J. I.; Yoshida, Y.; Nakano, T.; Tanaka, H.; Matsugi, T.; Kojoh, S. I.; Kashiwa, N.; Fujita, T. *Macromol. Rapid Commun.* **2001**, *22*, 1072-1075.
- (147) Saito, J.; Mitani, M.; Mohri, J.; Ishii, S.; Yoshida, Y.; Matsugi, T.; Kojoh, S.; Kashiwa, N.; Fujita, T. *Chem. Lett.* **2001**, 576-577.
- (148) Yoshida, Y.; Mohri, J.; Ishii, S.; Mitani, M.; Saito, J.; Matsui, S.; Makio, H.; Nakano, T.; Tanaka, H.; Onda, M.; Yamamoto, Y.; Mizuno, A.; Fujita, T. *J. Am. Chem. Soc.* **2004**, *126*, 12023-12032.
- (149) Furuyama, R.; Mitani, M.; Mohri, J.; Mori, R.; Tanaka, H.; Fujita, T. *Macromolecules* **2005**, *38*, 1546-1552.
- (150) Ishii, S.; Saito, J.; Matsuura, S.; Suzuki, Y.; Furuyama, R.; Mitani, M.; Nakano, T.; Kashiwa, N.; Fujita, T. *Macromol. Rapid Commun.* **2002**, *23*, 693-697.

- (151) Ishii, S.; Mitani, M.; Saito, J.; Matsuura, S.; Kojoh, S.; Kashiwa, N.; Fujita, T.  
*Chem. Lett.* **2002**, 740-741.
- (152) Milano, G.; Cavallo, L.; Guerra, G. *J. Am. Chem. Soc.* **2002**, *124*, 13368-13369.
- (153) Longo, P.; Amendola, A. G.; Fortunato, E.; Boccia, A. C.; Zambelli, A.  
*Macromol. Rapid Commun.* **2001**, *22*, 339-344.
- (154) Tian, J.; Hustad, P. D.; Coates, G. W. *J. Am. Chem. Soc.* **2001**, *123*, 5134-5135.
- (155) Mitani, M.; Furuyama, R.; Mohri, J.; Saito, J.; Ishii, S.; Terao, H.; Kashiwa, N.; Fujita, T. *J. Am. Chem. Soc.* **2002**, *124*, 7888-7889.
- (156) Prasad, A. V.; Makio, H.; Saito, J.; Onda, M.; Fujita, T. *Chem. Lett.* **2004**, *33*, 250-251.
- (157) Tshuva, E. Y.; Goldberg, I.; Kol, M. *J. Am. Chem. Soc.* **2000**, *122*, 10706-10707.
- (158) Tshuva, E. Y.; Groysman, S.; Goldberg, I.; Kol, M.; Goldschmidt, Z.  
*Organometallics* **2002**, *21*, 662-670.
- (159) Tshuva, E. Y.; Goldberg, I.; Kol, M.; Goldschmidt, Z. *Chem. Commun.* **2001**, 2120-2121.
- (160) Groysman, S.; Goldberg, I.; Kol, M.; Genizi, E.; Goldschmidt, Z. *Inorg. Chim. Acta* **2003**, *345*, 137-144.
- (161) Groysman, S.; Goldberg, I.; Kol, M.; Genizi, E.; Goldschmidt, Z.  
*Organometallics* **2003**, *22*, 3013-3015.
- (162) Keaton, R. J., 2003, dissertation, chapter 3.

- (163) Keaton, R. J.; Koterwas, L. A.; Fettinger, J. C.; Sita, L. R. *J. Am. Chem. Soc.* **2002**, *124*, 5932-5933.
- (164) Zhang, Y. H.; Keaton, R. J.; Sita, L. R. *J. Am. Chem. Soc.* **2003**, *125*, 9062-9069.
- (165) Jayaratne, K. C.; Sita, L. R. *Abstracts of Papers of the American Chemical Society* **2001**, *221*, U649-U649.
- (166) Keaton, R. J. Ph.D. Dissertation, 2003, chapter 4.
- (167) Coates, G. W. *Chem. Rev.* **2000**, *100*, 1223-1252.
- (168) Chen, Y. X.; Stern, C. L.; Yang, S. T.; Marks, T. J. *J. Am. Chem. Soc.* **1996**, *118*, 12451-12452.
- (169) Mehrkhodavandi, P.; Bonitatebus, P. J.; Schrock, R. R. *J. Am. Chem. Soc.* **2000**, *122*, 7841-7842.
- (170) Hawker, C. J.; Bosman, A. W.; Harth, E. *Chem. Rev.* **2001**, *101*, 3661-3688.
- (171) Wang, J. S.; Matyjaszewski, K. *Macromolecules* **1995**, *28*, 7901-7910.
- (172) Wang, J. S.; Matyjaszewski, K. *J. Am. Chem. Soc.* **1995**, *117*, 5614-5615.
- (173) Patten, T. E.; Xia, J. H.; Abernathy, T.; Matyjaszewski, K. *Science* **1996**, *272*, 866-868.
- (174) *Handbook of Radical Polymerization*; Chiefari, J.; Rizzardo, E., Eds.; Wiley-Inter-Science, 2002.
- (175) Gaynor, S. G.; Wang, J. S.; Matyjaszewski, K. *Macromolecules* **1995**, *28*, 8051-8056.
- (176) van Meurs, M.; Britovsek, G. J. P.; Gibson, V. C.; Cohen, S. A. *J. Am. Chem. Soc.* **2005**, *127*, 9913-9923.

- (177) Müller, A. H. E.; Zhuang, R. G.; Yan, D. Y.; Litvinenko, G. *Macromolecules* **1995**, *28*, 4326-4333.
- (178) Goto, A.; Fukuda, T. *Prog. in Polym. Sci.* **2004**, *29*, 329-385.
- (179) For a 25% activation MeDeT, with 2<sup>nd</sup> order polynomial fit,  $k_p = 0.189$  is obtained. If linear fitting is employed, a  $k_p$  of 0.169 is obtained. This stands for a 12% error. For a polymerization with more termination, the calculation error will be significantly bigger.
- (180) Sita, L. R.; Babcock, J. R. *Organometallics* **1998**, *17*, 5228-5230.
- (181) Jeener, J.; Meier, B. H.; Bachmann, P.; Ernst, R. R. *J. Chem. Phys.* **1979**, *71*, 4546-4553.
- (182) Perrin, C. L.; Dwyer, T. J. *Chem. Rev.* **1990**, *90*, 935-967.
- (183) Macura, S.; Westler, W. M.; Markley, J. L. *Methods Enzymol.* **1994**, *239*, 106-144.
- (184) Berger, S.; Braun, S. *200 and More NMR Experiments*; Wiley-VCH, 2004.
- (185) See experimentals part for detailed calculation.
- (186) <sup>13</sup>C-1-dodecene was prepared by Wittig reaction from undecylic aldehyde.
- (187) All the molecular weights  $M_n$  and  $M_w$  are detected by GPC, calibrated by seven polystyrene standards. This relative molecular weight from PS is slightly higher than the absolute molecular, as observed in our group and other research groups.
- (188) Detailed synthesis of **57** will be discussed in chapter 5.
- (189) Zhang, Y. H.; Reeder, E. K.; Keaton, R. J.; Sita, L. R. *Organometallics* **2004**, *23*, 3512-3520.

- (190) All molecular weight is round to the nearest hundred.
- (191) Kissounko, D. A.; Fettinger, J. C.; Sita, L. R. *Inorg. Chim. Acta* **2003**, *345*, 121-129.
- (192) Kissounko, D. A.; Zhang, Y. H.; Harney, M. B.; Sita, L. R. *Adv. Synth. & Catal.* **2005**, *347*, 426-432.
- (193) The synthesis of the hafnium derivative was done by Kissounko, D.A.
- (194) 2nd order polynomial curve fitting was employed to abstract  $k_p$  and  $k^{\ddagger}$ . Similar  $k_p$  was obtained.  $k_t$  was smaller than the experimental deviation.
- (195) Shibayama, K.; Seidel, S. W.; Novak, B. M. *Macromolecules* **1997**, *30*, 3159-3163.
- (196) Wu, F.; Jordan, R. F. *Organometallics* **2005**, *24*, 2688-2697.
- (197) Wrobel, O.; Schaper, F.; Wieser, U.; Gregorius, H.; Brintzinger, H. H. *Organometallics* **2003**, *22*, 1320-1325.
- (198) Leung, W.-P.; Song, F.-Q.; Zhou, Z.-Y.; Xue, F.; Mak, T. C. W. *J. Organomet. Chem.* **1999**, *575*, 232-241.
- (199) See Chapter 2 for more details.
- (200)  $\text{ArF}_4:(3,5\text{-CF}_3)_2\text{C}_6\text{H}_3$
- (201) Lambert, J. B.; Kuhlmann, B. *J. Chem. Soc.-Chem. Commun.* **1992**, 931-932.
- (202) Linear fitting was used to show the trend, and 2nd order polynomial fitting was used to abstract the kinetic parameters for each percentage activation, which is shown in Table 6.
- (203) See Chapter 2 for more details.
- (204) Matyjaszewski, K.; Xia, J. H. *Chem. Rev.* **2001**, *101*, 2921-2990.

- (205) Zhang, Y. H.; Keaton, R. J.; Sita, L. R. *J. Am. Chem. Soc.* **2003**, *125*, 8746-8747.
- (206) Buchwald, S. L.; LaMaire, S. J.; Nielsen, R. B.; Watson, B. T.; King, S. M. *Org. Synth.* **1993**, *71*, 77-82.
- (207) Kalesse, M. *Acros Organics Acta* **1995**, *1*, 29-31.
- (208) Fernandez-Megia, E. *Synlett* **1999**, 1179.
- (209) This number is expected by the fact that a poly(1-hexene) with 200 DP gives relative Mn of 20000 to 22000 based on polystyrene standards.
- (210) Unpublished results for  $\omega$ -alkenyl zirconium amidinates by Zhang, Y. H.
- (211) Hlatky, G. G. *Chem. Rev.* **2000**, *100*, 1347-1376.
- (212) Suzuki, t.; Suga, Y. *Polym. Prepr. (Am Chem Soc, Div. Polym. Chem.)* **1997**, *38*, 207-208.
- (213) Lee, D. H.; Yoon, K. B.; Hun, W. S. *Macromol. Symp.* **1995**, *97*, 185-193.
- (214) Soga, K.; Arai, T.; Hoang, B. T.; Uozumi, T. *Macromol. Rap. Commun.* **1995**, *16*, 905-911.
- (215) Young, A. E., M.S. Thesis, University of Maryland, 2004.
- (216) Woo, S. I.; Ko, Y. S.; Han, T. K. *Macromol. Rap. Commun.* **1995**, *16*, 489-494.
- (217) Zhang, Y. H.; Kissounko, D. A.; Fettinger, J. C.; Sita, L. R. *Organometallics* **2003**, *22*, 21-23.
- (218) Pretsch, E.; Bühlmann, P.; Affolter, C. *Structure Determination of Organic Compounds*; Springer, 2000.

- (219) Abiko, A.; Inoue, T.; Masamune, S. *J. Am. Chem. Soc.* **2002**, *124*, 10759-10764.
- (220) Barker, J.; Kilner, M. *Coord. Chem. Rev.* **1994**, *133*, 219-300.
- (221) Edelmann, F. T. *Coord. Chem. Rev.* **1994**, *137*, 403-481.
- (222) Koterwas, L. A.; Fettinger, J. C.; Sita, L. R. *Organometallics* **1999**, *18*, 4183-4190.
- (223) Kim, Y. H.; Kim, T. H.; Lee, B. Y.; Woodmansee, D.; Bu, X. H.; Bazan, G. *C. Organometallics* **2002**, *21*, 3082-3084.
- (224) Zhang, Y. H.; Sita, L. R. *Chem. Commun.* **2003**, 2358-2359.
- (225) Szwarc, M.; Beylen, M. *Ionic Polymerization and Living Polymers*; Chapman and Hall: New York, 1993.
- (226) Matyjaszewski, K. *J. Phys. Org. Chem.* **1995**, *8*, 197.
- (227) Sita group, unpublished data.
- (228) Woo, H. G.; Freeman, W. P.; Tilley, T. D. *Organometallics* **1992**, *11*, 2198-2205.
- (229) Richard, J. K., unpublished data.
- (230) Odian, G. *Principles of Polymerization*; 3 ed.; Wiley Interscience, 1991.
- (231) Mizuno, A.; Tsutsui, T.; Kashiwa, N. *Polymer* **1992**, *33*, 254-258.
- (232) Tsutsui, T.; Ishimaru, N.; Mizuno, A.; Toyota, A.; Kashiwa, N. *Polymer* **1989**, *30*, 1350-1356.
- (233) H. N. Cheng, J. A. E. *Die Makromol. Chem.* **1989**, *190*, 1931-1943.

- (234) Due to the lack of high temperature GPC system, all the samples were run at 50 °C in THF. This might cause some solubility issue and could cause a broader polydispersity.
- (235) See experiments for more details about the kinetic model.
- (236) This part of the work was done by Harney, M. B.
- (237) Author would like to thank Harney, M.B. and Hundert, S. N. for their contribution for the tensile test.
- (238) This part of the work was contributed by Wang, L.
- (239) Busico, V.; Cipullo, R.; Kretschmer, W. P.; Talarico, G.; Vacatello, M.; Castelli, V. V. *Angew. Chem., Int. Ed.* **2002**, *41*, 505-508.